University of South-Eastern Norway

Soheila Taghavi Hosnaroudi

Improved Multiphase Flow Performance Using AICV and its Potential Impact on Reservoir Recovery

Dissertation for the degree of Ph.D
Process, Energy and Automation Engineering

Faculty of Technology, Natural Sciences and Maritime Studies

University of
South-Eastern Norway

Soheila Taghavi Hosnaroudi

Improved Multiphase Flow Performance Using AICV and its Potential Impact on Reservoir Recovery

A PhD dissertation in
Process, Energy and Automation Engineering

Faculty of Technology, Natural Sciences and Maritime Studies
University of South-Eastern Norway
Porsgrunn

Doctoral dissertations at the University of South-Eastern Norway no. 198

ISSN: 2535-5244 (print)
ISSN: 2535-5252 (online)

ISBN: 978-82-7206-866-9 (print)
ISBN: 978-82-7206-867-6 (online)

Print: University of South-Eastern Norway

For

''Woman, Life, Freedom''

Preface

This thesis is submitted to the University of South-Eastern Norway (USN) as a partial fulfillment of the requirements for the degree of Philosophiae Doctor (PhD). The PhD research was carried out at the department of Process, Energy and Environmental Technology at USN, campus Porsgrunn, in the period from March 2021 to February 2024. This PhD is an industrial PhD which is a program offered by The Research Council of Norway (RCN). The program is funded by both RCN and InflowControl AS.

My PhD journey lasted for three years filled with opportunities and challenges. During this journey, they were many who supported me in ups and downs, and I would like to express my sincerest appreciations to them.

First and foremost, my gratitude goes to my main supervisor Britt Margrethe Emilie Moldestad. Words cannot express how grateful I am for her kindness, patience, understanding, availability, and encouragement. She supported me with her exceptional knowledge in fluid mechanics and reservoir engineering. She was meticulous in reviewing my results and manuscripts. Our long-lasted regular meetings were central in improving my theoretical foundation in the context of oil production. I did not have only a supervisor, but a life mentor; thank you Britt.

I am deeply grateful to Haavard Aakre, my manager and co-supervisor. Thanks for supporting me with the idea and desire of doing a PhD. In autumn 2020, he asked me if I want to be a ‘’Doctor’’ and I said yes. Since then, he supported me with his valuable inputs, original ideas, and insightful discussions. I learned a lot from him during my years at InflowControl AS.

My thanks extend to Nora Furuvik, my co-supervisor for her contribution and supportive supervision and collaboration in related projects to my PhD.

I would like to thank all my friends and colleagues at USN who made my stay at campus Porsgrunn welcoming and pleasant. Special thanks to Chidapha Deeraksa who always spread charm and positivity during lunch hours at Alkymisten; she made a difference at campus Porsgrunn. Thanks to the PhD coordinators Mariken Kjøhl-Røsand, Per Morten Hansen and Siri Luise Tveitan for guidance, and organizing the great PhD forums. I like to thank my fellow PhD candidates for a nice time at the campus and social gatherings: Vafa, Nima, Amir, Steven, Rune, Haytham, Agnieszka, Raghav, Vibeke, Peshalya and Jayangi.

Special thanks to Dag-Even Martinsen Torsøe at the library for providing the articles and books that I asked for; they were many. Thanks to Aleksander Svanberg and Martin Koklar Andersen at IT department for always being helpful in solving my technical software issues. Thanks to Sumudu S. Karunatathne for training me on use of the laboratory instruments at USN.

I am sincerely grateful to Ali Ghaderi for his great engagement in modelling work from the very beginning of my PhD. The long and interactive meetings with him made me more conscious on the importance of dimensional analysis and generally looking deep and fundamentally into the details of a problem.

Thanks to Seyed Amin Tahami for his professional assistance, valuable inputs, and expert suggestions in simulation work. Thanks to Farzan Farsi Madan, Farhan Hasin Alam, and Prakash Bhattarai whom I had the chance to be their supervisor on their master thesis which resulted into two scientific papers.

Thanks to my colleagues at R&D department at InflowControl AS, Einar Gisholt and Tilak Chand Dhital who helped me in the experimental work.

I would like to give a special thanks to my managers and colleagues at InflowControl AS, Vidar Mathiesen, Bjørnar Werswick, Merete Svartangen, Trond Mathisen, Alexander Løberg and many others both in Porsgrunn office and internationally. Haavard, Bjørnar and Vidar gave me the opportunity as a new graduate to start my career in 2014 as development engineer at InflowControl AS; their decision on that time resulted into this industrial PhD.

I want to thank my amazing friends who with their kindness, support, and love filled my heart with joy and happiness and made the challenging PhD period smoother, Mirela, Mehry, Atina & Mehrdad, Dilini & Mahesh, Mitra, and Sanaz; you are wonderful.

I would like to thank my beloved family in Iran, my parents, Dokhi and Hassan, and my lovely sister, Samira, for their endless moral support, encouragement, understanding and warm wishes. A huge warm thank to my brother, Amir, for always believing in me and for paving the success path for me. I could have never accomplished this achievement without them.

I would like to express my love and thank to my mother and father-in-law, Gunn and Torger, for always being kind, encouraging and supportive.

Finally, I want to thank the love of my life, my husband Robin for always believing in me. His support, encouragement, understanding, patience, and valuable consultations in almost everything, made this achievement possible for me.

Soheila Taghavi Hosnaroudi

Porsgrunn, February 2024

Acknowledgements

This thesis is an industrial PhD, which is a program funded partially by The Research Council of Norway. The Project number is 322802, and the title of the project is ‘’Improved Multiphase Flow Performance Using Autonomous Inflow Control Valve and its Potential Impact on Reservoir Recovery’’.

The candidate would like to thank USN for providing the necessary simulation tools. Also, some part of the experimental work is carried out at the laboratory facility at USN, Porsgrunn campus.

Abstract

The global energy demand is growing, and oil and gas supply and consumption will evolve in the coming years. It is important to maintain the current oil production to meet the global energy demand. A major challenge in oil production is low oil recovery. Inefficient oil recovery can be due to the early gas and/or water breakthrough in the production wells. It is therefore essential to develop technologies that can overcome the challenges related to gas and/or water breakthrough and consequently contribute to sustain the oil production and increase the oil recovery.

Different types of inflow control devices (ICDs), passive and autonomous, reduce the negative effects of early gas and/or water breakthrough. Passive ICD was first developed in the 1990s and is today a proven method to improve the oil production and recovery. Additionally, autonomous inflow control devices (AICDs) have become a standard solution for many horizontal wells at the Norwegian Continental Shelf due to the promising results from many field installations. The autonomous inflow control valve (AICV) was developed in 2012 as a result of a continuous effort to develop technologies that contribute to improve the oil recovery. AICVs can choke back gas and water more than other existing technologies.

This PhD thesis addresses the key issues related to improved oil recovery using different types of flow control devices. The thesis focuses on testing and simulation of AICV under different reservoir conditions and for different applications. When gas and water breakthrough occurs, the water cut (WC) and the gas volume fraction (GVF) vary over time in the breakthrough zones. The multiphase flow behavior of the AICV in these breakthrough zones is important for the total recovery along the well. The main goal is to improve the multiphase flow performance of the AICV for use in thin-oil-rim reservoirs, and reservoirs using enhanced oil recovery (EOR) methods. The potential impact of the improved AICV performance on increased oil recovery is investigated by utilizing different types of commercial simulators.

The AICV design and multiphase behavior of AICV are improved. Several AICV prototypes were tested under realistic reservoir conditions to find the optimum design. The piston dimension and shape, the combination and dimensions of pilot flow elements, the housing dimension, and the inlet dimension and design are changed to obtain a better multiphase flow behavior.

Experimental work and simulation study were combined to achieve the main objective. The experiments were conducted in different setups and consist of mainly one-phase and multiphase flow tests for ICD and AICV using water, gas, and oil as the reservoir fluid. Simulations were performed with selected reservoir simulation tools. Reservoirs using steam

assisted gravity drainage (SAGD) and CO_2 for EOR in addition to thin-oil-rim reservoirs face a number of challenges that AICV can potentially mitigate. The relevant conditions for SAGD/CO_2-EOR and thin-oil-rim reservoirs were used in the experiments and simulations.

The results from the experiments show that AICV restricts the gas and water flow rates significantly compared with an orifice-type ICD, in particular at higher GVF. This behavior makes the AICV technology unique compared with other inflow control technologies. The gas flow rates over the AICV and ICD at a 3-bar differential pressure are about 0.1 m^3/h and 3.8 m^3/h respectively, indicating that the gas reduction by using AICV is significant. The water flow rates for AICV and ICD at 3 bar are 0.07 m^3/h and 0.44 m^3/h, respectively. The simulations show that the gas/steam reduction can be up to 64% and the increase in oil production can reach up to 15%. Reduction in steam production will improve the overall SAGD operation performance. In addition, AICV in comparison with ICD, reduces the water and CO_2 volume flow rates by approximately 58% and 82%, respectively. The results obtained from the corresponding simulations for a case study with CO_2-EOR show that the production of water-CO_2 is reduced by 20%. Choking back CO_2 by using AICV may give a better distribution of CO_2 in a larger area of the reservoir. This leads to a broader contact between CO_2 and the residual oil in the reservoir, resulting in increased EOR. For the case study with light oil in a thin-oil-rim reservoir, at a 15-bar pressure drop, the gas and water flow rates through the passive ICD are approximately 7.35 and 2.4 times more than the flow rates through the AICV. The results indicate that the gas and water reduction by using AICV is significant. The simulations show that the oil production can be increased by approximately 48%. In addition, the wells completed with AICVs, keep the gas to oil ratio (GOR) at a relatively low level and this allows the wells to produce for a longer period at a high liquid rate without needing to choke back because of high GOR. It can be concluded that deployment of AICVs in the most challenging light oil reservoirs with high GOR can be beneficial in terms of increased production and recovery.

Mathematical models were developed for density and kinematic viscosity within the Bayesian statistical inference framework. The predictive accuracy of the models were validated against measurements, and it was within 90%. The models are based on the experimental data obtained during this work and can be used further to develop a model for AICV behavior. In addition, a model to describe the behavior of AICV was derived based on dimensional analysis. The model can be used in the experimental design and will significantly reduce the required number of experiments.

All the experiments and simulations demonstrate that the improved multiphase flow performance using AICV has a significant potential for increased oil production and recovery.

Keywords: AICV, ICD, Gas and/or water breakthrough, Oil recovery, GVF, GOR, IOR, CO_2-EOR, SAGD, Multiphase flow, Thin-oil-rim reservoir.

List of papers

Paper 1

S. Taghavi, E. Gisholt, H. Aakre, S. Håland, and K. Langaas, "Autonomous Inflow Control Valve Multiphase Flow Performance for Light Oil," in *Offshore Technology Conference*, 2021, vol. Day 1 Mon, August 16, 2021, D012S059R016, doi: 10.4043/31239-ms. [Online]. Available: https://doi.org/10.4043/31239-MS

Paper 2

S. Taghavi and A. Ghaderi, "On Uncertainty Analysis of the Rate Controlled Production (RCP) Model," in *First SIMS EUROSIM Conference on Modelling and Simulation*, Finland, 2021: Linköping Electronic Conference Proceedings, 2021, doi: DOI: https://doi.org/10.3384/ecp21185271

Paper 3

S. Taghavi, H. Aakre, and B. M. E. Moldestad, "Performance Analysis of Autonomous Inflow Control Valve in a SAGD Late Life Process with Non-Condensable Gases," in *SPE Canadian Energy Technology Conference*, 2022, vol. Day 1 Wed, March 16, 2022, D011S011R002, doi: 10.2118/208915-ms. [Online]. Available: https://doi.org/10.2118/208915-MS

Paper 4

S. Taghavi, F. Farsi Madan, R. Timsina, and B. M. E. Moldestad, "Application of Autonomous Inflow Control Valve for Enhanced Bitumen Recovery by Steam Assisted Gravity Drainage," in *The 63rd International Conference of Scandinavian Simulation Society, SIMS 2022*, Trondheim, Norway, 2022: Linköping Electronic Conference Proceedings 192, doi: https://doi.org/10.3384/ecp192009.

Paper 5

S. Taghavi, H. Aakre, and B. M. E. Moldestad, "The Impact of Autonomous Inflow Control Valve on Enhanced Bitumen Recovery in a SAGD Late Life Reservoir: Lab Experiment and Simulation," in *SPE Canadian Energy Technology Conference and Exhibition*, 2023, vol. Day 1 Wed, March 15, 2023, D012S001R002, doi: 10.2118/212783-ms. [Online]. Available: https://doi.org/10.2118/212783-MS

Paper 6

Farhan Hasin Alam, Amin Tahami, Nora C.I. Furuvik, Britt M.E. Moldestad, and S. Taghavi, "The Impact of Autonomous Inflow Control Valve on Enhanced Oil Recovery in SAGD

Application," in 64th International Conference of Scandinavian Simulation Society, SIMS2023, Västerås, Sweden, September 25–28, 2023. 2023: Linköping University Electronic Press (LiU E-press) in Linköping Electronic Conference Proceedings 200, 2023-10-19, pp. 278-285, doi: https://doi.org/10.3384/ecp200036. [Online]. Available: https://ecp.ep.liu.se/index.php/sims

Paper 7

S. Taghavi, S. A. Tahami, H. Aakre, N. C. I. Furuvik, and B. M. E. Moldestad, "Performance Analysis of Autonomous Inflow Control Valve in a Heterogenous Reservoir Using CO2 Enhanced Oil Recovery," in *SPE Annual Technical Conference and Exhibition*, 2023, vol. Day 3 Wed, October 18, 2023, D031S045R002, doi: 10.2118/215153-ms. [Online]. Available: https://doi.org/10.2118/215153-MS

Paper 8

S. Taghavi, H. Aakre, S. A. Tahami, and B. M. E. Moldestad, "The Impact of Autonomous Inflow Control Valve on Improved Oil Recovery in a Thin-Oil-Rim Reservoir," SPE Journal, pp. 1-15, 2024, https://doi.org/10.2118/218393-PA

Abbreviations

AICD	Autonomous Inflow Control Device
AICV	Autonomous Inflow Control Valve
API	Oil density defined from American Petroleum Institute
BHP	Bottomhole Pressure
CMG	Computer Modelling Group
EOR	Enhanced Oil Recovery
FCD	Flow Control Device
FW	FlexWell
GHG	Greenhouse Gas
GLR	Gas Liquid Ratio
GOC	Gas Oil Contact
GOR	Gas/Oil Ratio
GVF	Gas Volume Fraction
HMC	Hamilton Monte Carlo
ICD	Inflow Control Device
IEO	International Energy Outlook
IOR	Improved Oil Recovery
LFE	Laminar Flow Element
MCMC	Markov Chain Monte Carlo
MMP	Minimum Miscible Pressure
MRC	Maximum Reservoir Contact
NCS	Norwegian Continental Shelf
NPD	Norwegian Petroleum Directorate
OOIP	Original Oil In Place
PDO	Plan for Development and Operation
PI	Productivity Index
P&ID	Piping and Instrumentation Diagram
RC	Reservoir Condition
RCP	Rate-Controlled Production
SAGD	Steam Assisted Gravity Drainage
STG	Surface Gas Rate
STL	Surface Liquid Rate
TFE	Turbulent Flow Element
VTC	Viscosity Temperature Coefficient
WAG	Water Alternating Gas
WC	Water Cut

Nomenclature

Symbol	Description	Unit
a_{AICD}	RCP valve/AICV strength parameter	–
A_{vc}	Area in vena contracta	m^2
B_o	Oil formation volume factor	–
C	Geometrical constant	–
C_d	Discharge coefficient	–
D	Diameter	m
f	Friction factor	64/Re
K_r	Relative permeability	–
K_{rog}	Oil relative permeability at irreducible water saturation for an oil-gas system	–
K_{rg}	Relative permeability of gas phase	–
K_{row}	Oil relative permeability for a water-oil system	–
K_{rw}	Relative permeability of water phase	–
L	Length	m
n_g	Corey exponent	–
ΔP	Differential pressure	bar
Q	Volumetric flow rate	m^3/d
Re	Reynolds number	–
S	Slip	–
S_{orw}	Residual oil saturation in a water-oil system	–
S_w	Water saturation	–
S_{wc}	Connate (irreducible) water saturation	–
S_{or}	Residual oil saturation	–
S_g	Gas saturation	–
S_{gc}	Critical gas saturation	–
S_{lc}	Total critical liquid saturation	–
S/S_i	Source-sink term	–
U_{sg}	Superficial velocity of gas	m/s
U_{so}	Superficial velocity of oil	m/s
x	User-input parameter	–
y	User-input parameter	–
ρ	Fluid density	kg/m^3
ρ_{mix}	Mixed-fluid density	kg/m^3
ρ_{cal}	Calibration density	kg/m^3
μ	Fluid viscosity	cp
μ_{mix}	Mixed-fluid viscosity	cp
μ_{cal}	Calibration viscosity	cp
ε_g	Hold-up of gas	–
ε_o	Hold-up of oil	–
Ψ_{ji}	Rate of mass transfer between phase j to i	kg/s
Φ	Pipe angle relative to the gravitational vector	°
F^I_{ji}	Friction forces between the phase j to i	N

Table of contents

Part 1

Overview

1 Introduction

This section presents an overview of the background, motivation, and objectives of the thesis.

Background and motivation

According to the International Energy Outlook 2021, IEO2021, which provides long-term world energy projections, petroleum, and other liquid fuels together with natural gas remain the largest energy source in the world, see Figure 1-1. The IEO2021 projections indicate the constant growing pace in liquid fuels and natural gas consumption until 2050. However, renewable energy consumption nearly equals liquid fuels consumption by 2050. [1]

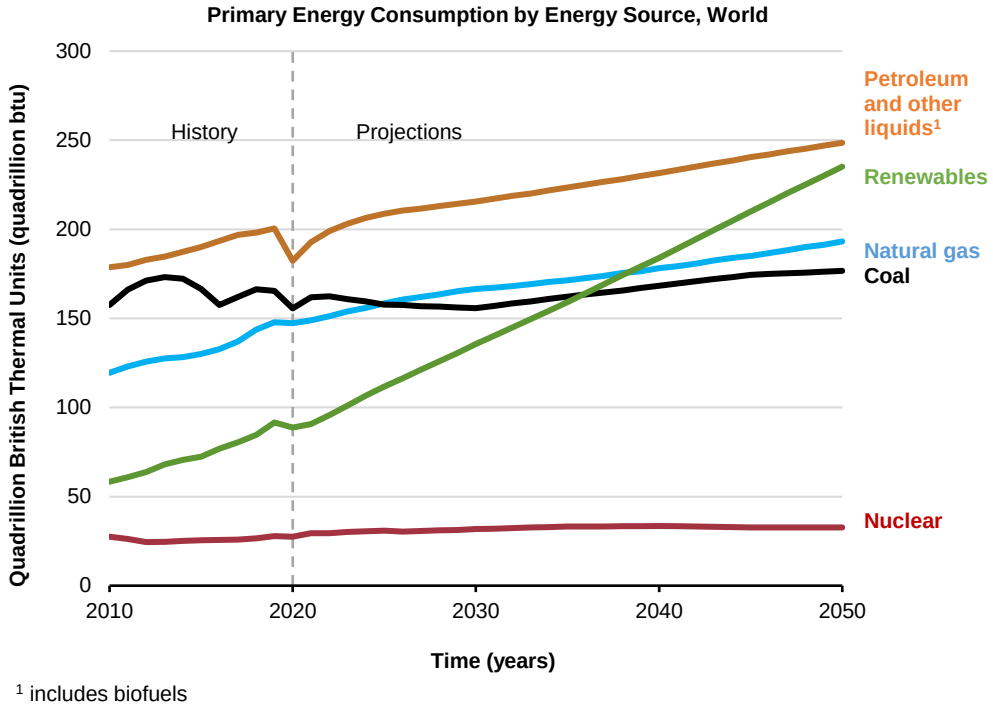

Figure 1-1: Global primary energy consumption by energy source, IEO2021 [1].

The newest report from the U.S Energy Information Administration, IEO2023, agrees with the previous projection from 2021, see Figure 1-2. Both projections confirm the continuous demand for fossil fuels throughout the year 2050. Due to the increasing energy demand and current policies, a steady growth in fossil fuel energy is expected. Besides, a faster growth in non-fossil fuel sources is predicted. The shaded regions in the figure represent maximum and minimum predicted values. [2]

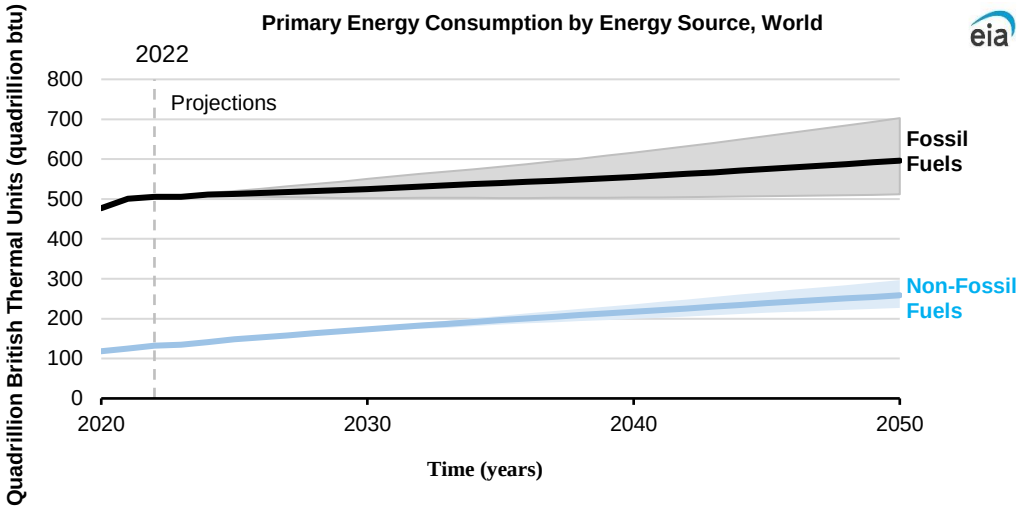

Figure 1-2: Global primary energy consumption, IEO2023 [2].

Due to the increase in the global energy demand, oil and gas will continue to meet a large share of this demand. However, it is believed that fossil fuels are a main contributor to the greenhouse gas (GHG) emissions. This urges the petroleum industry to implement measures that reduce the emissions from the production. The future of petroleum in the energy transition and how fast the transition will occur depend on many parameters. The important parameters in energy transition are willingness of global leaders in developing low-carbon energy policies, their success in implementation of binding agreements and policies, development cost of low-emission alternatives, and the technology advancements in this area. About half of today's oil demand is linked to the transport sector and can be addressed by large scale electrification, see Figure 1-3. Given that the electricity is generated from renewables or de-carbonized fossil fuels, the electrification of the transport sector becomes more attractive both environmentally and economically. Replacing the use of oil related to shipping and aviation are more challenging with today's electric battery capacity. Oil does not serve only as a source of energy, but it can also be refined into petrochemicals which are used as medicines, fertilizers, synthetic rubbers, paints, and plastics. Replacing this part of the oil use is also hard to achieve. [3]

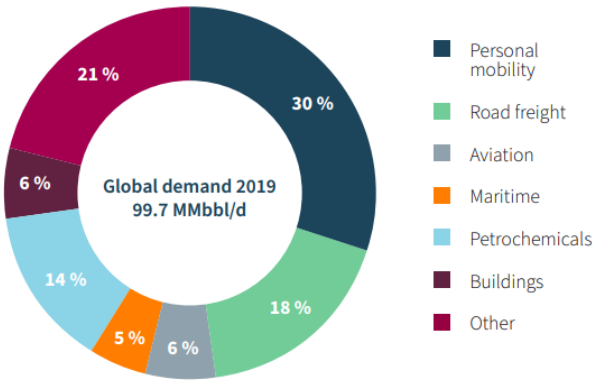

Figure 1-3: Oil usage share in different source and sectors in 2019 [3].

As oil is a product with a wide range of applications, it is important to develop methods to increase the oil production and recovery in an energy-efficient way. However, the major challenge in oil production is to increase the recovery factor. In the Norwegian continental shelf (NCS), using current technology and plan for development and operation (PDO plan), significant oil resources will not be recovered before shutting off the wells. Figure 1-4 shows the distribution of oil reserves and resources for the largest oil fields in Norway as of 31 December 2022. Although, NCS is one of the leading regions in oil recovery, about half of the oil is remaining in the reservoir after shutting down.

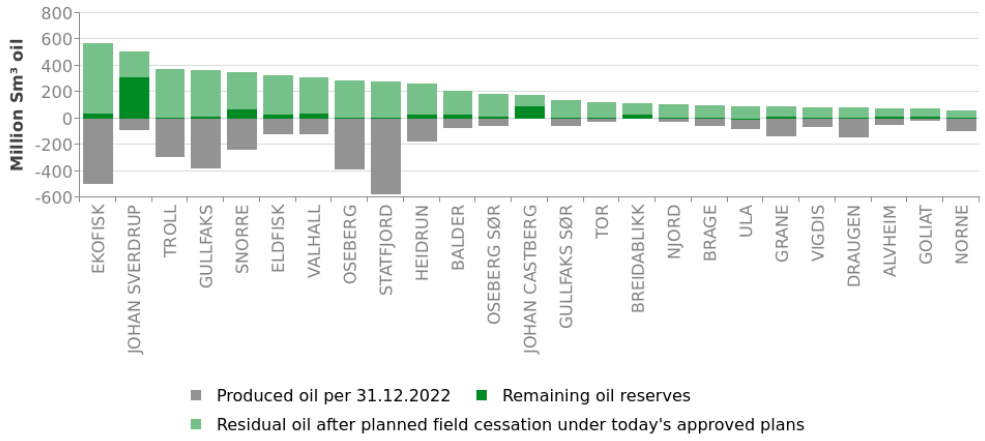

Figure 1-4: Distribution of oil reserves and resources for the largest oil fields as of 31 December 2022 [4].

These remaining resources require implementation of other methods beyond the methods in PDO to improve the oil recovery (IOR). ‘’*In the context of the Norwegian continental shelf (NCS), improved oil recovery (IOR) is the extra oil recovery achieved beyond what is described in the PDO.*’’ [5]. The oil recovery factor is the percentage of the oil that can be recovered from an oil reservoir. Increasing this factor by just a few percentage points would represent a significant value. [5]

One of the principal issues in IOR is to maximize the reservoir contact. This can be achieved by drilling long horizontal, and multilateral wells. Thus, more of the reservoir fluid that is trapped in the formation is accessible. Well placement, well type, well path, numbers and lengths of laterals, and completion methods are among the important factors that must be optimized to achieve a maximum reservoir contact (MRC) and well productivity [6, 7]. The Troll field at the Norwegian Continental Shelf is a good example of deploying these technologies. The oil production from the Troll West Oil and Gas Province started in 1995. Drilling of long and multilateral horizontal wells at Troll has contributed significantly to increased oil recovery [8].

Another crucial factor in IOR, is to reduce the negative effects of early gas and/or water breakthrough. Early gas and/or water breakthrough is one of the main challenges in oil production and results in inefficient oil recovery. This problem occurs due to uneven flow along the wells. Long horizontal wells experience higher pressure differences between the heel and toe section of the well due to the friction loss within the pipe. This leads to non-uniform flow and consequently fluid breakthrough in the heel section of the well. This phenomenon, which is known as the heel to toe effect, will limit the production rates from the other zones in the well. Some elements that can also create uneven flow along the well are permeability differences and heterogeneities in the reservoir [9, 10], changes in capillary pressure and relative permeability along the wellbore[11], localized skin damage or fractures [12, 13], and variations in viscosity of the reservoir fluids [14], see Figure 1-5.

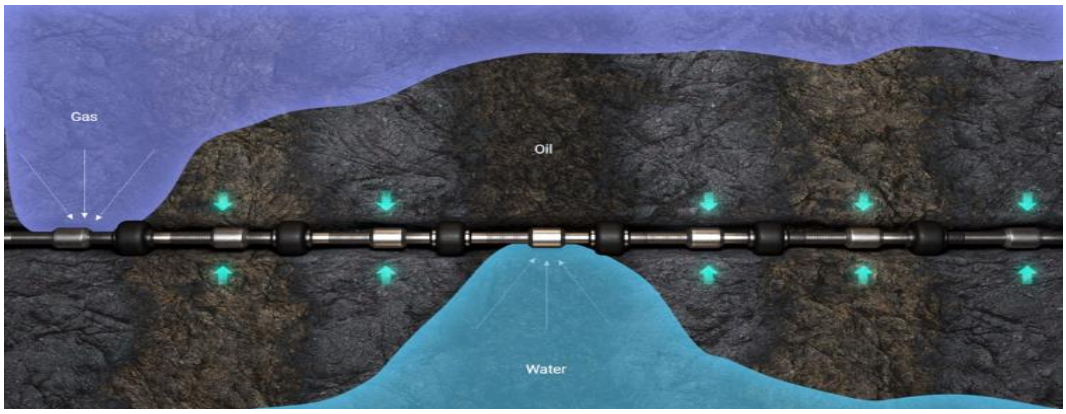

Figure 1-5: Uneven flow along the wellbore resulting into water and gas breakthrough.

Many new and advanced technologies have been developed to reduce the negative effects of early gas and/or water breakthrough. Inflow control technologies generally and passive and autonomous inflow control devices (ICDs and AICDs) particularly, are proven methods that can mitigate this problem and consequently increase oil production. The purpose of ICDs and AICDs is to introduce an additional flow resistance [15]. These devices can be installed in the base-pipe with sand screen mounted upstream the device. As it is illustrated in Figure 1-6, fluid from the reservoir flows towards the sand screen, passes through the device, enters the production tubing, and ultimately flows to the surface together with the fluids from the other connected joints.

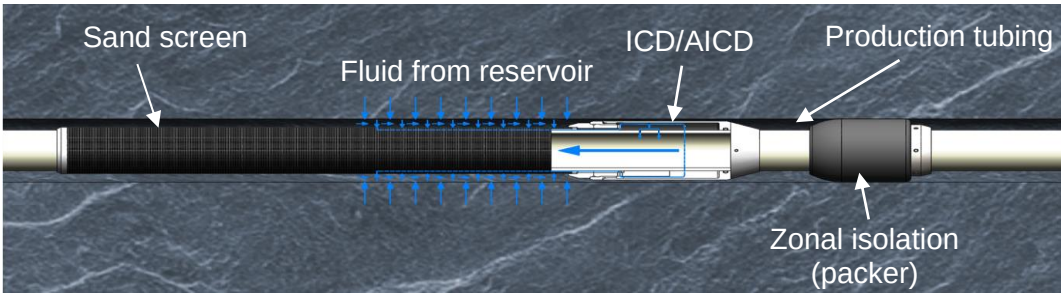

Figure 1-6: ICD/AICD mounted in base-pipe with sand screen.

Application of ICDs at the Troll field resulted in a higher oil production and recovery [16, 17]. Rate-controlled production valve (RCP valve) is one type of AICD. Many wells at Troll have been completed with RCP valves and the results demonstrate significant increase in cumulative oil production and a longer production period at low gas to oil ratio (GOR) [8]. Autonomous inflow control valve (AICV) is also one type of AICD. AICV delays the onset of breakthrough and restricts the gas and/or water production locally when these fluids flow into the well. The increased oil production and reduced water and gas production obtained by using AICV are demonstrated in several field installations worldwide and results are presented in several studies [18-20].

The reported results from simulations and field installations of passive and autonomous ICDs do not focus on the importance of the multiphase flow performance for IOR [21-24]. The ICD does not restrict the gas production after gas breakthrough occurs. Some AICDs restrict the gas production at lower gas volume fraction (GVF), but according to the available data none of the AICDs restrict the gas production at higher GVF [25]. The AICV developed prior to this project has an overall better multiphase flow performance than ICD but does not close for gas before GVF reaches 90%. A better gas choking than achieved with the existing flow control devices is needed to further improve the oil recovery.

In different zones along the well multiphase flow of gas/oil or water/oil flows through the completion. In some zones especially when there are fractures in the reservoir, pure phases of fluids enter the completion. Flow control devices must be able to choke or close when pure phases of unwanted fluids or mixtures of gas/oil or water/oil reach the completion. When selecting the flow control devices, it is crucial to have in mind that the performance of the devices for multiphase flow is of great importance. Therefore, utilizing flow control devices that have better performance in the presence of multiphase flow is crucial to obtain an improved IOR. In the breakthrough zones the water cut (WC) and the GVF vary over time. The multiphase flow behavior of the AICV in the breakthrough zones is important for the total recovery along the well. This thesis focuses on testing and simulation of AICV by focusing on multiphase flow performance under different reservoir conditions and recovery methods.

Research objectives

This PhD is an industrial PhD which is a program offered by The Research Council of Norway. This program has been established to encourage a closer cooperation between the industry and research organizations to promote knowledge transfer from researchers to society [26].

The main objective of this project is to improve the multiphase flow performance of the AICV for use in thin-oil-rim reservoirs, and reservoirs using enhanced oil recovery (EOR) methods. The potential impact of the improved AICV performance on increased oil recovery is

investigated by utilizing different types of commercial simulators. Increasing oil production and recovery will contribute to sustainable value creation for the Norwegian industry and society.

The main objective of this project is achieved through the following objectives:

- Developing and testing different AICV prototypes to find the optimum AICV design.
- Performing one-phase and multiphase flow tests for orifice ICD and AICV using water, gas, and oil at realistic reservoir conditions.
- Generate performance curves for one and two-phases for orifice ICD and AICV. Performance curves will give information about the amount of oil, water and gas produced at different reservoir drawdowns when the pure phases flow through the device and when the mixture of gas/oil or water/oil is passing through.
- Performing simulations using industry standard simulators such as ECLIPSE, NETool, OLGA/ROCX, and CMG.
- Evaluate the impact of improved multiphase performance using AICV on reservoir recovery and validation of the obtained results against experimental data.
- Modifying the existing RCP function through dimensional analysis.

Limitation

The PhD work was constrained by several factors including restricted access to field production data for history matching, limited availability of permeability and PVT data, and limited grids in developing reservoir models. The details of the implemented design modifications are not discussed in the thesis. The study of multiphase flow inside the AICV is not included in the thesis as it is beyond the scope of this work. The experimental and simulation study does only include ICD and AICV and no other AICD technologies. These limitations do not substantially affect the outcome of this work in which the performance of AICV and ICD/openhole under the same reservoir conditions are compared.

Main contribution

The main contribution of this industrial PhD is to extend the insight in advanced well completion with AICVs at different reservoir conditions and various applications. This is achieved by improving the AICV design and performance, and by developing coupled well-reservoir models to investigate the impact of AICV on increased oil production and recovery. The outcome of

this work can be utilized to address the challenges related to SAGD/CO_2 EOR and thin-oil-rim reservoirs.

The novelty of this work is the experimental data which demonstrate the unique behavior of AICV within multiphase flow. Furthermore, the experimental results are implemented in simulation tools, and new methods and workflows are developed in order to enable the modelling of advanced wells with AICVs under challenging reservoir conditions.

Outline of the thesis

This thesis is divided into two main parts. Part I consists of six chapters providing an overview of the thesis.

Chapter 1 presents the background and motivation of this research and describes why it is important to improve the oil recovery. This chapter also gives an idea of different inflow control technologies and how they can contribute to IOR.

Chapter 2 is the theory and literature review. The chapter presents an overview of IOR for thin-oil-rim reservoir and describes the EOR methods that this work focuses on. In addition, the functionality, and principles of the passive and autonomous ICDs that are of interest of this work are discussed in this chapter.

Chapter 3 summarizes the experimental setup and procedures. This section covers the test rigs and test conditions.

Chapter 4 describes the modelling methods and the simulation tools. Four commercial reservoir simulation tools are used in this work.

Chapter 5 presents a summary of the results from the experiments and simulations. The results are divided into subchapters based on the application of AICV in different types of reservoirs. This chapter also includes the results from mathematical modelling.

Chapter 6 is conclusions and some recommendations for further work.

Part II includes eight scientific papers as the main contributions of this research.

2 Theory and Literature Review

This chapter covers the most important theoretical topics and concepts that are relevant to this study. First, the history and development of inflow control technology are presented followed by different types of inflow control devices that are used in this work. The chapter investigates the IOR in thin-oil-rim reservoirs and EOR methods relevant to this PhD work. Finally, a brief explanation of relative permeability curves, stratified flow and slip which are necessary in order to understand part of the working principle of reservoir simulators is provided.

Inflow control technology

The petroleum industry raised attention to the concept of inflow control first after the introduction of ICDs in the early 1990s [27]. The motivation of ICDs development was first prompted after that the results from two horizontal wells at the Troll thin oil zone were not satisfactory. The productivity of the wells was severely limited by gas coning as a result of pressure loss along the wellbore [28]. ICDs were first developed in the 1990s to overcome this challenge. Two types of ICDs, passive and autonomous, are investigated in the following sub-chapters.

Passive inflow control device

Passive ICDs restrict the flow by generating additional pressure drop as the fluid travels between the reservoir and the production well [29]. They equalize the pressure drop along the entire length of the wellbore, promoting uniform flow of oil and gas through the formation so that the breakthrough of water and gas are delayed, see Figure 2-1.

A passive ICD has a constant flow area and no adjustment to its geometry is possible during operation. Different types of ICDs are commercially available, such as helical channel-type, nozzle-type, tube-type and hybrid-type [30].

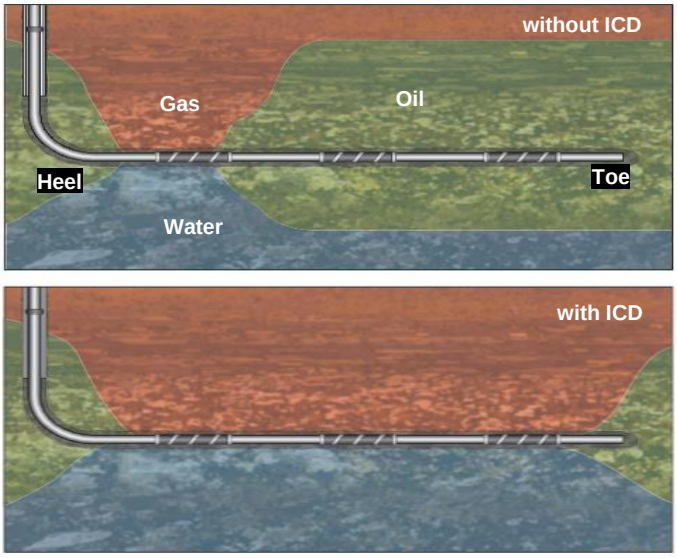

Figure 2-1: Gas and water breakthrough (without ICD) and uniform flow along the well (with ICD) [31].

In this work, the nozzle-type of ICD which is a sharp-edged orifice is used for the experiments and simulations. The governing equation for the nozzle-type ICD is as follows [32]:

$$\Delta P = \frac{8\rho Q^2}{d^4\pi^2 n^2 {C_d}^2} \qquad (1)$$

where ΔP is the pressure drop through the nozzle, ρ is the fluid density, Q is the volumetric flow rate of the fluid through the nozzle, d is the diameter of the nozzle, n is the number of tested nozzles, and C_d is the discharge coefficient. The discharge coefficient accounts for any non-reversible losses [15]. The discharge coefficient is a dimensionless number which is used to characterize the pressure loss behavior of an orifice or a nozzle and is defined as $C_d = A/A_{VC}$ [33]. A is the cross-sectional area of the orifice hole and A_{VC} is the area in vena contracta. Vena contracta is the minimum jet area that appears just downstream of the orifice where the fluid velocity is at its maximum. C_d is mostly a function of the Reynolds number (Re) [32]. It can be interpreted from equation (1) that the pressure drop through the nozzle is mainly dependent on the fluid density and the flow rate (velocity) squared.

Full scale experiments and field installations demonstrate the benefits of ICDs in mitigating the problem of gas and/or water breakthrough [34, 35]. Application of ICDs at the Troll field resulted in higher oil production and recovery [17, 36]. Successful examples of using ICDs to increase the oil production are provided in a scientific paper [37]. However, ICDs have some limitations in nature and once installed they cannot be adjusted. As ICDs are static and have a fixed opening, they do not choke or stop the water and/or gas production. Once the breakthrough occurs, extensive amount of water and/or gas is produced, and the solution is to

choke the whole well to sustain the operation of the downstream separation facilities. Choking the whole well, will also restrict the oil production.

Autonomous inflow control device, AICD

The next generation of ICDs is autonomous inflow control devices (AICDs). AICDs are self-regulated with no need to be controlled from the surface. AICDs are usually categorized as either with or without moving parts [38, 39]. Fluidic Diode [40], Schlumberger's AICD [41], and EQUALIZER SELECT™ [42] are the examples of AICDs without any moving parts. The internal geometry in these types of AICDs alters the flow pattern based on the fluid characteristics [39]. Rate-controlled production valve (RCP) and autonomous inflow control valve (AICV) are defined as AICDs with a moving part that is self-adjustable at downhole conditions [39]. In this work, RCP test results from literature are used for the purpose of comparison with experimental and simulation results obtained by using AICV.

Both the data from experiments in laboratories and the application of AICDs in reservoirs with high GOR or WC, have demonstrated that utilizing AICDs is a robust method in restriction of gas and/or water production and improving the oil recovery [43-48]. AICD completed wells in a super thin-oil-rim reservoir in the East and West Belumut fields in Malaysia produced 50% more oil compared with the ICD wells [23].

Rate-controlled production valve, RCP

RCP consists of a valve body (housing), a nozzle, and a movable disk, see Figure 2-2. The flow path is marked with red arrows. The fluid from the reservoir enters the nozzle, flows over the movable disk and spreads radially through the gap between the disk and the top plate of the housing, and is then discharged through the outlet ports in the body into the production well. The position of the disc which determines the valve opening (gap), depends on the fluid properties and the flow condition. The gap is a result of the balance between the three forces of momentum, drag and lift. The momentum and drag forces act to push the disk away from the top plate, while the lift force acts to pull the disk towards the top plate. When low-viscosity fluids like gas and water enter the valve, the velocity through the gap is increased and the pressure will be lower at the upper side of the disk, and the drag force is reduced. The higher pressure at rear side of the disk will press the disk upwards reducing the gap size until the forces balance. As a result, the overall pressure drop is increased. When higher viscosity fluids like oil flows through the disk, the drag force associated with friction loss increases, the pressure at the rear side of the disk decreases and the disk is pushed away from the top plate. Thus, the flow area and the flow rate are increased. [8, 49, 50]

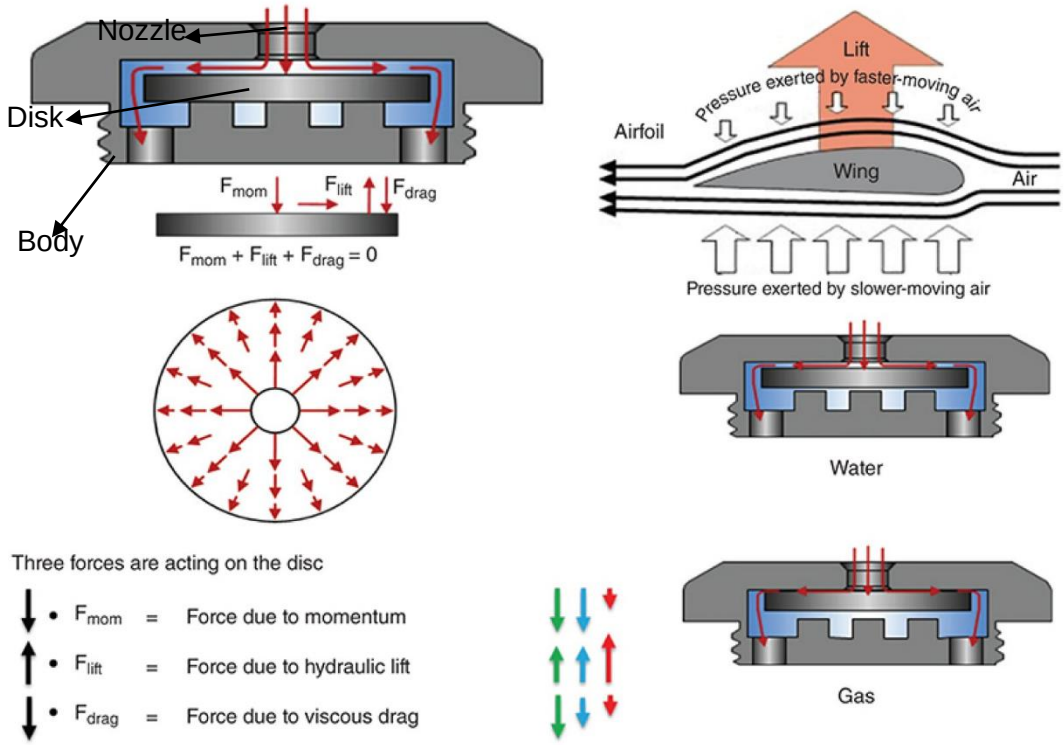

Figure 2-2: The RCP design and operation principle [49].

The mathematical model describing the performance of the RCP can be expressed as [51]:

$$\Delta P_{Tot} = \left(\frac{\rho_{mix}^2}{\rho_{cal}}\right) \cdot \left(\frac{\mu_{cal}}{\mu_{mix}}\right)^{y} \cdot a_{AICD} \cdot Q^{x} \qquad (2)$$

where ΔP_{Tot} is the differential pressure across the AICD, ρ_{cal} and μ_{cal} are the calibration fluid density and viscosity, and ρ_{mix} and μ_{mix} are the mixture fluid density and viscosity. The parameter a_{AICD} is a valve characteristic given by the ICD strength, Q is the volumetric flow rate of the mixture, and x and y are constants.

Many wells at Troll have been completed with RCP valves. The production results show approximately 20% higher cumulative oil production compared with ICDs [8]. In addition, the GOR in wells completed with ICDs is three times the GOR in wells completed with RCPs [8]. Also, analysis of the output from oil wells at Troll, demonstrates a clear improvement in the production rate after RCP installation [52]. This success made the RCP valves to be a part of standard lower completion solution at Troll, see Figure 2-3.

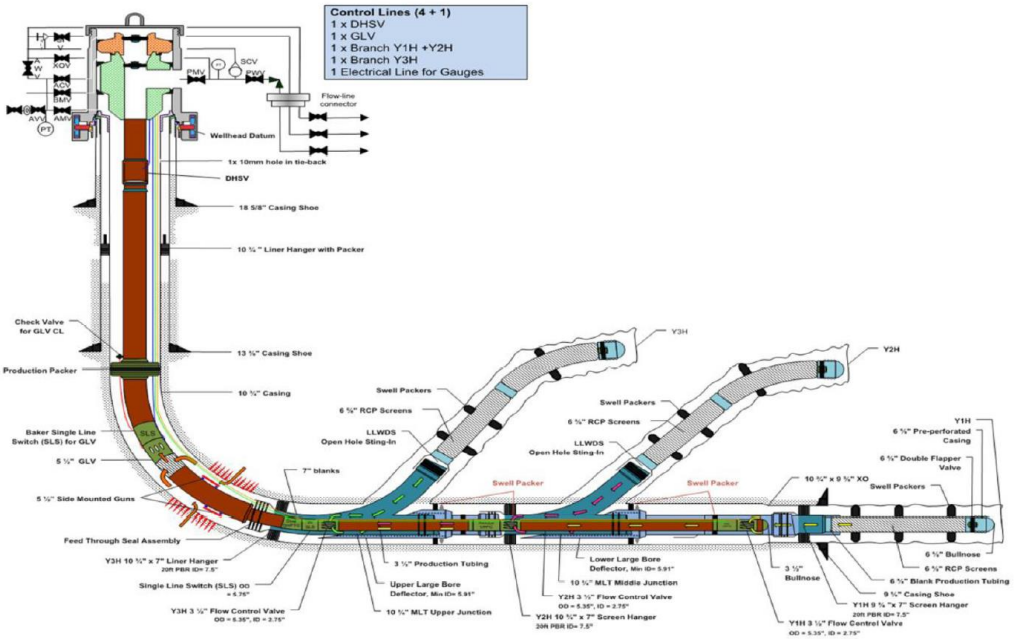

Figure 2-3: Typical completion at Troll; multilateral wells completed with RCP valves [17].

Autonomous inflow control valve, AICV

The AICV was invented in 2012. The first global installation of AICV was successfully executed in 2015. In 2022, over 220 AICV wells were deployed in five different continents and InflowControl AS passed a milestone. Since 2012, the AICV has been under continuous development. [53]

AICV delays the onset of breakthrough and restricts the gas production locally when the gas breakthrough occurs as shown in Figure 2-4. The figure shows a horizontal well completed with AICVs in a heterogenous reservoir. The pressure drops at different reservoir locations are plotted. Gas and water breakthrough occur in the high permeable zones in heterogenous reservoirs. In high permeable zones, the low resistance in the reservoir gives high flow rate of fluids resulting in higher pressure drop through the AICV, indicating that AICV is choking. In low permeable zones, the pressure drop in the reservoir is higher and as the total pressure drop from reservoir to the well is constant, the pressure drop over the AICV is lower. The reduction of gas production from the breakthrough zones allows to keep a low bottomhole pressure. This makes it possible to keep a higher sandface drawdown in the zones with oil, and thus maintaining the oil production from these zones. This results in maximizing oil production and recovery.

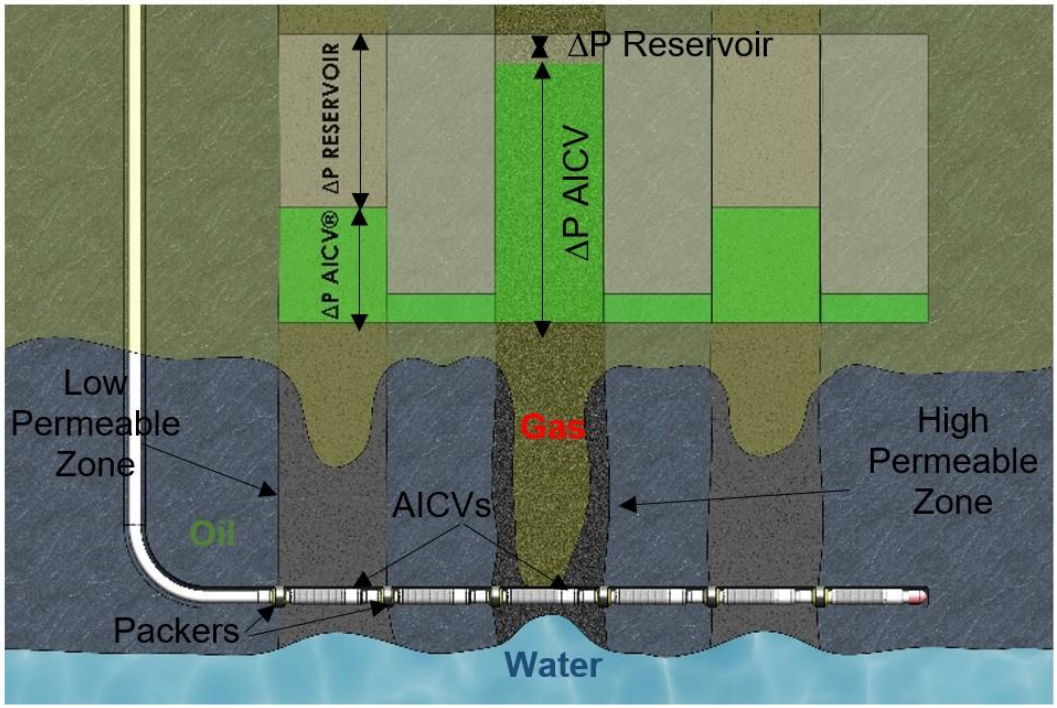

Figure 2-4: High pressure drop across AICV in high permeable zones with gas and water breakthrough [54].

The functionality of the AICV is controlled by a pilot flow parallel to the main flow, as it is illustrated in Figure 2-5. The main body, the inlet and the piston are the elements of the main flow path. The pilot flow consists of a pipe segment and a thin-plate orifice which are connected in series. The pipe segment serves as a laminar flow element (LFE) and the pressure drop through it is proportional to the fluid viscosity and the velocity. Equation (3) describes the pressure drop through the LFE:

$$\Delta P = f \times \frac{L\rho v^2}{2D} = \frac{64}{Re} \times \frac{L\rho v^2}{2D} = \frac{32\mu v L}{D^2} \qquad (3)$$

where ΔP is the pressure drop, f is the friction factor (64/Re), Re is Reynolds number, ρ is the fluid density, μ is the fluid viscosity, v is the fluid velocity, and L and D are the length and diameter of the LFE, respectively. A thin-plate orifice serves as a turbulent flow element (TFE) and the pressure drop through the orifice is given by equation (4):

$$\Delta P = \frac{1}{2\,C_d^2} \cdot \rho v^2 \qquad (4)$$

in which, C_d is the discharge coefficient that depends on the orifice design [55].

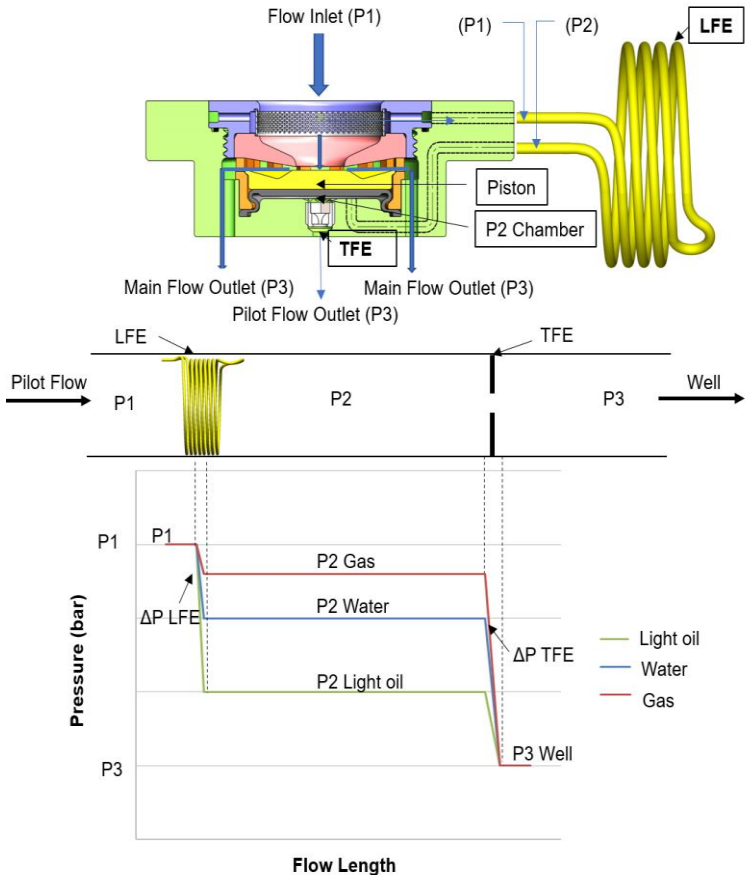

Figure 2-5: The pressure drop of reservoir fluids through the pilot flow of AICV [56].

As it is illustrated in Figure 2-5, the reservoir fluid at reservoir pressure P_1 enters the valve inlet, and a minor portion of the fluid is guided through the pilot flow elements, while the main flow passes through the small opening between the inlet seat and the piston. By passing through the LFE, the pressure of the fluid is reduced to P_2 at a chamber called the P_2 chamber.

As oil has higher viscosity than water and gas, the pressure drop through the LFE is higher, resulting in a lower P_2 in the pressure chamber. In contrast, the resulting P_2 in the chamber is much higher for gas and water due to the lower pressure drop through the LFE (see the lower part of the Figure 2-5). The resulting pressure, P_2, acting on the piston determines the piston movement, either upwards or downwards. If the pressure acting on the piston is high enough, the resulting force will push the piston upwards closing the AICV for water and/or gas. When the AICV is closed, meaning that the main flow path is closed, the only flow to the production well is the flow through the pilot flow. Lower pressure acting on the piston will keep the piston at its neutral position that maintains the oil production from both the main flow and the pilot flow.

Figure 2-6 presents the force balance around the piston. The inlet pressure, P_1, the resulting pressure in the chamber, P_2, and the pressure in the well, P_3, generate forces around the piston which control the piston position. [57]

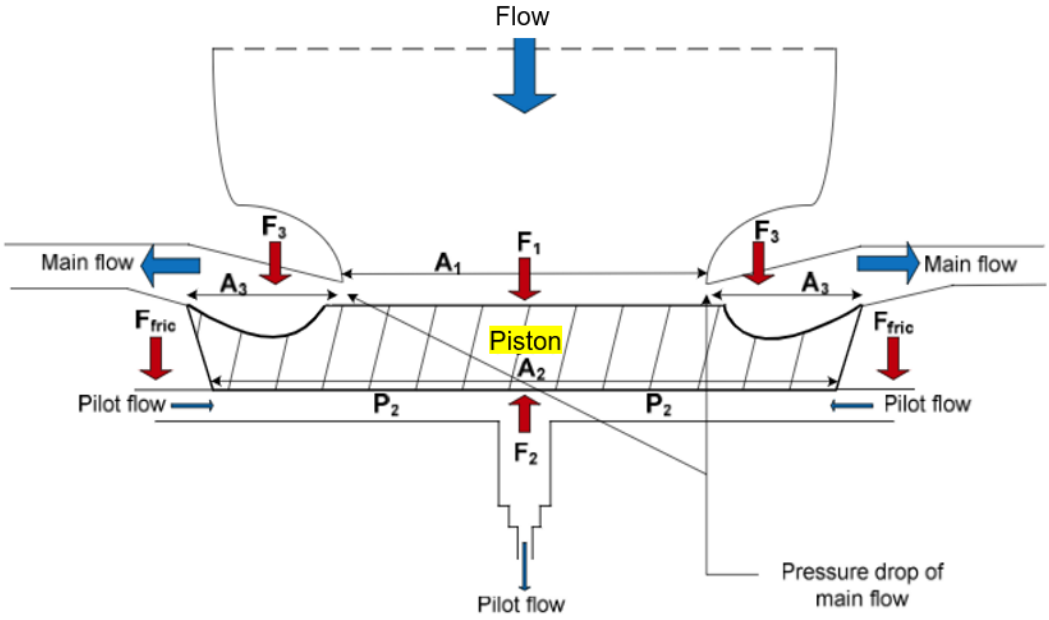

Figure 2-6: Forces acting on the different areas on piston [58].

The force F_1, (P_1A_1), is acting downwards on the upper side of the piston. The area A_1 is the same as the inlet area of the AICV. The force F_2, (P_2A_2), is below the piston and is acting upwards. The force F_3, (P_3A_3), is acting downwards on the outer part of the piston. The area A_3 is calculated as A_2- A_1. The ratio between A_1 and A_2 is a design parameter, and the optimum ratio is dependent on the reservoir fluid properties [57]. F_{fric} represents a friction force acting against the flow direction. When the net force acting on the piston (F_1-F_2+F_3±F_{fric}) is positive, the valve is in open position, and if the net force is negative, the valve is in close position. The inlet pressure, P_1, is always higher than P_2, and A_2 must be larger than A_1.

The first step in the AICV design is selecting the appropriate LFE and TFE design. The LFE and TFE which are placed in series are tested with water, model oil and gas. The pressure drop through each element is measured, and then based on the dimensions of the piston and the valve inlet, the net forces acting on the piston for different fluids are calculated. The net forces vary according to the choice of pilot flow, piston and AICV inlet. The choice of different AICV elements, regarding dimensions and material, is based on the fluid properties, the application (gas and/or water control) and the requirements defined by the field operators [59]. Figure 2-7 shows the net forces acting on the AICV piston for light oil, water, and gas. This AICV is constructed for water and gas control application in a light oil reservoir.

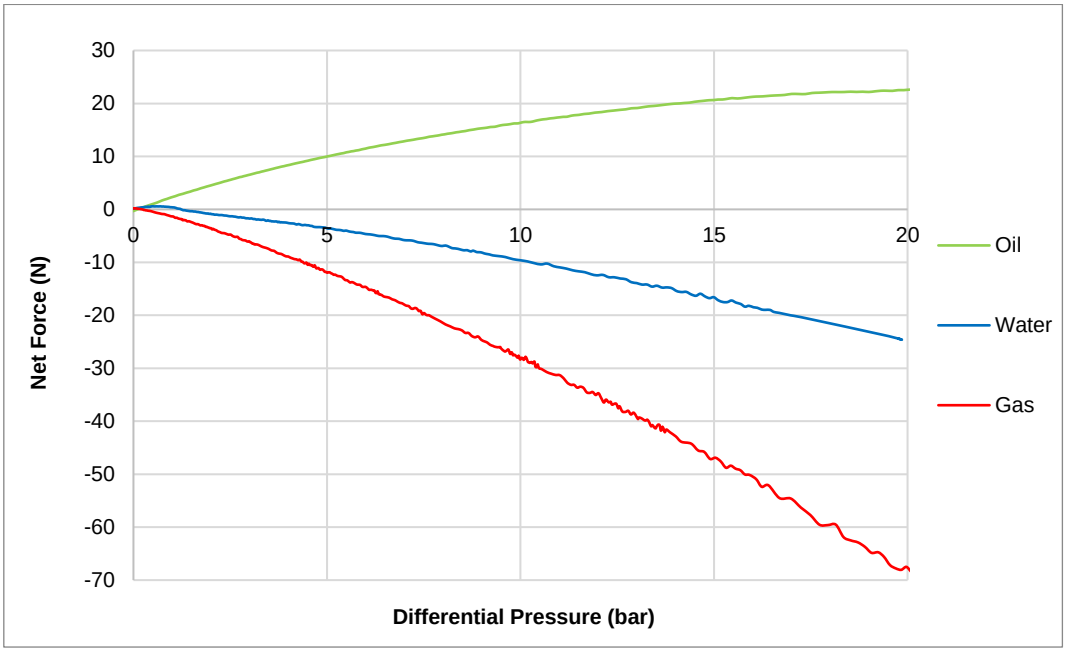

Figure 2-7: The calculated net forces acting on the AICV piston for different fluids.

Most of the pressure drop of the main flow over the piston occurs at the smallest passage, between the piston and the inlet seat. The size of this opening will define the ICD strength of the AICV. The ICD strength is the pressure drop over the valve when the oil flow rate is equal to 1 m^3/h. Figure 2-8 shows the AICV performance for different AICV strengths. Generally, performance curves for AICV describe the volumetric flow rates of different fluids through AICV at different differential pressures across the valve.

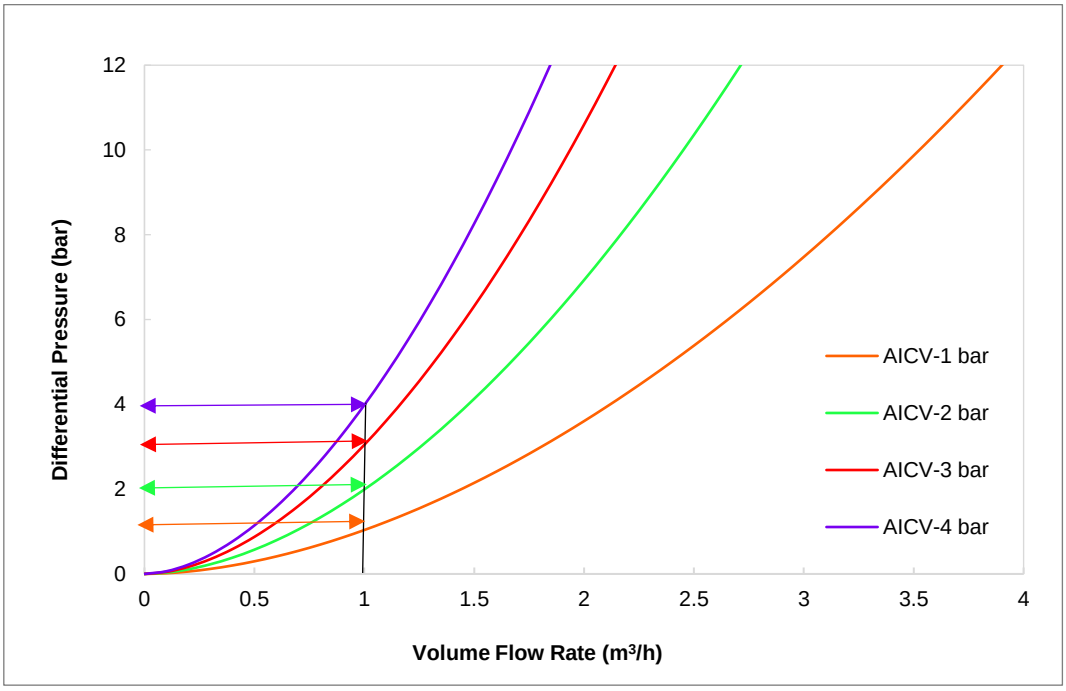

Figure 2-8: Performance curves of AICV for different strengths.

ICD and AICV for single-phase flow

Figure 2-9 illustrates an example of pressure drop versus normalized flow rate of single-phase oil with viscosity 2 cp, 12 cp, and 200 cp, together with water and gas for an orifice-type ICD and an AICV. The performance curves for oil 2 cp (black line) are the same for ICD and AICV.

The ICD performance is mainly density dependent while the AICV performance is mainly viscosity dependent. For ICD, the gas curve is far to the right from the oil and water curves due to the much lower gas density. According to equation (1), in case of gas breakthrough, the gas production from the wells with ICD is much higher than oil production. The oil 2 cp and water curves differ slightly from each other, the oil 12 cp and water curves are almost indistinguishable, and oil 200 cp deviates significantly from water and oil with lower viscosity. With increasing oil viscosity, the density difference between oil and water is compensated by the effect of discharge coefficient. Discharge coefficient is strongly dependent on Reynolds number and hence on fluid viscosity. For high Reynold numbers, the discharge coefficient approaches a constant value, and it decreases significantly for smaller Reynolds numbers meaning for high viscous fluids. Hence, for higher viscous fluids the effect of discharge coefficient becomes significant and ‘’oil choking’’ for oil 200 cp is observed from the figure. [32, 60]

The AICV is designed to keep open for oil and to close for water and gas. The location of performance curves for gas and water (red and blue lines) for AICV are changed compared with the performance curves for ICD. The oil with viscosities 2 cp, 12 cp and 200 cp curves differ significantly from water curve. The valve is more open for 12 cp oil than 2 cp oil due to its dependency on viscosity. However, at a point when the viscosity is high enough and due to the force balances around the AICV piston, the valve is at its maximum opening. At this point, the oil curves depend mainly on the density, the deviation between the oil curves are small and they are located to the left side of the oil curves with lower viscosity meaning that ‘’oil choking’’ occurs. This implies that the AICV performance for single-phase flow is significantly better than ICD. [59]

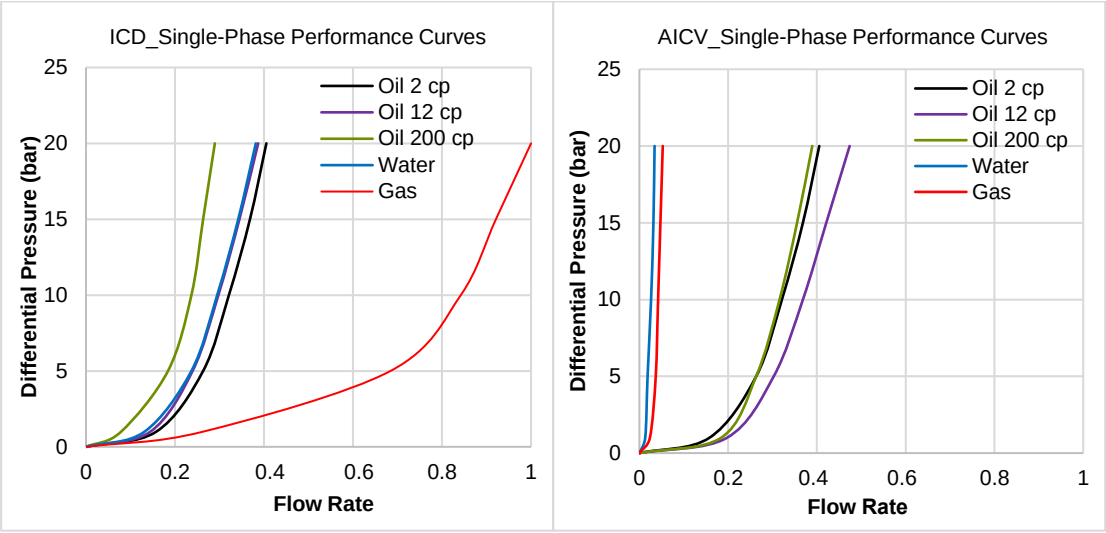

Figure 2-9: Single-phase performance curves for ICD (left) and AICV (right).

Improved oil recovery, IOR

IOR is the process of achieving a high ultimate recovery factor beyond the primary recovery factor. The analysis of 636 sandstone reservoirs demonstrates that the average primary recovery factor and ultimate recovery factor are 21% and 38.5%. Only 5% of the studied reservoirs has an ultimate recovery factor of 65.1%. [61]

Several factors are important to achieve an ultimate recovery factor ≥ 70%. These factors include, but are not limited to, the reservoir and fluid properties, wettability, development strategies and the IOR/EOR methods [61].

Different types of reservoirs based on their characteristics have different recovery factors. This study focuses on IOR in thin-oil-rim reservoirs. Thin-oil-rim reservoirs usually experience low primary recovery factor. Studies have reported higher recovery factors up to 48% in the case of implementing IOR methods [62-65] .

Thin-oil-rim reservoirs

In a typical thin-oil-rim field, a thin oil layer lies between a gas cap and an underlying aquifer. Oil may be produced from such fields by drilling long horizontal or long multilateral horizontal wells. Oil production from such fields will by time cause gas coning in some locations along the well. Generally, thin-oil-rim reservoirs are prone to gas coning [66]. Excessive gas production from a gas cap will result in upward movement and smearing of the tiny oil column [67]. Therefore, oil production from a thin-oil-rim field can be challenging. It is important to keep

a high oil production rate before and after the gas breakthrough occurs. The Troll field in the northern part of the North Sea is characterized as a thin-oil-rim reservoir. The Boa and Kameleon accumulations in the Alvheim field have also thin-oil-rims [67].

Well placement, well type, well path and completion methods are some important elements that must be evaluated to achieve an enhanced well performance and improved recovery in thin-oil-rim reservoirs [6]. In recent years, several measures at the Troll oil field have been in focus to produce the thin remaining oil columns. These measures include, but are not limited to, developing and implementing new technologies for cost effective drilling, more accurate well placement and technology for constraining the unwanted water and gas production from the oil wells [68].

In this work, the reservoir properties at the Troll oil field are used to develop a thin-oil-rim reservoir model. The Troll field is located in the North Sea 80 km from the west coast of Norway, see Figure 2-10. The oil production from the Troll West oil and gas province started in 1995. The thin oil layer was originally between 22 and 26 meters located at a depth of 1360 meters [69]. The oil column is now reduced to only 1 to 5 meters thickness [68]. However, a significant volume of residual oil is encountered directly below the oil column [68]. The newly drilled long horizontal multilateral wells at the Troll oil field, have a well length of more than 3500 m. These wells are positioned close to the oil-water contact to avoid early gas breakthrough. The Troll reservoir mostly consists of high-permeable homogeneous sandstones with permeability ranging from 1 Darcy to more than 20 Darcy. In addition, the porosity ranges from 30-35% [8].

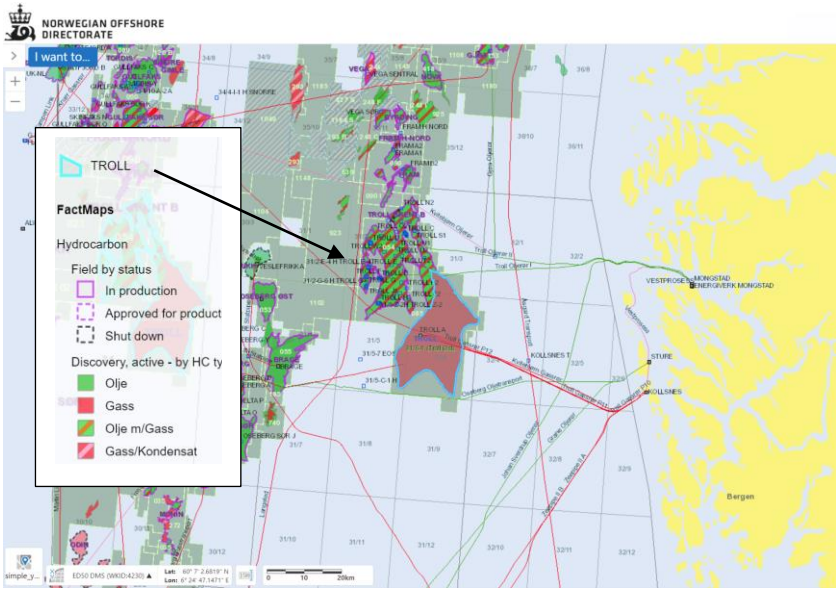

Figure 2-10: The Troll field [68].

Enhanced oil recovery, EOR

EOR refers to the tertiary phase of oil recovery and targets the immobile oil. EOR methods are categorized into thermal and non-thermal. Thermal EOR techniques are associated with heating of the oil and are generally applicable to heavy, viscous crudes, to reduce the viscosity and increase the mobility. Non-thermal EOR includes miscible gas injection methods and chemical methods. Hydrocarbon gas, nitrogen and CO_2 are used in gas injection EOR. However, CO_2 is the future of gas injection EOR as this generates income for the oil industry and at the same time motivates the industry to capture the CO_2 and sell it for further utilization for EOR. Injection of CO_2 for EOR is applicable to light oil reservoirs, in both carbonates and sandstones. Chemical EOR uses alkaline, surfactant, and surfactant polymer flooding to reduce the interfacial tension between the water and oil to recover more oil. [70]

Among the thermal and non-thermal methods, SAGD and CO_2-EOR are investigated in this work.

Steam assisted gravity drainage, SAGD

Thermal recovery methods such as SAGD is a viable method that is used widely by all the major operators in Athabasca and Cold Lake reservoirs in Alberta, Canada to recover the bitumen and heavy oil [71]. The viscosity of bitumen is in the range of 10^6 cp which makes it immobile and unable to flow towards the production well by gravity. Hence, the high viscosity bitumen is heated by high quality steam injected continuously from an injection well which is located about 4-6 m above the production well. The injected steam forms a steam chamber expanding vertically and laterally towards the cold bitumen. Steam transfers heat to the cold bitumen and the latent heat is released due to steam condensation. The transferred energy heats up the bitumen, resulting in decreasing the viscosity to below 20 cp and consequently increasing the oil mobility. As illustrated in Figure 2-11, the heated low viscous oil flows towards the production well. Thus, the mobilized oil and steam condensate are produced.

When horizontal wells are used in SAGD, reservoir contact, and the overall well productivity are both significantly improved. SAGD for recovery of heavy oil can achieve a recovery factor of 70-80% if favorable operational and reservoir conditions are met. [72]

An even steam distribution along the injector well and steam conformance improvement must be attained to ensure an efficient SAGD process [50]. Uneven liquid inflow from the reservoir to the well can result in steam and gas breakthrough in some parts of the well. This limits the oil production and consequently increases the SAGD operation cost.

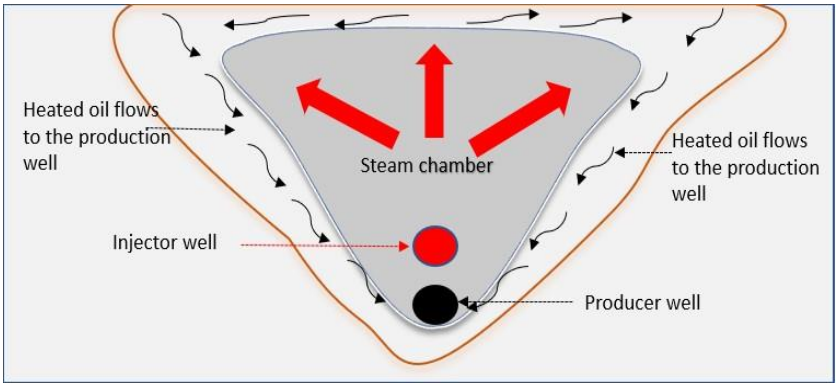

Figure 2-11: SAGD process [73].

Uneven steam distribution, and steam and water breakthrough are the challenges that AICV can potentially mitigate.

CO_2-EOR

Utilizing CO_2 in oil reservoirs is one of the proven methods of EOR. Since the first CO_2-EOR project in the Kelly-Snider oil field in Texas in 1972 until 2018, there were more than 160 projects of CO_2-EOR globally [74]. Most of these projects are still relying on CO_2 from geological formations. However, there is increasing interest in using anthropogenic CO_2 sources. This provides a potential solution to mitigate the effects of anthropogenic CO_2 on global warming [75]. One example of using anthropogenic CO_2 is in the Weyburn and Midale project, in southern Saskatchewan of Canada, where CO_2 from a gasification plant is utilized for EOR and sequestration [76].

The Norwegian petroleum directorate (NPD) has conducted several screening studies to evaluate the possibility and potential of using captured CO_2 for EOR at the Norwegian continental shelf [77, 78]. In most of the large oil fields at NCS, about half of the oil on average remains in the reservoir after shutting down the wells. About 50% of this oil is categorized as immobile oil [77]. To the authors knowledge, neither CO_2-EOR nor any other EOR methods to extract the immobile oil have been implemented on a full field scale at the NCS.

The expected CO_2-EOR potential varies between vertical and horizontal miscible flooding. In a vertical miscible flooding, the expected EOR potential is in the range of 15-40% original oil in place (OOIP) compared to upward water flood, while in a horizontal miscible flooding process, the expected EOR factor is 5-15% OOIP. The low EOR potential in horizontal miscible flooding may be associated with gravity override, viscous fingering and poor control of injection profiles [79]. NPD carried out a study on fields of interests at the NCS indicating an EOR potential of 3-7% [80]. Industry experience from onshore North America and the simulation results from the Brage field in the North Sea indicate an EOR potential of 4-12% OOIP and 9-

12% OOIP, respectively [79]. Also, research carried out by the department of energy in the US suggests that CO_2-EOR could improve the recovery factor by as much as 3-5% from unconventional shale reservoirs [81]. [82]

The best effect with CO_2-EOR is achieved when CO_2 is miscible in oil in the reservoir. To improve the sweep efficiency of CO_2 flooding, applying the alternating injection of CO_2 and water (WAG) is a widespread practice [80]. Figure 2-12 shows a cross section of a reservoir with CO_2 WAG in which oil and CO_2 displacement is illustrated. CO_2 is injected into the oil fields and can be dissolved in water. The injection process may also help to maintain the reservoir pressure above the minimum miscible pressure (MMP) of the oil, securing a more desirable miscible flood. After injection, CO_2 encounters the residual oil in the pores, and under miscible conditions the CO_2 is mixed with oil. The oil in the reservoir pore spaces swells and moves towards the production well. Four primary factors that affect the oil swelling in the presence of CO_2 are API oil gravity, temperature, CO_2 concentration and pressure [83]. CO_2 extracts the intermediate components of the oil through repeated contacts. In this process, the oil evaporates into lean gas. CO_2 and oil achieve multi-contact miscibility when CO_2 is sufficiently enriched with the intermediate components during vaporization [81]. [82]

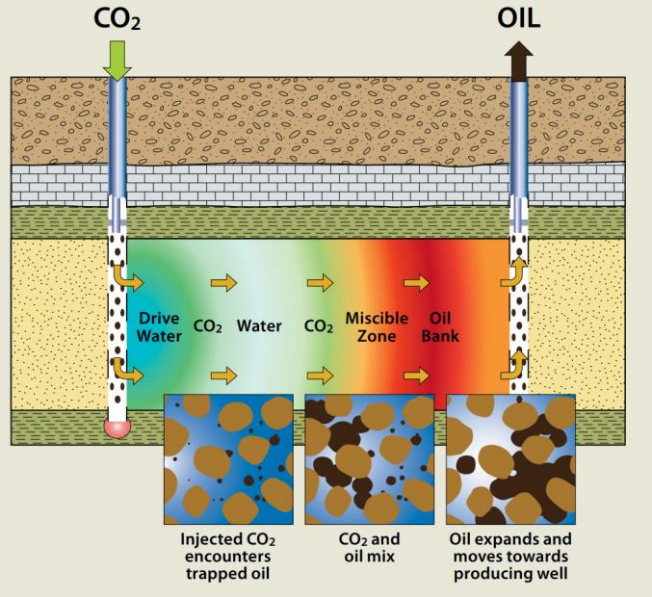

Figure 2-12: Cross section of a reservoir with CO_2 WAG [80].

Dense supercritical CO_2 can extract hydrocarbon components from oil easier. Dissolved CO_2 causes the oil to swell and thereby improves the oil mobility. Swelling is defined as the increase in the volume of the saturated liquid phase compared to the initial reference volume [84]. The swollen oil droplets force fluids to move out of the pores, hence causing drainage effect and consequently decreases the residual oil saturation [58]. In addition, CO_2 is soluble in water, can evaporate and extract the oil and it reduces the surface tension between oil and water [77]. Another effect of CO_2 on oil is observed in the relative permeability characteristics.

CO_2 flooding will affect the reservoir wettability and make the rock slightly more water-wet, making it easier to achieve a favorable oil displacement efficiency [85, 86].

Some challenges with CO_2-EOR are highlighted in this work. High permeable zones and fractures are prone to breakthrough and direct reproduction of CO_2 to the production well. In a miscible CO_2-EOR process, if the reservoir pressure drops below the MMP of CO_2 in oil, CO_2 will enter the production well [87]. This results in poor distribution of CO_2 in the reservoir. Also, CO_2 WAG often experience significant problems and challenges with short circuiting of CO_2 and water between the injectors and producers. Consequently, the CO_2 is reproduced without contributing to EOR. It is especially important to avoid reproduction of CO_2 if high-cost anthropogenic CO_2 is used for EOR and storage operations [79].

In summary, short circuiting of CO_2 and water between the injectors and producer, direct reproduction of CO_2 to the well, and production of the mixture of CO_2 and water which is extremely corrosive are the challenges that AICV can potentially mitigate.

Relative permeability

Results from the wells with RCP valves at the Troll oil field indicate that the reservoir simulation tools tend to underestimate the production and recovery. This was not the case when the wells were completed with ICDs [8]. After the gas breakthrough occurs, the RCP valves choke back the gas in contrast to the ICDs. In addition, throughout this study, there are some cases in which the increase in oil production with AICVs is not significant compared with ICDs or base cases, although the decrease in gas and/or water production is considerable. This is most probably due to the relative permeability curves that are being used for the simulations.

Oil production and recovery are largely dependent on the reservoir properties such as permeability, porosity, residual oil saturation, and the onset of breakthrough [88]. Relative permeability curves and how reservoir simulators utilize them have a significant effect on oil production. In the simulators, the saturation of the phases flowing from one cell to the adjacent cell is calculated using Darcy equation which is a function of the relative permeability (k_r) and the viscosity (μ) of the phases. Considering oil and gas phases with subscripts $'o'$ and $'g'$, respectively, the Darcy velocities are given by:

$$v_g = -k\frac{k_{rg}}{\mu_g}\left(\nabla P_g - \rho_g g\right) \tag{5}$$

$$v_o = -k\frac{k_{ro}}{\mu_o}\left(\nabla P_o - \rho_o g\right) \tag{6}$$

where k is the absolute permeability. In a two-phase scenario when gas has entered a cell and the saturation of gas is reaching to a certain level, the simulation tool considers that oil has a fraction of gas. For the simulator to be able to produce from that cell and into the well, it must consider oil and gas as a mixture, and produce that amount of gas along with the oil. In other words, if the simulator is not able to produce the gas, then it cannot produce the oil neither. For the ICD and base cases that do not impose any restriction on gas production, the simulator is able to produce the oil as it produces the gas. But, for the AICV and RCP cases in which the gas production is restricted, the oil production is reduced consequently. This can be illustrated through relative permeability curves. Figure 2-13 shows an example of relative permeability curves for oil and gas. When the gas saturation reaches for example 0.5, ICD has produced more oil and gas than AICV, as the AICV is partly closed at this gas saturation.

In a real case, oil and gas production rates are almost independent of each other. When the gas breakthrough occurs in the well completed with AICVs or RCPs, the oil flow rate is only dependent on the gas oil contact (GOC) angle, meaning that oil will continue to flow into the well even though the gas is choked back [59, 69].

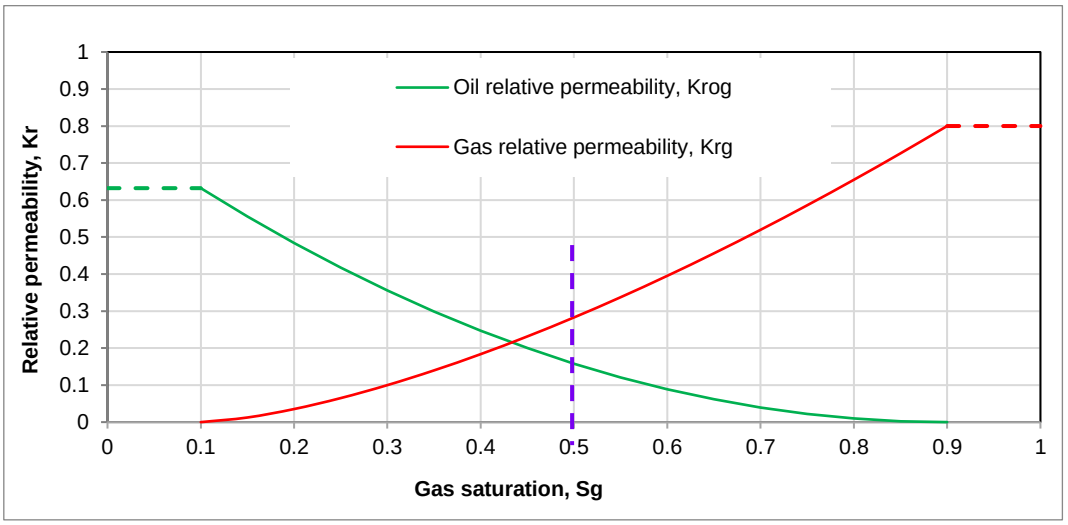

Figure 2-13: Oil and gas relative permeability curves.

Stratified flow and slip

Gaining insight into the mechanism of different simulators in calculating the multiphase flow properties is important. In stratified flow it is common to mention the slip between the phases. The slip ratio, usually referred to only as slip. The difference in velocity between the gas and liquid is defined as slip, S, and is as follows [89]:

$$S = \frac{A_o}{A_g}\frac{U_{sg}}{U_{so}} = \frac{1-\varepsilon_g}{\varepsilon_g}\frac{U_{sg}}{U_{so}} \quad (7)$$

where U_{sg} and U_{so} are the superficial velocity of gas and oil, A_g and A_o are area of a pipe segment occupied by the gas and oil, and ε_g and ε_o are the actual or the in-situ area fraction or hold-up of gas and oil, respectively. Superficial velocities of oil and gas are based on the input flow rates, Q_o and Q_g, and the pipe cross-sectional area, A:

$$U_{so} = \frac{Q_o}{A} \tag{8}$$

$$U_{sg} = \frac{Q_g}{A} \tag{9}$$

The definition of actual velocities of oil and gas are as follows:

$$U_o = \frac{Q_o}{A_o} \tag{10}$$

$$U_g = \frac{Q_g}{A_g} \tag{11}$$

The actual velocities always exceed the superficial velocities. The actual or the in-situ area fraction, hold-up, is defined as:

$$\varepsilon_o = \frac{A_o}{A} \tag{12}$$

$$\varepsilon_g = \frac{A_g}{A} \tag{13}$$

3 Experimental Setups

This chapter covers descriptions of the experimental setups included in this work. Two multiphase flow loop test rigs, one located at InflowControl AS and one at Equinor, were used for generating data related to performance curves, WC, and GVF behavior of ICD and AICV. Performance curves describe the differential pressure across the AICV and ICD as a function of volumetric flow rate of the fluid. In addition, density and viscosity measurements were performed at University of South-Eastern Norway for the purpose of model development.

Multiphase flow loop test rig at InflowControl AS

Most of the experimental tests are performed at the multiphase flow loop test rig at InflowControl AS in Porsgrunn, Norway.

Figure 3-1 shows a photo and the piping and instrumentation diagram (P&ID) of the flow loop test rig. The test facility is designed for single-phase and multiphase oil, water, and gas tests. Performance curves from single-phase tests with model oil, pressurized air, and water are obtained from the test rig. Data related to GVF and WC behavior of ICD and AICV is obtained from the multiphase tests with oil and pressurized air and/or oil and water.

Two pumps in series are used to increase the liquid pressure up to 50 bar from the oil and water supply. Compressed air at room temperature can be regulated to the desired pressure for each case, up to maximum 200 bar. A heat exchanger is used to regulate the temperature of the circulated fluid to the desired temperature. Flow rates, density and temperature are measured close to the inlet of the test vessel by a Coriolis flowmeter. The test vessel is built with the same geometry as in the screen joint [59]. A pressure transmitter measures the inlet pressure, whereas a differential pressure transmitter measures the differential pressure over the test vessel. Multiphase flow tests are performed by injecting the desired flow rate of oil from a separate test rig to the test vessel which is already filled with gas. The separate test rig is connected to the single-phase test rig. All the key elements and measuring instruments of the test rig are marked with red rectangles in the Figure 3-1b. [56]

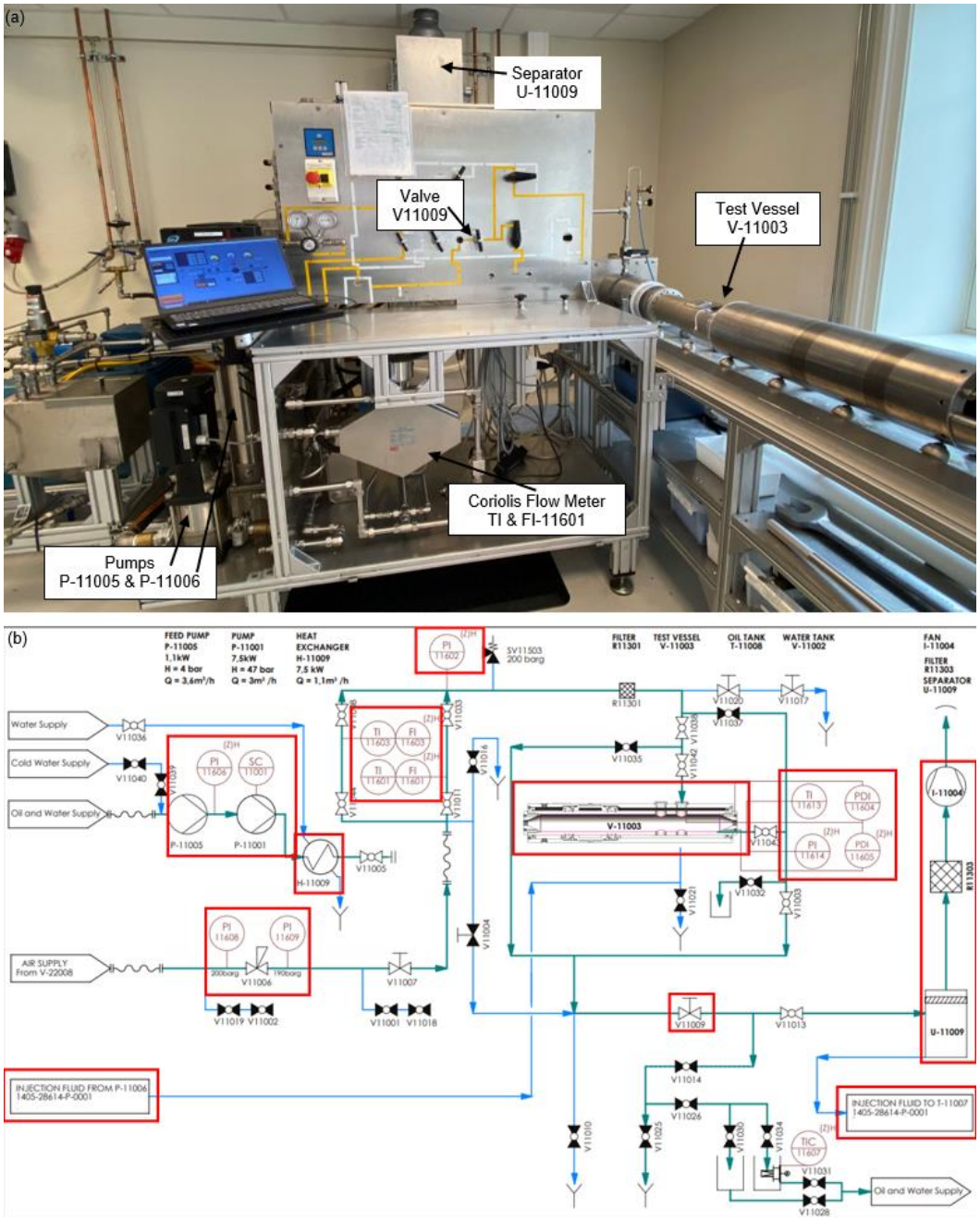

Figure 3-1: Photo (a) and P&ID (b) of the flow loop test rig.

The controlled and measured key variables for the tests were flow rates, differential pressure across the AICV or ICD, system conditions (pressure and temperature), and fluid properties, such as viscosity and density. LabVIEW is used for data logging.

In this test rig, the tests can be performed at different temperatures and pressures to obtain the viscosity and density of the fluids in the reservoir. In the tests, the air density is equivalent to the hydrocarbon gas density at the reservoir condition. Some specifications of the multiphase flow loop at InflowControl AS are listed in Table 3-1. The experiments presented in paper 2,3,5,7 and 8 were performed in this test rig.

For single-phase tests, the differential pressure across the AICV and/or ICD is increased gradually between 1 bar and 20 bar. The flow rate and differential pressure are continuously measured as the differential pressure is gradually varied. For multiphase tests, the differential pressure across the AICV and/or ICD is increased stepwise between 1 bar and 20 bar, and the volume flow rate of the mixture at corresponding differential pressure is measured.

Table 3-1: Multiphase flow loop specifications at InflowControl AS.

Description	Fluid Type	Pressure (bar)	Temperature (˚C)	Differential Pressure (bar)
Single-phase test	Pressurized air	Up to 200	Room Temperature	1–20
	Water	Up to 50	Up to 70	1–20
	Silicone oil	Up to 50	Up to 60	1–20
Multiphase test	Oil and gas	–	–	1,2,3,5,10,15,20
Multiphase test	Oil and water	–	–	1,2,3,5,10,15,20

Multiphase flow loop test rig at Equinor

Some experiments are performed at the multiphase flow loop test rig (AICD-HP) at the Equinor test facility located in Porsgrunn, Norway. The test rig is a full-scale rig that covers a wide range of reservoir conditions such as pressure, temperature, density, and viscosity. A photo and a simplified schematic of the flow loop showing key pieces of the equipment and key measurement locations are shown in Figure 3-2 [32, 38]. The main components in the rig are a three-phase separator, a multiphase pump and a test cell which is a pressurized vessel. The flow rates of the different fluids are regulated by flow controllers (CFM), and pressures and differential pressure are measured at various locations in the rig. The test facility is designed for single-phase and multiphase crude oil, synthetically produced formation water, and hydrocarbon gas tests. Single-phase tests were performed by establishing the desired differential pressure across the test section over periods of 10 minutes and measuring the corresponding stabilized flow rate. The results are presented as volumetric flow rates vs. pressure drops. Multiphase flow test data were obtained by logging stable values over periods of several minutes [38, 90]. The tests were performed by regulating the desired amount of oil/gas or oil/water flowing through the test unit at targeted differential pressure.

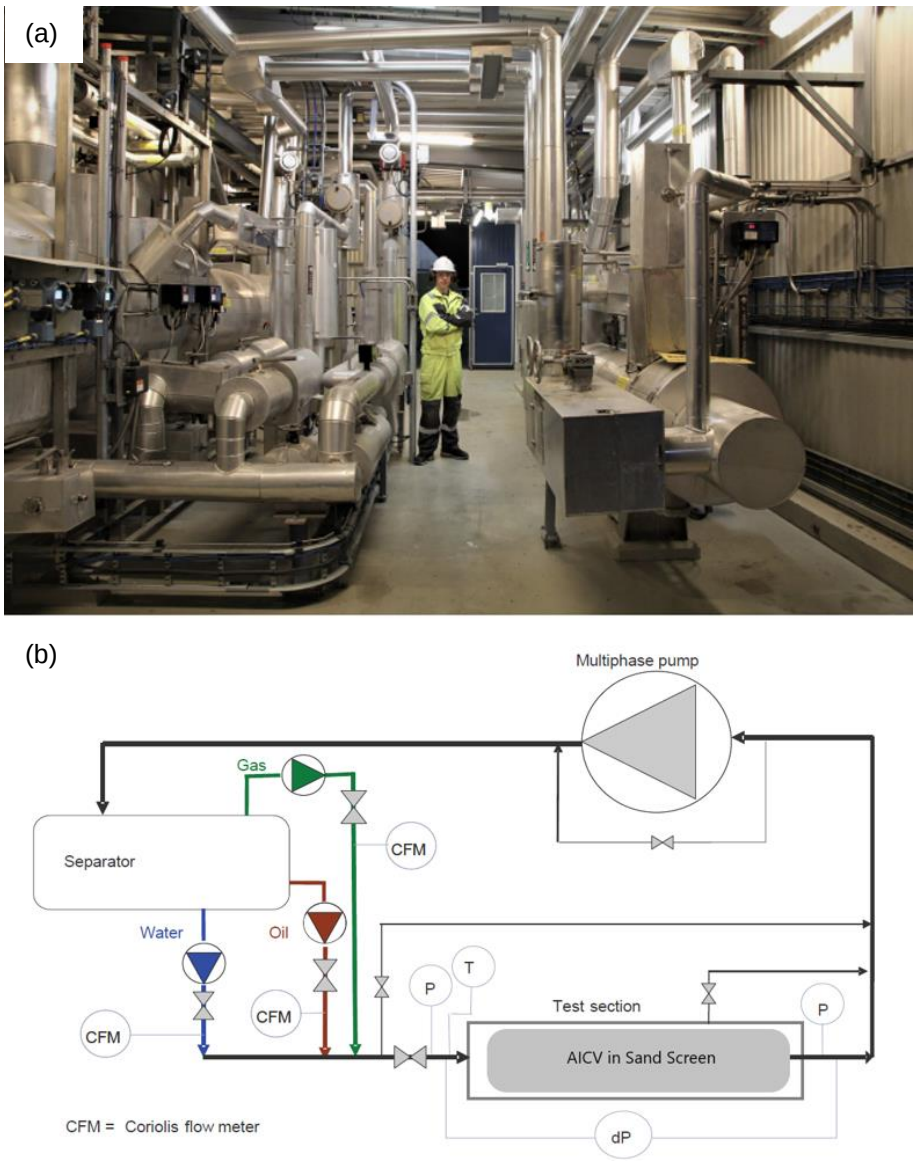

Figure 3-2: Photo (a) and schematic (b) of the flow loop test rig [32, 38].

The experiments presented in Paper 1 were performed at the multiphase flow loop test rig at Equinor. The tests and system conditions are summarized in Table 3-2.

Table 3-2: Tests and system conditions at the multiphase flow loop test rig at Equinor.

Description	Fluid Type	Pressure (bar)	Temperature (˚C)	Differential Pressure (bar)
Single-phase test	Hydrocarbon gas	200	70	1–40
	Formation water	200	70	1–40
	Crude Oil	200	70	1–40
Multiphase test	Oil and gas	200	70	10 and 20
Multiphase test	Oil and water	200	70	10 and 20

Density and viscosity measuring instruments at USN

This section describes the instruments used to perform the density and viscosity measurements of different silicone oils. The measurements were used to develop density and viscosity correlations that can be used further to develop a model for AICV performance.

Density meter

The density meter DMA 4500 from Anton Paar was used to measure the density of different silicone oils at atmospheric pressure and various temperatures. DMA 4500 is a high accuracy density meter with no requirements regarding ambient conditions. The density meter consists of a measuring cell and the measuring principle is the oscillating U-tube principle. The oscillation of the cell is electronically induced to oscillate at its characteristic frequency. The characteristic frequency changes depending on the density of the filled sample. [91]

The true density of the sample is determined by an accurate measurement of the characteristic frequency. This is described in detail in the PhD thesis of Sumudu S. Karunarathne [92].

Density measurements were conducted by injecting a sample with 3–5 *mL* volume into the U-shaped borosilicate glass. The transparent glass comprises 0.7*mL* of the injected sample [93]. The density of the sample at various temperatures up to 80°C was measured. When the measurement for each temperature is completed, the final calculated density is displayed on the screen. The schematic shown in Figure 3-3 illustrates the U-tube and the other parts of the density meter.

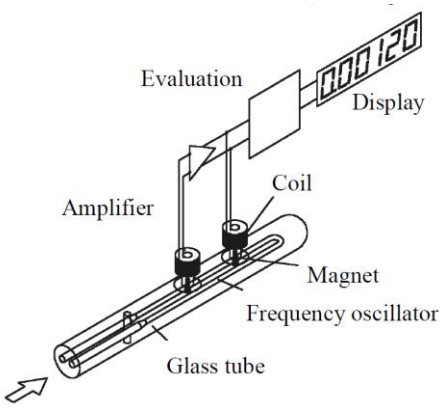

Figure 3-3: Measurement cell of the density meter [93].

The technical specification of the device is listed in Table 3-3.

Table 3-3: DMA 4500 technical specification [94].

Measuring range	Density :0–3 g.cm^{-3} Temperature: 0–100℃ Pressure: up to 10 bar
Repeatability standard deviation (According to ISO 5725)	Density: 5×10^{-5} g.cm^{-3} Temperature: 0.02℃
Accuracy (Under ideal conditions and for low densities/viscosities)	Density: 1×10^{-4} g.cm^{-3} Temperature: 0.03℃

Viscosity meter

A rheometer from Anton Paar (Physica MCR 101) shown in Figure 3-4a was used to measure the viscosity of different silicone oils at atmospheric pressure and various temperatures. The dynamic viscosity measurements are conducted via a double-gap pressure cell XL measuring system shown in Figure 3-4b. The rheometer is equipped with an internal temperature control system with standard temperature uncertainty of 0.03 K [95]. A sample of 7 mL shown by blue color in Figure 3-4b is injected using a clean syringe from the sample bottle into the gap of the pressure cell (the volume between R_3-R). Routine air checks and motor adjustment were carried out before the actual experiments as recommended by Anton Paar. The data reported in this work are the average values from at least 40 different readings. A detailed description of the rheometer and the working procedure is given in the PhD thesis of Sumudu S. Karunarathne [92].

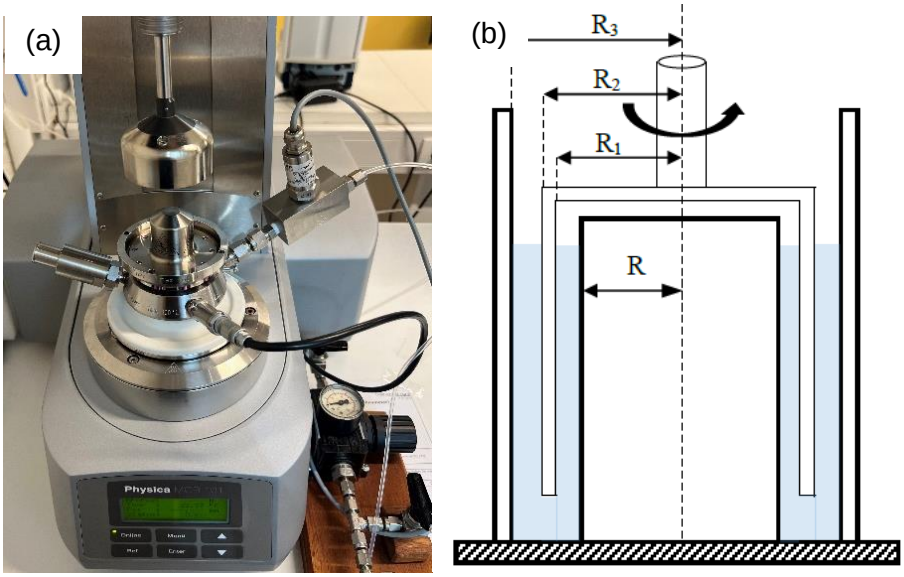

Figure 3-4: Rheometer (a) and schematic of a double-gap pressure cell XL (b) [96].

The technical specification of the device is listed in Table 3-4.

Table 3-4: Physica MCR 101 technical specification [92].

Maximum pressure	150 bar	
Maximum temperature	180℃	
Uncertainties related with standard oil	Viscosity range	Dynamic viscosity mPa.s (cp)
	0.3 to 7.4	±0.07%
	7.4 to 10	±0.09%
	10 to 30	±0.12%
	30 to 72	±0.14%

The viscosity and density measurements presented in ''Mathematical modelling'' section were performed by utilizing the devices described in this section.

4 Modelling and Simulation

The different modelling and simulation methods employed in this work are discussed in this section. Four commercial reservoir simulators –ECLIPSE 100 version 2021.4, NETool Well Simulator version 10.6.0, OLGA/ROCX version 2021.1.0, and CMG versions 2022.10 and 2023.20– are used to study the effect of AICV on reservoir oil recovery. In addition, Markov Chain Monte Carlo (MCMC) method that is often used in Bayesian inference is used for the modelling of the AICV performance. Dimensional analysis is employed to demonstrate the possibility of constructing models which are less sensitive to variations in their parameter values.

The purpose of using different simulation tools in this work is to investigate the ability of the simulators in modelling of oil production with advanced wells. NETool that shows the instantaneous inflow profile along the well is the most user-friendly simulator used in this work due to the short simulation time. However, NETool is a steady-state simulator that does not capture the dynamics of the reservoir and is only capable of calculation of multiphase flow with no-slip between phases. Coupling OLGA and ROCX enable the user to perform an integrated transient wellbore/reservoir modelling. The modelling of AICV and ICD in OLGA by using PID Controller was first developed by Haavard Aakre [59]. PID Controller was difficult to tune, and it resulted in high degree of inaccuracy. The method was further developed to use Table Controller instead of the PID Controller in order to implement the autonomous behavior of the RCP valve in the simulator [33]. The Table Controller option is used in this work for simulations with AICV and ICD. Although, coupling OLGA/ROCX is a robust method for modelling near-well oil production, the long simulation time in the scale of days caused challenges during this work. In contrast, CMG and ECLIPSE are dynamic reservoir simulators that simulates the near-well oil production in a relatively short time. AICV modelling in CMG is one of the novelties of this work. This work proposes a workflow for modelling of AICV in CMG. FlexWell is implemented in CMG STARS for well modelling that makes is possible to model fluid flow into a well with AICV/ICD. CMG STARS is especially developed for thermal application, and it is used in this work for SAGD application. However, due to the FlexWell option that is only available in CMG STARS, it is also used for CO_2-EOR application. As CMG STARS using K-value correlation or tables for the fluid model, it is possible to use CMG STARS for the miscible CO_2-EOR application. Both ECLIPSE and CMG are robust simulation tools suitable for simulations with AICV/ICD. However, in this work, CMG is chosen as the primary simulation tool due to its robustness and a wide range of applications.

ECLIPSE

The black-oil simulator ECLIPSE 100 is a fully implicit, three-phase, three-dimensional reservoir simulator. The following features in ECLIPSE are important to consider:

- The black-oil model which is a three-phase, three-component model is implemented in ECLIPSE.
- The ICD and RCP models are available in ECLIPSE. The RCP model is used to adjust the functionality of the implemented AICVs for single and multiphase flow. The model parameters and coefficients are modified to obtain the performance based on experimental data.
- The Drift Flux Model in ECLIPSE allows for slip between the phases in annulus as well as in the tubing. When using the keyword WELSEGS together with DF the model considers the slip between the phases [97].
- ECLIPSE 100 uses the generalized Corey model for estimating the relative permeability for the different phases. According to the model, the following functions can be used to estimate the relative permeabilities of oil and gas (k_{ro} and k_{rg}) in an oil-gas system [98]:

$$k_{ro} = k_{rogc}\left(\frac{S_o - S_{ro}}{1 - S_{or} - S_{gc}}\right)^{n_o} \tag{14}$$

$$k_{rg} = k_{rgor}\left(\frac{S_g - S_{gc}}{1 - S_{or} - S_{gc}}\right)^{n_g} \tag{15}$$

- S_o and S_g are the oil and gas saturations, S_{gc} is the critical gas saturation, S_{or} is the residual oil saturation, k_{rogc} and k_{rgor} are the maximum relative permeabilities for oil and gas, and n_o and n_g are the Corey exponents for oil and gas
- Multilateral wells, both injectors and producers, can be simulated in ECLIPSE 100.
- A multi-segment well model containing options for modeling advanced wells is available in ECLIPSE 100. The tubing and annulus are divided into one-dimensional segments where each segment has a set of independent variables describing the local fluid conditions. Flow control devices can be implemented in specific segments. Figure 4-1 shows an example of a multi-segment well defined in ECLIPSE 100. The tubing and the wellbore are designed as two branches and are connected through the FCD [99].

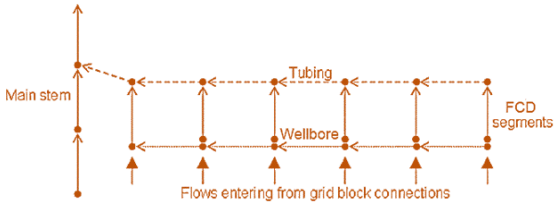

Figure 4-1: Schematic of a multi-segment well model in ECLIPSE [99].

A wellbore design includes annulus, pipeline, inflow control devices, screens, and packers. In addition, the well location and the choice of multilateral wells are important. The simulations in Paper 1 are performed with ECLIPSE 100, where the performance of AICV in multilateral wells in a thin-oil-rim was tested.

NETool

NETool is a one-dimensional steady state near-well simulation tool which can be used for performance analysis of several types of inflow control devices. One of the most important benefits of using NETool is providing a user-friendly modeling for relative complex wells within a short simulation time [100]. In this study, the following features in NETool are important to consider:

- The RCP model that is available in NETool is used to adjust the functionality of the implemented AICVs for single and multiphase flow. The model parameters and coefficients are modified to obtain the desired performance.
- The black-oil model, which is a three-phase, three-component model is implemented in NETool. The basic modelling assumption in the black-oil model is that oil is treated as a single component and there is a full instant equilibrium between the components in a cell [101, 102]. In the black-oil model, the composition of the gaseous phase is assumed the same at all pressures and temperatures [103].
- NETool calculates the multiphase flow properties in annulus with no-slip. The no-slip correlation assumes homogeneous flow with no slip between the phases.
- NETool uses the modified Darcy's law for flow in annulus filled with formation or gravel:

$$v = k\left(\frac{k_{ro}}{\mu_o} + \frac{k_{rg}}{\mu_g}\right)\frac{\partial p}{\partial x} \tag{16}$$

where, v is the total volumetric flux, $\frac{\partial p}{\partial x}$ is the pressure gradient, μ_g and μ_o are gas and oil viscosity, k is gravel permeability, k_{rg} and k_{ro} are gas and oil relative permeabilities and are calculated as:

$$k_{ro} = \alpha^c \tag{17}$$

$$k_{rg} = (1-\alpha)^c \tag{18}$$

C is Corey index and the value of 2 is commonly used, and α is the oil fraction.

- Via the Corey index, the modified Darcy's model considers both gas and oil flow along the annulus through the gravel and the effect of relative permeability on this flow. This is a homogeneous model which assumes that all phases travel with same speed in the form of a mixture. Thus, NETool allows only a single true velocity at each node, and the slip effect is not entirely utilized in the output results.
- The incorporated Joshi model is used for modelling the fluid flow from the reservoir to a horizontal wellbore. The Joshi model, used to calculate the productivity of horizontal wells, considers an ellipsoidal drainage area. For simplicity, the Joshi model converts the 3D horizontal-well oil production into two 2D problems [104]. As it is illustrated in Figure 4-2, the oil flow into the production well is divided into two horizontal (A-A/*x-y*) and vertical planes (B-B/*y-z*).

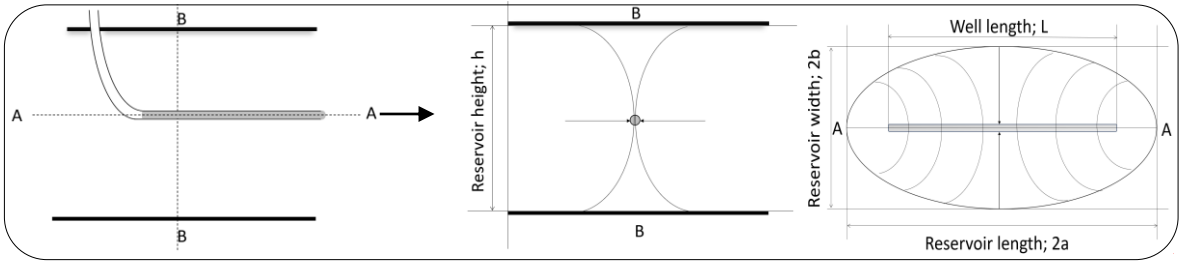

Figure 4-2: The Joshi productivity index (PI) model and the division into two horizontal and vertical planes.

For calculating oil production from a horizontal well, the following expression is used in the Joshi model [104]:

$$q_H = \frac{2\pi k_o h \Delta P/(\mu B_o)}{ln\left[\frac{a+\sqrt{a^2-(L/2)^2}}{L/2}\right]+\frac{h}{L}ln\left(\frac{h}{2r_w}\right)} \tag{19}$$

where q_H is the horizontal well flow rate, k_o is the average permeability, μ is the viscosity, B_o is the oil formation volume factor, ΔP is the pressure drop from the drainage boundary to the wellbore, and r_w is the wellbore radius. This applies for $L > h$ and $(L/2) < 0.9\ r_{eH}$, where L is the well length, h is the reservoir thickness, and r_{eH} is the drainage radius. In addition, a is half the major axis of drainage ellipse and given by [105]:

$$a = \left(\frac{L}{2}\right)\left[0.5 + \sqrt{0.25 + \frac{1}{\left(\frac{0.5L}{r_{eH}}\right)}}\right]^{0.5} \tag{20}$$

Generally, in NETool, the input information regarding the reservoir is set either manually or by coupling the wellbore model to a reservoir model, e.g., ECLIPSE. In this work, the input to NETool including the reservoir conditions, fluid properties, and wellbore design is specified manually. The reservoir depth, porosity, permeability, the saturation of phases, and the relative permeabilities are specified to define the reservoir conditions. The Corey correlation is used to calculate the relative permeability curves. The oil and water saturations in the reservoir are specified for each zone.

A wellbore design includes annulus, pipeline, inflow control devices, screens, and packers. A sketch of a well is shown in Figure 4-3.

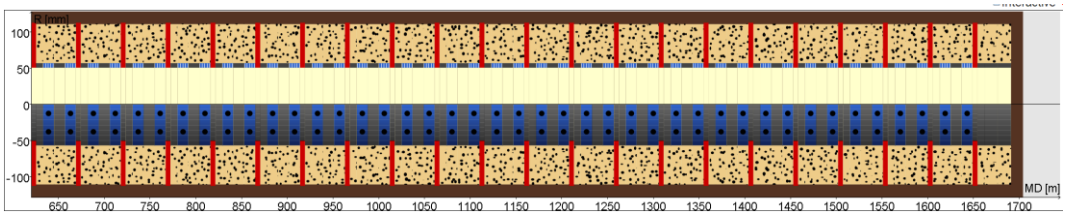

Figure 4-3: Sketch of the production well with AICVs (blue rectangles), packers (red rectangles), and annulus which is filled with gravel (black dots).

The simulations in Paper 3 and Paper 5 are performed with NETool. The papers investigate the effect of AICV in a SAGD late-life reservoir.

OLGA/ROCX

OLGA is an industry-standard dynamic multiphase flow simulator. In this work OLGA is coupled implicitly to ROCX to perform an integrated transient wellbore/reservoir modelling [106]. ROCX which is one of the available tools in OLGA, is a three-dimensional near-wellbore reservoir model. Reservoir and fluid properties are specified in ROCX, and the wellbore model is developed in OLGA. Coupling OLGA and ROCX enable the user to simulate the fluid production from the reservoir into the well. The initial and boundary reservoir conditions and the well pressure are set as input in ROCX. In addition, the pressure and pressure drop in the well and through the inflow control devices are estimated by the flow models in OLGA. Based on the reservoir and fluid information in OLGA and ROCX, the production rates from the reservoir into the wellbore for each phase are calculated [59].

OLGA/ROCX is a robust transient simulation tool to perform integrated well-reservoir simulations, while NETool is a static one-dimensional steady state simulation tool that shows the instantaneous inflow profile along the well.

ROCX

Input data to the reservoir model in ROCX are grid dimensions, fluid, and reservoir properties. The input data regarding the reservoir properties include the permeabilities, porosities of the porous medium, capillary pressure, and in addition thermal properties of the rock and fluids. Initial conditions such as fluid saturations, temperature, and the boundary conditions at the well and at the outer near-well boundary are specified in ROCX. The fluid flow in a porous medium is calculated based on the conservation equations for the different phases [59].

In this work, data for relative permeabilities are either set manually in table-form in ROCX or are calculated from the Corey and Stone II correlations.

The Corey correlation is used to estimate the relative permeability of the water phase in a water-oil system:

$$K_{rw} = (k_{rw})_{S_{orw}} \left(\frac{S_w - S_{wc}}{1 - S_{wc} - S_{orw}}\right)^{n_w} \tag{21}$$

where K_{rw} is the relative permeability of water, S_{orw} is the residual oil saturation in the water oil system, $(k_{rw})_{S_{orw}}$ is the water relative permeability at the residual oil saturation, S_w is the water saturation, S_{wc} is the connate (irreducible) water saturation, S_{orw} is the residual oil saturation, and n_w is the Corey exponent [107].

The Corey correlation is also used to estimate the relative permeability of the gas phase in a gas-oil system:

$$K_{rg} = (k_{rg})_{S_{wc}} \left(\frac{S_g - S_{gc}}{1 - S_{lc} - S_{gc}}\right)^{n_g} \tag{22}$$

with

$$S_{lc} = S_{wc} + S_{org} \tag{23}$$

where K_{rg} is the relative permeability of gas, $(k_{rg})_{S_{wc}}$ is the gas relative permeability at the connate (irreducible) water saturation, S_g is the gas saturation, S_{gc} is the critical gas saturation, S_{lc} is the total critical liquid saturation, S_{org} is the residual oil saturation in the gas oil system, and n_g is the Corey exponent [107].

The Corey exponents are usually determined by the least-squares method to match the experimental data or field relative permeability and capillary pressure data [107].

The Stone's II model is used to estimate the relative permeability of oil in an oil-water and an oil-gas system. This model was developed to estimate three-phase relative permeability data and uses two sets of two-phase data of water and gas in which they are displacing oil [108]. The following expression is used for the relative permeability of the oil phase [107]:

$$K_{ro} = (k_{ro})_{S_{wc}} \left[\left(\frac{k_{row}}{(k_{ro})_{S_{wc}}} + k_{rw} \right) \left(\frac{k_{rog}}{(k_{ro})_{S_{wc}}} + k_{rg} \right) - \left(k_{rw} + k_{rg} \right) \right] \qquad (24)$$

where k_{ro} is the relative permeability of oil, $(k_{ro})_{S_{wc}}$ is the oil relative permeability at connate (irreducible) water saturation, k_{row} is the oil relative permeability as determined from the water-oil two-phase relative permeability at S_w, and k_{rog} is the oil relative permeability as determined from the gas-oil two-phase relative permeability at S_g.

The fluid properties are specified either by use of PVT table or black-oil model. The black-oil model is used in this work. For the GOR model, LASATER correlation which is used to estimate the bubble point pressure for a black-oil system is selected. The correlation was developed based on data of black-oil systems produced in Canada, Western and Mid-Continental US and south America. LASATER is often considered to be more accurate than other correlations such as STANDING [109].

The reservoir model in ROCX is initialized by specifying the reservoir pressure, temperature, and saturations of the phases. In addition, the near-well source is the flow source from the reservoir to the annulus and is given as input from ROCX to OLGA. The boundary conditions of the reservoir grid elements are matched with inflow points of the components that are placed in the wellbore model. This will define the flow from the reservoir model. So, the pressure boundary for the reservoir model is provided by the wellbore model while the reservoir model provides the flow and the fluid temperatures into the pipeline [110]. A gas cap is placed at the top of the reservoir and/or a water aquifer is placed at the bottom in the boundary conditions section. Hence, a gas and/or a water feed in addition to the oil feed are defined.

OLGA; model and setup

Wellbore model

In OLGA, separate continuity equations are applied for gas, oil (or condensate) and water liquids and also for oil (or condensate) and water droplets. Three momentum equations are also used: one for each of the continuous liquid phases (oil/condensate and water) and one for the combination of gas with liquid droplets. One mixture energy equation is also applied. Totally, seven conservation equations and one equation of state have to be solved: the seven conservation equations are three for mass, three for momentum, and one for energy, while the equation of state is for pressure. [111, 112]

- Mass transport equation:

$$\partial_t m_i + \partial_z (m_i U_i) = \sum_i \Psi_{ji} + G_i \tag{25}$$

where m_i and U_i denote the mass field (gas, oil in liquid layers, water in liquid layers, oil droplets in gas layer, and water droplets in gas layer), and velocity, respectively. In addition, ∂_t is differentiation in time, ∂_z is spatial differentiation, Ψ_{ji} is the rate of mass transfer between the j-th and i-th mass field. The mass transfer between the mass fields includes, dispersions, droplet deposition and entrainment, and phase transitions. G_i is any mass source/sink.

- Momentum balance equation

$$\partial_t (m_i U_i) + \partial_z \left(m_i {U_i}^2\right) = m_i . g . \cos(\varphi) + \mathcal{p}_i + G_i U_i + \sum_j \left(\Psi_{ji}^{+} U_i - \Psi_{ji}^{-} U_i\right) + \sum_j F_{ji}^{I} \left(U_j - U_i\right) - F_i^{w} U_i \tag{26}$$

where g is the acceleration of gravity, φ is the pipe angle relative to the gravitational vector, $\mathcal{p}_i$ is the pressure force, $G_i U_i$ is the momentum contribution corresponding to the mass source/sink, G_i. Also, F_{ji}^{I} are friction forces between the i-th and j-th mass field, and F_i^{w} denotes the wall friction. Ψ_{ji} is momentum contributions corresponding to the mass transfer between the j-th and i-th mass field. In the equation (26), Ψ_{ji}^{+} accounts for a net contribution from the mass field i to j while Ψ_{ji}^{-} accounts for a net contribution from the mass field j to i.

- Energy balance equation

$$\partial_t (m_i E_i) + \partial_z (m_i U_i H_i) = \mathcal{S}_i + \mathcal{Q}_i + \sum_i T_{ij} E_j \tag{27}$$

where E_i is the field energy, H_i is the field enthalpy, $\mathcal{S}_i$ denotes enthalpy source/sink, $\mathcal{Q}_i$ is the heat flux through the pipe wall, and T_{ij} models the energy transfer between the fields. [111, 113]

Wellbore setup

In this work, a basic case is selected to generate the wellbore model in OLGA. The model consists of the two components PIPELINE and FLOWPATH. FLOWPATH represents the production tubing, and PIPELINE represents the annulus and the inflow from annulus to the well. On PIPLINE, the flow components such as inflow controls and packers are placed. Figure 4-4 shows the setup in OLGA for one production zone which consists of two sections. This modelling approach was developed and proposed for the first time in 2012 [59]. The PIPELINE

includes a near-well source (NWSOUR) which connects ROCX to OLGA. The near-well source is the flow source from the reservoir to the annulus. In addition, PIPELINE consists of one inflow controller (VALVE-A), two packers (VALVE-1 and 2 with zero opening), and leak (LEAK). The leak delivers the flow through the inflow control to the production well (FLOWPATH) and towards the heel (OUTLET). Each production zone is divided into two sections and is isolated by packers. The near-well source is placed in one section and the leak in the other one. In this setup, the packers, and the inflow controllers are the section boundaries.

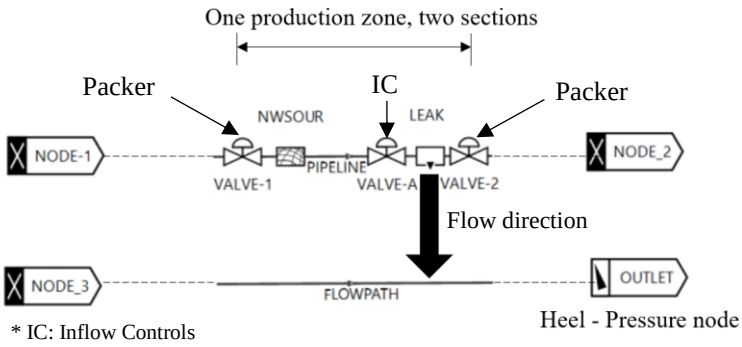

Figure 4-4: Setup of a single production zone with inflow controller in OLGA.

The inflow control (VALVE-A) in Figure 4-4 is an orifice with constant diameter and a specified discharge coefficient. To model the autonomous closure and opening behavior of an autonomous inflow control, either PID controller [59] or table controller can be used. The table controller method is used in this work and it is described in detail in earlier work by Moradi & Moldestad, 2021 [33] . The setup of a single production zone with AICV in OLGA is illustrated in Figure 4-5.

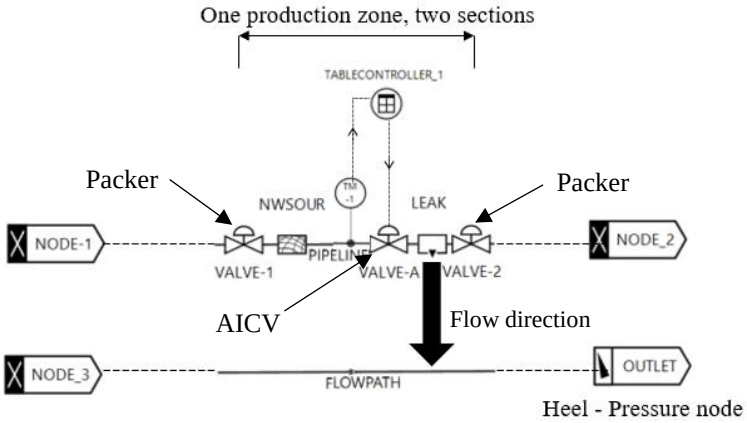

Figure 4-5: Setup of a single production zone for AICV in OLGA.

The table controller is created based on the characteristics of AICV and the reservoir fluid mixture. The table gets the measured GVF data from the transmitter (TM-1) and provides corresponding control signals for choking the AICV. The AICV with improved GVF behavior opens gradually when the oil/gas mixture flows through the valve. Afterwards, the AICV

restricts the gas flow when the GVF is getting higher, until pure gas flows through the valve and the valve is almost closed. The control signal table in the OLGA for controlling the AICV, consists of independent and dependent variables. In this case, the percentage of the valve opening is a function of the GVF. Indeed, the valve opening is getting less and less by increasing the GVF. This behavior is illustrated in Figure 4-6.

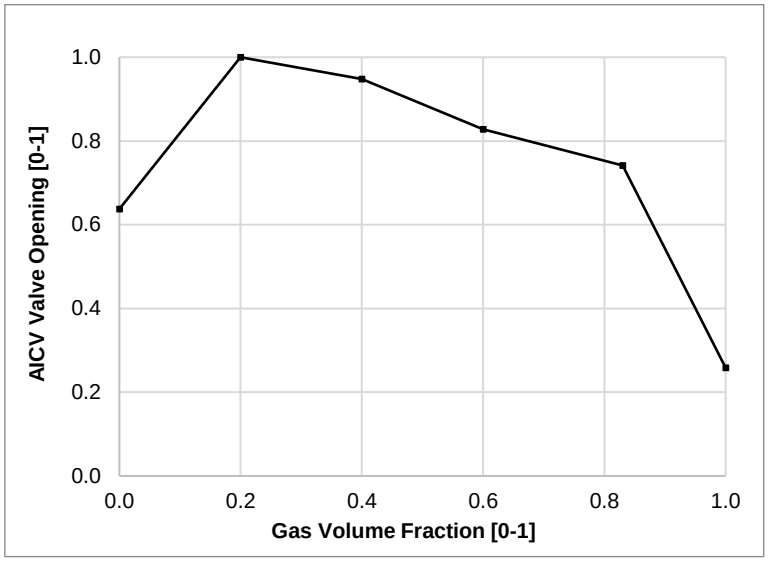

Figure 4-6: Valve opening versus GVF for AICV valve.

If a well with length of 1000 m is assumed, the well is divided into 10 segments, each 100 m long. One equivalent orifice valve with diameter of 7 mm is considered for every segment of the well. The flow area of this equivalent orifice should be equal to the total flow area of 8 ICDs. As, in a standard completion the length of one joint is approximately 12.4 m and there is enough space for 8 single ICDs per segment. So, the corresponding size of the 8 single ICDs is 2.5 mm. Most of the experiments in this work are performed with an orifice-type ICD with a diameter of 2.5mm. This methodology is used for designing the wellbore completion for all the simulation cases in this work. The wellbore setup in OLGA for ICD and AICV completion is shown in Figure 4-7 and Figure 4-8, respectively. In this setup, a table controller is also used to regulate the well choke. The dependent variable that is transmitted to the table controller is the GOR at standard condition (GORST [Sm^3/Sm^3]). The total gas processing capacity is an active constraint in many oil fields, hence, in this well setup, the GOR value is determined based on this constraint and the table controller is generated accordingly.

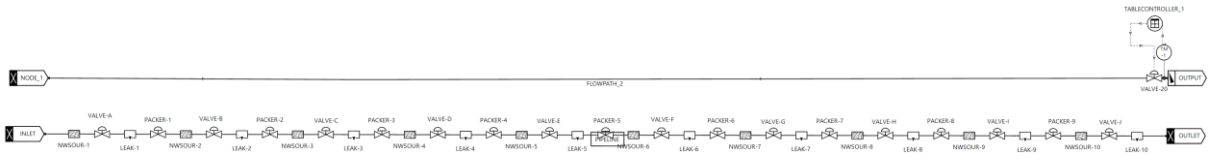

Figure 4-7: Well setup for a case with 10 ICDs, packers, near-well sources, leaks, and well choke.

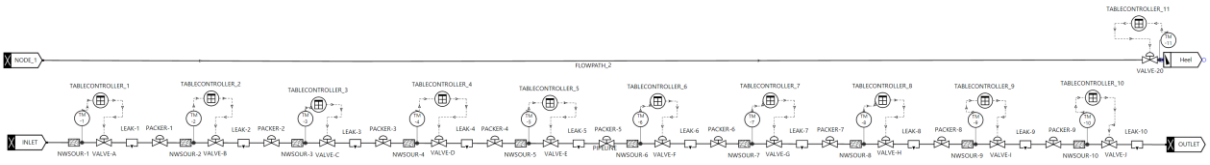

Figure 4-8: Well setup for the case with 10 AICVs, table controllers, packers, near-well sources, leaks, and well choke.

The simulations presented in Papers 4 and Paper 5 are performed with OLGA/ROCX. Paper 4 investigates the effect of AICV in a reservoir using SAGD for EOR. Paper 5 presents the optimized performance analysis of AICV for SAGD application. In addition, the annular flow in a well completed with inflow controllers was studied by using OLGA and NETool. This was an attempt to investigate a fundamental problem that almost all the reservoir simulators are dealing with.

CMG

CMG 2022.10 general release by Computer Modeling Group Ltd. is used in this work. The software has 13 modules, each for a specific purpose. The modules that are used in this work are Builder, CEDIT, Results, WINPROP, GEM and STARS.

Generating reservoir grid and well modelling are conducted in Builder. In addition, the input to Builder is the reservoir rock and fluid properties.

CEDIT facilitates the edition and manipulation of all sorts of data-input which are initially implemented in Builder.

The output can be graphically and quantitatively analyzed in the RESULTS module.

WINPROP applies an equation of state methodology to generate PVT data by analyzing oil and gas samples within a laboratory environment. WINPROP is used for fluid characterization, matching the experimental data, and constructing the phase diagram [82].

GEM is the compositional simulation tool which simulates the important mechanisms of a miscible gas injection process, i.e., in the CO_2-EOR process. The important mechanisms in the CO_2-EOR process are vaporization and swelling of oil, viscosity reduction and the multiple contacts of CO_2-oil in a miscible CO_2 injection.

STARS is a three-phase multi-component thermal and steam additive simulator. The governing equations for modelling the reservoir in STARS are the mass balance, heat balance and the auxiliary equations containing the momentum equation. The governing equation for modelling the wellbore in residual form is:

$$R_i = Acc_i + flow_i \frac{S}{S_i} \tag{28}$$

$\frac{S}{S_i}$ is the source-sink term, and the treatment of this term can be done through the source/sink model and FlexWell (FW) model. A simple source/sink model may be used in some specific situations. These situations are included but not limited to where the horizontal well is short, the wellbore-reservoir communication in a homogenous reservoir is uniform, the flow rate is low, or the pipe diameter is large [114]. FW is used to model the fluid flow in the wellbore and between the wellbore and the reservoir. FW is an advanced discretized mechanistic wellbore model which models the complex well completions [115]. The governing equations in FW modelling are mass balance, energy balance, momentum balance and pipe flow equation by assuming that the wellbore is discretized in space. The sum of inflow and outflow is equal to the sum of the accumulation and injection or accumulation and production, see Figure 4-9 to the left. In addition, FW modeling incorporates a two-way interaction between the wellbore and reservoir simulator, capturing dynamic interactions, see Figure 4-9 to the right. This modelling process involves solving the wellbore and reservoir models alternately at each time step, with the reservoir slightly trailing behind by one iteration. As a result, to enhance the precision of the well modelling calculations, STARS/GEM is employed for reservoir modelling, and the FlexWell option is chosen for modelling the wells equipped with ICDs and AICVs.

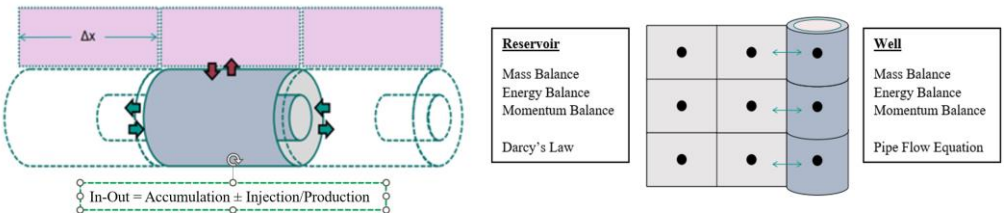

Figure 4-9: Wellbore in FlexWell (left) and coupling between wellbore and reservoir in FlexWell (right) [114].

The simulations in the papers 6,7 and 8 are performed with CMG. The impact of AICV on the reservoir recovery in a SAGD reservoir is studied by utilizing CMG STARS and the results are presented in Paper 6. Paper 7 investigates the effect of AICV in a heterogenous reservoir using CO_2 for EOR. In addition, paper 8 presents the performance analysis of AICV in a thin-oil-rim reservoir.

Mathematical modelling

A mathematical model describing the performance of the RCP valve was originally developed by Mathiesen et. al. in 2011 [51]. This model is also used to describe the AICV performance. The model is presented in the section *''Rate-controlled production valve, RCP ''*, equation (2). However, there are some indications that the RCP model does not explain all the variations in the data [116, 117]. In addition, the RCP model is dimensionally inconsistent. Paper 2 [118] presented an uncertainty analysis of the RCP model. The study was an attempt to quantify and model the sources of the uncertainty and check how well the model explains the variations in the measurements. This was done within the Bayesian statistical inference framework.

To achieve the objective of paper 2, the first step was to avoid handling the dimensionally inconsistency of the model and its consequences. Hence, the flow rate vs. pressure drop was studied with respect to a reference fluid at the same temperature. Water at 20℃ and a flow rate around 120 l/h was chosen as a reference fluid. Also, a_{AICD} is a geometric parameter and hence independent of the fluid type, it will not play a role in the analysis. In addition, a multiplicative noise term was proposed to quantify possible model discrepancies. The modified dimensionless RCP model is:

$$\frac{\Delta P_{oil}}{\Delta p_{water}} = \alpha \left(\frac{\rho_{oil}}{\rho_{water}}\right)^2 \left(\frac{\mu_{water}}{\mu_{oil}}\right)^y \left(\frac{Q_{oil}}{Q_{water}}\right)^x \tag{29}$$

where α denotes the multiplicative noise term. An α-value very close to one is an indication that the model can adequately describe the variations in the data.

The statistical inference will reveal the probable values of α. Equation (29) along with the experimental data were used to estimate the parameters α, x and y. These estimates were used to evaluate the performance of the modified RCP model.

Bayesian inference

The calculus of Bayesian inference is based on the application of two rules, the product, and the sum rules of the probability theory. One of the useful forms of the product rule is the Bayes theorem. In the present context, there are noisy measurements, D and a model, M with unknown parameters represented by θ that should be estimated. Then by the Bayes theorem:

$$P(\theta|D,M,I) = P(D|\theta,M,I) \times \frac{P(\theta|M,I)}{P(D|I)} \tag{30}$$

$P(\theta|D,M,I)$ is the posterior distribution over the possible values of θ consistent with the measurements. The model and any other available and relevant background information is denoted by 'I.' 'I' is any information about the AICV construction. On the right-hand side of equation (30), $P(D|\theta,M,I)$ is the likelihood, which is a statement about how likely it is to measure D given the model and specific values for θ. The term $P(\theta|M,I)$ is known as the prior distribution. In the present context, it models the expert opinion about the possible values of θ. The last term $P(D|I)$ functions as the normalization constant and is independent of θ and hence not relevant in the present context. The reader is referred to John K. Kruschke [119] for further information about Bayesian inference. [118]

Markov Chain Monte Carlos (MCMC) simulation

By the Bayes theorem, the joint posterior distribution is:

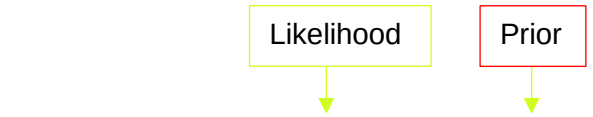

$$p(\theta,\omega|D,M,I) \propto p(D|\theta,\omega,M,I) \times p(\theta,\omega|M,I) \quad (31)$$

where θ is the model parameters, ω is the nuisance parameters, D is the data, and M is the model. The main reason for the choice of the nuisance parameter vector ω, is the uncertainty about the true values of parameters like viscosity. The dataset D used in the MCMC simulation in this work is generated by running experiments on different oil viscosities.

Since it is often difficult to find an analytical expression for the joint posterior distribution, a common approach is to approximate the joint posterior distribution by a large number of samples. The generation of samples are conducted by the MCMC method. The method works by sampling the distribution relative to the height of the distribution function on its domain. The frequency distribution of these samples will on the long run converge to the true distribution. Computationally, the process starts with a random sample and generates a chain of samples following certain sets of rules, which will guarantee that the chain will eventually visit all the regions relative to their probability mass. Since in practice only a finite number of samples can be generated, it is important to check if the chain has found the regions of highest probability mass. There is a so-called burn-in period, below which all the samples are discarded. The reason for this is to make sure that in a set containing a finite number of samples, the samples from regions with low probability mass are not over-represented. [118]

A MCMC method known as Hamilton Monte Carlo (HMC) is used to draw samples from the joint posterior probability distribution. The MCMC method is described in detail in a tutorial by John K. Kruschke [120].

5 Results and Discussions

This chapter presents an overview of the key findings from the experiments and simulations. Most of the results have been presented and published in the papers attached to this thesis. The presentation of results is divided into subsections based on different applications in which AICV shows a potential in increasing the oil production and reducing the production of un-wanted fluids. In this work, the performance of an orifice-type ICD and AICV is compared. In the experiments, by using the same strength for AICV and ICD, the performance curve for oil will be the same. This will make it more illustrative to compare the gas and water performance curves for ICD and AICV. The volumetric gas flow rates are presented at the AICV/ICD inlet pressure and temperature condition. The oil flow rate through the AICV is equivalent with the oil flow rate through an ICD. The orifice-type ICD throat sizes used in this work are in the range from 1.45 mm to 2.5 mm depending on the applications.

One sub-chapter is allocated to the modelling and uncertainty analysis of the RCP model.

Improved AICV design

The AICV design is improved. Several AICV prototypes were tested to find the optimum design. The piston dimension and shape, the combination and dimensions of LFE and TFE, the housing dimension, and the inlet dimension and design are changed to obtain a better multiphase flow behavior. Figure 5-1 illustrates the multiphase flow behavior of ICD, the AICV prior to this work and an improved AICV as an example.

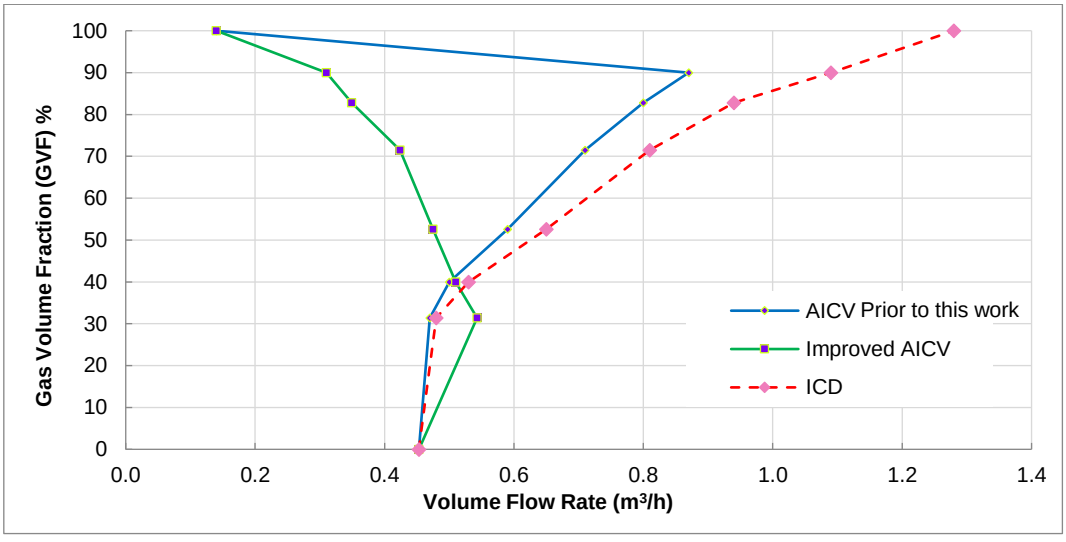

Figure 5-1: Total volume flow rate of gas and oil versus GVF.

Utilizing the ICD shown in the figure delays the onset of gas breakthrough but does not reduce or stop the gas production after breakthrough occurs [8, 60]. The AICV that was developed before this project restricts the gas production more than the ICD, and it closes for gas when the GVF reaches approximately 90%. The results from field installations showed that the use of this AICV reduces the gas production and thereby increases the oil production efficiency [19, 57]. The improved AICV has a better performance in multiphase flow compared to the previous version of AICV and any other existing AICDs reported in the literature [25]. The improved AICV chokes the gas flow rate when the GVF reaches approximately 30%. This reduces the gas production even more and may improve the total oil recovery. The unique behavior of AICV within multiphase flow is that the total volume flow rate is decreasing (from approximately 30% GVF) with increasing GVF and the valve is closed when GVF reaches 100%.

SAGD application

Utilizing AICV in SAGD reservoirs are discussed in papers 3,4,5, and 6. Both single and multiphase flow tests under SAGD late-life conditions are performed at the multiphase test facility at InflowControl AS.

AICV performance under SAGD conditions, lab experiments

The tests are performed at different temperatures and pressures to obtain the viscosity and density of the fluids under SAGD conditions. For single-phase tests, the differential pressure across the AICV and ICD is varied gradually between 1 bar and 8 bar. The flow rates and differential pressure are continuously measured as the differential pressure is gradually varied from 1 bar to 8 bar. Multiphase tests are performed at 1, 2, 3 and 5-bar differential pressure across the AICV. The tests are performed by regulating the desired amount of oil flowing through the test-unit that is already filled with gas. The gas density is equivalent to the hydrocarbon gas density at the reservoir condition. Also, the steam density is approximately the same as the hydrocarbon gas density at the SAGD late-life condition. The mixture of non-condensable gases (NCGs) and steam in a SAGD late-life reservoir will behave as gas through the AICV. Thus, in the simulations and the experiments, the gas represents the mixture of steam and hydrocarbon gas. The test matrix and system conditions applied in the experiments are given in Table 5-1.

Table 5-1:Test conditions.

Description	Fluid type	System conditions and/or fluid properties	Differential pressure across AICV (bar)
Single-phase test	Gas	≈11 bar, ρ ≈11.5 kg/m^3	1–8
Single-phase test	Water	≈ 70°C / 0.40 cp	1–8
Single-phase test	Oil	44 cp	1–8
Multiphase test	Oil and gas	≈11 bar	1–5

Figure 5-2 presents the single-phase performance data of the AICV and an orifice-type ICD. The oil flow rates through the ICD and AICV are equal at 3-bar pressure drop and the differences in the flow characteristics are studied. The gas flow rate at 3 bar for the ICD is about 3.8 m^3/h while it is about 0.1 m^3/h for the AICV indicating that the gas reduction by using AICV is significant. The results for ICD illustrate that at constant pressure drop, the volume flow rates of oil and water differ slightly as the density differences are minor (1000 kg/m^3 for water vs. 955 kg/m^3 for oil, the dashed black and blue lines), while the volume flow rate of gas is much higher due to the much lower density (about 11.5 kg/m^3). The AICV chokes the water considerably compared with ICD (solid blue line vs. dashed blue line). It can also be observed that AICV is able to distinguish between the fluid viscosities and adjust the performance accordingly.

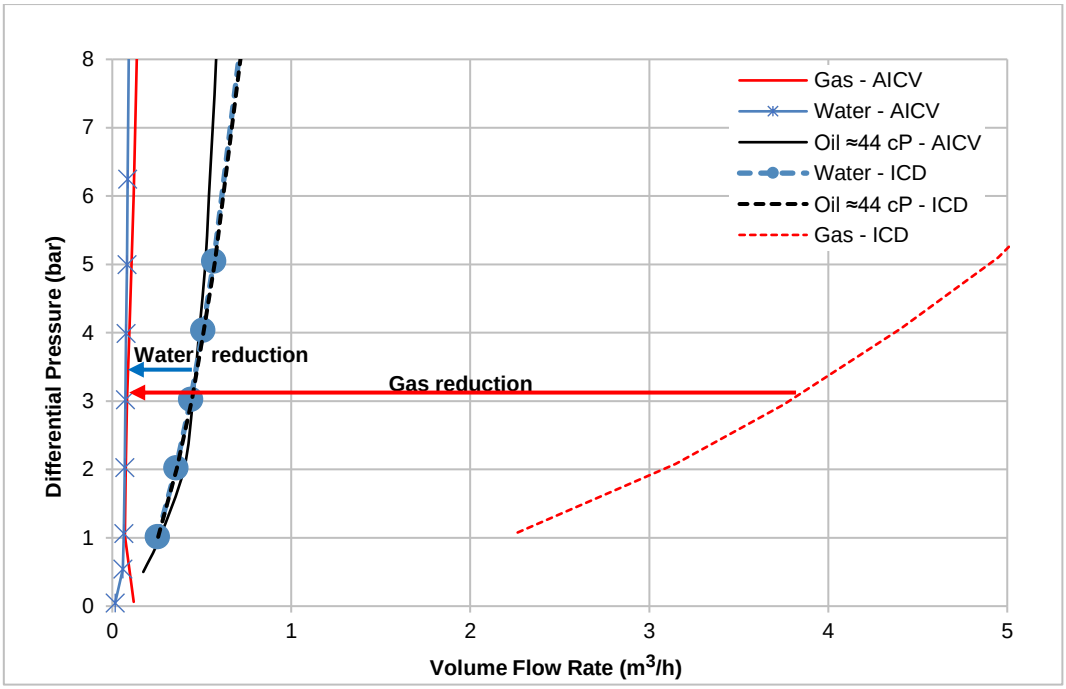

Figure 5-2: Comparison of single-phase flow performance of the ICD (dashed lines) and AICV (solid lines) for oil, water, and gas.

Figure 5-3 shows the pressure drop versus total volume flow rate of the fluids. The total volume flow rate is the volume flow rate of gas and oil. The tests are performed in the GVF range of 40% to 80%. The AICV restricts the gas flow when the GVF is between 40% to 80%. The AICV

closes totally when pure gas flows through the valve. The green point over the red curve (pure gas) at 5 bar is an illustration of 100% GVF when the valve is closed, and the gas is only flowing through the pilot flow.

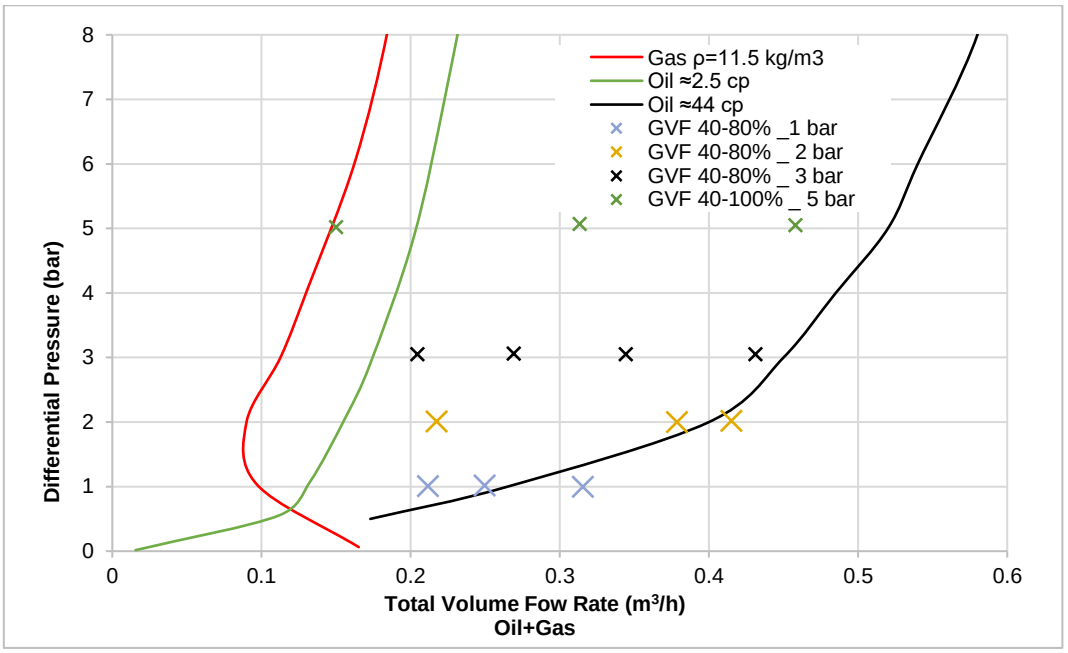

Figure 5-3: Two-phase performance of AICV at 1,2,3, and 5-bar differential pressure and the single-phase tests of AICV.

Viscosity dependency of AICV

As the temperature can vary along the well, fluid with different viscosities flows through the AICV. The AICV performance is modelled for different bitumen/water emulsion viscosities at different temperatures as shown in Figure 5-4.

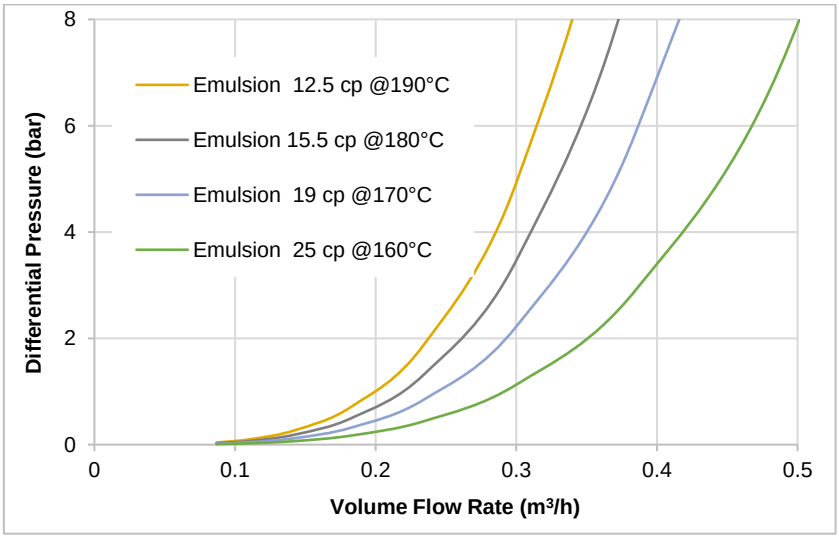

Figure 5-4: The AICV performance for emulsion at different viscosities.

It is common that bitumen/water emulsion is present in a SAGD reservoir. Bitumen viscosity data selected from literature [121] are presented in Figure 5-5.

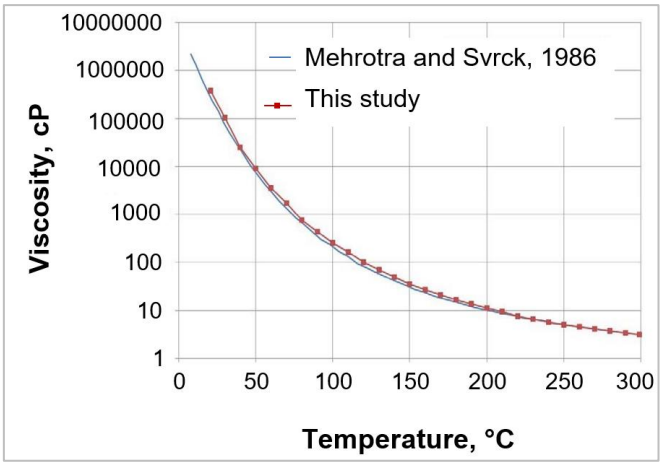

Figure 5-5: Viscosity of Athabasca bitumen sample versus temperature [121].

AICV performance under SAGD conditions, simulations with NETool

In paper 3, NETool simulations are used to analyze the performance of AICV based on the results from the experiments. The performance curves for AICV in Figure 5-2 and Figure 5-4 are considered. The estimated model parameters, a_{AICD}, x and y, in equation (2), and the density and the viscosity for water as the calibration fluid, have been used in NETool. The density and viscosity of the calibration fluid are 1000 kg/m^3 and 0.5 cp, respectively. The estimated model parameters for the AICVs are listed in Table 5-2.

Table 5-2: The estimated model parameters for AICVs in NETool.

	AICVs in Z3	AICVs in Z4	AICVs in Z2	AICVs in Z1
	Emulsion 12.5 cp	Emulsion 15.5 cp	Emulsion 19 cp	Emulsion 25 cp
a_{AICV}	0.00038	0.00065	0.00065	0.00065
x	3.7	3.9	3.9	3.8
y	1.95	1.73	1.75	1.75

A homogenous sandstone reservoir with a production well completed with AICVs is assumed in NETool. For the case study in this work, a SAGD late-life reservoir is considered. At the later stage of the SAGD process, non-condensable gases such as methane, nitrogen, carbon dioxide are co-injected with the steam to maintain the pressure and assist the bitumen to flow towards the producer well. The partial pressure of the steam is lowered, and consequently the temperature is being decreased from 230°C to about 160°C. For the simulation case in this work, it is assumed that the temperature along the well varies from 160°C to 190°C and the

corresponding viscosity range is 25 cp to 12.5 cp. It is assumed that the initial reservoir pressure is 27.5 bar and is less than the bubble point pressure and that the oil is saturated. The length of the openhole well is about 1045 m, and the top measured depth, MD, is 620 m. Based on the temperature differences along the well, the production well is divided into four zones. The temperature and viscosity of the fluid in each zone are illustrated in Figure 5-6. In total, 84 AICVs are distributed in 21 compartments isolated with packers (red rectangles). In this setup, the gas saturation (S_g) and permeability are highest in zone 3 (Z3). This is to simulate a SAGD late-life scenario in which gas breakthrough will occur more likely in the warmest zone close to the toe section of the well.

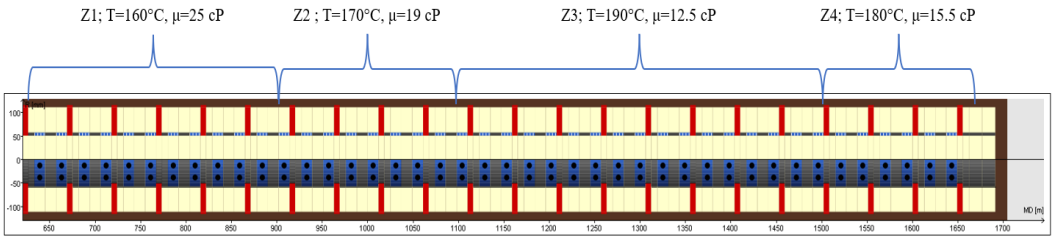

Figure 5-6: Fluid temperature and viscosity along the well.

Some of the important input data to NETool are listed in Table 5-3.

Table 5-3: Input data used in NETool.

Parameter	Value	Unit
Vertical /horizontal permeability, k_v/k_h	0.6	–
Gas density, ρ	11.5	kg/m^3
Gas viscosity, μ	0.016	cp
Saturations in zone 1	S_g=0, S_o=1	–
Saturations in zone 2	S_g=0, S_o=1	–
Saturations in zone 3	S_g=0.03, S_o=0.97	–
Saturations in zone 4	S_g=0, S_o=1	–
Horizontal permeability in zone 1, K_h	3000	md
Horizontal permeability in zone 2, K_h	3000	md
Horizontal permeability in zone 3, K_h	6000	md
Horizontal permeability in zone 4, K_h	3000	md
Target oil production, Q	423	stock-tank m^3/d

Results from three simulated cases are presented and discussed. One case with openhole and two cases with AICVs with different drawdowns are simulated. The drawdown represents the total drawdown which is the sum of the drawdown through the sandface and across the completion. The target oil production in the simulated cases is set to 423 stock-tank m^3/d. Stock-tank oil refers to the volume of oil after separation treatment when gas is removed (at storage temperature and pressure) [122]. Figure 5-7 shows a comparison of the stock-tank oil

and the gas rates from the reservoir to the well together with the differential pressure along the well for the three simulation cases. As it can be seen from the figure, gas breakthrough occurs in zone 3, from MD 1100 m to 1500 m. However, the gas production is much higher for the case of openhole compared with the AICV cases. AICV restricts the gas production, and this allows reducing the bottomhole pressure and thus increasing the drawdown. Since the bottomhole pressure is being decreased, a higher drawdown in the sandface from the zones 1, 2, and 4 is obtained. Thus, a higher production from the colder zones with less mobile oil is achieved, and the steam chamber is thereby forced to be more evenly distributed along the different zones resulting in increased oil recovery. When the total drawdown is increased to 5 bar, the oil production from zones 1, 2, and 4 is increased, compared with the openhole case and the AICV case with 3.5-bar total drawdown.

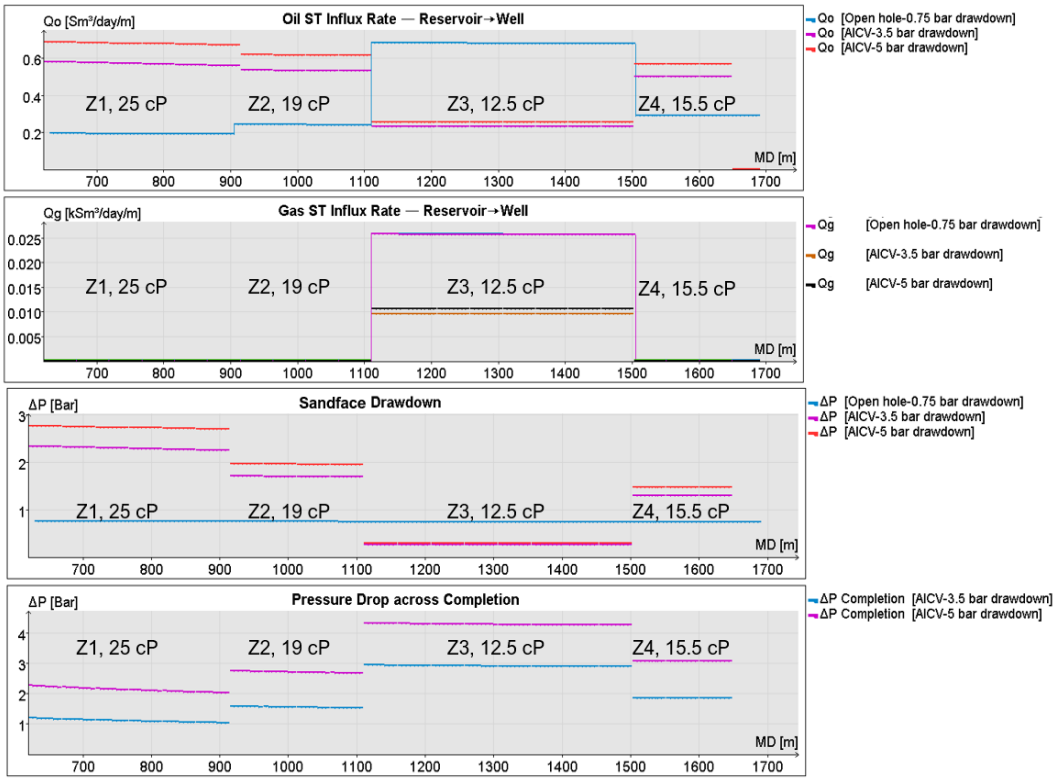

Figure 5-7: Oil and gas production and differential pressure along the well for three simulation cases.

The production zone 1 has the highest fluid viscosity which is 25 cp. The pressure drop across the AICV in this production zone is lowest with highest sandface drawdown. This indicates that the AICV is more open, producing the colder viscous bitumen/water emulsion. The summary of the results from the simulations are presented in Table 5-4.

Table 5-4: Comparison of the results for three simulation cases.

Simulation case	Reservoir pressure (bar)	Bottomhole pressure (BHP) (bar)	Gas liquid ratio (GLR) (std m^3/ std m^3)	Emulsion increase	Gas reduction
Openhole_0.75-bar drawdown	27.50	26.75	24.01	–	–
AICV_3.5-bar drawdown	27.50	24.00	8.66	0.16%	64%
AICV_5-bar drawdown	27.50	22.50	8.31	15%	60%

The results indicate that AICV can decrease the production of gas and steam by 64% compared with an openhole well. In addition, the emulsion production can be increased by 15% when AICV is used at higher drawdown.

Simulation of AICV under SAGD conditions in NETool provided a general insight into AICV modelling. The knowledge gained in this work is used further to perform simulations in dynamic reservoir simulators OLGA/ROCX and CMG.

AICV performance under SAGD conditions, simulations with OLGA/ROCX

In paper 4 [112] and 5 [123], OLGA/ROCX simulations are used to analyze the performance of AICV based on the results from the experiments.

In paper 4, a higher rock permeability is specified in the toe section of the well. In paper 5, a homogeneous reservoir with a high gas saturation in the toe section of the well is considered. This is to simulate a scenario of SAGD in which it is assumed that the well has been in production for several years, and at the late-life stage a strong gas breakthrough has occurred in the toe section of the production well.

The setup in OLGA for well modeling with ICDs and AICVs is shown in Figure 4-7 and Figure 4-8. This setup is used in both paper 4 and 5. The key input to OLGA/ROCX that is common for the two papers are presented in Table 5-5. Generally, it is challenging to obtain information about the relative permeability for different fields. Data for relative permeabilities are set manually in table form in ROCX. The “Stone II” model with exponent 2 is used to evaluate the oil-phase relative permeability, while the Corey correlation with exponent 1.5 is used to estimate the gas-phase relative permeability.

Table 5-5: Input information used in OLGA/ROCX for homogeneous and heterogeneous reservoirs.

Property	Value	Unit
Oil viscosity (cp)	15.5	cp
Oil and gas specific gravity	0.9 and 0.64	–
Porosity	0.3	–
Initial reservoir temperature	180	°C
Initial reservoir pressure	27	bar
Wellbore diameter, and tubing outer diameter	8.74 and 4.5	in
Roughness in wellbore and tubing	0.028 and 0.050	mm
Reservoir length, width, height	1000,117,40	m
Drawdown ($P_{reservoir}$ - P_{well})	7	bar

The purpose of the studies is to evaluate the ICD/AICV performance in the case of steam breakthrough. The well is located as near as possible to the bottom of the drainage area to delay the probable steam breakthrough as long as possible. As the fluid properties vary significantly around the well and in the *y-z* plane, a finer mesh is considered in the grid setup to achieve more accurate results. The grid resolution in the *y-z* and *x-z* plane, and the well location are shown in Figure 5-8.

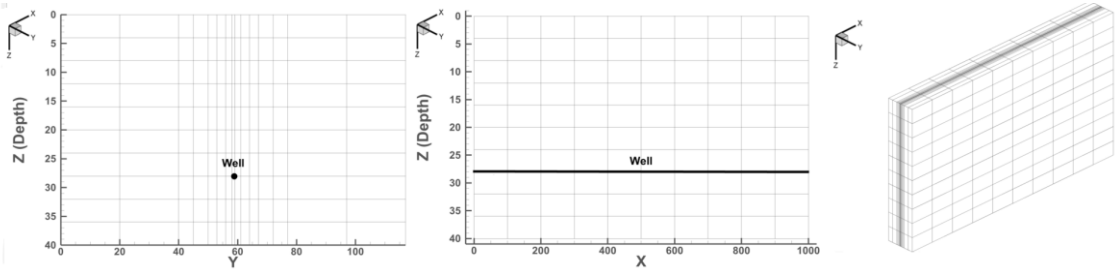

Figure 5-8: Grid resolution in y-z, and x-z plane and the well location for homogeneous and heterogeneous reservoirs.

Homogeneous reservoir

The initial oil saturation profile of the homogeneous reservoir is shown in Figure 5-9. The horizontal and vertical permeabilities are 3000 md and 500 md, respectively. In the toe section of the well (green color) the gas saturation is set to 0.7. The length, height and width of the toe section are 100 m, 40 m and 117m, respectively.

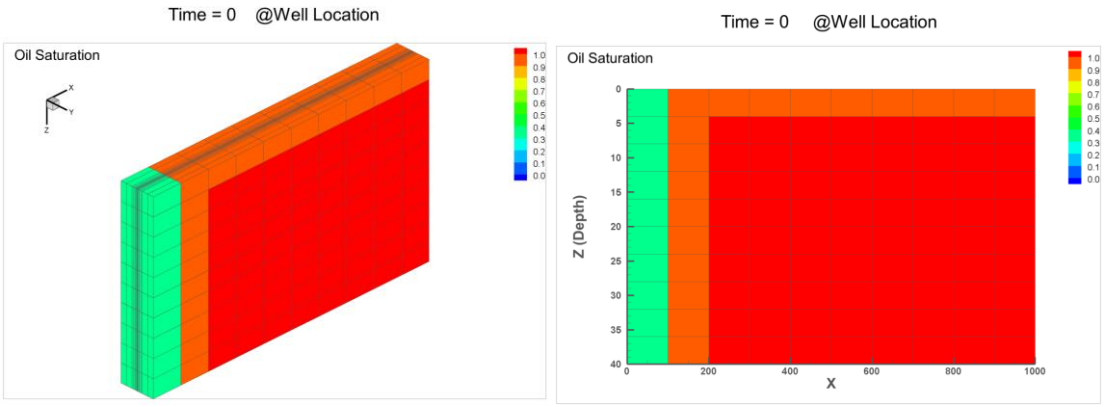

Figure 5-9: 3D plot of initial oil saturation (left) and 2D plot in x-z direction (right).

The model is run for 365 days to investigate the oil production. Figure 5-10 shows a 2D plot of the reservoir in the *x-z* direction and the well location. The plot shows the oil saturation right after that gas reaches the heel at day 58 (left), and after 365 days of production (right). The plot to the left illustrates that the oil saturation in the heel at day 58 is less than the oil saturation in the adjacent zones.

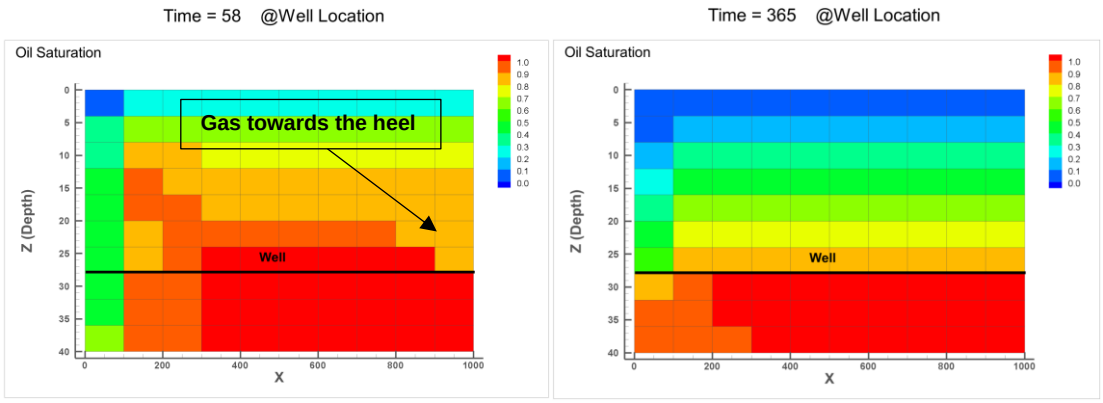

Figure 5-10: Oil saturation in the reservoir in the x-z direction after 58 days (left) and after 365 days (right).

The minimum opening of the AICVs is specified as 10% of fully open AICV and the transmitted parameter to the table controllers is GVF. When the GVF reaches to 100%, the opening of AICV is 10%. The well choke is also regulated with a table controller, see Figure 4-8. GOR is the transmitted parameter for choking the well. The minimum possible opening of the choke is set to 10% opening when the GOR reaches 20 std m^3/std m^3. Figure 5-11 shows the instantaneous GOR development over time for both the ICD and the AICV case. The figure also shows how a well completed with AICVs and ICDs is choked. The well completed with ICDs chokes instantly to its minimum value as the gas enters the well and GOR is equal to 20 std m^3/std m^3. ICDs do not restrict the gas production and GOR reaches to about 500 std m^3/std m^3 at the end of the production. For the AICV case, when gas reaches the toe section of the well, the AICVs in the toe and adjacent zone, restrict the gas production, keeping the

GOR low and the well choke in fully open position. After some time, gas reaches the heel due to the heel to toe effect and the GOR increases gradually. When the GOR passes 20 std m^3/std m^3, the controller starts to reduce the choke-opening and chokes the well. The choke position reaches its minimum after almost 80 days of production. After this, the valve position is constant at its minimum opening and the GOR gradually increases to approximately 300 std m^3/std m^3.

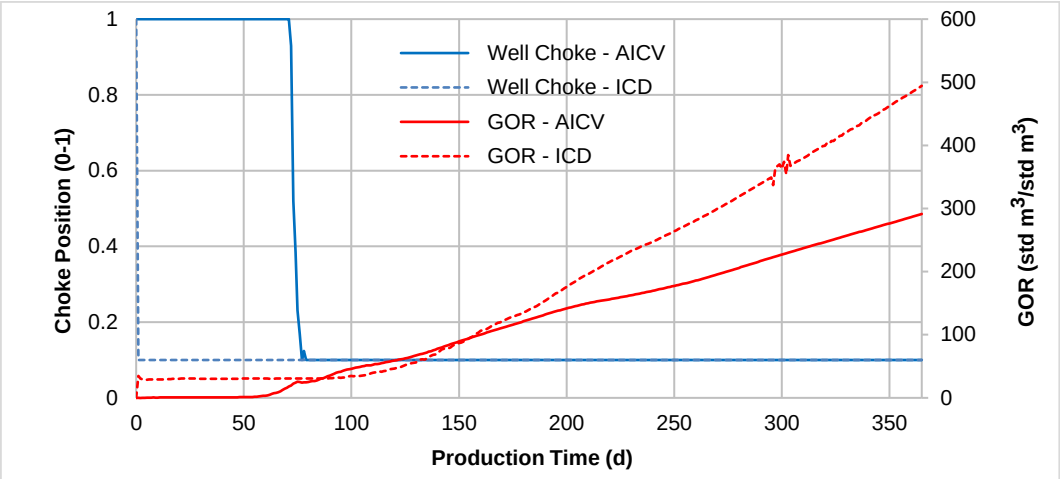

Figure 5-11: GOR development and well choke position.

Figure 5-12 shows the cumulative oil and gas production versus time for ICD and AICV. The gas is produced from the beginning of the production time for the ICD case. For the AICV case, gas is produced from day 58; when the gas reaches the heel. As it is shown in Figure 5-11, the well choking begins from the first day for the ICD case. This choking leads to reduction of the drawdown in the gas production zone, and consequently reduction of the oil production. The well choking continues until day 58, when gas reaches the heel, and the GOR increases until day 80. In this period, the cumulative oil production for AICV is approximately 48% higher than for ICD. At day 80, when the GOR passes 20 std m^3/std m^3, the controller starts to reduce the choke opening and chokes the well for the AICV case. This can be observed by the change in the curve slope resulting in a decline in the oil production. At the end of the production period, the cumulative oil production for AICV is about 3% more than for ICD. The cumulative gas production is reduced significantly from 1.68 Mm^3 for ICD to 0.97 Mm^3 for the AICV (42% reduction) after 365 days of production. It must be noted that although excessive amount of gas is produced from the ICD well, almost the same amount of oil as from the AICV well is produced. To the author's knowledge and the results from AICDs installations at the Troll field [8], dynamic reservoir simulators tend to underestimate the oil production after that the breakthrough of gas to the wells occurs.

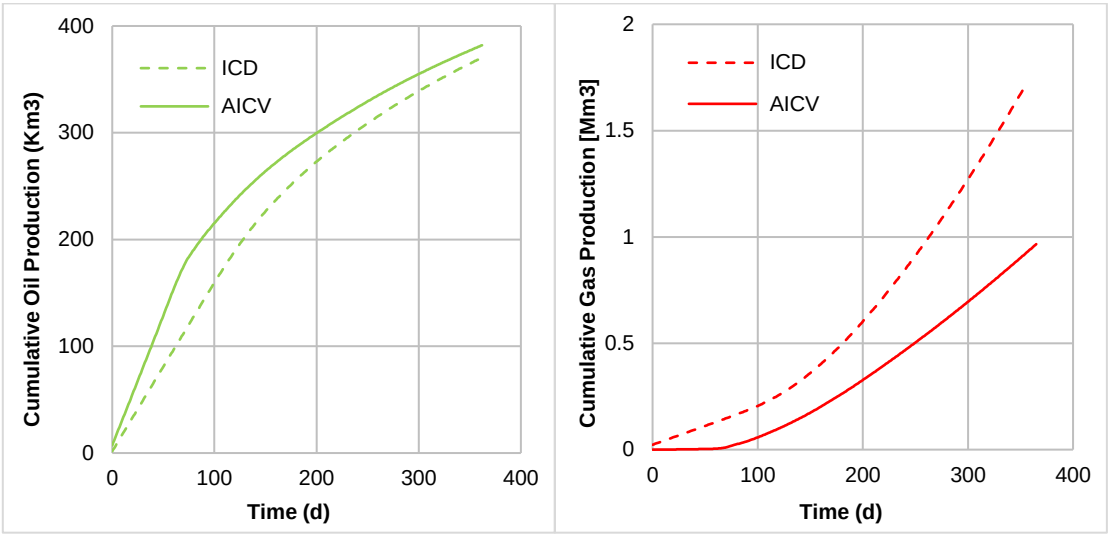

Figure 5-12: Cumulative oil (left) and gas (right) production for the homogeneous reservoir versus time.

Heterogeneous reservoir

Different permeabilities are specified for each block to simulate a heterogenous reservoir. It is assumed that the reservoir rock where the toe section of the well is placed has a higher permeability in all directions. The permeability in both *x* and *y*-direction, varies from 3000 md to 6000 md. The vertical permeability varies from 300 md to 600 md. The horizontal permeability profile of the heterogenous reservoir is illustrated in Figure 5-13.

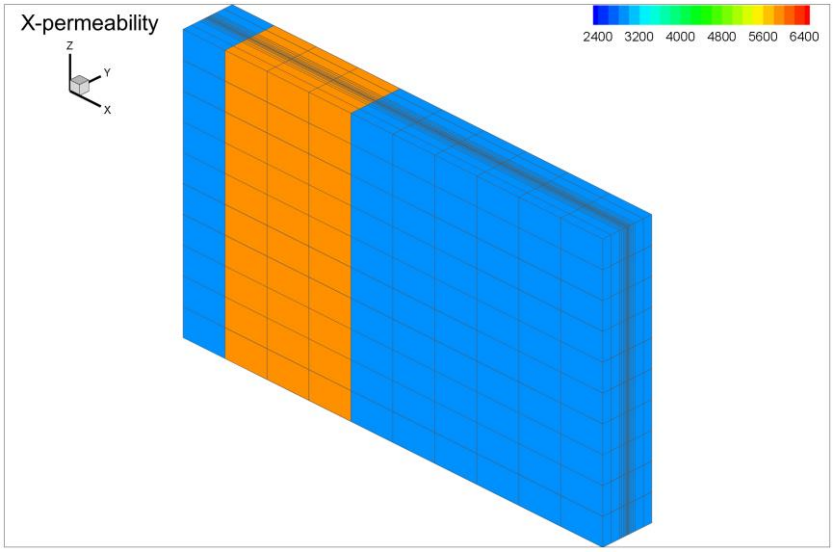

Figure 5-13: Horizontal permeability profile.

The model is run for 300 days. Figure 5-14 illustrates the accumulated oil and gas produced from the well after 300 days of production. After 300 days, the cumulative oil production for ICD is higher than for AICV. However, due to the better single and multiphase flow

performance of AICV, the amount of cumulative gas drops significantly from 4.8 Mm^3 to 1.9 Mm^3 after 300 days of production. This corresponds to approximately 60% reduction. When the gas breakthrough occurs, the AICV closes gradually as the GOR increases. The choking behavior, which is based on experimental data, is implemented in the table controllers in OLGA.

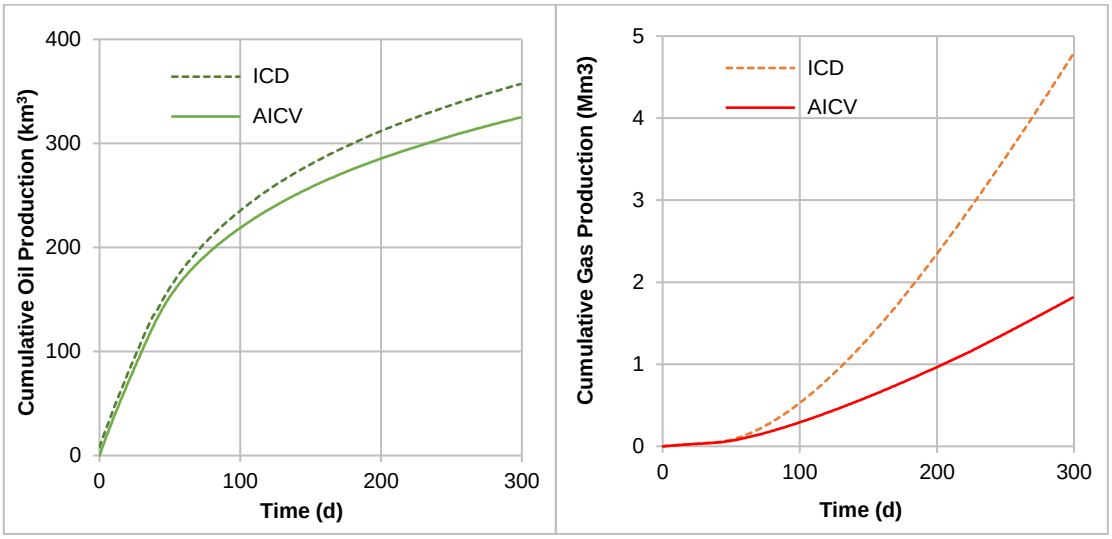

Figure 5-14: Cumulative oil (left) and gas (right) production for the heterogeneous reservoir versus time.

Figure 5-15 shows the GOR development versus accumulated oil at standard conditions. The figure illustrates how the GOR varies with accumulated oil. The total allowable gas production is usually limited and the total gas processing capacity is an active constraint [69, 124]. This highlights the importance of developing new inflow control technologies which guarantee a higher maximum oil production while meeting the GOR constraint. In this case, the accumulated oil at a specific GOR, for example 600 std m^3/std m^3, is approximately 15% more for AICV than for ICD.

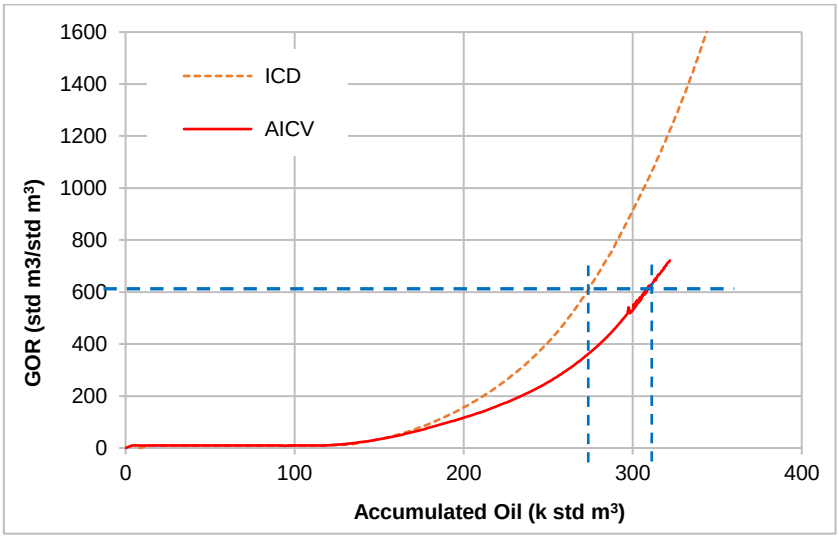

Figure 5-15: GOR versus accumulated oil for AICV and ICD.

AICV performance under SAGD conditions, simulations with CMG STARS

Simulations with coupling OLGA/ROCX are generally time-consuming. In addition, the physics involved in thermal recovery processes are incorporated in simulators such as CMG. In paper 6 [125], CMG STARS simulations are used to analyze the performance of AICV. The reservoir construction developed for the SAGD model is shown in Figure 5-16, and the gravitational force is acting along the *k*-direction (vertical). The injector and producer wells are placed in the area with the finest mesh both in the *x-z* and *y-z* plane (areas marked in blue). The vertical distance between injector and producer wells is 6 m.

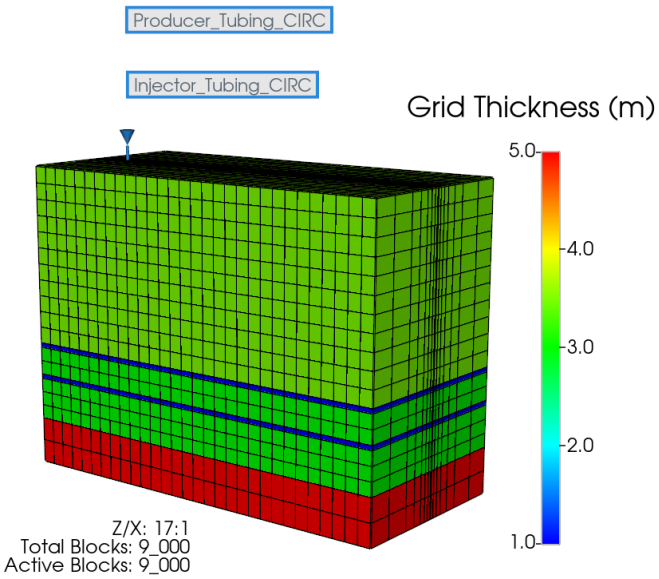

Figure 5-16: 3D view of the reservoir grid.

The reservoir characteristics and parameters for initialization are presented in Table 5-6. The Stone II model is used to calculate the relative permeability data.

Table 5-6: Reservoir Characteristics initialization details.

Property	Value	Unit
Reservoir length *(X)*	1500	m
Reservoir width *(Y)*	141	m
Reservoir depth *(Z)*	65.5	m
Porosity	0.3	-
Rock wettability	water-wet	-
Reservoir top depth	400	m
Initial pressure at top of the reservoir	1500	kPa
Initial temperature	12	^{o}C
Initial water saturation	0.10	-
Reference depth	430	m
Water-oil contact depth	455.5	m
Oil mole fraction (dead oil)	0.80	-
Oil mole fraction (solution gas)	0.20	-

The simulation time has been set to 10 years for the SAGD operation, and these 10 years have been divided into two phases. The first phase, also known as the circulation period, starts from 1st of January 2023 and continues for six months until 1st of July 2023. The SAGD period starts from 1st of July 2023 and continue until 1st of January 2033. FW is used for well modelling. The injector and producer well are 1201 meters long and are placed horizontally in the I direction. The wells trajectory is shown in Figure 5-17. During the circulation period, steam is injected from both wells. This is to establish thermal communication between the injector and producer and warm up the reservoir. The temperature at the end of the circulation period is between 70 to 100ºC.

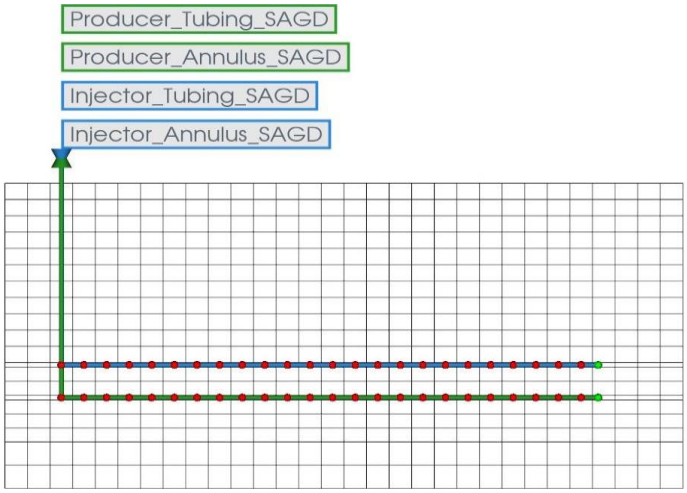

Figure 5-17: The wells trajectory.

The outer and inner diameter of annulus wall are 0.177 m and 0.166 m. For the injector FW annulus, the maximum BHP is 4000 kPa, the injection temperature is 250°C, the steam quality is 0.9, and the maximum surface water rate is 500 m^3/d. For the producer FW annulus, the minimum BHP is 2000 kPa, and the maximum surface liquid rate is 1500 m^3/d.

Six cases have been established for the simulations. The simulation cases are well perforations (without any inflow controllers), well completed with 4 ICDs for each 50 meters of the horizontal length, and well completed with 4 AICVs for each 50 meters of the horizontal length. The simulations are performed both for a homogenous and a heterogeneous reservoir. The horizontal permeability of the homogeneous reservoir is 1800 md in all the blocks. The permeability distribution of the heterogeneous reservoir in the *x-z* plane is illustrated Figure 5-18.

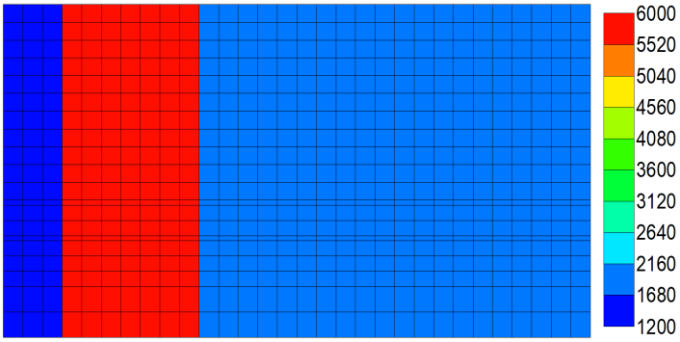

Figure 5-18: Permeability distribution of heterogeneous reservoir.

Figure 5-19 shows the steam chamber distribution along *y-z* plane for the simulated cases. It can be interpreted that due to the high steam production for well perforations, the steam chamber has not reached the maximum temperature after 5 years, see Figure 5-19a. In addition, Figure 5-19c illustrates that the AICV case has a slightly better steam distribution than the ICD case shown in Figure 5-19b. The AICV case has a uniform steam chamber distribution which has reached the maximum temperature after 5 years. The same pattern is observed for both homogenous and heterogenous cases. This means that AICVs are better in handling steam breakthrough than ICDs and well perforations.

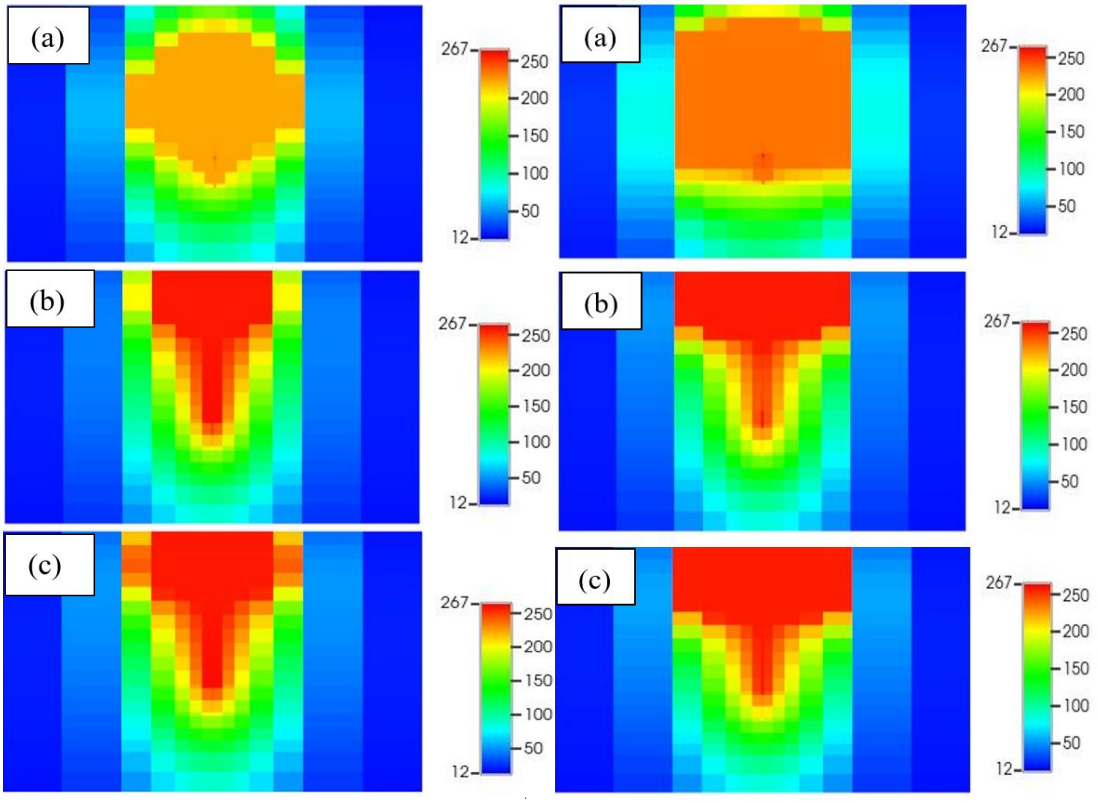

Figure 5-19: Steam chamber conformance along J-K plane for (a) perforations, (b) ICDs, and (c) AICVs; homogenous (left) and heterogenous (right) cases.

The cumulative oil, water, and gas production for the homogeneous and the heterogenous cases are presented in Figure 5-20. Perforation case has the lowest oil production and the highest gas production in both homogeneous and heterogenous cases. AICV has the highest oil production and the lowest gas production in both reservoir types. This indicates that AICVs are better in recovery of heavy oil, in reduction of gas (steam) and water production, and in steam chamber distribution, compared with ICDs and well perforations. A more uniform temperature distribution, and steam chamber conformance are observed in the AICV cases.

Reduction in steam production with AICV is observed in all the simulation cases that are performed in this work with static (NETool) and dynamic (OLGA/ROCX and STARS) reservoir simulators. This will improve the overall SAGD operation performance. This also will result in a more cost-effective oil production, as less steam is needed to be generated for production of each barrel of oil. Less steam generation means less energy demand, that consequently contribute to reduce the intensity of greenhouse gas emissions.

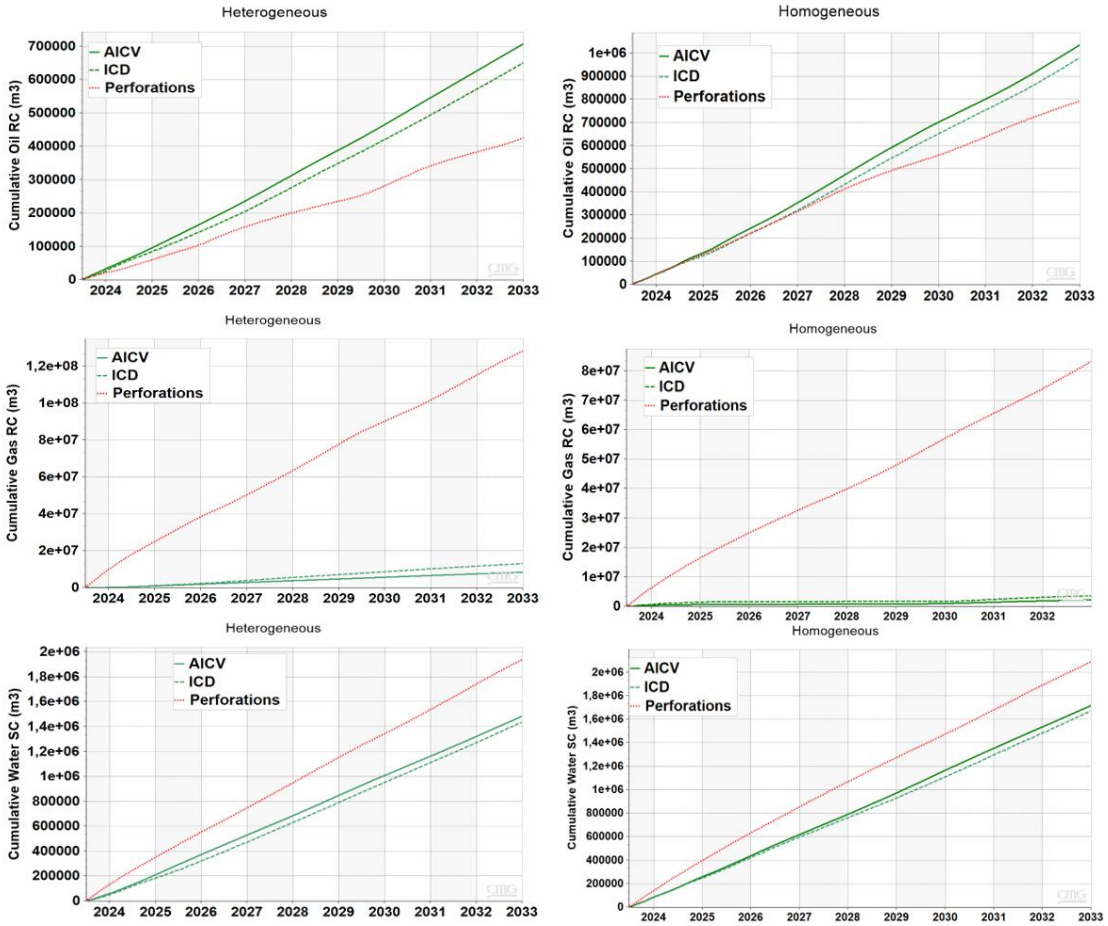

Figure 5-20: Cumulative oil, gas, and water production for perforations, ICDs and AICVs in a heterogeneous (left) and homogenous (right) reservoir.

CO_2-EOR application

Utilizing AICV in reservoirs using CO_2 for EOR is discussed in paper 7 [82]. The AICV performance curves for reservoir fluids are obtained based on experimental data and the RCP model. It is assumed that CO_2 is at supercritical conditions. This corresponds to a density of 600 kg/m^3 and a viscosity of 0.1 cp. Also, it is assumed that the oil viscosity in the reservoir is 1.32 cp with a density of 811.6 kg/m^3.

AICV performance in fields with CO_2-EOR, performance curves

The comparison of the AICV and ICD performance curves for the reservoir fluids for the CO_2-EOR application is presented in Figure 5-21. The orifice-type ICD has the same strength as the AICV. Under the same conditions and at a given Δp, AICV compared with ICD, reduces the water and CO_2 volume flow rates by approximately 58% and 82%, respectively. The results indicate that the gas and water reduction by using AICV is significant. According to the

experimental results, the volume flow rate of unwanted fluids like gas and water is always less than the oil flow rate at a given Δp, as AICV is mainly viscosity dependent.

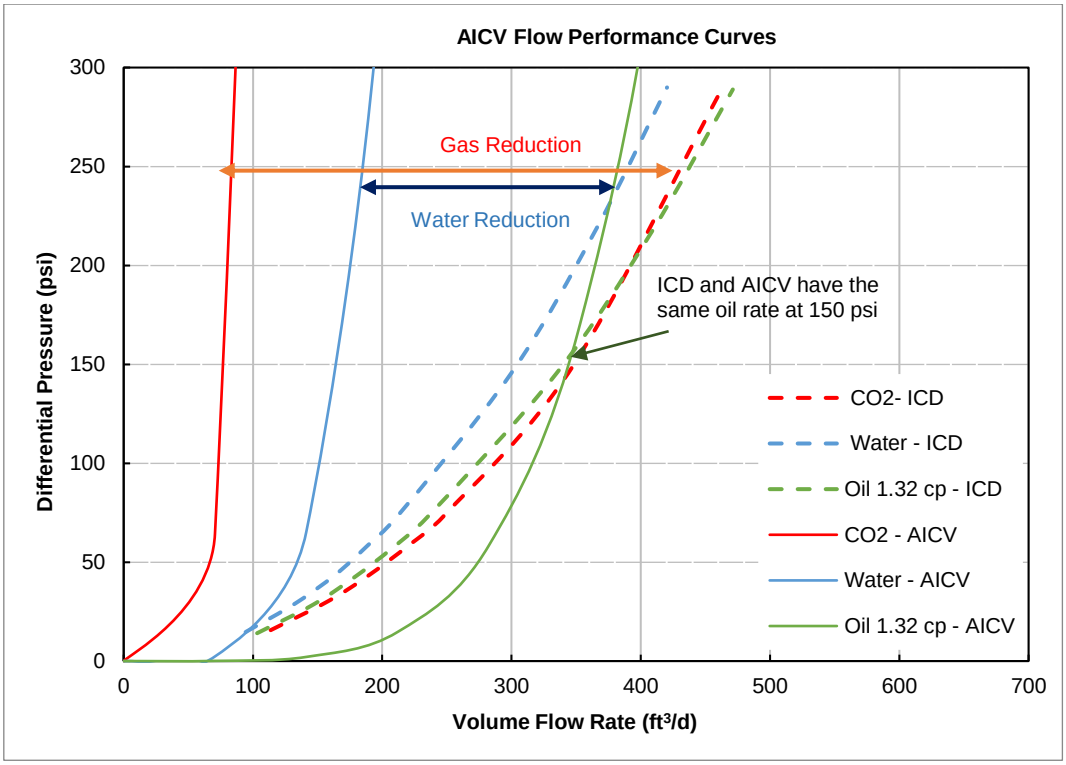

Figure 5-21: Comparison of flow performance curves of the ICD and AICV.

AICV performance in fields with CO_2-EOR, simulations

In paper 7, CMG STARS simulations are used to study the performance of AICV in a heterogenous reservoir where CO_2 is injected from a horizontal well under miscible condition.

The reservoir and well model are developed in STARS. WINPROP is used for fluid characterization, matching the experimental data, and to construct the phase diagram. The MMP at reservoir temperature (186°F) is calculated by WINPROP to be 3217 psi. The reservoir temperature is considered constant and equal to 186°F. The oil viscosity at standard condition is 1.32 cp. To assure that the reservoir pressure is always higher than MMP, the initial reservoir pressure at the top and the bottom of the reservoir are 4184 psi and 4248 psi, respectively. Also, CO_2 is injected by a constraint of a maximum BHP of 5000 psi. The porosity ranges from 0.23 to 0.32 and the horizontal permeability varies from 0 md to 2588 md. The top of the reservoir is at a defined depth of 5835 ft, while the bottom is at a depth of 6016 ft.

Two horizontal producer wells and one horizontal injector well are considered to develop the well model. The length of the wells is approximately 2200 ft, and they are placed in the *J*-

direction. The injector well is placed between the two producer wells, see Figure 5-22. The maximum surface liquid rate from each well is 2000 bbl/d and minimum BHP is 500 psi. The simulations are conducted for five years; from January 2023 to February 2028. The CO_2 WAG injection starts with water injection in three months followed by CO_2 injection in three months. This cycle is repeated in almost five years. Three different cases are simulated: one case without any completion in the producer wells, one case with AICV completion in the producer wells, and one case with AICV in one producer well and without AICV in another producer well. There are in total 18 production zones in each well. The production zones are isolated with packers.

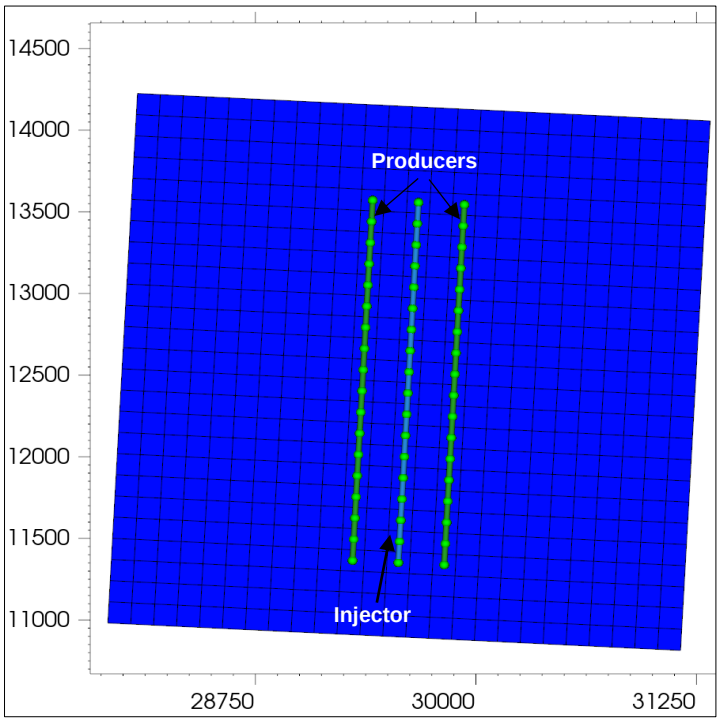

Figure 5-22: The producer and injector wells.

Figure 5-23 shows the field cumulative oil and water production for different completion scenarios. The results indicate that the wells completed with AICVs have the highest oil production with the lowest water production (solid green and blue lines). The cumulative water production is reduced by approximately 25% by using AICVs compared with the perforated casing completion. It is assumed that the CO_2 is dissolved in water and oil, indicating that reduction in water production will minimize the recirculation of CO_2. The reduction in the production of carbonated water will mitigate the problem related to the corrosion of the production wells and process equipment on the platform.

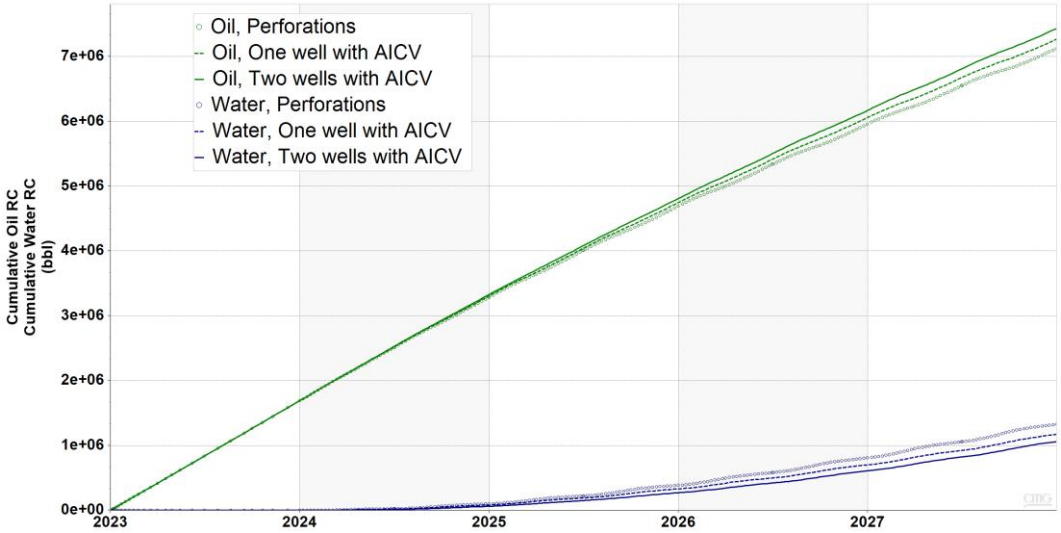

Figure 5-23: Field cumulative oil and water production of different completion scenarios.

The increased oil production and reduced water and gas production obtained by using AICV are demonstrated in several field installations worldwide and the results are presented in several studies [18-20]. However, the dynamic reservoir simulators tend to underestimate the oil production and recovery compared with the reality and the actual well tests.

It can be concluded that utilizing AICV in CO_2-EOR projects will contribute significantly to reduction of greenhouse gas emissions as it mitigates the problem with breakthrough and direct reproduction of CO_2 to the well. Choking back CO_2

gas or supercritical CO_2 by using AICV may give a better distribution of CO_2 in a larger area of the reservoir. This leads to a broader contact between CO_2 and the residual oil in the reservoir, resulting in increased EOR. Choking back CO_2 by using AICV may also result in increased drawdown in the zones with high oil saturation, and thereby increased oil production and recovery. A better distribution of CO_2 in the reservoir contributes to a larger storage capacity of CO_2 in the reservoir, and thereby more CO_2 storage.

Thin-oil-rim reservoir with light oil

The experiments with light oil are performed in the test facilities at Equinor and InflowControl AS, and the obtained results are presented in paper 1 and 8, respectively. Light oil is defined as oil with density less than 875.7 kg/m^3 (API gravity greater than 30.1° API). In this study the viscosity and density of the oil samples are 1.02 cp and 760 kg/m^3 (paper 1), and 2.1 cp and 870 kg/m^3 (paper 8) at reservoir condition. Simulations are performed with ECLIPSE 100 (paper 1) and CMG (paper 8). The purpose of the tests and simulations is to evaluate the impact of AICV on the IOR in a thin-oil-rim reservoir.

AICV performance with light oil, lab experiments

The performance curves presented in paper 1 for both ICD and AICV are shown in Figure 5-24. The density of the hydrocarbon gas and the oil are 140 kg/m^3 and 760 kg/m^3, respectively. Oil viscosity is measured to be 1.02 cp at 70°C and 200 bar. The oil flow rates through the ICD and AICV are equal at 20-bar pressure drop. The gas flow rate is significantly reduced from approximately 0.84 m^3/h for the ICD at 20 bar, to 0.14 m^3/h for the AICV (about 83% reduction). A considerable reduction in the water flow rate from 0.34 m^3/h for the ICD to 0.23 m^3/h for the AICV (about 33% reduction) is also obtained.

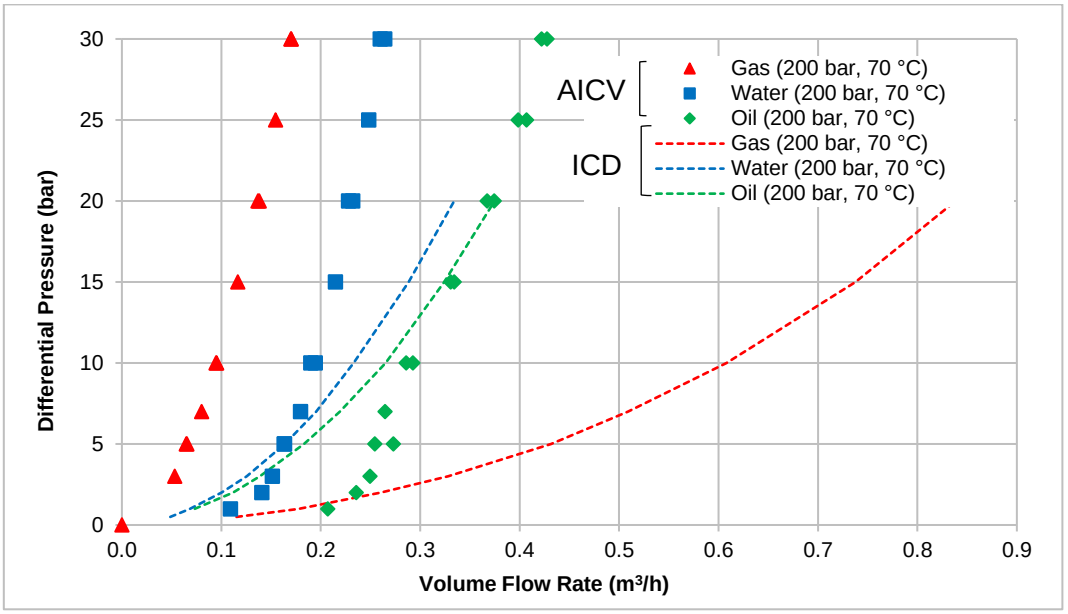

Figure 5-24: Comparison of single-phase flow performance of the ICD (dashed lines) and AICV (points) for oil 1.02 cp, water 0.41 cp, and gas 0.02 cp.

Two-phase oil/water and oil/gas performance of AICV is shown in Figure 5-25, and the total volume flow rate vs. GVF and WC at 10-bar and 20-bar pressure drop are plotted. As can be seen from the figure to the left, the total volume flow rates decrease significantly from 60% until 100% WC. The AICV gradually chokes when the WC increases from 60% to 100%. The maximum flow rate through the AICV at 60% WC is 0.5 m^3/h at 20 bar. The two-phase oil/water performance for ICD is known to be linear, which means that oil flow rate decreases linearly with an increasing WC, while the AICV performance does not follow the linear trend. This behavior allows the AICV to obtain more oil at the lower WC ranges. The GVF behavior is shown in the figure to the right. If oil flashes in the reservoir towards the inflow zones, gas will be released. AICV is open when the local GVF is up to 20% allowing the oil together with gas to flow through the valve. AICV closes from 20% GVF until 100% pure gas flows through the valve. At this point AICV is closed for gas and the only remaining flow is through the pilot flow.

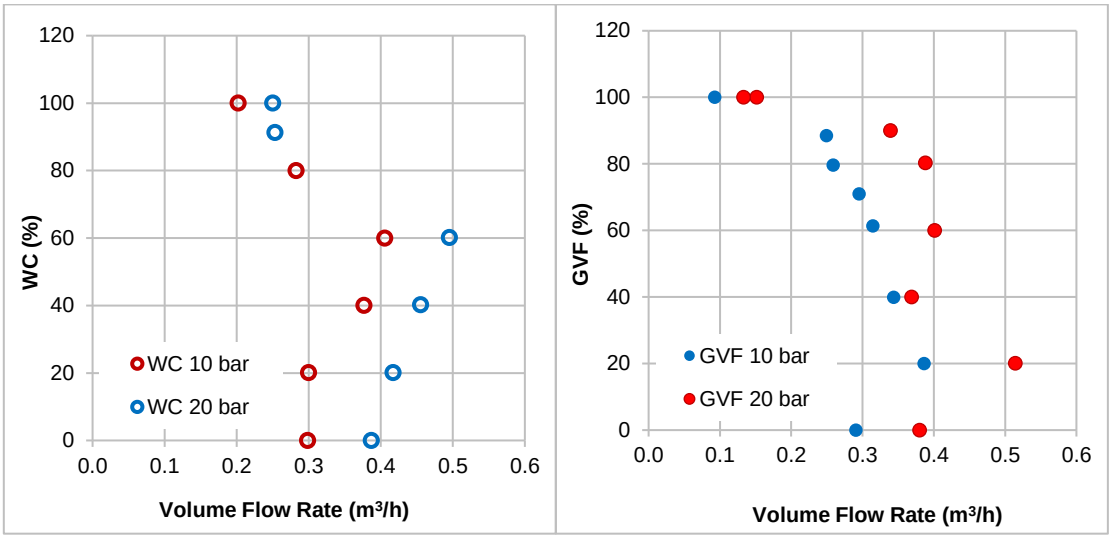

Figure 5-25: Two-phase behavior of AICV in the WC (left) and GVF (right) range from 0-100% at 10-bar and 20-bar ∆p.

Paper 8 presents the experimental results that are performed using the test facilities at InflowControl AS. The results are obtained using model oil with viscosity 2.1 cp, pressurized air with density 92 kg/m^3, and water with viscosity 0.41 cp. These conditions represent the Troll field conditions. At a 15-bar pressure drop, the oil/water ratio for AICV is 2.60, while it is 1.08 for ICD. Also, the oil/gas ratio at the same pressure drop for AICV is 3.20, while it is 0.36 for ICD, see Figure 5-26. The corresponding values of the oil/water ratio and oil/gas ratio for the RCP valve are 1.33 and 0.55 [17].

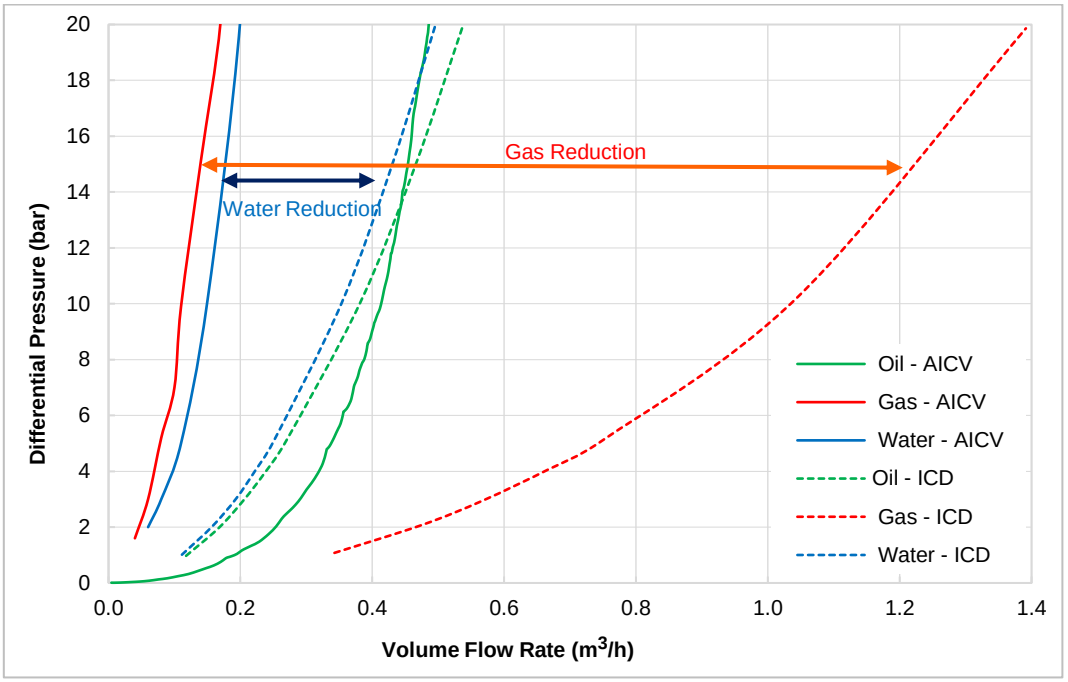

Figure 5-26: Performance curves for oil 2.1 cp, gas 0.02 cp, and water 0.41 cp for ICD and AICV.

The GVF behavior of AICV and ICD is shown in Figure 5-27. The oil flow rate at 15-bar differential pressure through both ICD and AICV is 0.45 m^3/h. As the amount of gas (GVF) increases, AICV chokes the gas flow, while ICD does not restrict the gas production. When the GVF reaches 100%, the volume flow rate through the ICD is 1.27 m^3/h, which is three times more than the volume flow rate for pure oil through the ICD.

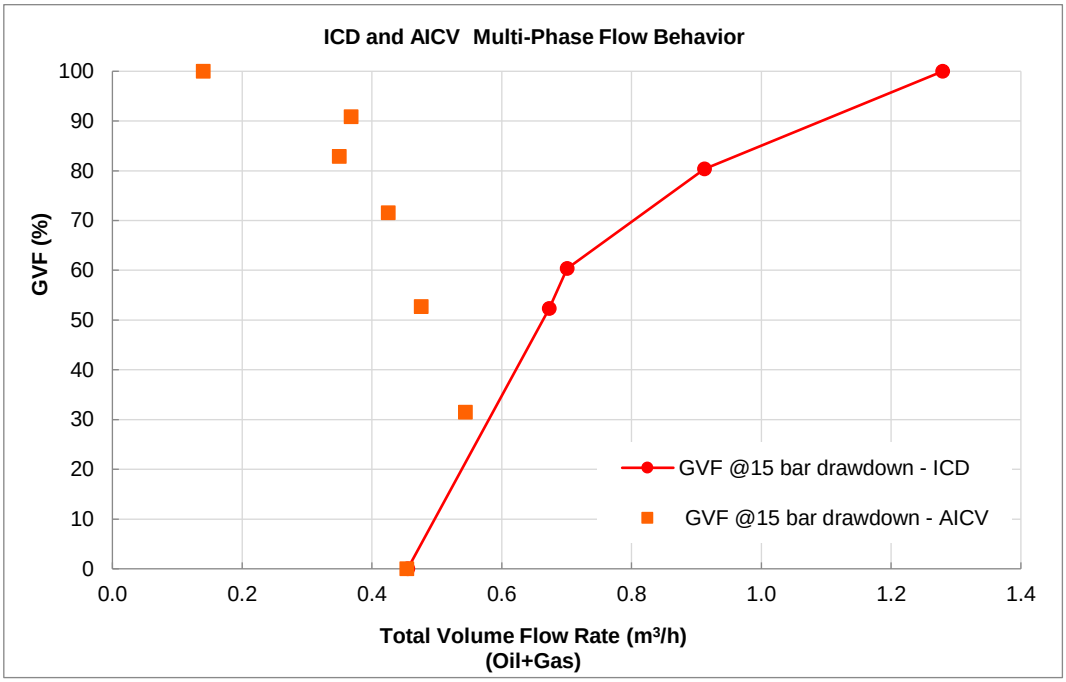

Figure 5-27: Multiphase flow behavior for ICD and AICV.

The AICV restricts the gas flow significantly, specifically at higher GVF, which is what makes this technology unique compared with other inflow control technologies including passive and autonomous AICDs [25].The single and multiphase tests results performed at the InflowControl AS laboratory confirm that AICV significantly restricts the gas and water flow rates compared with ICD. The results are consistent with the results obtained from the Equinor laboratory.

AICV performance in a thin-oil-rim reservoir, simulations

The experiments performed at the Equinor laboratory with 1.02 cp oil is used to develop a reservoir case study in ECLIPSE 100. The oil viscosity in the reservoir case study is assumed to be 0.6 cp. Ideally the test condition and reservoir condition should be the same. In this case, the best to do was to calculate the performance curve for 0.6 cp oil based on the RCP model. The result of the changed oil viscosity and the model match are shown in Figure 5-28. All the other fluid properties in the experiments were very close to the reservoir case study and needed no correction.

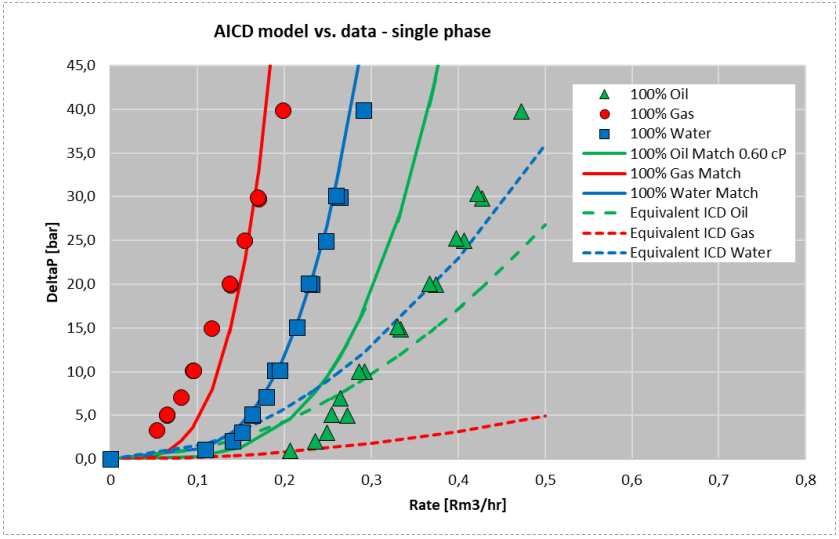

Figure 5-28: RCP model match vs. experimental data. 1.02 cp oil viscosity in experiment and 0.6 cp oil viscosity in model.

The matched model is tested in a North Sea thin-oil-rim development scenario. The reservoir is a thin-oil-rim reservoir with a large gas cap and a strong underlying aquifer. The oil column is only around 6.5 m, while the gas cap average column is approximately 30 m, and the aquifer is considered as an unlimited regional aquifer. The reservoir model as shown in Figure 5-29 has a grid size of 50 m x 50 m orthogonal grid, with a varying cell thickness vertically refined in the oil column down to 0.5 m. The development strategy is long horizontal tri-lateral wells with a dense well spacing. All wells are placed 2.5 m below the gas cap in the 6.5 m oil column. The maximum production is 2500 std m^3/d of liquid, with a GOR lower than 600 std m^3/std m^3, for the first 5 years. The wells are modelled as multilateral segmented wells with inflow control devices along the entire horizontal section. The inflow devices are upscaled to the reservoir grid of 50 m, and do not include annular flow. This is equivalent to having production swell packers for every 50 m. Less swell packers will be used commonly, but this can be an optimization for later studies. Three completion scenarios are compared; 4x4 mm ICD per 12 m as an approximation for sand screens only, 1x1.6 mm ICD per 12 m, and 1xAICV per 12 m. [126]

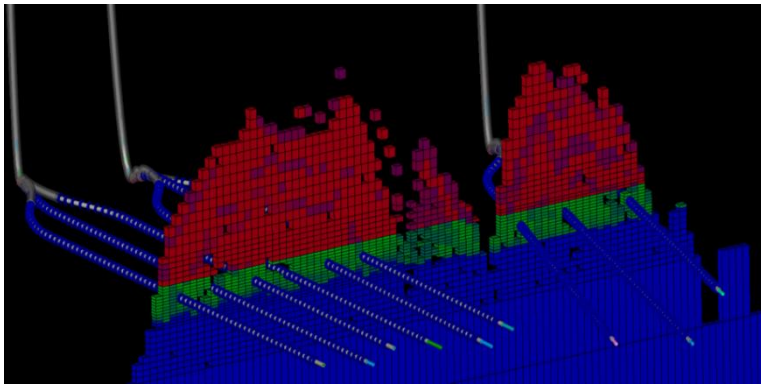

Figure 5-29: Reservoir model showing gas in red, oil in green and water in blue at initial conditions. Vertical to horizontal scale is aggregated 30:1 [126].

The results from the simulations are shown in Figure 5-30 and demonstrate that, by using AICVs, 17.5% and 4.2% extra cumulative oil relative to the screen case and the ICD case is obtained. In addition, the GOR development for the cases, demonstrate that the GOR level is reduced when AICVs are utilized. AICVs produce less unwanted gas from the gas cap and allow the well to produce for a longer period at a high liquid rate without needing to choke back due to high GOR.

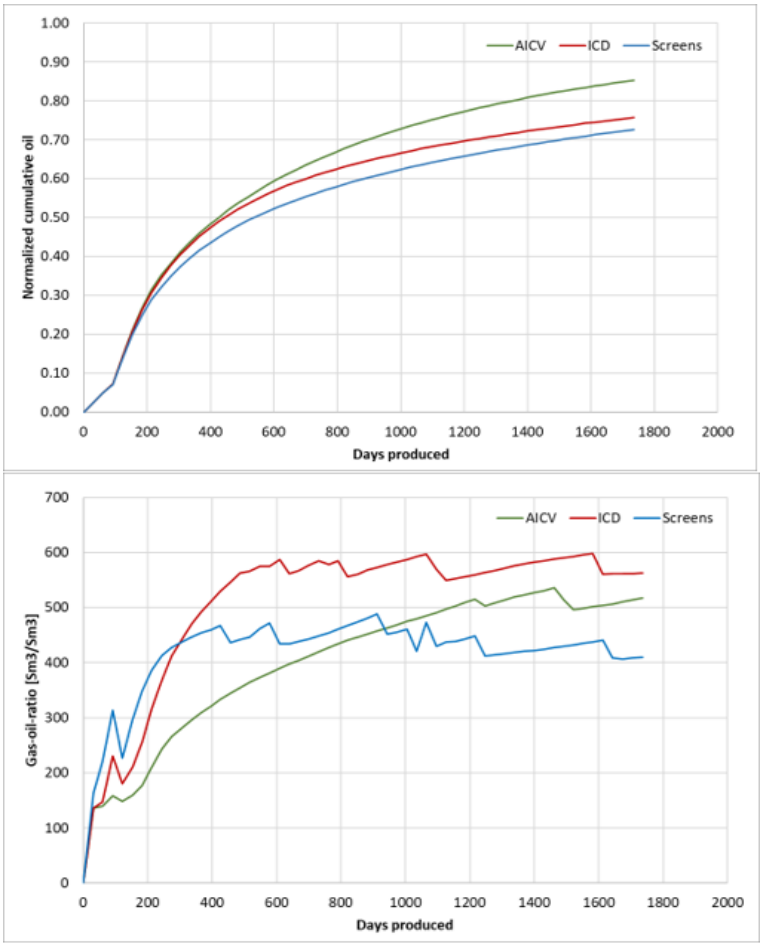

Figure 5-30: Cumulative oil and GOR development for the simulation cases.

Another thin-oil-rim reservoir case study with the typical Troll field reservoir conditions is considered for simulations, and the results are presented in paper 8. The most important properties of the heterogenous reservoir and the fluids used for the simulations are presented in Table 5-7.

Table 5-7: Reservoir and fluid properties.

Parameter	Value	Unit
Viscosity	2.1	cp
Density	870	kg/m^3
Gas/oil ratio	42	std m^3 /std m^3
Bubble point pressure	12500	kPa
Initial temperature	68	°C
Initial pressure	12500	kPa
Porosity	0.3	–
Horizontal permeability	42–7282	md
Vertical permeability	20–5058	md
Reservoir length, width, height	4500, 201, 73	m
Oil column thickness	7	m
Initial oil saturation	0.85	–
Initial water saturation	0.15	–

The well model consists of two pipes that represent the wellbore and the production tubing. The wellbore is a pipe with a length and inner diameter of 3500 m and 0.2159 m (8.5 in.), and the production tubing is a pipe with a length and inner diameter of 3500 m and 0.1397 m (5.5 in.). It is assumed that the well is located at a depth of 2096 m in the thin oil column and 4 m below the gas cap.

In the simulations, AICV/ICD tables (FCD tables) are developed in CMG STARS based on data from the experiments (Figure 5-26 and Figure 5-27). The FCD tables are used to implement the behavior of the AICV/ICD using their characteristics and the reservoir fluid properties. In addition, a workflow for developing the AICV/ICD tables in the simulator is proposed in the paper.

The model is run for 5 years to investigate the oil production. The minimum and maximum timesteps are set to 0.00001 days and 0.25 days, respectively. In addition to the main case study with AICV completion, the simulations are conducted for similar cases with ICD completion and one case that represents sand screens only.

Figure 5-31 illustrates the pressure in the tubing for the completion scenarios during the production period. As can be seen from the figure, AICV has the highest pressure drop ($P_{reservoir} - P_{tubing}$) over the whole production period. The higher pressure drop indicates that AICV chokes the gas flow entering the well for a longer period. This will delay the excessive gas production that will eventually take over the oil production.

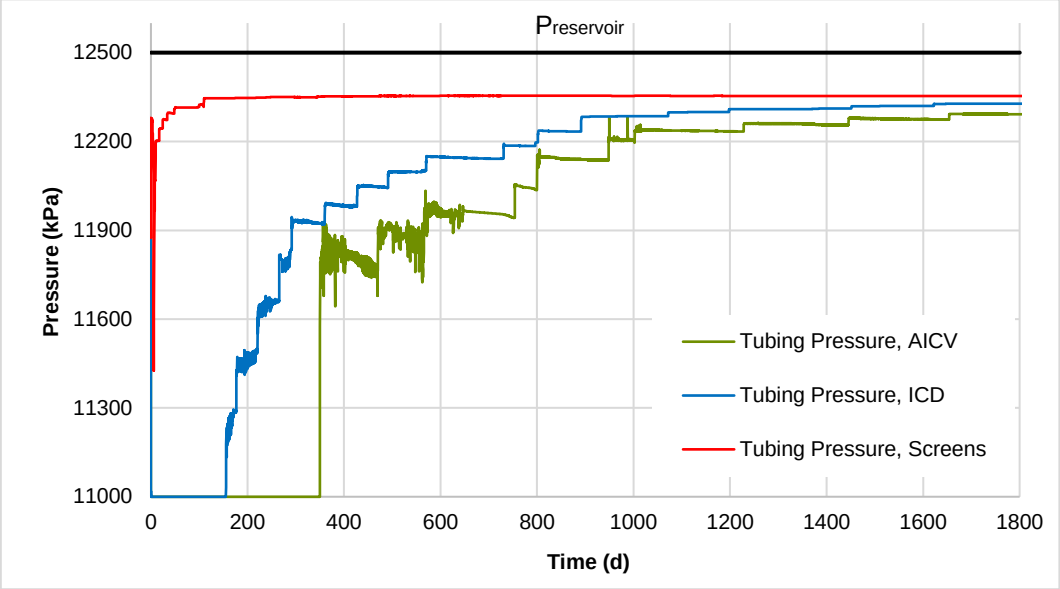

Figure 5-31: Pressure changes of the completion scenarios with time.

Figure 5-32 illustrates the cumulative oil and gas produced for the simulated cases by time. There is an insignificant difference between accumulated oil in the ICD and sand screen cases, whereas the accumulated gas drops by using ICDs compared with sand screens. However, the difference between accumulated oil in the AICV case compared with the two other cases is significant. Also, because of the choking effect of the AICVs on low-viscosity fluids like gas, the amount of accumulated gas drops significantly when the well is completed with AICVs. The cumulative oil produced is 48.7% more when using AICVs compared with using ICDs and sand screens. Owing to the better performance of AICV in both single- and multiphase flow regions, the amount of accumulated gas after 1,825 days of production is reduced by 22.5% and 26.7% relative to the ICD and sand screen cases, respectively. When the gas enters the well, AICV starts to close gradually as the gas mass fraction increases. This behavior, which is based on the experimental data, was implemented in the FCD control tables.

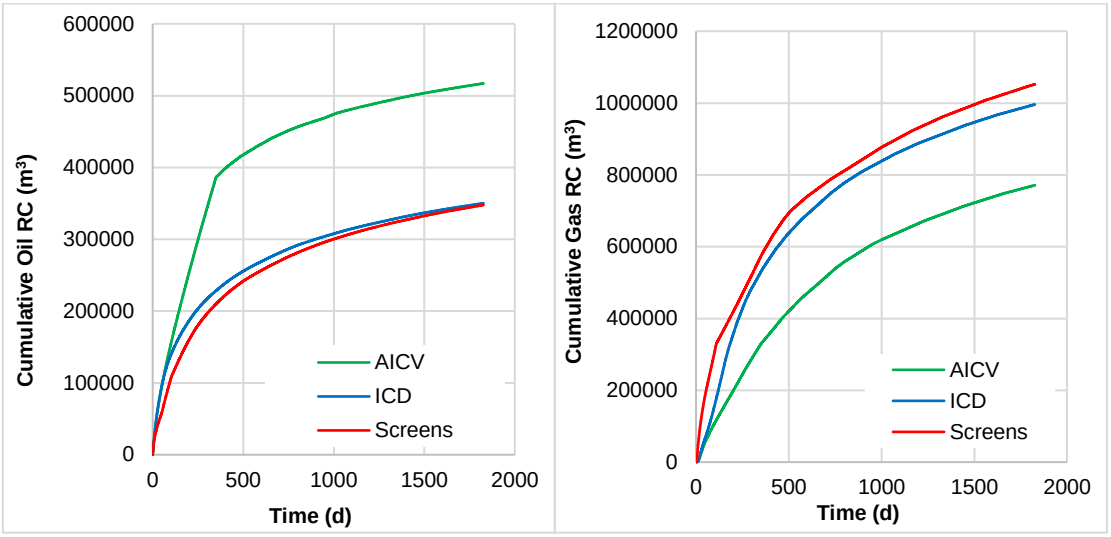

Figure 5-32: Accumulated oil and gas from the well by time.

The simulated oil production agrees with the AICV performance results from the experiments, see Figure 5-33. This shows that the implementation of the workflow for generating the FCD tables in the simulator has been successful.

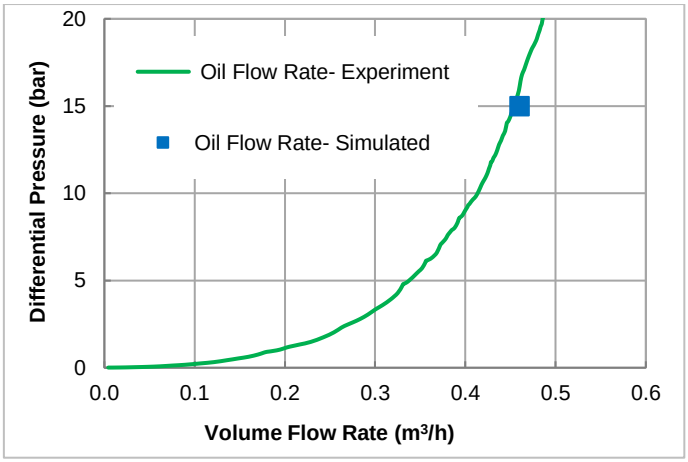

Figure 5-33: Oil flow rate from experiment and simulation.

By evaluation of the experimental and simulation results for thin-oil-rim reservoirs, it can be concluded that the wells are producing at a beneficial GOR for a longer period for the AICV case compared with the cases with ICDs and sand screens. Keeping the GOR at a relatively low level allows the production wells to stay longer at a high liquid rate without needing to choke back because of high GOR. This can be achieved by using advanced inflow control technologies such as AICVs. It can be concluded that, deploying AICVs in the most challenging light oil reservoirs with high GOR can be beneficial with respect to increased production and recovery.

Annulus flow simulations with OLGA and NETool

A simple case is proposed in this section to understand the mechanism of different simulators in calculating the multiphase flow properties. NETool uses modified Darcy's law, which is a no-slip correlation, for flow in annulus filled with formation or gravel, while OLGA utilizes correlation with considering slip between the phases. However, it is also possible to perform the simulations in OLGA without slip. In both cases it is assumed that a gas breakthrough occurs in the toe section of the well.

Figure 5-34 shows the comparison of the GVF behavior along the annulus in OLGA (with and without slip) and NETool (without slip). The GVF performance along the annulus is almost the same for the NETool case and OLGA case with no-slip assumption. The GVF is almost constant along the annulus towards the heel. NETool uses a homogeneous model which assumes that all phases travel with same speed in the form of a mixture (no-slip). However, in the case of gas breakthrough in a real case, the gas travels much faster than the oil along the annulus with low pressure gradients because of much lower gas viscosity compared with the oil viscosity.

The GVF performance along the annulus simulated using NETool and OLGA illustrates how different the reservoir simulators behave for similar cases. The difference is most probably due to the fact that NETool and most of the reservoir simulation tools (except for OLGA) calculate the multiphase flow properties in annulus with no-slip assumption.

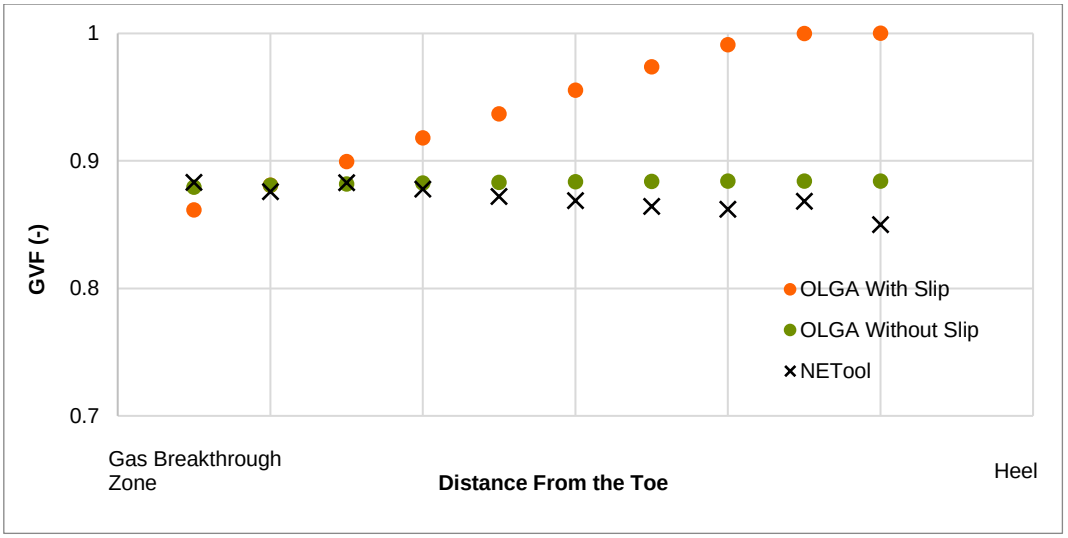

Figure 5-34: Comparison of GVF behavior along the annulus in OLGA and NETool.

Mathematical modelling

This chapter includes the results from uncertainty analysis of the RCP model, the proposed density and viscosity model, and modelling through dimensional analysis approach.

Uncertainty analysis

The study in paper 2 is an attempt to revise the original RCP model. This is done initially and as the first phase through the quantification of the uncertainties within the model and the measurements. A number of experiments with different oil viscosities were carried out to obtain the performance curves and to form the basis for fulfillment of the objective of paper 2. Figure 5-35 shows the AICV performance curves for oil at different viscosities.

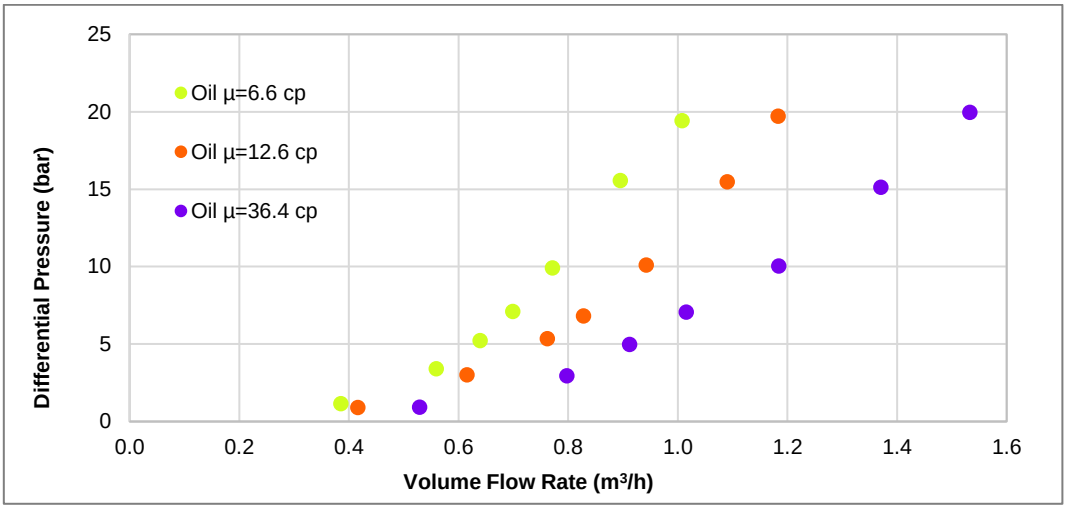

Figure 5-35: AICV performance curves.

The model parameters in equation (29), α, x and y, are denoted with θ and are estimated within the Bayesian inference. The choices of the priors and the likelihoods for each parameter are illustrated in Figure 5-36.

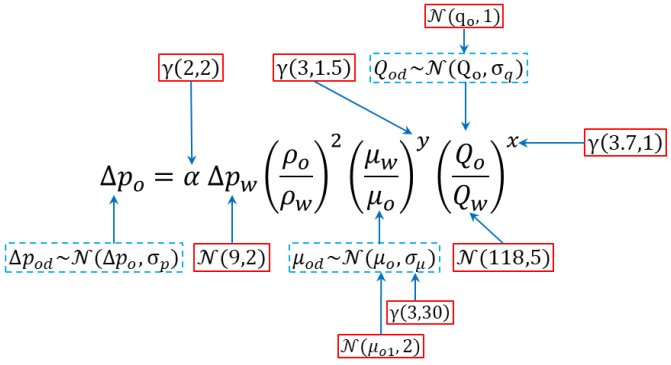

Figure 5-36: The choice of prior distribution (in red/whole) and the likelihood (in blue/dashed).

The dataset used in the MCMC simulation is the performance curves for oil with viscosities 6.6 cp and 36.4 cp, see Figure 5-35. The marginal posterior distributions of the model parameters are shown through the pairs plot in Figure 5-37. It is basically 1D and 2D histogram of the samples of the model parameters. The histogram density of the parameter α reveals that the model is hugely over predicting the relative pressure drop over the valve. More specifically, the pressure drops over the valve have to be scaled down to 2.2%-3.2% of their predicted values by the model in order to be consistent with the measurements. [118]

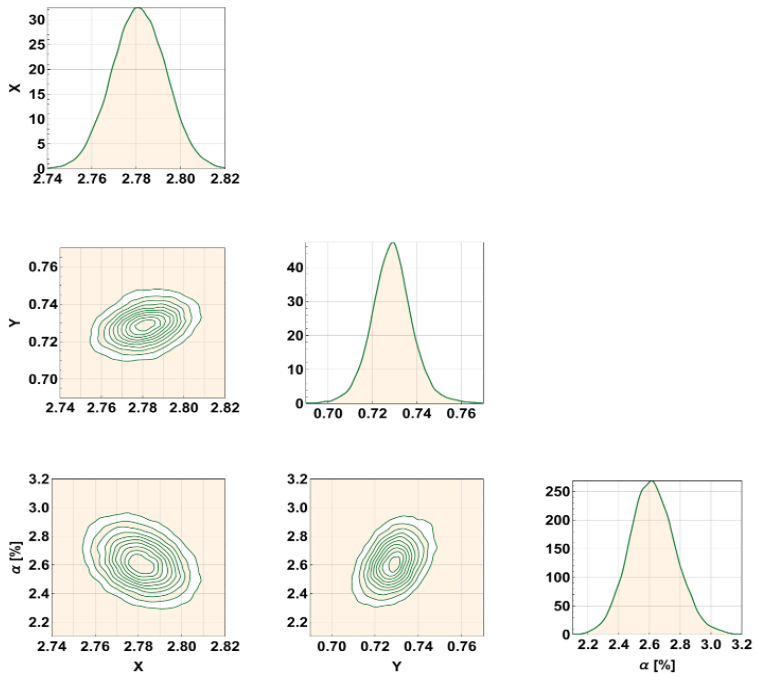

Figure 5-37: Pairs plot of the model parameters.

The measurements and the posterior samples from the MCMC with 99% credible intervals are plotted in Figure 5-38. As it can be seen from the figure (top row), at the calibration step, the model can describe most of the variations in the measurements.

The validation is conducted on a new dataset with viscosity 12.6 cp, which was not used in the estimation of the model parameters. The result of the cross-validation with 99% credible error-bars is given in Figure 5-38 (bottom row). For low flow rates, the model prediction is within the 99% credible interval of the measurements. However, it appears that for high flow rates, the model has tendency to over-predict the differential pressure over the valve.

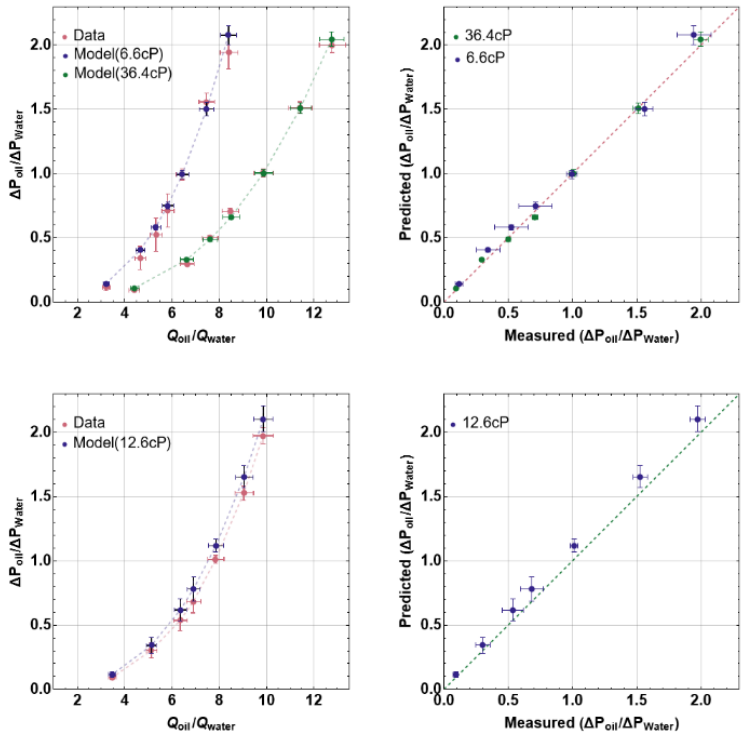

Figure 5-38: Calibration (top row) and validation (bottom row). The dashed lines are drawn for visualization purpose.

The model validation has revealed that there is a tendency for the modified model to over-predict the pressure drop. The deviation of the model described in Figure 5-38 also indicates that the model is very sensitive to small changes in viscosity. The results imply that the original RCP model needs revision. This leads the study to perform accurate measurements of density and viscosity for different oils to develop correlations. The correlations can be used further to develop a model within Bayesian approach that can represent and explain the AICV behavior. However, this has not been completed in this thesis, but will be studied as future work.

Density, modelling and estimation

The density of silicone oils at different temperatures were measured by using the measuring devices presented in ‘’*Density and viscosity measuring instruments at USN”* section. The test results are presented in Figure 5-39. Consistent with the behavior of most liquids, the density of silicone oil inversely correlates with increasing temperature.

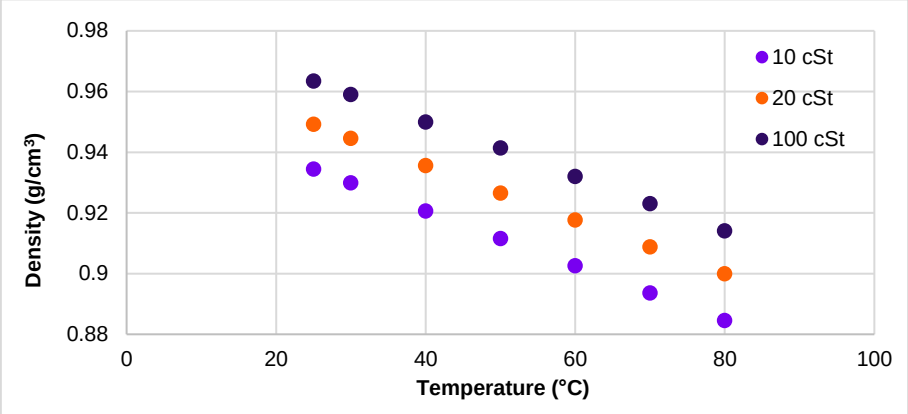

Figure 5-39: Density vs. temperature for 10, 20, and 100 cSt oil.

This study aims to develop a model capable of accurately predicting oil density in response to temperature variations within a confined temperature range. It is assumed that, similar to gases, the molecules in the oil are loosely packed. Then according to Charles's law, the volume of the oil (V) is positively proportional to its absolute temperature (T) at constant pressure. This means that,

$$V \propto T \tag{32}$$

As a first-order approximation, it is assumed that the relative change in volume is proportional to the relative change in temperature. For a minor change in temperature, it is expected a slight change in the volume. Furthermore, this change in volume is assumed to be linear and proportional with the change in temperature, and is expressed as follows:

$$V(T + \Delta T) = V(T) + c\Delta T\, V(T) \tag{33}$$

in which c is a dimensionless constant greater than zero, representing the dimensionless coefficient of thermal expansion. The arranged form of the equation (33) is as follows:

$$\frac{1}{V(t)} \frac{V(T + \Delta T) - V(T)}{\Delta T} = c \tag{34}$$

Letting $\Delta T \rightarrow 0$:

$$\frac{d\ln(V)}{dT} = c \tag{35}$$

Solving the equation (35) with respect to the reference temperature and volume, T_0 and $V_0 = V(T_0)$, gives the following equation:

$$V(T) = V_0 \exp\left(c \frac{T - T_0}{T_0}\right) \tag{36}$$

Note that although, in general, the liquids do expand and contract with temperature changes, the rate of expansion (or the coefficient of thermal expansion c) is much lower than that of gases. Density is defined as the amount of mass per unit volume. Since the mass does not change with temperature, then the change in density is only caused by the change in volume. Accordingly, the expression has the following form:

$$\frac{M(T)}{V(T)} = \rho(T) = \rho_0 \exp\left(-c\frac{T-T_0}{T_0}\right), \tag{37}$$

in which ρ_0 is the density of the liquid at the reference temperature. As previously argued, the value of c should be small for liquids. Thus, for the temperatures in the neighborhood of T_0, the exponential term is approximately linear and is as follows:

$$\rho(T) \approx \rho_0\left(1 - c\frac{T-T_0}{T_0}\right) \tag{38}$$

Therefore, the analysis suggests that within a reasonable temperature range around T_0, the density of a silicone oil changes linearly with respect to the relative temperature change. In this work it is assumed that T_0=298.15 K (25℃).

In summary, it is proposed that within a narrow temperature range around T_0 (25℃), the density behaves as a linear function of relative temperature, which is:

$$\frac{\rho(T)}{\rho_0} = 1 - c\frac{T-25}{298.15}, c > 0 \tag{39}$$

in which, for sake of simplicity, the unit of T is chosen to be Celsius. It is expected that as the temperature increases away from T_0, the deviation from linearity become more evident. The dimensionless coefficient of thermal expansion, c, is expressed as [127]:

$$c = \alpha \times 298.15 \times 10^{-4} \tag{40}$$

in which, α is known as coefficient of thermal expansion with unit of K^{-1}. Thus, the equation (39) can be rewritten as:

$$\frac{\rho(T)}{\rho_0} = 1 - \alpha \times 10^{-4}(T-25), \alpha > 0 \tag{41}$$

$$\varepsilon \sim \mathcal{N}(0, \sigma^2)$$

where ε represents the model error. For silicone oils the α values vary slightly from 9.2 for the high viscosity oils (~10^6 cSt) to 13.4 for the low viscosity oils (~10^{-2} cSt) [127]. At the present case, the temperature ranges of the interest are between 25℃ and 100℃. Then according to the model, for the temperatures 25℃≤ T≤100℃, it is expected that,

$$0.9\rho_0 < \rho < \rho_0 \tag{42}$$

This means that as the temperature is increased from 25℃ to 100℃, it is expected that the density would at most fall by 10%.

Estimation of the coefficient of thermal expansion

The focus is on estimating α within the linear model described in equation (41). It is crucial to acknowledge at least two primary factors contributing to deviations between the model predictions and empirical observations. The first major source is due to the assumption that the density is a linear function of relative change in temperature. The model generates a value for density for each given temperature. However, due to the simplifying assumptions, the densities predicted by the model might deviate from the true density values. Thus, the model error which is normally distributed; $\varepsilon \sim \mathcal{N}(0, \sigma^2)$ is taken into account. The model parameters, σ^2 and α, are estimated through Bayesian approach and the choice of prior distributions and the likelihoods are illustrated in Figure 5-40 .

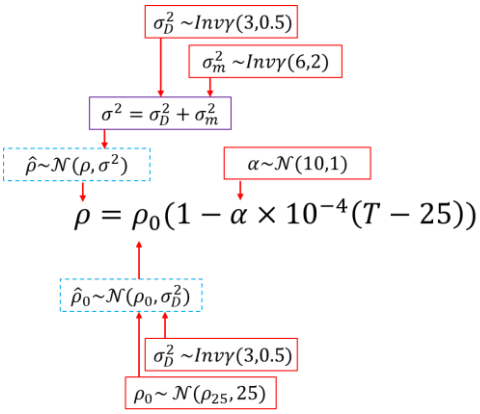

Figure 5-40: The choice of prior distribution (in red/whole) and the likelihood (in blue/dashed).

The marginal posterior distributions, with proposed analytical form in red is given in the Figure 5-41.

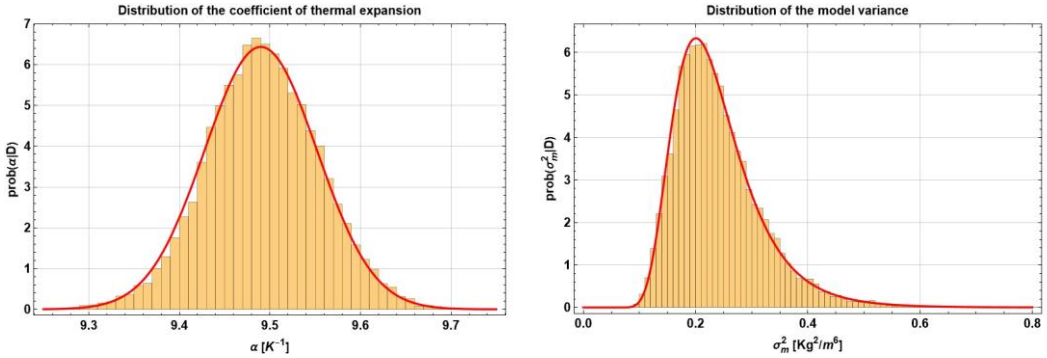

$\alpha \sim \mathcal{N}(9.49, 3.8 \times 10^{-3}$

$\sigma_m^2 \sim Invγ(11.21, 2.45)$

Figure 5-41: Marginal posteriors of the model parameters.

The measurements and the prediction of the model with 90% credible intervals are plotted in Figure 5-42. As it can be seen from the figure, the proposed density correlation can describe most of the variations in the measurements.

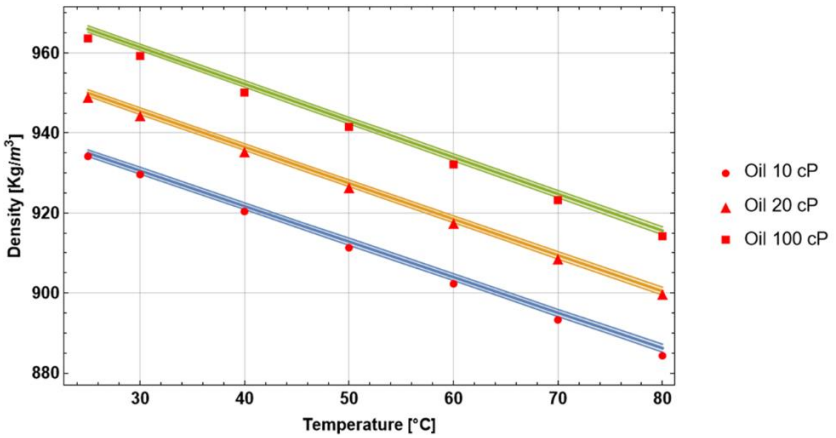

Figure 5-42: Experimental vs. model with 90% credible band.

Kinematic viscosity, modelling and estimation

The viscosity of silicone oils at different temperatures were measured by using the measuring devices presented in ‘’*Density and viscosity measuring instruments at USN”* section. The test results are presented in Figure 5-43.

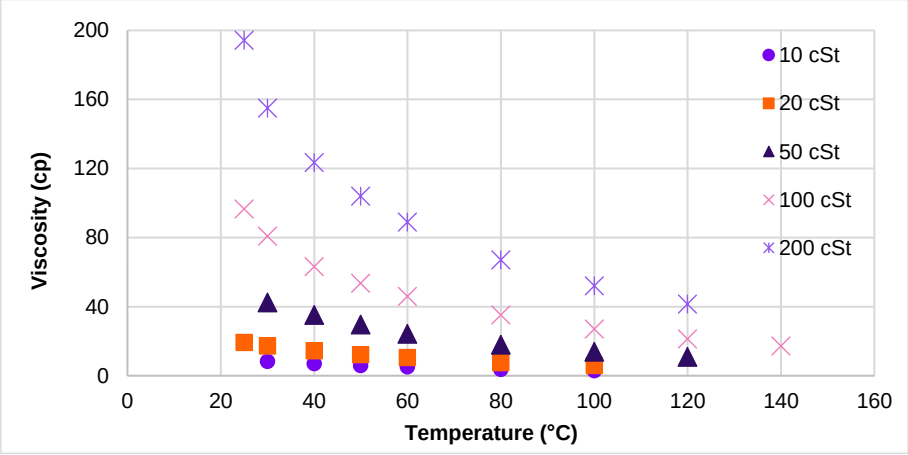

Figure 5-43: Viscosity vs. temperature for 10, 20, 50, 100, and 200 cSt oil.

The viscosity changes decrease as the temperature increases. The kinematic viscosity of silicone oils as a function of temperature is given by the following equation:

$$\nu(T) = \nu_0 e^{-\beta(T-25)} \tag{43}$$

where, ν_0 is the kinematic viscosity at 25°C, and β is viscosity-temperature coefficient (VTC). A model which predicts the β as a function of ν_0 at 25℃ is proposed:

$$\beta(\nu_0) = \frac{\beta_\infty}{1-\exp\left(-r(\nu_0-\gamma)\right)} \qquad (44)$$

$$\varepsilon \sim \mathcal{N}(0,\sigma^2)$$

where β_∞ is the maximum value of VTC, γ is the viscosity at which $\beta = \beta_\infty/2$ and is called the inflection viscosity. The inflection viscosity is the viscosity at which the rate of change of β with respect to ν_0 is at its highest value. Moreover, r is logistic rate and influences how quickly β grows to its maximum value. Basically, r sets the upper limit for the rate of change of β and therefore it is called the logistic rate. The model generates β-value for each given ν_0. However, due to the simplifying assumptions, the β-values predicted by the model might deviate from the true β-values. Hence, ε is the model error and is estimated by allocating a normal distribution, and σ is the standard deviation of the model mismatch. The values of VTC are tabulated for number of silicone oils, with respect to their kinematic viscosities at 25℃ [127].

The model parameters, β_∞, r, γ, and σ^2, are estimated through Bayesian approach and the choice of prior distributions and the likelihoods are illustrated in Figure 5-44.

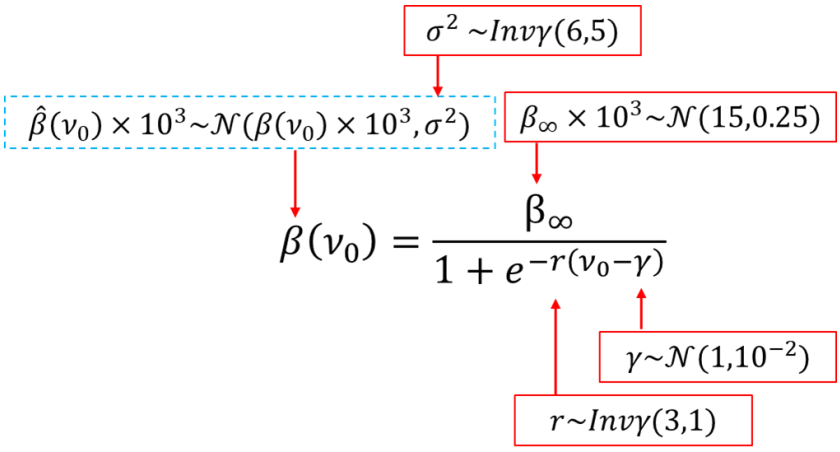

Figure 5-44: The choice of prior distribution (in red/whole) and the likelihood (in blue/dashed).

The marginal posterior distributions, with proposed analytical form in red is given Figure 5-45.

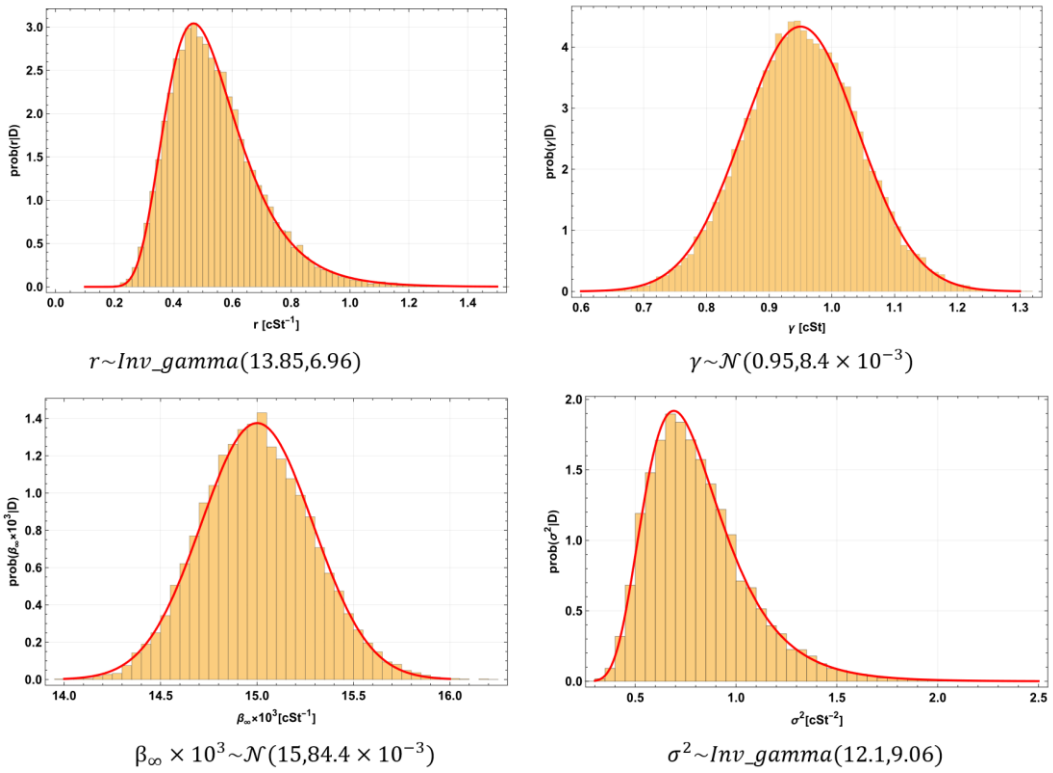

Figure 5-45: Marginal posteriors of the model parameters.

The values from literature [127] and the prediction of the model with 90% credible interval are plotted in Figure 5-46.

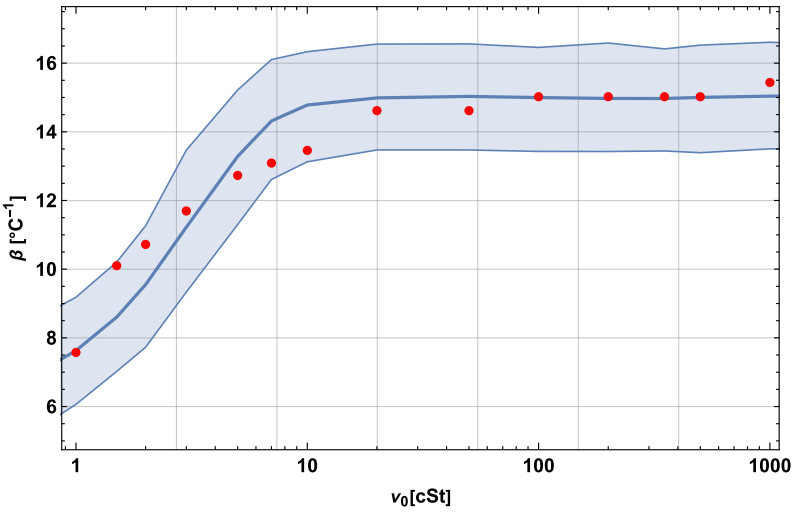

Figure 5-46: VTC with 90% credible band.

Finally, by applying the model with the estimated parameters, its predictive accuracy against the empirical data is validated and is shown in Figure 5-47. The figure incorporates the

uncertainty in ν_0, which may reach up to 10%. As it can be seen from the figure, the proposed model possesses a high predictive accuracy.

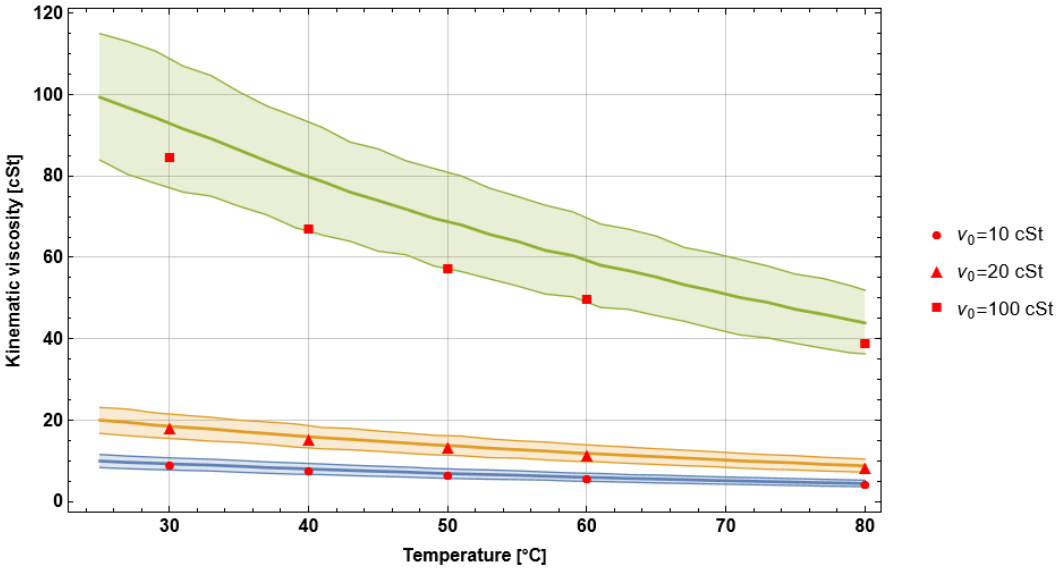

Figure 5-47: Experimental vs. model with 90% credible band.

Dimensional analysis approach

The results from paper 2 indicates that the original RCP model is very sensitive to small changes in viscosity. Hence, the dimensional analysis approach is employed in this work to demonstrate that it is possible to construct models which are less sensitive to variations in their parameter values.

The performance curves with different oils for three AICVs with different dimensions are presented in Figure 5-48. The valves have different inlet and pilot flow elements dimensions. The tests were performed at the flow loop test rig at InflowControl AS. Valve #1 is designed to close for water and keep fully open for oils at SAGD reservoir conditions. The typical viscosities for oil in SAGD reservoirs is above 10 cp. Valve #1 closes for water, is partly open for oil 2 cp and is fully open for oil 39 cp. Valves # 2 and #3 are open for the tested oils. The volume flow rates through the valves depend on the oil viscosities.

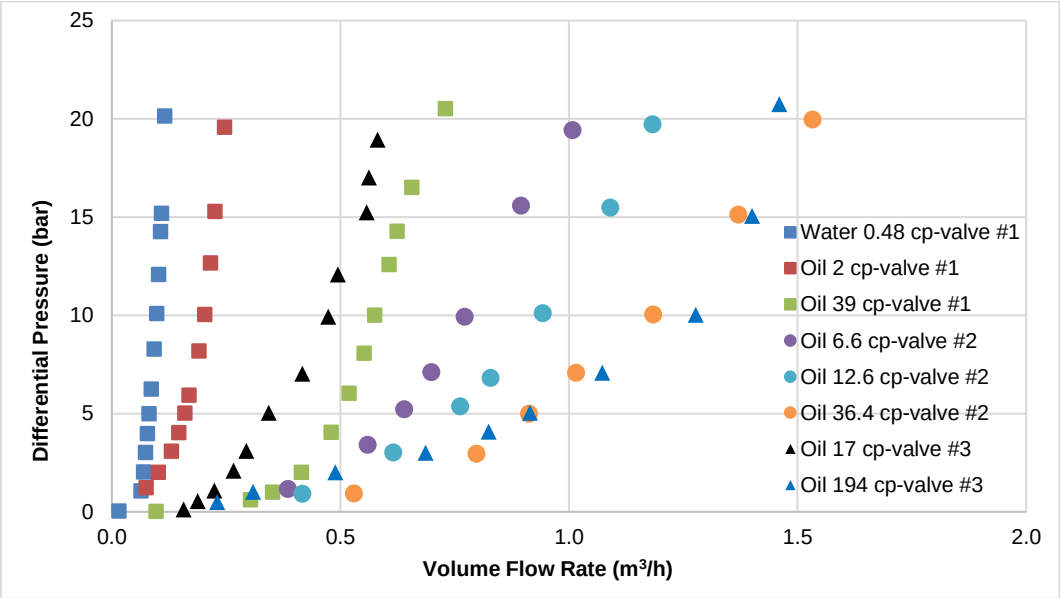

Figure 5-48: Performance curves for three different AICVs.

In this work, by following the steps in Buckingham's Π-theorem [128], the dimensionless groups for the experimental system with AICV are as follows:

$$\begin{cases} \Pi_1 = \left(\frac{D_m}{\nu}\right)^2 \frac{\Delta P_{13}}{\rho} \\ \Pi_2 = Re = \frac{4}{\pi} \frac{Q}{\nu D_m} \\ \Pi_3 = \frac{L_L}{D_L} \\ \Pi_4 = \frac{D_L}{D_m} \\ \Pi_5 = \frac{D_T}{D_L} \end{cases} \tag{45}$$

where the subscripts m, L, and T refer to the main flow, laminar flow element, and turbulent flow element, respectively. D and L are the diameter and length, Q is the total volumetric flow rate exiting the valve, Re is Reynolds number, ΔP_{13} is the total pressure drop across AICV, and ν is the kinematic viscosity. The presentation of data using the dimensionless groups is shown in Figure 5-49.

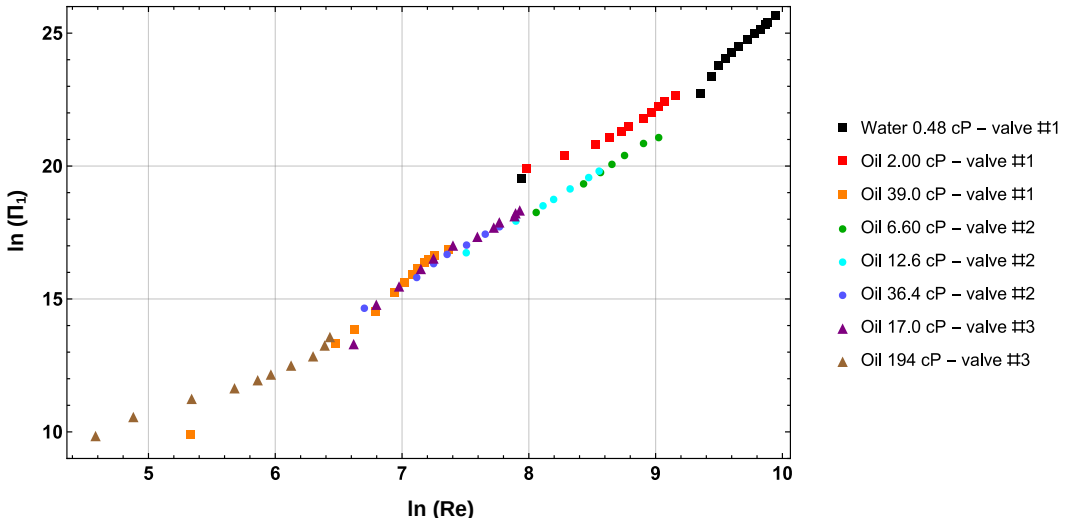

Figure 5-49: Presentation of data using the dimensionless groups.

The momentum of the total flow exiting the valve is the combined momentum of the pilot and main streams. With considering incompressible flow, the pressure and mass balance are as follows:

$$\frac{\Delta P_{13}}{\rho} = \frac{\Delta P_{12}}{\rho} + \frac{\Delta P_{23}}{\rho} \tag{46}$$

$$Q = Q_m + Q_p \tag{47}$$

where the subscript 'p' and 'm' refer to the pilot flow and main flow respectively, ΔP_{12} is the pressure drop through LFE and ΔP_{23} is the pressure drop through TFE. The pressure drop through LFE and TFE are expressed as:

$$\frac{\Delta P_{12}}{\rho} = \frac{1}{2} f_l \frac{L}{D_L} \langle v_l \rangle^2 \tag{48}$$

$$\frac{\Delta P_{23}}{\rho} = \frac{1}{2} f_t \langle v_t \rangle^2 \tag{49}$$

where f_l and f_t are the friction factor and the loss coefficient for LFE and TFE. In addition, $\langle v_l \rangle$ and $\langle v_t \rangle$ are the average fluid velocity through LFE and TFE, respectively and are defined as:

$$\langle v_l \rangle = \frac{Q_p}{A_l} \tag{50}$$

$$\langle v_t \rangle = \frac{Q_p}{A_t} \tag{51}$$

in which A_l and A_t is the flow area for LFE and TFE. Assuming that α denotes the fraction of the total flow that goes through the main line, the volume flow through the main and pilot lines are:

$$Q_m = \alpha Q \tag{52}$$

$$Q_p = (1-\alpha)Q \tag{53}$$

By using equations (47) to (53) in the equation (46) :

$$\left(\frac{D_m}{\nu}\right)^2 \frac{\Delta P_{13}}{\rho} = \frac{1}{2}\left(f_l\left(\frac{L}{D_L}\right)\left(\frac{D_m}{D_L}\right)^4 + f_t\left(\frac{D_m}{D_t}\right)^4\right)(1-\alpha)^2\left(\frac{4}{\pi}\frac{Q}{\nu D_m}\right)^2 \tag{54}$$

Equation (54) by using the dimensionless groups in equation (45) is rewritten as:

$$\boxed{\Pi_1 = \frac{1}{2}\left(\Pi_3 f_l + {\Pi_5}^{-4} f_t\right){\Pi_4}^{-4}(1-\alpha)^2 Re^2} \tag{55}$$

The Reynolds number for LFE is given as :

$$Re_p = {\Pi_4}^{-1}(1-\alpha)Re \tag{56}$$

The models used for calculation of friction factor through LFE depend on the Reynolds number and are given as :

$$f_l = \frac{64}{Re_p} \qquad 0 < Re_p < 400 \tag{57}$$

$$f_l = 27.836\, Re_p^{-0.839} \qquad 400 \le Re_p < 2000 \tag{58}$$

$$f_l = \left[1.8\, Log\left(\left(\frac{\varepsilon}{3.7\, D_L}\right)^{1.11} + \frac{6.9}{Re_p}\right)\right] \qquad 2000 \le Re_p < 20000 \tag{59}$$

$$f_l = 0.002 \qquad 20000 \le Re_p \tag{60}$$

Further, in the present test set-up the LFE roughness is measured as $\varepsilon = 0.0000002$.

By assuming that $$f_t = C_D^{-2} \tag{61}$$

where C_D is the TFE discharge coefficient. The measured C_D values for oil and water through TFE which is a thin-plate orifice are 0.61 and 0.62, respectively.

By using the equations (57) to (60) and the corresponding loss coefficients for oil and water in equation (55), the values for α are estimated. The estimated values for α are shown in Figure 5-50. The figure shows that for oil viscosities in the range of 6.6 cp – 194 cp, the α is almost

constant and close to 1 indicating that the AICV is fully open and that the main fraction of the total flow goes through the main line. For oil 2 cp, α varies with Re from approximately 0.95 to 0.72. This implies that the AICV is partly open for oil 2 cp. For water, α reaches to 0.1 when ln(Re) is about 10, meaning that the fluid is mainly flowing through the pilot flow and the AICV is closed.

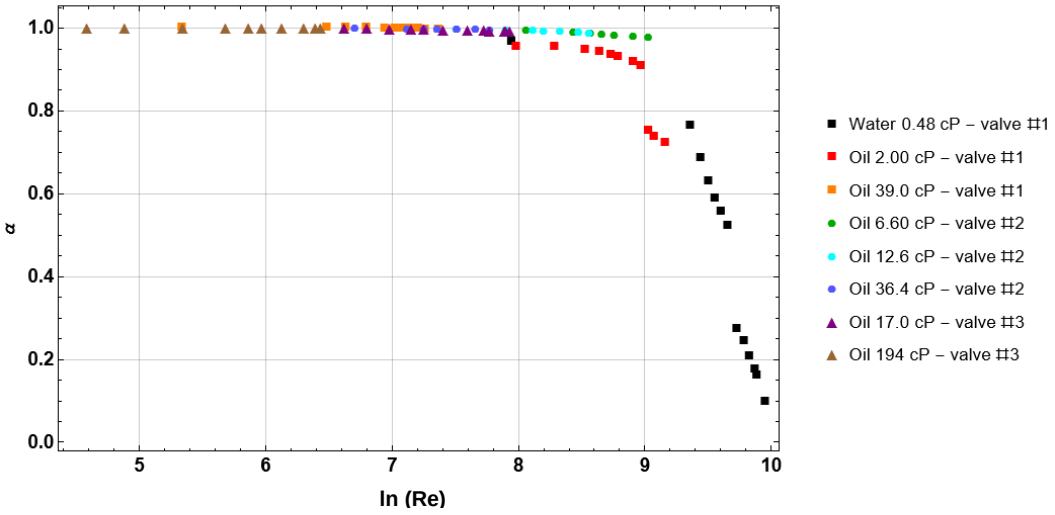

Figure 5-50: Estimated values for α.

The estimated values for α is used to calculate the Re_p in equation (56). The dimensionless group Π_1 is plotted versus ln(Re_p) in Figure 5-51. Π_1 is the dimensionless group containing the total differential pressure across the AICV. The figure illustrates that all points fall on a common curve, as predicted by dimensional analysis. The model indicates that the AICV design parameters described by the dimensionless groups and the flow regime characterized by Re_p are affecting the valve performance. The model can be used in the experimental design and will significantly reduce the required number of experiments. The derived model is less sensitive to variations in the parameter values.

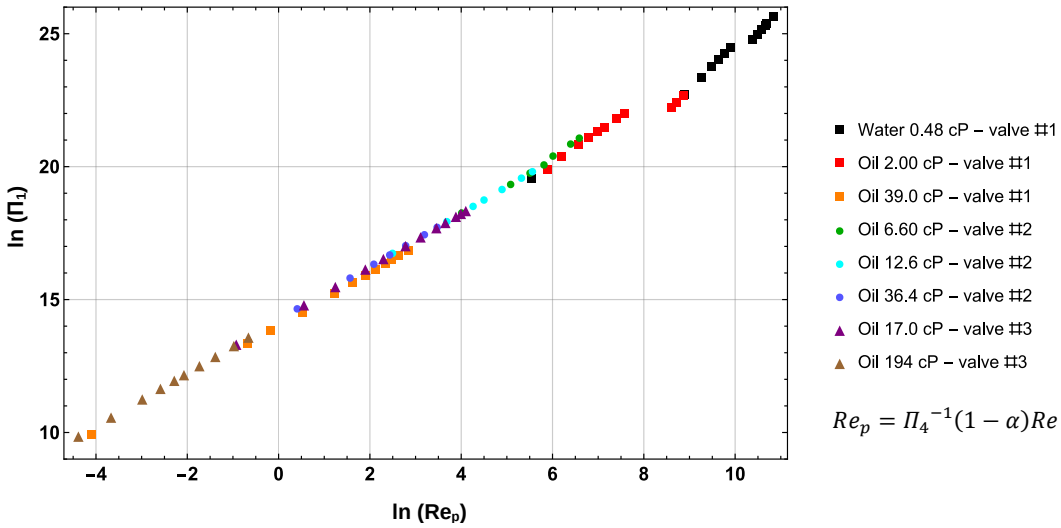

Figure 5-51: Presentation of Π_1 as a function of Re_p.

6 Conclusions and Future Works

This chapter comprises of the main conclusions that has been drawn in the published articles in this thesis, and the recommendations for further works.

Conclusions

The aim of this research work was to improve the multiphase flow performance of the AICV for use in thin-oil-rim reservoirs, and reservoirs using EOR methods. The potential impact of the improved AICV performance on increased oil recovery was investigated by utilizing different types of commercial simulators.

The AICV has been under continuous development since 2012 with main focus on multiphase behavior improvement. The AICV design and multiphase behavior of AICV were improved during this work. Several AICV prototypes were tested under realistic reservoir conditions to find the optimum design. The piston dimension and shape, the combination and dimensions of LFE and TFE, the housing dimension, and the inlet dimension and design are changed to obtain a better multiphase flow behavior.

To evaluate the potential of increased oil production and recovery when using the improved AICV, the results were mainly compared with corresponding cases for ICD and openhole. The experiments were conducted under realistic reservoir conditions and simulations were performed with selected reservoir simulators. Reservoirs using SAGD and CO_2 for EOR in addition to the thin-oil-rim reservoirs face a number of challenges that AICV can potentially mitigate and therefore this work were limited to these applications.

The experimental work consisted of one-phase and multi-phase flow tests for orifice ICD and AICV using water, gas, and oil as the reservoir fluids. The results from the experiments show that AICV restricts the gas and water flow rates significantly compared with an orifice-type ICD, in particular at higher GVF. This behavior makes the AICV technology unique compared with other inflow control technologies.

Performance curves for one and two-phases for orifice ICD and AICV were generated. The results show that under SAGD conditions, the gas flow rate at a 3-bar differential pressure for the ICD is about 3.8 m^3/h while it is about 0.1 m^3/h for the AICV. This indicates that the gas reduction by using AICV is significant. The water flow rates for AICV and ICD at 3 bar are 0.07 m^3/h and 0.44 m^3/h, respectively. Corresponding simulations were conducted in NETool, OLGA/ROCX, and CMG, and the results show that the steam reduction can be up to 64% and

the oil increase can reach 15%. Reduction in steam production will improve the overall SAGD operation performance and will also result in a more cost-effective oil production, as less steam is required to produce each barrel of oil. In addition, a more uniform temperature distribution, and steam conformance are observed in the AICV cases.

For CO_2-EOR application, the results from the experiments show that AICV in comparison with ICD, reduces the water and CO_2 volume flow rates by approximately 58% and 82%, respectively. The results obtained from the corresponding simulations for a case study show that the production of the mixture of water and CO_2 is reduced by 20%. Choking back CO_2 by using AICV may give a better distribution of CO_2 in a larger area of the reservoir. This leads to a broader contact between CO_2 and the residual oil in the reservoir, resulting in increased EOR.

For the case study with light oil in a thin-oil-rim reservoir, at a 15-bar pressure drop, the gas and water flow rates through the passive ICD are approximately 7.35 and 2.4 times more than the flow rates through the AICV. The results indicate that the gas and water reduction by using AICV is significant. The simulations show that the oil production can be increased by approximately 48%. In addition, the wells completed with AICVs, keep the GOR at a relatively low level and this allows the production wells to run at a high liquid rate for a longer period of time. It can be concluded that, deploying AICVs in the most challenging light oil reservoirs with high GOR can be beneficial in terms of increased production and recovery.

Mathematical models were developed for density and kinematic viscosity using the Bayesian approach. The models are based on the experimental data obtained during this work. A model to describe the behavior of AICV was derived based on dimensional analysis. The model can be used in the experimental design and will significantly reduce the required number of experiments.

All the experiments and simulations demonstrate that the improved AICV has a significant potential for increased oil production and recovery.

Recommendations for future works

Despite many efforts that have been devoted to developing realistic reservoir models in order to investigate the effect of AICV on IOR, there are many aspects for further improvements.

There is a possibility to model simple reservoir grids in CFD and for example CMG, conduct a comparative study, and use the gained knowledge to improve the reservoir models in existing reservoir simulation tools. Another recommendation for future work is related to the challenges

with simulations that were described in this work. The challenges may be solved by developing an in-house simulation tool with incorporated black-oil model; a simulation tool that focuses on modelling of the dynamics of AICDs and AICVs and utilizes the reservoir properties such as relative permeability curves, accordingly. The author's intention to modify the RCP model by using Bayesian approach can be pursued through utilizing the developed density and viscosity models.

References

[1] "International Energy Outlook 2021 (IEO2021)." U.S. Energy Information Administration. https://www.eia.gov/todayinenergy/detail.php?id=49856 (accessed.

[2] "International Energy Outlook 2023 (IEO2023)." U.S. Energy Information Administration. https://www.eia.gov/outlooks/ieo/ (accessed 11.10.2023).

[3] "OG21 Strategy - A New Chapter." The Research Council of Norway. https://www.og21.no/strategi-og-analyser/ny-og21-strategi-2021/ (accessed.

[4] "Effective resource management in mature areas " Norwegian Petroleum https://www.norskpetroleum.no/en/developments-and-operations/resource-management-in-mature-areas/ (accessed.

[5] "Improved oil recovery (IOR)." The Norwegian Petroleum Directorate. https://www.npd.no/en/facts/production/improved-oil-recovery-ior/ (accessed.

[6] C. Carpenter, "Smart Horizontal Wells for Development of Thin-Oil-Rim Reservoirs," *Journal of Petroleum Technology,* vol. 67, no. 11, pp. 87-89, 2015, doi: https://doi.org/10.2118/1115-0087-JPT.

[7] A. Hussain, A. T. A. Kumar, S. A. Garni, and M. A. Shammari, "Optimizing Maximum Reservoir Contact Wells: Application to Saudi Arabian Reservoirs," in *International Petroleum Technology Conference*, 2005, vol. All Days, IPTC-10395-MS, doi: 10.2523/iptc-10395-ms. [Online]. Available: https://doi.org/10.2523/IPTC-10395-MS

[8] M. Halvorsen, G. Elseth, and O. M. Nævdal, "Increased oil production at Troll by autonomous inflow control with RCP valves," in *SPE Annual Technical Conference and Exhibition*, 2012, vol. All Days, SPE-159634-MS, doi: 10.2118/159634-ms. [Online]. Available: https://doi.org/10.2118/159634-MS

[9] F. T. T. Al-Khelaiwi, V. M. M. Birchenko, M. R. R. Konopczynski, and D. R. R. Davies, "Advanced Wells: A Comprehensive Approach to the Selection Between Passive and Active Inflow-Control Completions," *SPE Production & Operations,* vol. 25, no. 03, pp. 305-326, 2010, doi: 10.2118/132976-pa.

[10] P. E. Llaguno, F. Moreno, R. Garcia, Z. Mendez, and E. Escobar, "A Reservoir Screening Methodology for SAGD Applications," in *Canadian International Petroleum Conference*, 2002, vol. All Days, PETSOC-2002-124, doi: 10.2118/2002-124. [Online]. Available: https://doi.org/10.2118/2002-124

[11] C. Wang and J. Y. Leung, "Characterizing the Effects of Lean Zones and Shale Distribution in Steam-Assisted-Gravity-Drainage Recovery Performance," *SPE Reservoir Evaluation & Engineering,* vol. 18, no. 03, pp. 329-345, 2015, doi: 10.2118/170101-pa.

[12] K. Furui, D. Zhu, and A. D. Hill, "A Comprehensive Skin-Factor Model of Horizontal-Well Completion Performance," *SPE Production & Facilities,* vol. 20, no. 03, pp. 207-220, 2005, doi: 10.2118/84401-pa.

[13] E. S. Tam, R. M. Modien, and D. A. Best, "The Effect Of Production Well Open Interval On Steamflood Performance," *Journal of Canadian Petroleum Technology,* vol. 27, no. 03, 1988, doi: 10.2118/88-03-07.

[14] I. D. Gates, J. Adams, and S. Larter, "The Impact of Oil Viscosity Heterogeneity on the Production Characteristics of Tar Sand and Heavy Oil Reservoirs. Part II: Intelligent,

Geotailored Recovery Processes in Compositionally Graded Reservoirs," *Journal of Canadian Petroleum Technology,* vol. 47, no. 09, 2008, doi: 10.2118/08-09-40.

[15] G. A. Rosi, D. Zhu, I. D. Gates, and J. Wang, "Passive flow control devices—well design and physics of their different flow regimes: A review," *Journal of Petroleum Science and Engineering,* vol. 218, p. 110999, 2022/11/01/ 2022, doi: https://doi.org/10.1016/j.petrol.2022.110999.

[16] K. H. Henriksen, E. I. Gule, and J. R. Augustine, "Case Study: The Application of Inflow Control Devices in the Troll Field," in *SPE Europec/EAGE Annual Conference and Exhibition*, 2006, vol. All Days, SPE-100308-MS, doi: 10.2118/100308-ms. [Online]. Available: https://doi.org/10.2118/100308-MS

[17] M. Halvorsen, M. Madsen, M. Vikøren Mo, I. Isma Mohd, and A. Green, "Enhanced Oil Recovery On Troll Field By Implementing Autonomous Inflow Control Device," in *SPE Bergen One Day Seminar*, 2016, vol. Day 1 Wed, April 20, 2016, SPE-180037-MS, doi: https://doi.org/10.2118/180037-MS. [Online]. Available: https://doi.org/10.2118/180037-MS

[18] K. Kearns *et al.*, "Autonomous Inflow Control Valves Restore Oil Production by Controlling Gas and Water Breakthrough in Acordionero Field, Colombia: A Case Study," in *SPE Annual Technical Conference and Exhibition*, 2022, vol. Day 3 Wed, October 05, 2022, D031S044R007, doi: 10.2118/210163-ms. [Online]. Available: https://doi.org/10.2118/210163-MS

[19] R. S. Alakberi, O. F. Igein, and S. A. Aljasmi, "Successful Smart Completion Deployment of Autonomous Inflow Control Valve with 13 Open Hole Segmentation Lower Completion Using a Light Workover Rig," in *SPE/IADC Middle East Drilling Technology Conference and Exhibition*, 2023, vol. Day 2 Wed, May 24, 2023, D021S011R002, doi: 10.2118/214582-ms. [Online]. Available: https://doi.org/10.2118/214582-MS

[20] S. Buwauqi *et al.*, "Application of Autonomous Inflow Control Valve AICV in Increasing the Field Recovery in One of the Matured Fields in the Sultanate of Oman: Case Study," in *SPE Annual Caspian Technical Conference*, 2021, vol. Day 1 Tue, October 05, 2021, D012S014R010, doi: 10.2118/207069-ms. [Online]. Available: https://doi.org/10.2118/207069-MS

[21] N. F. A. Sapian *et al.*, "Maximizing Production Recovery Through Autonomous Inflow Device AICD Configuration in Challenging Long Horizontal Open-Hole Oil Producer with High Gas-Oil-Ratio and Un-Even Fluid Contacts," in *IADC/SPE Asia Pacific Drilling Technology Conference and Exhibition*, 2022, vol. Day 2 Wed, August 10, 2022, D021S011R004, doi: 10.2118/209871-ms. [Online]. Available: https://doi.org/10.2118/209871-MS

[22] M. Martinez Santiago, B. Priyadarshini, and J. Ortiz, "A Success Story of Implementing Autonomous Inflow Control Devices (AICD) for Gas Control in a Brownfield Asset - What Can We Learn?," in *ADIPEC*, 2023, vol. Day 1 Mon, October 02, 2023, D012S154R002, doi: 10.2118/215954-ms. [Online]. Available: https://doi.org/10.2118/215954-MS

[23] I. Mohd Ismail, N. A. Che Sidik, F. Syarani Wahi, G. L. Tan, F. Tom, and F. Hillis, "Increased Oil Production in Super Thin Oil Rim Using the Application of Autonomous Inflow Control Devices," in *SPE Annual Technical Conference and Exhibition*, 2018,

vol. Day 1 Mon, September 24, 2018, D011S002R002, doi: 10.2118/191590-ms. [Online]. Available: https://doi.org/10.2118/191590-MS

[24] M. MoradiDowlatabad, F. Zarei, and M. Akbari, "The Improvement of Production Profile While Managing Reservoir Uncertainties with Inflow Control Devices Completions," in *SPE Bergen One Day Seminar*, 2015, vol. All Days, SPE-173841-MS, doi: 10.2118/173841-ms. [Online]. Available: https://doi.org/10.2118/173841-MS

[25] G. Elseth *et al.*, "Implementation of Autonomous Inflow Control and the Effect on Carbon Intensity," in *SPE Annual Technical Conference and Exhibition*, 2022, vol. Day 3 Wed, October 05, 2022, D031S053R004, doi: 10.2118/210379-ms. [Online]. Available: https://doi.org/10.2118/210379-MS

[26] T. R. C. o. Norway. "Industrial PhD Scheme – Doctoral Projects in Industry." The Research Council of Norway. https://www.forskningsradet.no/en/call-for-proposals/2019/industrial-ph.d.-scheme--doctoral-projects-in-industry/ (accessed.

[27] E. Eltaher, K. Muradov, D. Davies, and I. Grebenkin, "Autonomous Inflow Control Valves - their Modelling and "Added Value"," in *SPE Annual Technical Conference and Exhibition*, 2014, vol. All Days, SPE-170780-MS, doi: 10.2118/170780-ms. [Online]. Available: https://doi.org/10.2118/170780-MS

[28] K. Brekke and S. C. Lien, "New, Simple Completion Methods for Horizontal Wells Improve Production Performance in High-Permeability Thin Oil Zones," *SPE Drilling & Completion,* vol. 9, no. 03, pp. 205-209, 1994, doi: 10.2118/24762-pa.

[29] S. Banerjee and B. Hascakir, "Design of flow control devices in steam-assisted gravity drainage (SAGD) completion," *Journal of Petroleum Exploration and Production Technology,* vol. 8, no. 3, pp. 785-797, 2018/09/01 2018, doi: 10.1007/s13202-017-0393-4.

[30] Q. Zeng, Z. Wang, and G. Yang, "Comparative Study on Passive Inflow Control Devices by Numerical Simulation," *Structural Longevity,* vol. 9, no. 3, pp. 169--180, 2013. [Online]. Available: http://www.techscience.com/sl/v9n3/42912.

[31] T. Jokela *et al.*, "Inflow Control Devices — Raising Profiles," 2010.

[32] J. E. Lauritzen and I. B. Martiniussen, "Single and Multi-phase Flow Loop Testing Results for Industry Standard Inflow Control Devices," in *SPE Offshore Europe Oil and Gas Conference and Exhibition*, 2011, vol. All Days, SPE-146347-MS, doi: 10.2118/146347-ms. [Online]. Available: https://doi.org/10.2118/146347-MS

[33] A. Moradi and B. M. E. Moldestad, "A Proposed Method for Simulation of Rate-Controlled Production Valves for Reduced Water Cut," *SPE Production & Operations,* vol. 36, no. 03, pp. 669-684, 2021, doi: 10.2118/205377-pa.

[34] B. O. Lee, M. N. Rabeh, R. Vicario, P. Gavioli, and G. Garcia, "Multi-Phase (Oil-Water) Loop Flow Test for Helical and Hybrid Passive Inflow Control Devices," in *International Petroleum Technology Conference*, 2013, vol. All Days, IPTC-17125-MS, doi: 10.2523/iptc-17125-ms. [Online]. Available: https://doi.org/10.2523/IPTC-17125-MS

[35] A. K. Rahimah, N. M. Azrul, K. F. GordonGoh, A. N. Asyikin, E. Leung, and M. Johan, "Horizontal Well Optimization With Inflow Control Devices (ICDs) Application in Heterogeneous and Dipping Gas-Capped Oil Reservoirs," in *SPE Annual Technical Conference and Exhibition*, 2010, vol. All Days, SPE-133336-MS, doi: 10.2118/133336-ms. [Online]. Available: https://doi.org/10.2118/133336-MS

[36] K. H. Henriksen, E. I. Gule, and J. Augustine, "Case Study: The Application of Inflow Control Devices in the Troll Oil Field," in *SPE Europec/EAGE Annual Conference and*

Exhibition, 2006, vol. All Days, SPE-100308-MS, doi: 10.2118/100308-ms. [Online]. Available: https://doi.org/10.2118/100308-MS

[37] T. C. Emegano, S. A. Baloch, M. M. Al. Alrefaai, S. M. Al Nuimi, and E. S. Radwan, "Inflow Control Devices ICD – A Historical Performance Analysis," in *Abu Dhabi International Petroleum Exhibition & Conference*, 2020, vol. Day 1 Mon, November 09, 2020, D012S116R112, doi: 10.2118/202847-ms. [Online]. Available: https://doi.org/10.2118/202847-MS

[38] K. Langaas, E. Gisholt, A. Bjerke, and V. Mathiesen, "Autonomous Inflow Control Valve for Medium-Light Oil and Its Effective Performance," *SPE Production & Operations,* pp. 1-13, 2023, doi: 10.2118/214342-pa.

[39] *API SPEC 19ICD, Inflow Control Devices*, G19ICD01, A. P. Institute., Washington, D.C, 2020.

[40] T. Kalyani, G. Corona, and K. Ross, "Fluidic Diode Autonomous ICD Selection Criteria, Design Methodology, and Performance Analysis for Multiple Completion Designs: Case Studies," in *SPE Conference at Oman Petroleum & Energy Show*, 2022, vol. Day 1 Mon, March 21, 2022, D012S029R001, doi: 10.2118/200255-ms. [Online]. Available: https://doi.org/10.2118/200255-MS

[41] "Autonomous ICD, Dynamically controls and delays gas and water influx." Schlumberger. https://www.slb.com/-/media/files/sand-control/product-sheet/aicd-ps.ashx (accessed.

[42] "EQUALIZER SELECT inflow and injection control device." Baker Hughes. https://www.bakerhughes.com/completions/subsurface-flow-control/inflow-control-devices/passive-inflow-control/equalizer-select-inflow-and-injection-control-device (accessed.

[43] K. Langaas, E. J. Jeurissen, and H. K. Abay, "Combining Passive and Autonomous Inflow-Control Devices in a Trilateral Horizontal Well in the Alvheim Field," *SPE Production & Operations,* vol. 34, no. 03, pp. 446-460, 2018, doi: https://doi.org/10.2118/195485-PA.

[44] F. Tusimin, L. Riyanto, N. Ahmad Tajuddin, M. Moradi, R. Marimuthu, and M. Konopczynski, "Enhanced Oil Production with Autonomous Inflow Control Devices in a Thin Oil Rim Reservoir Malaysia," in *Offshore Technology Conference Asia*, 2020, vol. Day 1 Mon, November 02, 2020, D012S001R072, doi: 10.4043/30363-ms. [Online]. Available: https://doi.org/10.4043/30363-MS

[45] M. Konopczynski, M. Moradi, T. Krishnan, H. Sandhu, and C.-L. Lai, "Case Study: Oil Production Optimized With Autonomous Inflow Control Devices Offshore Malaysia," *Journal of Petroleum Technology,* vol. 74, no. 09, pp. 44-51, 2022, doi: 10.2118/0922-0044-jpt.

[46] B. Least, S. Greci, A. Wileman, and A. Ufford, "Fluidic Diode Autonomous Inflow Control Device Range 3B - Oil, Water, and Gas Flow Performance Testing," in *SPE Kuwait Oil and Gas Show and Conference*, 2013, vol. All Days, SPE-167379-MS, doi: 10.2118/167379-ms. [Online]. Available: https://doi.org/10.2118/167379-MS

[47] G. Corona, W. Yin, M. Fripp, M. Coffin, and N. Shahreyar, "Testing of a Novel Autonomous ICD with Low-Viscosity Multiphase Fluids," in *Offshore Technology Conference*, 2017, vol. Day 2 Tue, May 02, 2017, D021S017R006, doi: 10.4043/27789-ms. [Online]. Available: https://doi.org/10.4043/27789-MS

[48] G. Corona, M. Fripp, T. Kalyani, and W. Yin, "Fluidic Diode Autonomous Inflow Control Device for Heavy Oil Application," in *SPE Heavy Oil Conference and Exhibition*, 2016, vol. Day 2 Wed, December 07, 2016, D021S009R002, doi: 10.2118/184094-ms. [Online]. Available: https://doi.org/10.2118/184094-MS

[49] M. R. Konopczynski and M. Moradi, "Annular Phase Separation with AICD Completions – The Impact on Well Flow Performance and Control of Unwanted Effluents," in *SPE Offshore Europe Conference & Exhibition*, 2021, vol. Day 2 Wed, September 08, 2021, D022S016R002, doi: 10.2118/205407-ms. [Online]. Available: https://doi.org/10.2118/205407-MS

[50] M. Konopczynski, "Thermodynamic Analysis of a Modified Autonomous Flow Control Device for SAGD Sub-Cool Management," in *SPE Thermal Well Integrity and Design Symposium*, 2018, vol. Day 2 Wed, November 28, 2018, D023S006R002, doi: 10.2118/193365-ms. [Online]. Available: https://doi.org/10.2118/193365-MS

[51] V. Mathiesen, H. Aakre, B. Werswick, and G. Elseth, "The Autonomous RCP Valve - New Technology for Inflow Control In Horizontal Wells," in *SPE Offshore Europe Oil and Gas Conference and Exhibition*, 2011, vol. All Days, SPE-145737-MS, doi: 10.2118/145737-ms. [Online]. Available: https://doi.org/10.2118/145737-MS

[52] T. N. P. Directorate. "Zone control for improved recovery and lower costs." https://www.npd.no/en/facts/publications/reports/resource-report/resource-report-2019/fields/Zone-control-for-improved-recovery-and-lower-costs/ (accessed.

[53] "The historical development of Inflow Control Technology." https://www.inflowcontrol.no/who-we-are#history (accessed.

[54] H. Aakre, B. Halvorsen, B. Werswick, and V. Mathiesen, "Autonomous Inflow Control Valve for Heavy and Extra-Heavy Oil," in *SPE Heavy and Extra Heavy Oil Conference: Latin America*, 2014, vol. Day 2 Thu, September 25, 2014, D021S014R001, doi: https://doi.org/10.2118/171141-MS. [Online]. Available: https://doi.org/10.2118/171141-MS

[55] A. Moradi, N. A. Samani, A. S. Kumara, and B. M. E. Moldestad, "Evaluating the performance of advanced wells in heavy oil reservoirs under uncertainty in permeability parameters," *Energy Reports,* vol. 8, pp. 8605-8617, 2022/11/01/ 2022, doi: https://doi.org/10.1016/j.egyr.2022.06.077.

[56] S. Taghavi, H. Aakre, S. A. Tahami, and B. M. E. Moldestad, "The Impact of Autonomous Inflow Control Valve on Improved Oil Recovery in a Thin-Oil-Rim Reservoir," *SPE Journal,* pp. 1-15, 2024, doi: 10.2118/218393-pa.

[57] R. Kais, V. Mathiesen, H. Aakre, G. Woiceshyn, A. Elarabi, and R. Hernandez, "First Autonomous Inflow Control Valve AICV Well Completion Deployed in a Field Under an EOR Water & CO2 Injection Scheme," in *SPE Annual Technical Conference and Exhibition*, 2016, vol. Day 1 Mon, September 26, 2016, D011S013R001, doi: 10.2118/181552-ms. [Online]. Available: https://doi.org/10.2118/181552-MS

[58] H. Aakre, V. Mathiesen, and B. Moldestad, "Performance of CO2 flooding in a heterogeneous oil reservoir using autonomous inflow control," *Journal of Petroleum Science and Engineering,* vol. 167, pp. 654-663, 2018/08/01/ 2018, doi: https://doi.org/10.1016/j.petrol.2018.04.008.

[59] H. Aakre, "The impact of autonomous inflow control valve on increased oil production and recovery," no. 32, University College of Southeast Norway, Faculty of Technology, Natural Sciences and Maritime Sciences, Kongsberg, 2017.

[60] C. S. Mayer, P. M. Spiecker, C. E. Shuchart, R. Burkey, A. Ufford, and J. Brysch, "Multiphase Flow Performance of Inflow Control Devices – Characterizing Downhole Flow Behavior in Lab Experiments," in *Abu Dhabi International Petroleum Exhibition and Conference*, 2014, vol. Day 1 Mon, November 10, 2014, D011S015R002, doi: 10.2118/171890-ms. [Online]. Available: https://doi.org/10.2118/171890-MS

[61] X. Lu, S. Sun, and R. Dodds, "Toward 70% Recovery Factor: Knowledge of Reservoir Characteristics and IOR/EOR Methods from Global Analogs," in *SPE Improved Oil Recovery Conference*, 2016, vol. All Days, SPE-179586-MS, doi: 10.2118/179586-ms. [Online]. Available: https://doi.org/10.2118/179586-MS

[62] A. N. Onukwuri and I. I. A. , "Improved Oil Recovery for Developed Oil Rim Reservoir Using Gas Blow Down Strategy (A Case Study of Cefa Field in Niger Delta)," *International Research Journal of Advanced Engineering and Science,* vol. 5, no. 2, p. 8, 2020. [Online]. Available: https://irjaes.com/wp-content/uploads/2020/10/IRJAES-V5N2P101Y20.pdf.

[63] E. A. Razak, K. S. Chan, and N. Darman, "Breaking Oil Recovery Limit in Malaysian Thin Oil Rim Reservoirs: Force Balance Revisited," in *SPE EUROPEC/EAGE Annual Conference and Exhibition*, 2010, vol. All Days, SPE-130388-MS, doi: 10.2118/130388-ms. [Online]. Available: https://doi.org/10.2118/130388-MS

[64] P. Obidike, M. Onyekonwu, and C. E. Ubani, "Horizontal Well Standoff Performance and Exploitation of Thin Oil Rim," in *SPE Nigeria Annual International Conference and Exhibition*, 2019, vol. Day 2 Tue, August 06, 2019, D023S025R010, doi: 10.2118/198725-ms. [Online]. Available: https://doi.org/10.2118/198725-MS

[65] N. A. Ogolo, V. C. Molokwu, and M. O. Onyekonwu, "Proposed Technique for Improved Oil Recovery from Thin Oil Rim Reservoirs with Strong Aquifers and Large Gas Caps," in *SPE Nigeria Annual International Conference and Exhibition*, 2017, vol. Day 2 Tue, August 01, 2017, D023S010R005, doi: 10.2118/189126-ms. [Online]. Available: https://doi.org/10.2118/189126-MS

[66] A. Hasan, S. Sagatun, and B. Foss, *Well Rate Control Design for Gas Coning Problems*. 2010, pp. 5845-5850.

[67] K. Langaas, O. Urazovskaya, N. Gueze, and E. Jeurissen, "Attic Oil Recovery in the Alvheim Field," in *SPE Norway Subsurface Conference*, 2020, vol. Day 1 Mon, November 02, 2020, D011S002R001, doi: https://doi.org/10.2118/200719-MS. [Online]. Available: https://doi.org/10.2118/200719-MS

[68] "NPD FactPages." The Norwegian Petroleum Directorate. https://factpages.npd.no/en/field/PageView/Producing/46437 (accessed.

[69] A. Mjaavatten, R. Aasheim, S. Saelid, and O. Groenning, "A Model for Gas Coning and Rate-Dependent Gas/Oil Ratio in an Oil-Rim Resevoir," in *SPE Russian Oil and Gas Technical Conference and Exhibition*, 2006, vol. All Days, SPE-102390-MS, doi: 10.2118/102390-ms. [Online]. Available: https://doi.org/10.2118/102390-MS

[70] S. L. Kokal and A. U. Al-Kaabi, "Enhanced oil recovery: challenges & opportunities," 2010.

[71] I. D. Gates and C. Leskiw, "Impact of steam trap control on performance of steam-assisted gravity drainage," *Journal of Petroleum Science and Engineering,* vol. 75, no. 1, pp. 215-222, 2010/12/01/ 2010, doi: https://doi.org/10.1016/j.petrol.2010.11.014.

[72] C. Shen, "Chapter 17 - SAGD for Heavy Oil Recovery," in *Enhanced Oil Recovery Field Case Studies*, J. J. Sheng Ed. Boston: Gulf Professional Publishing, 2013, pp. 413-445.

[73] S. Taghavi, H. Aakre, S. Swaffield, and R. B. Brough, "Verification of Autonomous Inflow Control Valve Flow Performance Within Heavy Oil-SAGD Thermal Flow Loop," in *SPE Annual Technical Conference and Exhibition*, 2019, vol. Day 2 Tue, October 01, 2019, D022S091R001, doi: 10.2118/196216-ms. [Online]. Available: https://doi.org/10.2118/196216-MS

[74] R. Nasralla, R. Farajzadeh, S. Ketkar, J. Van Wunnik, D. Mahruqi, and R. Al Mjeni, "Towards Low Carbon Oil – A Comprehensive Portfolio Analysis for CO2 EOR/CCUS Opportunities in Oil Reservoirs in the Sultanate of Oman," in *ADIPEC*, 2022, vol. Day 2 Tue, November 01, 2022, D022S168R001, doi: 10.2118/210944-ms. [Online]. Available: https://doi.org/10.2118/210944-MS

[75] R. Safi, R. K. Agarwal, and S. Banerjee, "Numerical simulation and optimization of CO2 utilization for enhanced oil recovery from depleted reservoirs," *Chemical Engineering Science,* vol. 144, pp. 30-38, 2016/04/22/ 2016, doi: https://doi.org/10.1016/j.ces.2016.01.021.

[76] G. Protti, "Win-Win: Enhanced Oil Recovery And CO2 Storage At EnCana's Weyburn Oilfield," in *18th World Petroleum Congress*, 2005, vol. All Days, WPC-18-0986.

[77] E. K. Halland, V. Pham, F. Riis, and A.-H. Hansen, "CO2 for EOR Combined with Storage in the Norwegian North Sea," presented at the 14th Greenhouse Gas Control Technologies Conference (GHGT-14), Melbourne, 21-26 October 2018, 2019. [Online]. Available: http://dx.doi.org/10.2139/ssrn.3365602.

[78] E. K. Halland, W. T. Johansen, and F. Riis, "CO2 Storage Atlas Norwegian Continental Shelf ", 2014. [Online]. Available: https://www.npd.no/en/facts/publications/co2-atlases/co2-atlas-for-the-norwegian-continental-shelf/

[79] F. Gozalpour, S. R. Ren, and B. Tohidi, "CO2 Eor and Storage in Oil Reservoir," *Oil & Gas Science and Technology - Rev. IFP,* vol. 60, no. 3, pp. 537-546, 2005. [Online]. Available: https://doi.org/10.2516/ogst:2005036.

[80] E. K. Halland, W. T. Johansen, and F. Riis, "CO2 Storage ATLAS Norwegian Sea," Norway, 2012. [Online]. Available: https://www.npd.no/en/facts/publications/co2-atlases/co2-storage-atlas-of-the-norwegian-sea/

[81] "MEETING THE DUAL CHALLENGE ; A Roadmap to At-Scale Deployment of CARBON CAPTURE, USE, AND STORAGE," National Petroleum Council, 2021. [Online]. Available: https://www.energy.gov/sites/default/files/2022-10/CCUS-Chap_8-030521.pdf

[82] S. Taghavi, S. A. Tahami, H. Aakre, N. C. I. Furuvik, and B. M. E. Moldestad, "Performance Analysis of Autonomous Inflow Control Valve in a Heterogenous Reservoir Using CO2 Enhanced Oil Recovery," in *SPE Annual Technical Conference and Exhibition*, 2023, vol. Day 3 Wed, October 18, 2023, D031S045R002, doi: 10.2118/215153-ms. [Online]. Available: https://doi.org/10.2118/215153-MS

[83] M. A. Ahmadi, S. Zendehboudi, and L. A. James, "Hybrid connectionist model determines CO2–oil swelling factor," *Petroleum Science,* vol. 15, no. 3, pp. 591-604, 2018/08/01 2018, doi: 10.1007/s12182-018-0230-5.

[84] E. M. Mansour, A. M. Al-Sabagh, S. M. Desouky, F. M. Zawawy, and M. Ramzi, "A laboratory investigation of carbon dioxide-enhanced oil recovery by focusing on CO2-

oil physical properties," *Egyptian Journal of Petroleum,* vol. 28, no. 1, pp. 21-26, 2019/03/01/ 2019, doi: https://doi.org/10.1016/j.ejpe.2018.10.004.

[85] A. R. Y. Zekri, S. A. Shedid, and R. A. Almehaideb, "Experimental investigations of variations in petrophysical rock properties due to carbon dioxide flooding in oil heterogeneous low permeability carbonate reservoirs," *Journal of Petroleum Exploration and Production Technology,* vol. 3, no. 4, pp. 265-277, 2013/12/01 2013, doi: 10.1007/s13202-013-0063-0.

[86] G. F. Potter, "The Effects of CO2 Flooding on Wettability of West Texas Dolomitic Formations," in *SPE Annual Technical Conference and Exhibition*, 1987, vol. All Days, SPE-16716-MS, doi: 10.2118/16716-ms. [Online]. Available: https://doi.org/10.2118/16716-MS

[87] L. Zhang *et al.*, "CO2 EOR and storage in Jilin oilfield China: Monitoring program and preliminary results," *Journal of Petroleum Science and Engineering,* vol. 125, pp. 1-12, 2015/01/01/ 2015, doi: https://doi.org/10.1016/j.petrol.2014.11.005.

[88] O. Ezeaneche, M. Wobo, C. Uzoho, and M. Onyekonwu, "Investigation On the Effect of Change in Relative Permeability On Oil Recovery," in *SPE Nigeria Annual International Conference and Exhibition*, 2020, vol. Day 1 Tue, August 11, 2020, D013S007R004, doi: 10.2118/203707-ms. [Online]. Available: https://doi.org/10.2118/203707-MS

[89] G. Elseth, "An experimental study of oil/water flow in horizontal pipes," 2001:102, Norges teknisk-naturvitenskapelige universitet, Trondheim, 2001.

[90] M. Negrescu and I. L. F. Leitao Junior, "ICD/AICD for Heavy Oil - Technology Qualification at the Peregrino Field," in *OTC Brasil*, 2013, vol. All Days, OTC-24503-MS, doi: 10.4043/24503-ms. [Online]. Available: https://doi.org/10.4043/24503-MS

[91] "U-tube technology in digital laboratory density meters." Anton Paar GmbH. https://wiki.anton-paar.com/kr-en/u-tube-technology-in-digital-laboratory-density-meters/ (accessed 01.11.2023.

[92] S. S. Karunarathne, n. o. m. f. Universitetet i Sørøst-Norge Fakultet for teknologi, and S.-N. Universitetet i, "Physicochemical data for amine based CO_2 capture process," no. 72, Faculty of Technology, Natural Sciences and Maritime Studies, University of South-Eastern Norway, Porsgrunn, 2020.

[93] A. Furtado, E. Batista, I. Spohr, and E. Filipe, *Measurement of density using oscillation-type density meters. Calibration, traceability and Uncertainties*. 2009.

[94] "Density meter: DMA 4500 M." Anton Paar https://www.anton-paar.com/kr-en/products/details/benchtop-density-meter-dma-4500-m/ (accessed 02.11.2023.

[95] Z. Idris, N. B. Kummamuru, and D. A. Eimer, "Viscosity measurement of unloaded and CO2-loaded aqueous monoethanolamine at higher concentrations," *Journal of Molecular Liquids,* vol. 243, pp. 638-645, 2017/10/01/ 2017, doi: https://doi.org/10.1016/j.molliq.2017.08.089.

[96] S. S. Karunarathne, D. A. Eimer, and L. E. Øi, "Uncertainty comparison of viscosity measurements of CO2 loaded MEA and water mixtures in a coaxial rheometer using Monte Carlo simulation and GUM method," (in English), *International Journal of Energy and Environment,* vol. 10, no. 2, pp. 77-86, Mar 2019 2019.

[97] *ECLIPSE Technical Descriptions*, Version 2020.1 ed., Schlumberger, pp. 692-709. Accessed: 23.04.2024.

[98] "Relative permeability models." SPE. https://petrowiki.spe.org/Relative_permeability_models#Brooks-Corey_and_related_models (accessed 23.04.2024.
[99] *ECLIPSE Technical Descriptions*, Version 2020.1 ed., Schlumberger, p. 689. Accessed: 23.04.2024.
[100] S. Taghavi, H. Aakre, and B. M. E. Moldestad, "Performance Analysis of Autonomous Inflow Control Valve in a SAGD Late Life Process with Non-Condensable Gases," in *SPE Canadian Energy Technology Conference*, 2022, vol. Day 1 Wed, March 16, 2022, D011S011R002, doi: 10.2118/208915-ms. [Online]. Available: https://doi.org/10.2118/208915-MS
[101] M. Mesbah, M. Jamialahmadi, and A. Helalizadeh, "Black Oil and Compositional Reservoir Simulation for Increasing the Recovery Performance of an Iranian Fractured Carbonate Reservoir," *Petroleum Science and Technology,* vol. 30, no. 13, pp. 1404-1415, 2012/04/30 2012, doi: 10.1080/10916466.2010.506459.
[102] "The Mathematical Formulation of the Black Oil Model." OpenGoSim. https://docs.opengosim.com/theory/mathematical_formulation_of_black_oil/#the-mathematical-formulation-of-the-black-oil-model (accessed.
[103] "Black-Oil Simulations." wikitext. https://dwsim.org/wiki/index.php?title=Black-Oil_Simulations (accessed.
[104] S. R. Shadizadeh, M. Kargarpour, and M. Zoveidavianpoor, "Modeling of Inflow Well Performance of Multilateral Wells: Employing the Concept of Well Interference and the Joshi's Expression," *Iranian Journal of Chemistry and Chemical Engineering,* vol. 30, pp. 119-133, 03/01 2011.
[105] F. A. Adesina, A. Churchill, and F. Olugbenga, "Modeling productivity index for long horizontal well," 2011.
[106] G. Chupin, B. Hu, T. Haugset, J. Sagen, and M. Claudel, "Integrated Wellbore/Reservoir Model Predicts Flow Transients in Liquid-Loaded Gas Wells," in *SPE Annual Technical Conference and Exhibition*, 2007, vol. All Days, SPE-110461-MS, doi: https://doi.org/10.2118/110461-MS. [Online]. Available: https://doi.org/10.2118/110461-MS
[107] T. Ahmed, "Chapter 5 - Relative Permeability Concepts," in *Reservoir Engineering Handbook (Fifth Edition)*, T. Ahmed Ed.: Gulf Professional Publishing, 2019, pp. 283-329.
[108] H. L. Stone, "Estimation of Three-Phase Relative Permeability And Residual Oil Data," *Journal of Canadian Petroleum Technology,* vol. 12, no. 04, 1973, doi: 10.2118/73-04-06.
[109] M. Vasquez and H. D. Beggs, "Correlations for Fluid Physical Property Prediction," *Journal of Petroleum Technology,* vol. 32, no. 06, pp. 968-970, 1980, doi: 10.2118/6719-pa.
[110] J. Sagen, T. Sira, A. Ek, S. Selberg, M. Chaib, and H. Eidsmoen, "A Coupled Dynamic Reservoir and Pipeline Model – Development and Initial Experience," in *13th International Conference on Multiphase Production Technology*, 2007, vol. All Days, BHR-2007-G1.
[111] K. H. Bendlksen, D. Malnes, R. Moe, and S. Nuland, "The Dynamic Two-Fluid Model OLGA: Theory and Application," *SPE Production Engineering,* vol. 6, no. 02, pp. 171-180, 1991, doi: 10.2118/19451-pa.

[112] S. Taghavi, F. Farsi Madan, R. Timsina, and B. M. E. Moldestad, "Application of Autonomous Inflow Control Valve for Enhanced Bitumen Recovery by Steam Assisted Gravity Drainage," in *The 63rd International Conference of Scandinavian Simulation Society, SIMS 2022*, Trondheim, Norway, 2022: Linköping Electronic Conference Proceedings 192, doi: https://doi.org/10.3384/ecp192009.
[113] Schlumberger, "Transport Equations ", ed, p. OLGA User Manual.
[114] C. M. Group. Advanced Wellbore Modelling Using STARS, CMG Tutorial
[115] I. Mohd Ismail, V. Mathiesen, A. Abraham, E. Ranjbar, F. Zarei, and J. Walter, "An Innovative Modelling Approach in Characterization of Autonomous Inflow Control Valve Performance to Maximizing Oil Recovery in Heavy Oil-SAGD Application," in *SPE Thermal Well Integrity and Design Symposium*, 2021, vol. Day 3 Thu, January 28, 2021, D032S003R003, doi: 10.2118/203859-ms. [Online]. Available: https://doi.org/10.2118/203859-MS
[116] K. Langaas, O. Urazovskaya, N. Gueze, and E. Jeurissen, *Attic Oil Recovery in the Alvheim Field*. 2020.
[117] B. A. Voll, I. M. Ismail, and I. Oguche, "Sustaining Production by Limiting Water Cut and Gas Break through with Autonomous Inflow Control Technology," in *SPE Russian Oil and Gas Exploration & Production Technical Conference and Exhibition*, 2014, vol. All Days, SPE-171149-MS, doi: 10.2118/171149-ms. [Online]. Available: https://doi.org/10.2118/171149-MS
[118] S. Taghavi and A. Ghaderi, "On Uncertainty Analysis of the Rate Controlled Production (RCP) Model," in *First SIMS EUROSIM Conference on Modelling and Simulation*, Finland, 2021: Linköping Electronic Conference Proceedings, 2021, doi: DOI: https://doi.org/10.3384/ecp21185271.
[119] J. K. Kruschke, "Chapter 5 - Bayes' Rule," in *Doing Bayesian Data Analysis (Second Edition)*, J. K. Kruschke Ed. Boston: Academic Press, 2015, pp. 99-120.
[120] J. K. Kruschke, "Chapter 7 - Markov Chain Monte Carlo," in *Doing Bayesian Data Analysis (Second Edition)*, J. K. Kruschke Ed. Boston: Academic Press, 2015, pp. 143-191.
[121] A. J. Ghahfarokhi, T. A. Jelmert, J. Kleppe, M. Ashrafi, Y. Souraki, and O. Torsaeter, "Investigation of the Applicability of Thermal Well Test Analysis in Steam Injection Wells for Athabasca Heavy Oil," in *SPE Europec/EAGE Annual Conference*, 2012, vol. All Days, SPE-154182-MS, doi: 10.2118/154182-ms. [Online]. Available: https://doi.org/10.2118/154182-MS
[122] C. H. Whitson, S. Ø. Martinsen, and B. Younus, "Chapter 2 - Sampling petroleum fluids," in *Fluid Chemistry, Drilling and Completion*, Q. Wang Ed.: Gulf Professional Publishing, 2022, pp. 41-93.
[123] S. Taghavi, H. Aakre, and B. M. E. Moldestad, "The Impact of Autonomous Inflow Control Valve on Enhanced Bitumen Recovery in a SAGD Late Life Reservoir: Lab Experiment and Simulation," in *SPE Canadian Energy Technology Conference and Exhibition*, 2023, vol. Day 1 Wed, March 15, 2023, D012S001R002, doi: 10.2118/212783-ms. [Online]. Available: https://doi.org/10.2118/212783-MS
[124] S. A. Halvorsen, A. Mjaavatten, and R. Aasheim, "Improved near-well approximation for prediction of the gas/oil production ratio from oil-rim reservoirs," *Computational Geosciences,* vol. 16, no. 2, pp. 231-246, 2012/03/01 2012, doi: 10.1007/s10596-011-9250-6.

[125] Farhan Hasin Alam, Amin Tahami, Nora C.I. Furuvik, Britt M.E. Moldestad, and S. Taghavi, "The Impact of Autonomous Inflow Control Valve on Enhanced Oil Recovery in SAGD Application," in *64th International Conference of Scandinavian Simulation Society, SIMS2023*, Västerås, Sweden, September 25–28, 2023. 2023: Linköping University Electronic Press (LiU E-press) in Linköping Electronic Conference Proceedings 200, 2023-10-19, pp. 278-285, doi: https://doi.org/10.3384/ecp200036. [Online]. Available: https://ecp.ep.liu.se/index.php/sims

[126] S. Taghavi, E. Gisholt, H. Aakre, S. Håland, and K. Langaas, "Autonomous Inflow Control Valve Multiphase Flow Performance for Light Oil," in *Offshore Technology Conference*, 2021, vol. Day 1 Mon, August 16, 2021, D012S059R016, doi: 10.4043/31239-ms. [Online]. Available: https://doi.org/10.4043/31239-MS

[127] Gelest. *Silicone fluids: property profile guide, Gelest, 2013*, 2013. [Online]. Available: https://www.gelest.com/themencode-pdf-viewer/?file=https://www.gelest.com/wp-content/uploads/Goods-PDF-brochures-inert_silicones_2013.pdf.

[128] V. Simon, B. Weigand, and H. Gomaa, "Some Fundamentals of Dimensional Analysis," in *Dimensional Analysis for Engineers*, V. Simon, B. Weigand, and H. Gomaa Eds. Cham: Springer International Publishing, 2017, pp. 1-25.

Part 2

Scientific Papers

Paper 1

Autonomous Inflow Control Valve Multiphase Flow Performance for Light Oil

OTC-31239-MS

This paper was prepared for presentation at the Offshore Technology Conference held in Houston, TX, USA, 16 - 19 August 2021.

Paper presented by Soheila Taghavi

Authors: Soheila Taghavi, Einar Gisholt, Haavard Aakre, Stian Håland, and Kåre Langaas

OTC-31239-MS

Autonomous Inflow Control Valve Multiphase Flow Performance for Light Oil

Soheila Taghavi, Einar Gisholt, and Haavard Aakre, InflowControl AS; Stian Håland and Kåre Langaas, Aker BP ASA

This paper was prepared for presentation at the Offshore Technology Conference held in Houston, TX, USA, 16 - 19 August 2021.

Abstract

Early water and/or gas breakthrough is one of the main challenges in oil production which results in inefficient oil recovery. Existing mature wells must stop the production and shut down due to high gas oil ratio (GOR) and/or water cut (WC) although considerable amounts of oil still present along the reservoir. It is important to develop technologies that can increase oil production and recovery for marginal, mature, and challenging oil reservoirs. In most fields the drainage mechanism is pressure support from gas and/or water and the multiphase flow performance is particularly important. Autonomous Inflow Control Valve (AICV) can delay the onset of breakthrough by balancing the inflow along the horizontal section and control or shut off completely the unwanted fluid production when the breakthrough occurs. The AICV was tested in a world-leading full-scale multiphase flow loop located in Porsgrunn, Norway. Tests were performed with realistic reservoir conditions, i.e. reservoir pressure and temperature, crude oil, formation water and hydrocarbon gas at various gas oil ratio and water cut in addition to single phase performances. A summary of the flow loop, test conditions, the operating procedures, and test results are presented. In addition, how to represent the well with AICVs in a standard reservoir simulation model are discussed. The AICV flow performance curves for both single phase and multiphase flow are presented, discussed, and compared to conventional Inflow Control Device (ICD) performance. The test results demonstrate that the AICV flow performance is significantly better than conventional ICD. The AICV impact on a simplified model of a thin oil rim reservoir is shown and modelling limitations are discussed.

The simulation results along with the experimental results demonstrated considerable benefit of deploying AICV in this thin oil rim reservoir. Furthermore, this paper describes a novel approach towards the application of testing the AICV for use within light oil completion designs and how the AICV flow performance results can be utilized in marginal, mature, and other challenging oil reservoirs.

Introduction

Inefficient oil recovery due to early breakthrough of unwanted fluids is one of the main challenges in oil production. Mature wells are forced to stop the production while there still are considerable amounts of oil left in the reservoir, due to high WCs and/or GORs.

As it stands today, more than 50% of the oil in most fields on the Norwegian Continental Shelf will not be recovered. This problem is partly due to uneven flow along the wells. Fluid friction within the pipe,

permeability differences and heterogeneities are some elements which can create uneven drainage along the wells. Long horizontal wells are likely to experience more pressure differences between the heel and toe section, which leads to non-uniform flow and consequently breakthrough of unwanted fluids in the heel section of the well which is shown in Figure 1. This phenomenon is known as heel to toe effect [1]. Hence these challenges, developing new technologies that can help enhance the oil production and increase the total oil recovery of the fields is of great interest.

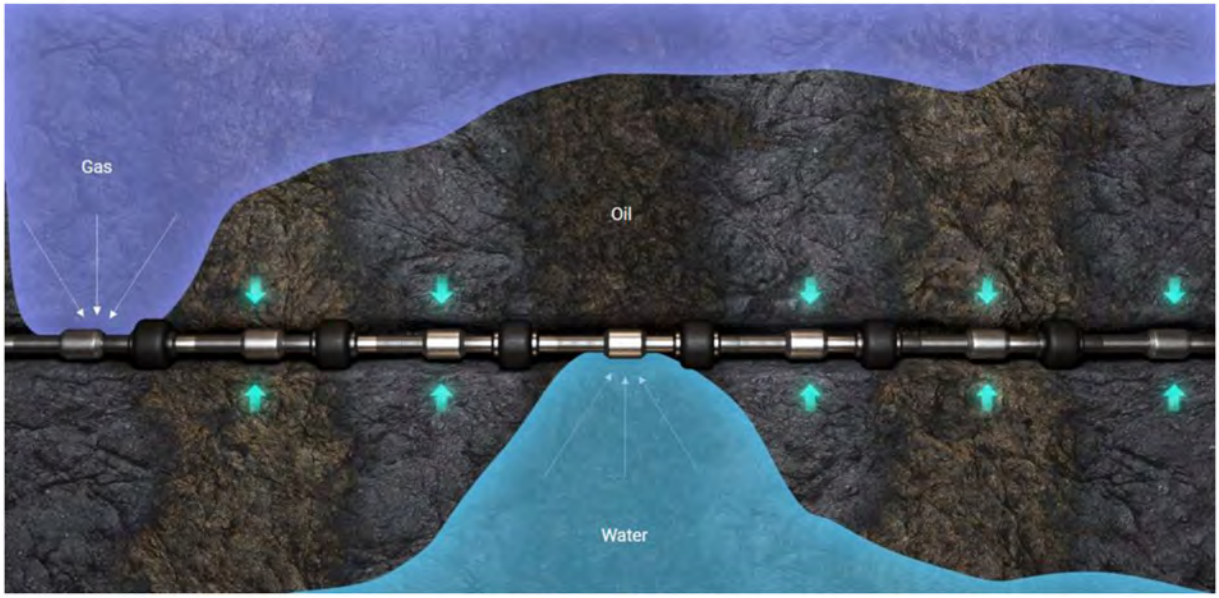

Figure 1—Uneven Flow along the wellbore resulting into water and gas breakthrough.

Inflow control technologies have been widely used during the last decades to make the wells more profitable by attaining uniform flow, delaying the unwanted fluid breakthrough, and consequently maximizing the oil production and recovery.

Optimizing well performance and increasing oil production in challenging oil reservoirs by implementing autonomous Flow Control Devices (FCD) have been achieved and results have been published in previous work, see e.g. Mohd Ismail et al. (2018) [2] and Langaas et al. (2018) [3].

Among the other inflow control technologies is the patented Autonomous Inflow Control Valve (AICV) which can delay the onset of breakthrough and control or shut off completely the unwanted fluid production locally when the breakthrough occurs. This restriction of unwanted fluids can result in a significant increase in oil production and ultimate recovery.

In the breakthrough zones WC and GVF varies over time. The two-phase flow behavior of the inflow control devices in these breakthrough zones is important for the total recovery along the well.

AICV Technology

The function of the Autonomous Inflow Control Valve (AICV) is based on two physical principles: Darcy's law and Bernoulli's principle. AICV utilize viscosity and density differences between fluids in such a way that it will keep the valve open for oil and closed for fluids like gas and water. This is achieved by taking advantage of the pressure differences in the Laminar Flow Element (LFE) and Turbulent Flow Element. Figure 2 illustrates AICV in open and closed position, respectively. The concept and principles of AICV is described in detail in earlier SPE papers [4] and [5].

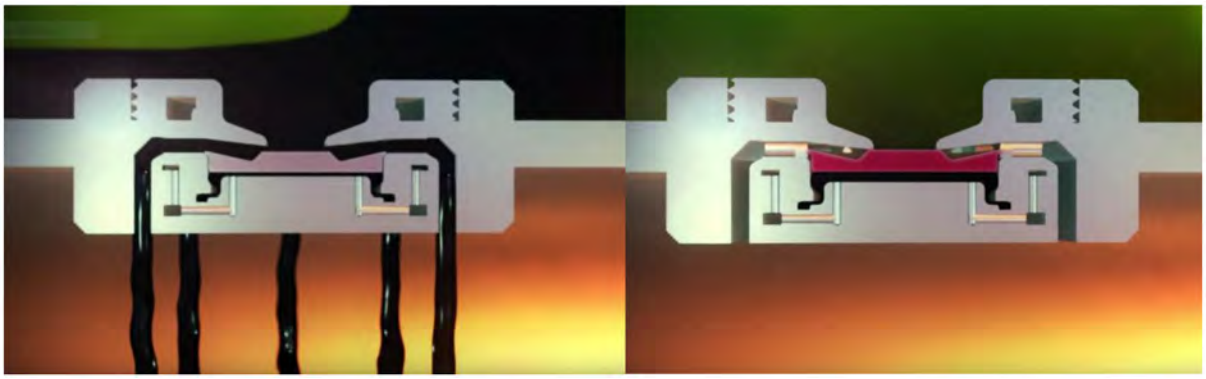

Figure 2—AICV is open for oil (left) and closed for gas (right).

AICV can be mounted into sand screen joints as it is shown in Figure 3. The flow path for a single AICV fitted joint is illustrated with blue arrows. Fluids from the reservoir enters the sand screen and flows further towards the AICV housing where the AICV is installed. After having passed through the AICV, the fluid together with the fluid produced from the other joints will flow all the way up to the surface through the production tubing.

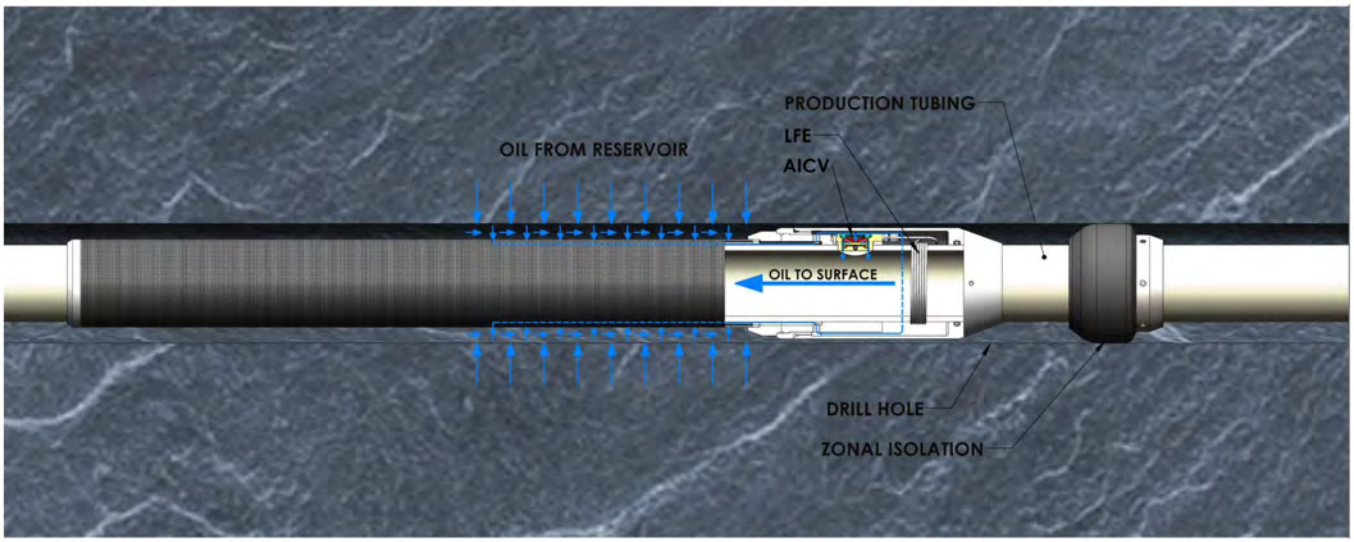

Figure 3—AICV mounted into sand screen joint.

Multiphase flow loop and test conditions

The experimental tests were performed at multiphase flow loop test rig at Equinor test facility located in Porsgrunn, Norway. The test rig is a full-scale dimension rig that covers a wide range of reservoir conditions such as pressure (P), temperature(T), density (ρ), and viscosity (μ). A simplified schematic of the flow loop showing key pieces of equipment and key measurement locations is shown in Figure 4 [6].

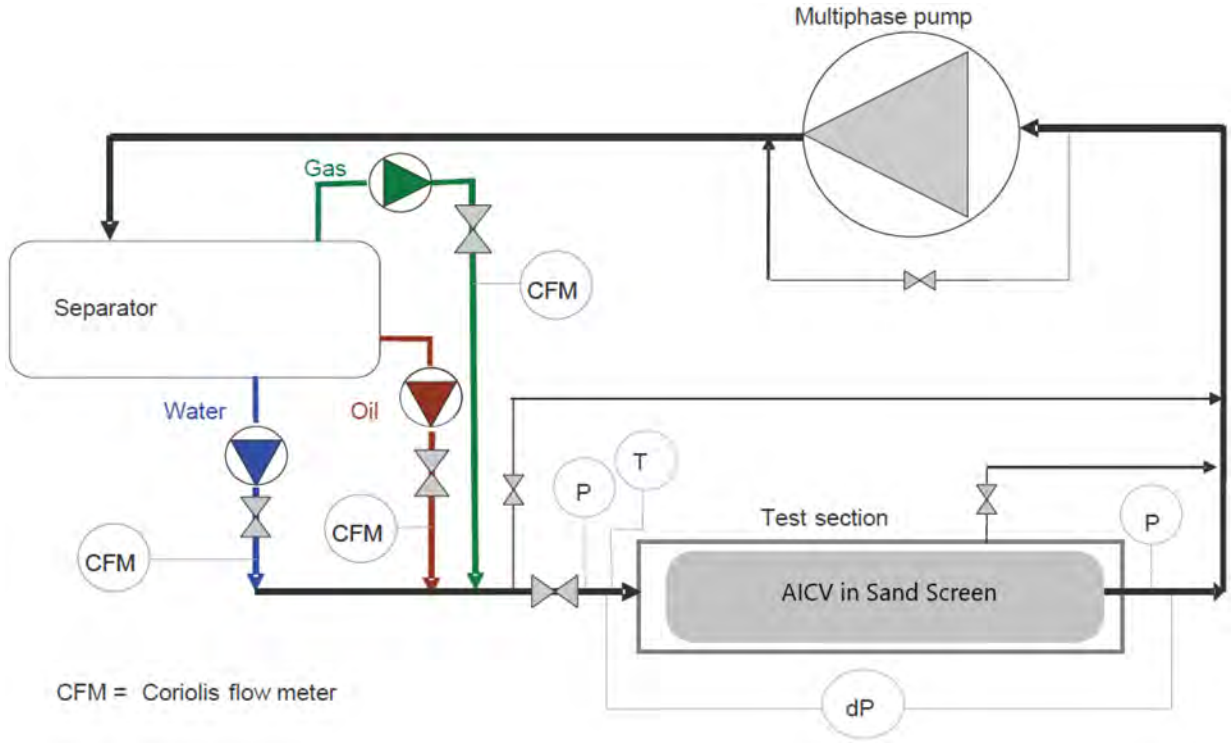

Figure 4—Multiphase flow loop test setup.

The main components in the rig are three phase separator, a multiphase pump and a test cell. The flow rates of the different fluids are regulated by flow controllers (FIC) and pressures and differential pressure are measured at different locations in the rig.

Single phase tests were performed by establishing the desired differential pressure across the test section and measuring the stabilized flow rate [7]. Multiphase flow tests were performed by regulating the desired amount of oil/gas or oil/water flowing through the test section at targeted differential pressure.

Tests were carried out with fluids at realistic reservoir conditions. The crude oil used in these tests is from North Sea saturated with natural gas giving 1cP viscosity at test conditions. Synthetic formation water with density of 1035 kg/m^3 at test conditions was used in the tests.

Test matrix

Table 1 shows the experimental test matrix for the flow tests conducted. The key controlled and measured variables for the test program were flow rates, differential pressure across the AICV, system conditions (pressure and temperature), and fluid properties, such as viscosity and density.

Natural gas and oil density were 140 kg/m^3 and 760 kg/m^{3,} respectively. Oil viscosity was measured 1.02cP at 70 °C and 200bar.

Table 1—Experimental test conditions

Description	Fluid Type	System Conditions: Pressure (bar) and Temperature (˚C)	Differential pressure across AICV (bar)
Single-phase test	Gas	200 bar/70˚C	1-40
	Water		
	Oil		
Multi -phase test	Oil and Gas	200 bar/70˚C	10, and 20
	Oil and Water		

Results and discussions

Single and multi-phase tests were performed with fluids at reservoir conditions in Equinor's full scale laboratory test facility located in Porsgrunn, Norway.

Single phase flow test results

The results plotted in Figure 5 represent the characteristic of the AICV described by pressure drop across the AICV as a function of volumetric flow rate for single phases. At 20 bar pressure drop the oil/gas and oil/water ratio is about 2.7 and 1.6 respectively, which illustrates the choking capability of AICV when breakthrough of unwanted fluids occurs. For Rate Controlled Production (RCP) valve deployed at Troll oil field the oil/gas and oil water ratio is 0.73 and 1.5 respectively [8]. Troll oil viscosity is about 2 cP, while the viscosity of the oil used in the tests is about 1.02 cP. This indicates that RCP valve requires greater viscosity contrast than the AICV to control water breakthrough/production effectively and consequently obtain additional oil production and recovery.

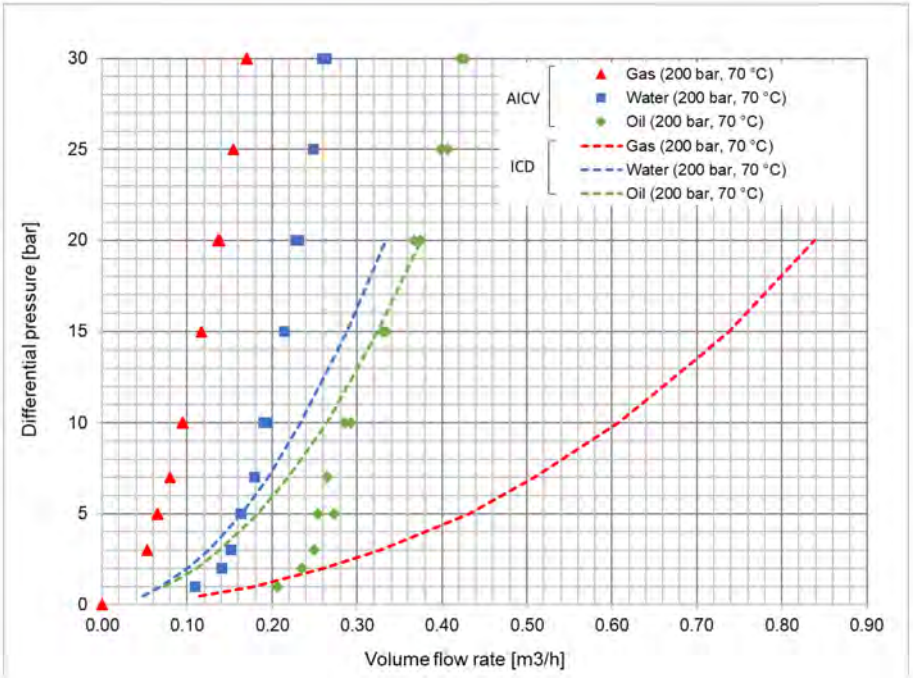

Figure 5—Comparison of single-phase flow performance of the ICD (dashed lines) and AICV (points) for oil, water, and gas.

Figure 5 also shows how a conventional/passive inflow control device (ICD) would behave for the same fluids, matched for 20 bar differential pressure oil flow. The AICV provides a considerably more restrictive gas flow rate than the passive ICD.

Indeed, the gas production is dramatically reduced from approximately 0.84 m^3 /h for the ICD at 20 bar differential pressure, to 0.14 m^3 /h for the AICV (about 83% reduction). The considerable reduction in water flow rate from 0.34 m^3 /h for the ICD to 0.23 m^3 /h for the AICV (about 33% reduction) is demonstrated as well. These results show that the AICV technology is able to significantly reduce the production of unwanted fluids compared to conventional/passive ICDs.

As Figure 5 shows, the AICV provides significantly higher oil rates at lower differential pressures when compared to the ICD. When studying the figure, it is evident that the AICV curves are steeper than what is the case for the ICD. Having this fluid choking ability with increasing differential pressure allows the AICV to prevent massive initial inflow from high permeable zones in the reservoir. This is desired behavior, as high permeable zones are susceptible to breakthrough of unwanted fluids if produced too fast. Due to this

feature more drawdown is distributed to zones with lower permeability, while desirable production rates are maintained. This will secure even inflow across the whole well length, consequently, delay unwanted fluid breakthrough in high permeable zones and ensure a more efficient total recovery of the reservoir.

Multi-phase flow test results

Figure 6 shows two-phase oil/gas tests performed at 10 and 20 bar differential pressure across the AICV along with the single-phase performance of oil and gas for reference. Pressure drop as a function of total volume flow rate is plotted. AICV gradually opens when the oil/gas mixture flows through the valve however, the maximum flow through the AICV is 0.52 m^3 /h.

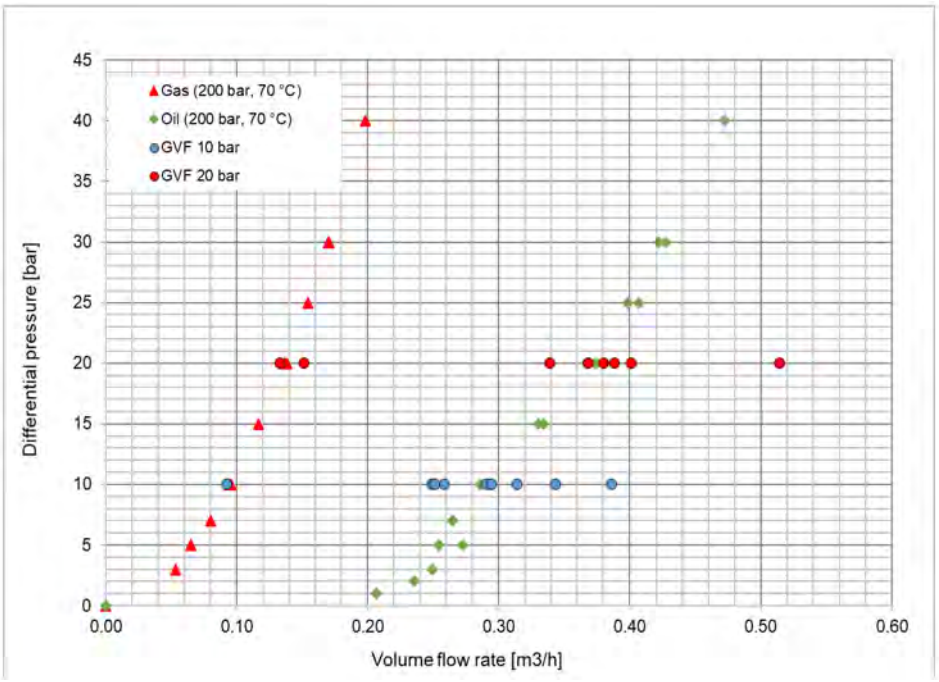

Figure 6—Two-phase performance of AICV at 10 and 20bar differential pressure together with single phase tests of AICV.

Gas volume fraction in the range of 0-100 % at 10 and 20 bar pressure drops are shown in Figure 7. If oil flashes in the reservoir towards the inflow zones, then it releases gas. When the local GVF is up to 20% GVF the AICV opens, allowing all the oil together with gas to flow through the valve. As it is demonstrated in Figure 7 AICV closes gradually and effectively from 20% GVF until 100 % pure gas flows through the valve. At this point AICV is closed for gas and the only remaining flow is through pilot flow.

AICV will restrict gas flow significantly, specifically in higher GVF which is what makes this technology unique when compared to other inflow control technologies.

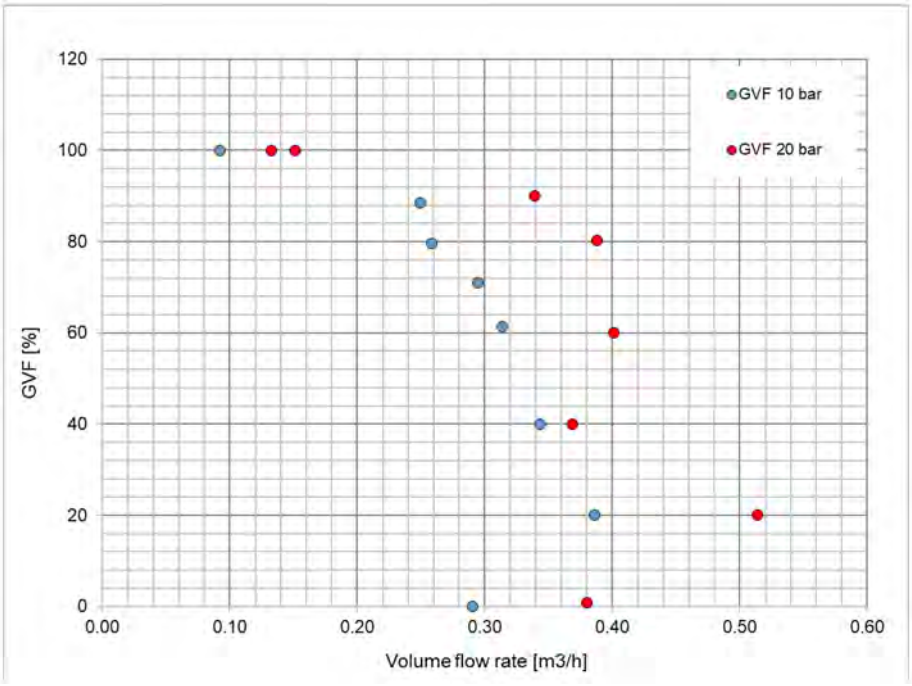

Figure 7—Two-phase behavior of AICV in the GVF range from 0-100% at 10and 20 bar differential pressure.

Figure 8 shows two-phase oil/water tests performed at various pressure drops across AICV at three specific water cuts, together with single phase curves of oil and water for reference. The pressure drops as a function of total volume flow rate is plotted. AICV gradually chokes when WC increases from 60% to 100% pure water. The maximum flow rate through the AICV in the WC range is 0.5 m^3 /h at 20 bar.

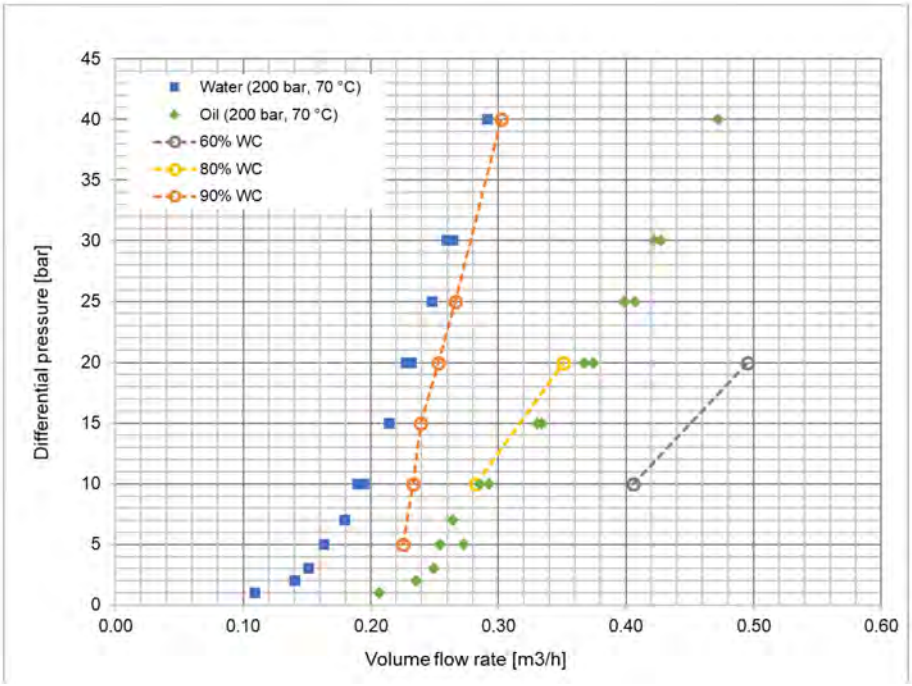

Figure 8—Two-phase performance of AICV as a function of differential pressure at 60%, 80% and 90% water cut.

Two-phase oil/water performance of AICV is shown in Figure 9, and total volume flow rate vs water cut at 10 and 20 bar pressure drop is plotted. The total volume flow rates decrease significantly from 60% until 100% WC.

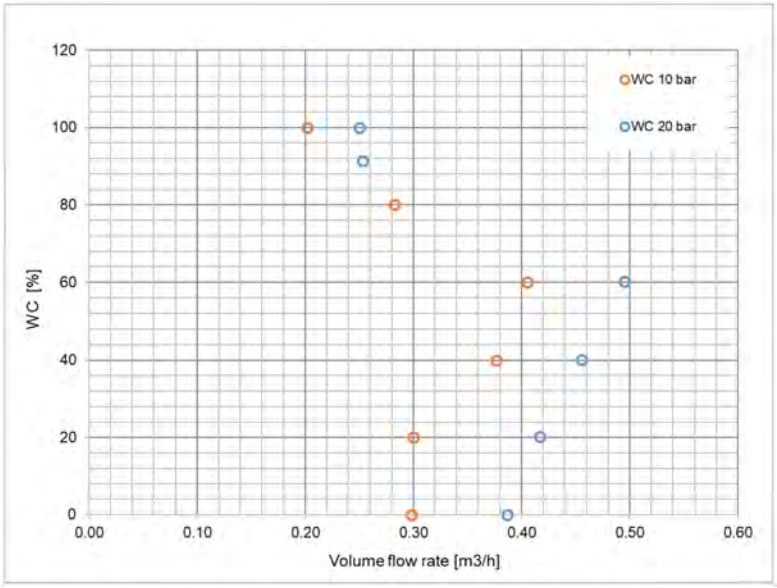

Figure 9—Two-phase behavior of AICV in the WC range from 0-100% at 10and 20 bar differential pressure.

Figure 10 illustrates the WC behavior of AICV and how this can be beneficial to obtain more oil than passive ICD from zones in which water breakthrough has occurred. Indeed, AICV will produce more oil than ICD in all WC ranges up to 80% (left plot in Figure 10). AICV chokes water more than ICD in higher WC ranges from 80% (right plot in Figure 10). The two-phase oil/water performance for ICD is linear, which means that oil flow rate decreases linearly with an increasing water cut while the AICV performance does not follow the linear trend. This behavior allows the AICV to obtain more oil in lower WC ranges.

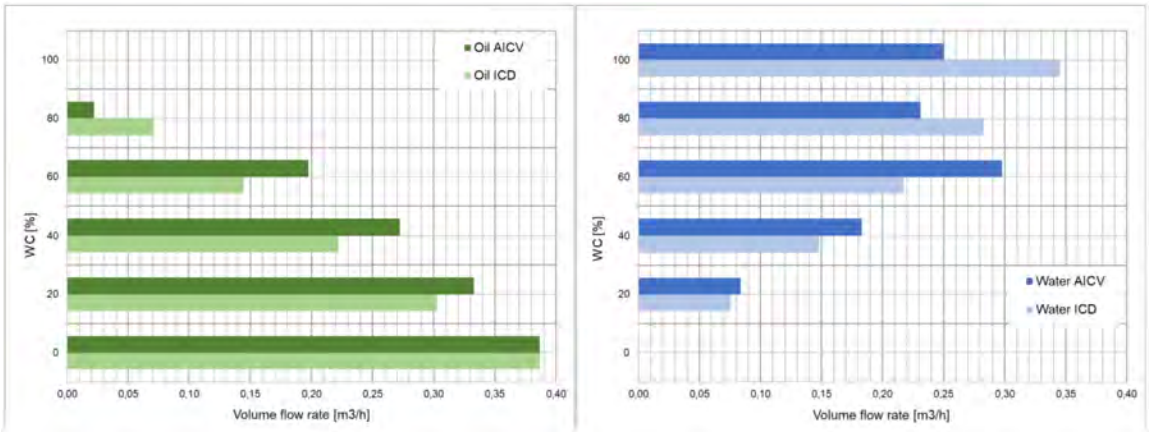

Figure 10—Comparison of AICV and ICD in the WC range from 0-100% at 20 bar differential pressure.

AICV model match

The AICV has been modelled with the equation described by [8] and later extended with density and viscosity exponents. Regression coefficients have been fitted to the experimental data, with fluid parameters equal to actual test conditions. These data are shown in Table 2 and the model match vs. experimental data for single phase flow are shown in Figure 11.

Table 2—Fluid properties in experimental test and AICD model match parameters.

Fluid parameters			
Name	**Unit**	**Symbol**	**Value**
Density: Oil	[kg/m3]	rho_oil	**759**
Density: Water	[kg/m3]	rho_water	**1014**
Density. Gas	[kg/m3]	rho_gas	**140**
Viscosity: Oil	[cp]	mu_oil	**1.02**
Viscosity: Water	[cp]	mu_water	**0.46**
Viscosity: Gas	[cp]	mu_gas	**0.0196**
AICD model parameters			
Name	**Unit**	**Symbol**	**Value**
Calibration density	[kg/m3]	rho_cal	**1000.00**
Calibration viscosity	[cp]	mu_cal	**1.00**
Viscosity function exponent	[-]	y	**1.770**
Flow rate exponent	[-]	x	**3.75**
AICD strength	[Bar/((kg/m3) *(Rm3/day))]	a_aicd	**8.06E-06**
Density exponents: Oil	[-]	a	**4.63**
Density exponents: Water	[-]	b	**1.00**
Density exponents: Gas	[-]	c	**1.00**
Viscosity exponents: Oil	[-]	d	**2.28**
Viscosity exponents: Water	[-]	e	**1.00**
Viscosity exponents: Gas	[-]	f	**1.00**

The regression shows a good match with the single-phase experimental data. An equivalent ICD is plotted alongside the AICV plot for comparison (dotted lines). To match oil rate at 10 bar pressure drop, a 1.45mm effective diameter ICD is used. For the test conditions, the AICV chokes much better the unwanted phases (water and gas) than is the case for the ICD.

For fluids with lower viscosity than the measured lab oil viscosity, the oil curve is expected to shift to the left. Ideally the test condition and reservoir condition should be exactly same. The best we could do for the reservoir case study with an oil of 0.6 cp oil viscosity, was to trust the AICD model and change the oil viscosity after the regression in Figure 11. The result of the changed oil viscosity is shown in Figure 12. All other fluid properties in the experiments were very close to the reservoir case study and needed no correction.

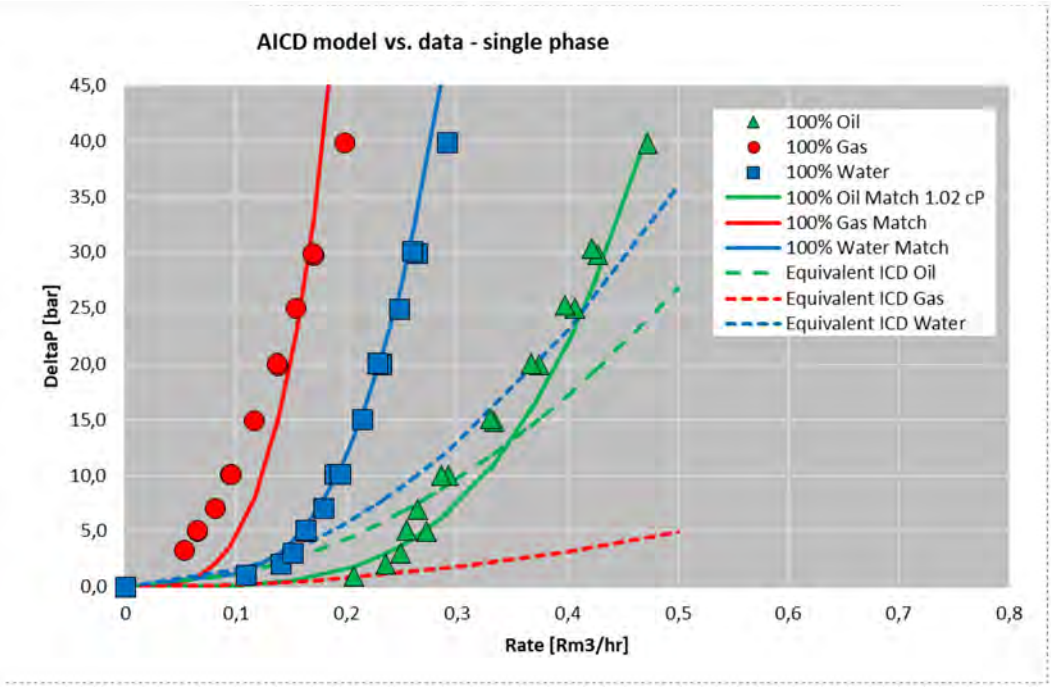

Figure 11—AICD model match vs. experimental data. Same fluid properties in model and experiments.

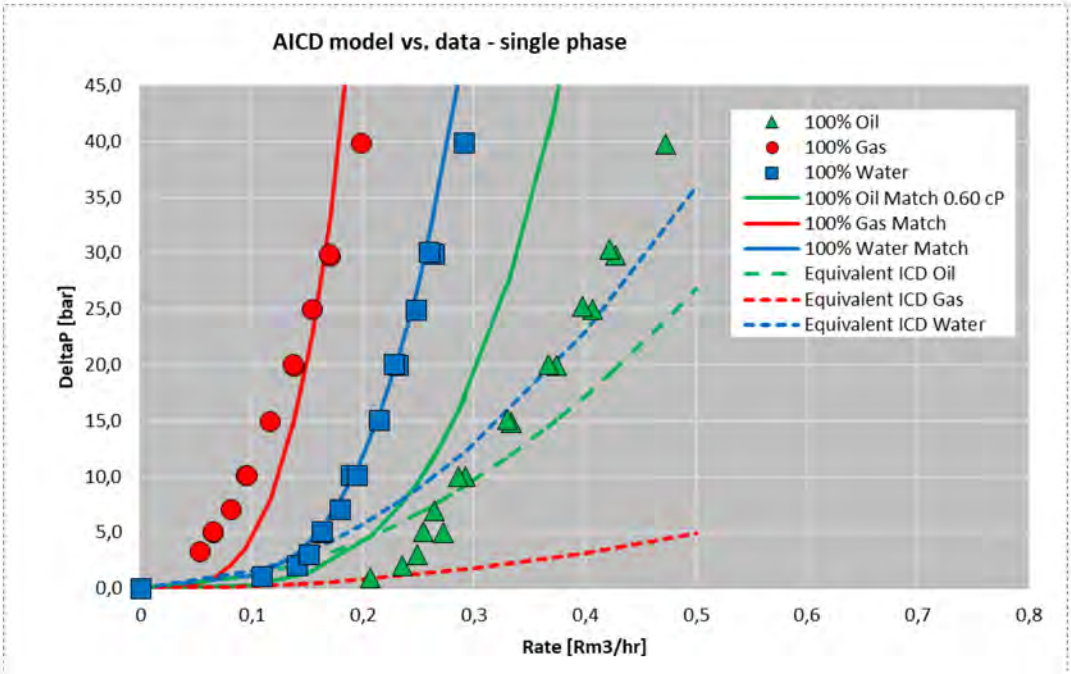

Figure 12—AICD model match vs. experimental data. 1.02 cp oil viscosity in experiment and 0.6 cP oil viscosity in model.

The effective AICV model in the reservoir model could be a mix of individual AICV performances and is somewhat uncertain. Further, standard reservoir simulators as used here has its limitations on representing the physics ongoing in the annulus of a horizontal well. In the study below, we assume that the effective AICV performance is as Table 2 except for 0.6 cp oil viscosity. We can name this model the "single valve AICV model".

Reservoir case study

The single valve AICV model has been tested in a North Sea thin oil rim development scenario using an industry standard reservoir simulator. The reservoir is a thin oil rim reservoir with excellent properties, with a large gas cap and a strong underlying aquifer. The oil column is only around 6.5 m, while the gas cap average column is around 30m and the aquifer is considered an unlimited regional aquifer. The oil is a light oil of around 0.6 cP viscosity. The reservoir model as shown in Figure 13 has a grid size of 50m × 50m orthogonal grid, with a varying cell thickness vertically refined in the oil column down to 0.5m.

The development strategy is long horizontal tri-lateral wells with a dense well spacing. All wells are placed 2.5 m below the gas cap in the 6.5m oil column.

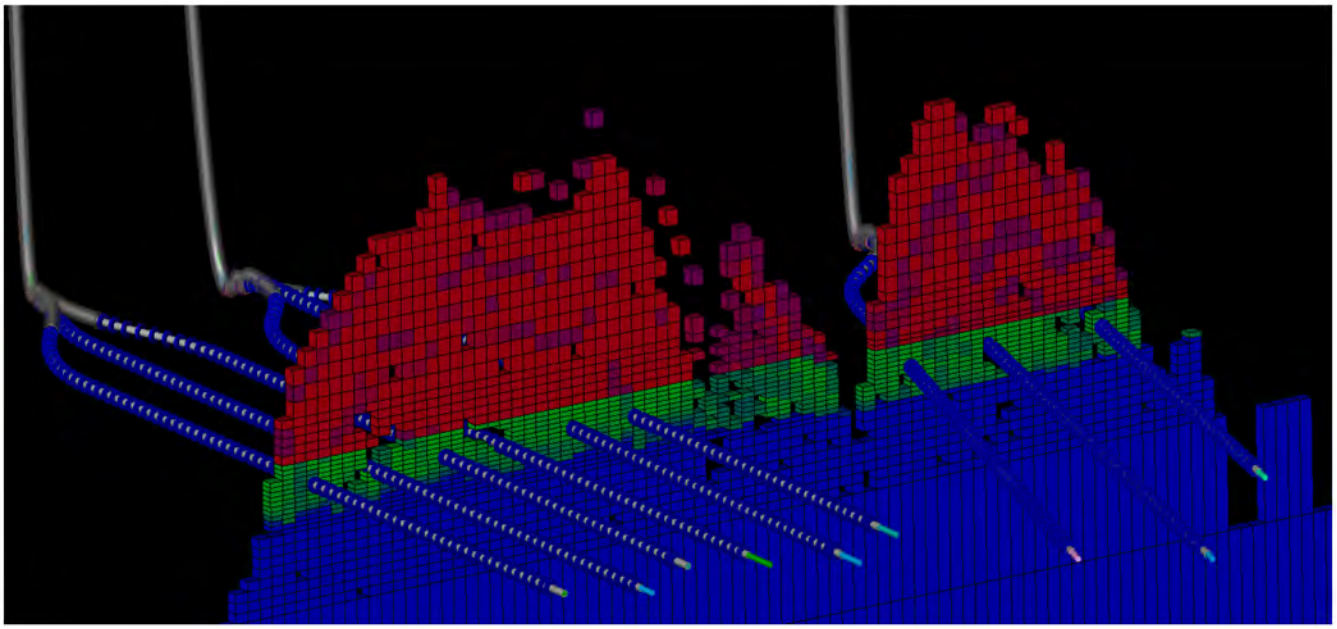

Figure 13—Reservoir model showing gas in red, oil in green and water in blue at initial conditions. Vertical to horizontal scale is aggregated 30:1.

The wells are modelled to produce 2500 sm3/d of liquid, with a GOR control scheme to stay below 600 sm3/sm3, for the first 5 years. The wells are modelled as multilateral segmented wells with inflow control devices along the entire horizontal section. The inflow devices are upscaled to the reservoir grid of 50m, and do not include annular flow. This is equivalent to having production swell packers every 50m. Less swell packers will be used commonly, but this is an optimization for later.

The completion is set as a constant configuration along all wellbores. No optimization along the wellbore has been done here. Some optimizations like some lower AICV/ICD density in the heel part of the well is expected as part of later optimization work. The three following completion scenarios are compared:

- 4x4mm ICD per 12m as an approximation for sand screens only
- 1x1.6mm ICD per 12m
- 1xAICV per 12m

Results from the full field simulation is shown in Figure 14 and Table 3 and demonstrate an incremental oil recovery gain between the 3 cases. For a thin oil rim development like this, it is beneficial for long term recovery to limit the production from the gas cap, as this limits the upward movement of the oil rim. The early GOR level is highest w screens, reduced somewhat with ICDs, and even more with AICVs. Advanced inflow control produces less unwanted gas from the gas cap and allow the well to stay longer at high liquid

rate without needing to choke back due to high GOR. By gaining 17.5% extra oil relatively, autonomous inflow control technology seems beneficial for this thin oil rim reservoir. AICD has been used extensively in similar reservoir conditions [3], [9], and will also be evaluated for this reservoir case.

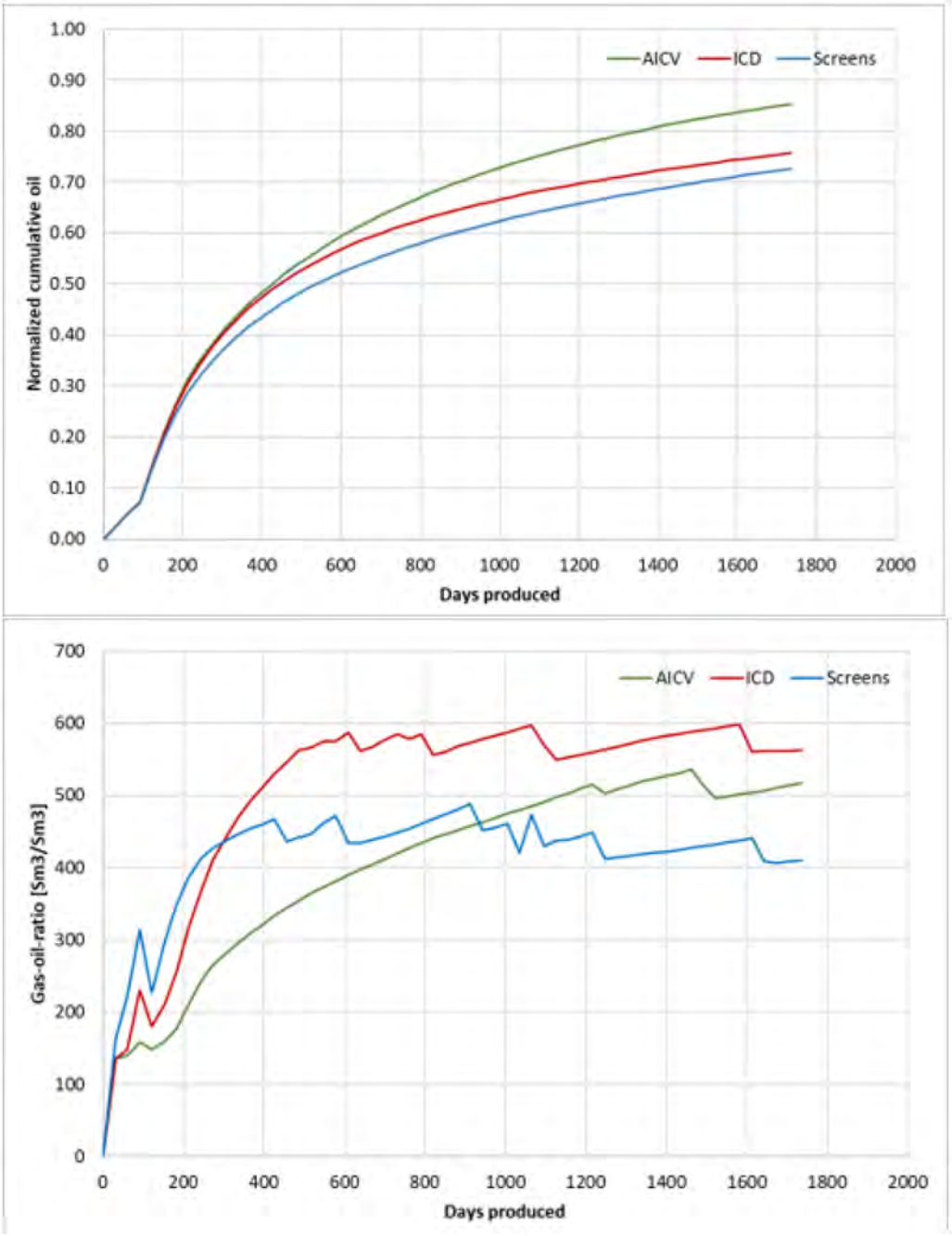

Figure 14—Full field simulation results comparing ICD, screen and AICV performance.

Table 3—Simulation results for three completion scenarios.

Completion scenario	Normalized cumulative oil	Relative increase from Screens case
4x4mm ICD (Screens)	0.726	**0 %**
1x1.6mm ICD	0.756	**+ 4.2 %**
1xAICV	0.853	**+ 17.5 %**

Future work on implementation of AICV in light oil reservoirs

As it is demonstrated in this work, deploying AICV can be beneficial in the most challenging light oil reservoirs with high GOR and WC. Future installations of AICV's in these kinds of reservoirs, ensuring a successful installation and eventually gaining field data will provide a comprehensive illustration of the AICV performance. This will provide the necessary knowledge for future installations and further development of this promising technology.

A proper compartmentalization and zonal isolation are among the criteria of having a successful installation, which is crucial in gaining the desired results in well completion with AICV's.

Conclusions

Detailed single and multiphase flow performance for the AICV were presented, discussed, and compared to conventional Inflow Control Device (ICD) performance. The test results demonstrate that the AICV flow performance is significantly better than conventional ICD for both single phase and multiphase flow.

A reservoir modelling method have been used to evaluate the AICV performance in a light oil reservoir compared to sand screens and ICD completion. The model was tested in a North Sea thin oil rim development scenario using an industry standard reservoir simulator. The simulation study showed that in case of well completion with AICV, oil production will be increased by 17.5% and 13.3% relative to completion with sand screens and ICDs, respectively.

Acknowledgements

The authors would like to thank Aker BP, ConocoPhillips, and Lundin for the permission to publish the work. We acknowledge Equinor test center in Porsgrunn for excellent laboratory work.

References

1. Mathiesen, Vidar; Werswick, Bjørnar; Aakre, Haavard, «The Next Generation Inflow Control the Next Step to Increase Oil Recovery on the Norwegian Continental Shelf, SPE 169223,» i *SPE Bergen one day seminar*, 2 April, Bergen, Norway, 2014.
2. Ismarrullizam Mohd Ismail, Nor Azuairi Che Sidik, Faez Syarani Wahi, Giok Lin Tan, Focht Tom, Frazer Hillis, «Increased Oil Production in Super Thin Oil Rim Using the Application of Autonomous Inflow Control Devices,» i SPE Annual Technical Conference and Exhibition, Dallas, Texas, 24-26 September 2018.
3. Kåre Langaas, Emile Jeurissen, Hailu Kebede Abay, «Combining Passive and autonomous Inflow-Control Devices in a Trilateral Horizontal Well in the Alvheim Field,» *SPE Production and Operations*, vol. **34**, nr. 03, pp. 446–460, 2018.
4. Aakre, Haavard; Halvorsen, Britt; Werswick, Bjornar; Mathiesen, Vidar, «Autonomous Inflow Control Valve for Heavy and Extra-Heavy Oil,» i SPE Heavy and Extra Heavy Oil Conference, Latin America,, Medellín, Colombia, 2014.
5. Soheila Taghavi, Haavard Aakre, Steven Swaffield, R. Brent Brough, «Verification of Autonomous Inflow Control Valve Flow Performance Within Heavy Oil-SAGD Thermal Flow Loop,» i SPE Annual Technical Conference and Exhibition, Calgary, Alberta, Canada, 2019.
6. J. Eric Lauritzen, Ingvild Berg Martiniussen, «single and Multi-phase Flow Loop Testing results for Industry Standard Inflow Control devices,» i SPE Offshore Europe Oil and Gas Conference and Exhibition, Aberdeen, 2011.
7. I. Leitão Junior, M. Negrescu, «ICD/AICD for Heavy Oil - Technology Qualification at the Peregrino Field,» i Offshore Technology Conference Brasil, Rio de Janeiro, 29-31 October 2013.

8. Martin Halvorsen, Martin Madsen, Mathias Vikøren Mo, Ismail Isma Mohd, Annabel Green, «Enhanced Oil Recovery on Troll Field by implementing Autonomous Inflow Control Device,» i *SPE Bergen One Day Seminar*, Bergen, Norway, 2016.
9. Kåre Langaas, Oxana Urazovskaya, Nicolas Gueze, Emile Jeurissen, «Attic Oil Recovery in the Alvheim Field,» i SPE Norway Subsurface Conference, Virtual, Bergen, Norway, 2020.

Paper 2

On Uncertainty Analysis of the Rate-Controlled Production (RCP) Model

This paper is published in the Proceeding of The First SIMS EUROSIM Conference on Modelling and Simulation, SIMS EUROSIM 2021, and 62nd International Conference of Scandinavian Simulation Society, SIMS 2021, September 21-23, Virtual Conference, Finland, 2021.

Paper presented by Soheila Taghavi

Authors: Soheila Taghavi and Ali Ghaderi

On Uncertainty Analysis of the Rate Controlled Production (RCP) Model

Conference Paper · March 2022

DOI: 10.3384/ecp21185271

2 authors:

Soheila Taghavi
University of South-Eastern Norway
5 PUBLICATIONS **1** CITATION
SEE PROFILE

Ali Ghaderi
University of South-Eastern Norway
48 PUBLICATIONS **55** CITATIONS
SEE PROFILE

On Uncertainty Analysis of the Rate Controlled Production (RCP) Model

Soheila Taghavi[1,2] Ali Ghaderi[3]

[1]Process, Energy and Environmental Technology, University of South-Eastern Norway, Norway, Soheila.t.hosnaroudi@usn.no

[2]InflowControl AS, Norway, Soheila.taghavi@inflowcontrol.no

[3]Mathematics and Science Education, University of South-Eastern Norway, Norway, Ali.Ghaderi@usn.no

Abstract

Rate controlled production (RCP) model is used to simulate and investigate the performance of the oil wells which are completed by autonomous inflow control devices. In order to quantify the performance of the RCP model, a dimensionless version of the model is considered, and its parameters are estimated. We demonstrate how the model and the measurement uncertainties can be quantified within the Bayesian statistical inference framework. In this relation, Hamilton Monte Carlo (HMC) is used to draw samples from the joint posterior probability distribution. We demonstrate that at the calibration step the modified model is able to capture the variations in the measurements. However, the cross- validation with the new data has revealed that the modified model tends to overpredict the pressure drop. This inadequacy cannot be explained by the measurement noise or the uncertainty in the estimated parameters. These results also imply that the original RCP model needs revision.

Keywords: AICV performance, RCP model, Bayesian inference, parameter estimation, MCMC, Stan

1 Introduction

Increase in oil production and recovery have been always the main objective of the oil industry. Hence, different methods and technologies have been developed to achieve this goal. One of the proven methods is to drill long horizontal wells, which increases the reservoir contact and consequently makes the oil production feasible and more economical.

However, long horizontal wells are likely to experience more pressure differences between the heel and toe section. This leads to non-uniform flow and consequently breakthrough of unwanted fluids in the heel section of the well, as shown in Figure 1.This phenomenon is known as heel to toe effect (Mathiesen, et al., 2014).

Autonomous Inflow Control Valve (AICV) together with Autonomous Inflow Control Devices (AICD's) like RCP valves are among the newest technologies that have been developed for Increased Oil Recovery (IOR). By balancing reservoir drawdown, these valves delay the onset of water and/or gas breakthrough and in case of breakthrough, it will restrict the production of these unwanted fluids significantly.

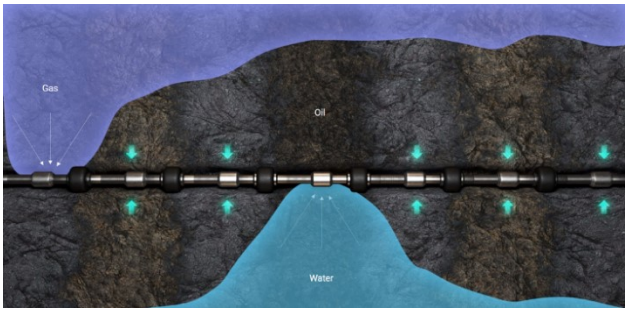

Figure 1.Uneven flow along the wellbore resulting in water and gas breakthrough.

A mathematical model describing the performance of the RCP valve was originally developed by Mathiesen et. al. in 2011 (Mathiesen, et al., 2011).This model is later being used to describe the AICV performance too. In recent years, both lab and production data from various oil wells have been used to check the validity of the model (Mohd Ismail, et al., 2018; Langaas, et al., 2020). This model has been implemented in reservoir simulators such as NETool and Eclipse in order to simulate the performance of the valve under static and dynamic conditions.

In order to be able to employ the model, one needs to estimate the model parameters prior to its deployment. It appears that one of the methods used by many practitioners for parameter estimation prior to utilization of the model in NETool is the trial-and-error method (Aakre, et al., 2018; Halvorsen, et al., 2016). Nevertheless, if one assumes that the model is correct, in most practical cases, the classical least square or similar methods are sufficient to produce good estimates for the model parameters (Moradi, et al., 2021). However, there are some evidences that the model does not explain all the variations in the data (Langaas, et al., 2020). There has also been attempts to modify the model (Voll, et al., 2014).

In order to be able to verify model inadequacy, two pre-conditions are needed to be satisfied. The first one

is accurate and precis measurements of the valve behaviour and the second one is the quantification of the different sources of the uncertainty. In this short paper, we will demonstrate how results from accurate measurements can be used within the Bayesian statistical inference framework to quantify and model the sources of the uncertainty and check how good the model explains the variations in the measurements.

2 AICV Principle

AICV utilizes viscosity and density differences between the reservoir fluids in such a way that it will keep the valve open for oil and closed for unwanted fluids like gas and water. Figure 2 illustrates AICV in open and closed position, respectively.

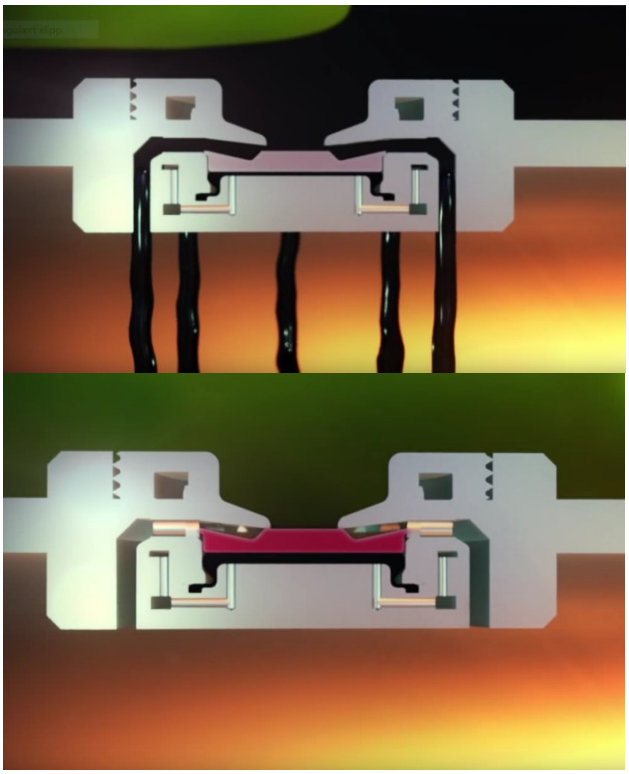

Figure 2. AICV is open for oil, illustrated by the black region (top) and closed for gas, illustrated by the green region (bottom).

This is achieved by taking advantage of the pressure differences in the Laminar Flow Element (LFE) and Turbulent Flow Element (TFE). These two flow restrictors are connected in series, which is illustrated in Figure 3 . AICV consists of two flow paths: the main flow path and the pilot flow path. Pilot flow path consists of two flow restrictors of LFE and TFE. When reservoir fluid enters the main path, a small portion of the flow is guided through the pilot flow, which is located near the main path. If a fluid with high viscosity enters the AICV, its flow through LFE will lead to a higher pressure drop over LFE. This phenomenon can be explained by Darcy-Weisbachs equation:

$$\Delta P = f \times \frac{L\rho v^2}{2D} = \frac{64}{Re} \times \frac{L\rho v^2}{2D} = \frac{32\mu v L}{D^2} \qquad (1)$$

where

ΔP is the pressure drop.

f is the friction factor (64/Re)

Re is Reynolds number.

ρ is the fluid density.

μ is the fluid viscosity.

v is the fluid velocity.

L and D are the length and diameter of the LFE respectively.

After passing through the LFE, which is a pipe segment, fluid enters a chamber. The second flow restrictor TFE, which is a nozzle, is placed in this chamber. The pressure drop across the TFE as described by Bernoulli, is calculated using the equation:

$$\Delta P = \frac{C}{2}\rho v^2, \qquad (2)$$

in which, C is a geometrical constant. Combination of these two flow restrictors results in a pressure drop, which determines how the AICV functions. As it is shown in Figure 3, high P2 will move the piston upwards closing the AICV for unwanted fluids while low P2 will keep the piston at its neutral position that maintains the oil production.

The concept and principle of AICV is described in detail in earlier SPE papers (Taghavi, et al., 2019; Aakre, et al., 2014).

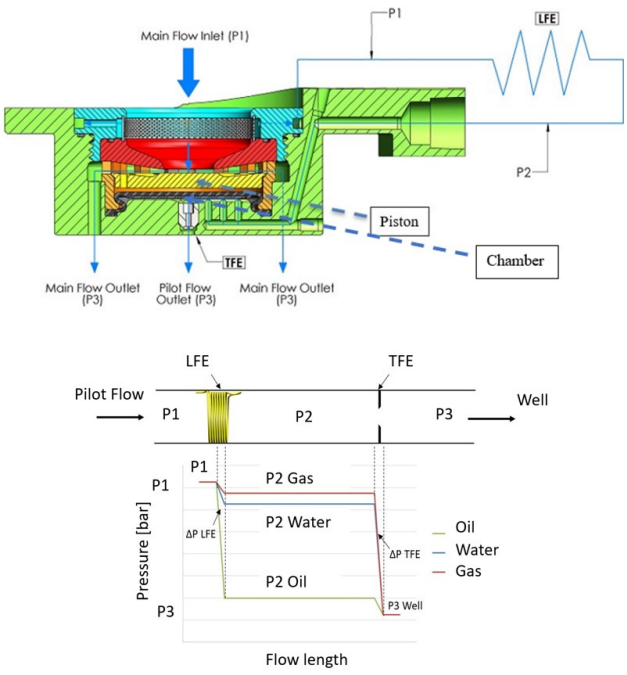

Figure 3. Combination of the laminar and turbulent flow restrictors in series in the AICV pilot flow.

3 RCP Model

The RCP model for the valve can be described as:

$$\Delta P_{Tot} = \left(\frac{\rho_{mix}^2}{\rho_{cal}}\right) \cdot \left(\frac{\mu_{cal}}{\mu_{mix}}\right)^y \cdot a_{AICD} \cdot Q^x \qquad (3)$$

where ΔP_{Tot} is the differential pressure across the AICV ρ_{cal} and μ_{cal} are the calibration fluid density and viscosity, and ρ_{mix} and μ_{mix} are the mixture fluid density and viscosity. The parameter a_{AICD} is a valve characteristic given by the ICD strength, Q is the volumetric mixture flow rate, and x and y are constants (Mathiesen, et al., 2011).

In order to reduce the complexity in this short article, we will concentrate our efforts on a single-phase oil flow. In addition, the model will be evaluated for three types of oil with different densities and viscosities.

The model described by Eq. (3), is dimensionally inconsistent. In order to avoid handling this inconsistency and its consequences, we study the flow rate vs. pressure drop with respect to a reference fluid at the same temperature. Therefore, we have chosen water at 20 degrees and a flow rate around 120 l/h. The measured pressure drop for water under these conditions is around 10 bar. Consequently, since a_{AICD} is a geometric parameter and hence independent of the fluid type, it will not play a role in the analysis. Then from Eq. (3) follows that the relative pressure drop with respect to water is

$$\frac{\Delta P_{oil}}{\Delta p_{water}} = \left(\frac{\rho_{oil}}{\rho_{water}}\right)^2 \left(\frac{\mu_{water}}{\mu_{oil}}\right)^y \left(\frac{Q_{oil}}{Q_{water}}\right)^x \qquad (4)$$

As it was mentioned earlier, there are some indications that the RCP model does not explain all the variations in the data. For this reason, we propose to use a multiplicative noise term in order to quantify possible model discrepancies. The *modified dimensionless RCP model* is

$$\frac{\Delta P_{oil}}{\Delta p_{water}} = \alpha \left(\frac{\rho_{oil}}{\rho_{water}}\right)^2 \left(\frac{\mu_{water}}{\mu_{oil}}\right)^y \left(\frac{Q_{oil}}{Q_{water}}\right)^x \qquad (5)$$

where α denotes the multiplicative noise term. Since the relative pressure drop is positive, we assume that a priori α is distributed according to Gamma distribution, with its mode at one. An α-value very close to one is an indication that the model can adequately describe the variations in the data. The statistical inference will reveal the probable values of α. In the following, Eq. (5) along with the experimental data are used to estimate the parameters α, x and y. These estimates are used to evaluate the performance of the modified RCP model.

4 Experimental Setup

The experiments were performed on the AICV prototype test rig at InflowControl's multiphase test facility located in Porsgrunn, Norway. A simplified schematic of the test rig showing the key elements of equipment and key measurement locations is shown in Figure 4. The tests can be carried out with water, pressurized air, and silicone oil as test fluid. The test facility is designed for single- and multiphase oil, water, and gas. A multistage centrifugal pump increases the water/oil pressure from the water/oil supply. Compressed air at room temperature can be regulated to the desired pressure for each case, up to maximum 200 bar. Flow rates, density and temperature are measured close to the inlet of the test vessel by a Coriolis flowmeter. A pressure transmitter measures the inlet pressure, whereas a differential pressure transmitter measures the differential pressure over the test vessel. Multiphase flow tests can be performed by injecting the desired oil flow rate to the test vessel, which is already filled with gas. The desired oil flow rate is injected from a separate test rig, which is connected to the single-phase test rig. The green dashed line in Figure 4 show the multiphase test flow path.

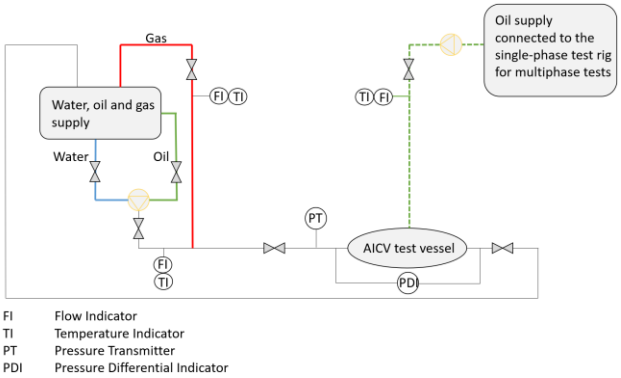

Figure 4. AICV prototype test rig setup.

4.1 Test Conditions and Data

Single-phase flow tests were performed with silicone oil as test fluid. The system conditions such as temperature and pressure, flow rates, pressure drops over the AICV and fluid properties, such as viscosity and density are controlled and measured in each test. The data obtained during the tests are listed in Table 1 in the Appendix. Temperature, density, and mass flow rate were measured using a Coriolis flow meter and the differential pressure across the AICV were measured by using a high precision pressure transmitter. Viscosity was measured and calculated manually using an Ubbelohde type viscometer. Viscosity measurements were performed several times under stable conditions in order to minimize the uncertainties. The accuracy of the different measuring tools employed in the tests are listed in Table 2 in the Appendix.

5 Bayesian Inference

The calculus of Bayesian inference is based on the application of two rules, the product, and the sum rules of the probability theory. One of the useful forms of the

product rule is the Bayes theorem. In the present context, we have noisy measurements, D and a model, M with unknown parameters represented by θ. We are seeking to estimate θ. Then by the Bayes theorem we have

$$P(\theta|D,M,I) = P(D|\theta,M,I) \times \frac{P(\theta|M,I)}{P(D|I)} \qquad (6)$$

$P(\theta|D,M,I)$ is the posterior distribution over the possible values of θ consistent with the measurements, the model and any other available and relevant background information denoted by I; like any information about the valve construction. On the right-hand side of the above equation, $P(D|\theta,M,I)$ is the likelihood, which is a statement about how likely it is to measure D given the model and specific values for θ. The term $P(\theta|M,I)$ is known as the prior distribution. In the present context, it models the expert opinion about the possible values of the θ. The last term $P(D|I)$ functions as the normalization constant and is independent of θ and hence not relevant in the present context. We remind the reader that the letters in the parentheses stand for logical propositions and "," denotes the logical "AND" operation. However, in calculations we work with algebraic expressions. The context will determine the use.

Often, as in the present case, the inference on θ also depends on some other parameters, for which neither their true values are known nor are they of primary interests. Nevertheless, due to dependency of inference on them, they must be part of the estimation process. These parameters are known as the *nuisance parameters*. Here the sum rule of the probability theory can be useful. Let ω denote the vector of the nuisance parameters, then by the sum rule we have

$$P(\theta|D,M,I) = \int_{\Omega} P(\theta,\omega|D,M,I)d\omega \qquad (7)$$

The above operation is called marginalization. Basically, calculating the above integral is the same as averaging the integrant over all possible values of ω. Marginalization is a very powerful concept and will be used in the next section. The reader is referred to (Kruschke, 2015) for further reading on Bayesian inference.

6 Statement of the Inference

In the following, let the model parameters, the nuisance parameters, data, and the model be denoted by θ, ω, D and M, respectively. That is,

$\theta = (\alpha, x, y)$
$\omega = (\Delta p_w, Q_w, \sigma_\mu, Q_o, \mu_o)$
$D = (\Delta p_{od}, Q_{od}, \mu_{od}, \rho_o, \rho_w, \mu_w, \sigma_p, \sigma_q)$
$M = M(\theta,\omega) = \Delta p_o(\theta,\omega)$

The description of each symbol is listed in Table 3 in the Appendix. The main reason for the choice of the nuisance parameter vector ω, is that we are uncertain about the true values of these parameters. For example, even though we have taken great care in measuring the viscosity, there is no guaranty that the conditions under which the oil flows through the valve are exactly the same as the viscometer. Therefore, we have chosen to include σ_μ as one of the nuisance parameters. Similar reasons are behind the choice of other components of ω. We emphasise that this is an important component in quantification of the sources of the uncertainty. The lack of knowledge about the true values of the parameters under different test conditions, which are not possible to be controlled during the experiments, constitute an important source of the uncertainty.

By the Bayes theorem, the joint posterior distribution is

$$p(\theta,\omega|D,M,I) \propto p(D|\theta,\omega,M,I) \times p(\theta,\omega|M,I). \quad (8)$$

The choice of the likelihood is determined by the measurements noise, while the choice of the prior distribution is based on the uncertainty in the expert knowledge about the true values of the parameters, before considering the measurements. For example, as was mentioned previously, α represents the multiplicative noise. It is positive and we expect its value to be one. However, there are reasons to believe that the model tends to overestimate the pressure drop over the valve. Therefore, we suspect that there is a good chance that α can attain values below one. For these reasons, we choose $\gamma(2,2)$, the gamma distribution with the parameters $(2,2)$, to represent our prior knowledge about α. The expected value of this distribution is one and its mode is at one-half. However, after seeing the data, the posterior distribution of α might be different, which as we shall see, is indeed the case. Note that $\gamma(2,2)$ has non-zero mass for all $\alpha > 0$. That is, the prior distribution does not exclude any positive values of α. It only makes some values less probable. The marginal posterior distribution of α will allow the data to modify the belief represented by the prior. In a similar manner, the expert knowledge on the other parameters can be incorporated in the inference process through appropriate choice of the prior distributions for each parameter. We have summarized the choices of the priors and the likelihoods for each parameter in Figure 5.

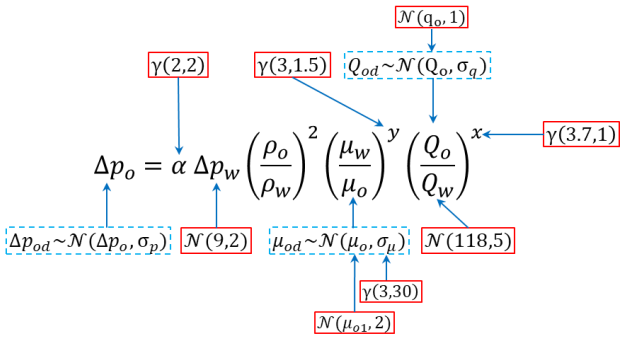

Figure 5. The choice of prior distribution (in red/whole) and the likelihood (in blue/dashed).

Due to *logical* independence between the parameters, the joint posterior distribution in Eq. (8) is the product of all the distributions listed in Figure 5. All the parameters are positive and in case of x, it is larger than 2. This means that all the normal distributions are truncated at zero. In the case of x, we have a truncated gamma distribution with lower limit being 2. The marginal posterior distribution is found by integrating over the domain of ω.

7 Markov Chain Monte Carlo Simulation

It is difficult to find an analytical expression for the joint- and the marginal posterior distributions of the parameters. This is generally a challenging task in Bayesian statistics. A common approach is to approximate the joint posterior distribution by large number of samples. The generation of samples are often conducted by a class of dependent sampling methods known as Markov Chain Monte Carlo (MCMC). Roughly explained, the method works by sampling the distribution relative to the height of the distribution function on its domain. The frequency distribution of these samples will on the long run converge to the true distribution. Computationally, one starts with a random sample and generates a chain of samples following certain sets of rules, which will guaranty that the chain will eventually visit all the regions relative to their probability mass. Since in practice one can only generate finite number of samples, it is important to check if the chain has found the regions of highest probability mass. There is a so-called *burn-in* period, below which all the samples are discarded. The reason for this is to make sure that in a set containing a finite number of samples, the samples from regions with low probability mass are not over-represented.

For the purpose of this study, we run a MCMC method known as *Hamiltonian Monte Carlo* (HMC), using the statistical software known as *Stan*, which comes also as a R package known as *RStan* (Stan development team, 2019). We have run four chains, each with different starting points. Figure 6 shows the output of the chains for each of the model parameters.

As it can be seen, regardless of the initial starting point of the chain, after a burn-in period of roughly 10K, all the chains are stabilized and converged. For more details, we refer the reader to (Kruschke, 2015).

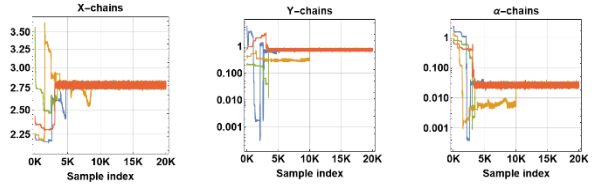

Figure 6. The trace plot of the MCMC chains for model parameters.

After ignoring the burn-in samples, the pairs plot can be used to represent the marginal posterior distributions of the model parameters. The plot consists of both single and pairwise marginal posterior distributions of the model parameters. It is basically 1D and 2D histogram of the samples of the model parameters (see Figure 7).

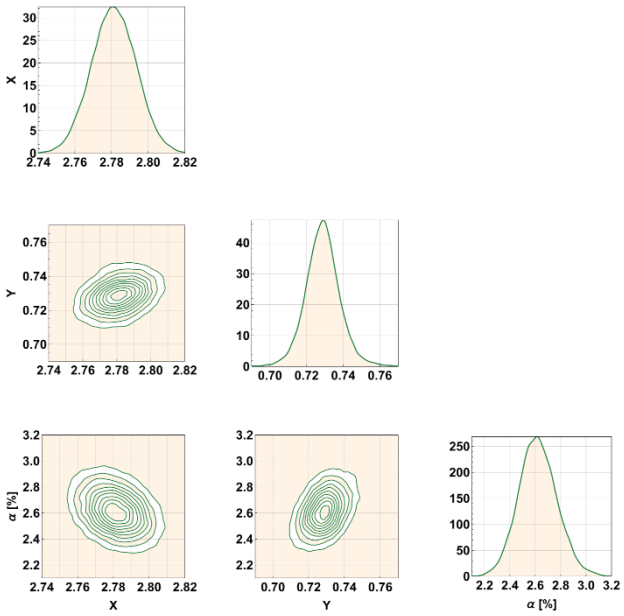

Figure 7. Pairs plot of the model parameters.

The histogram density of the parameter α reveals that the model is hugely over predicting the relative pressure drop over the valve. More specifically, the pressure drops over the valve have to be scaled down to 2.2%-3.2% of their predicted values by the model in order to be consistent with the measurements.

7.1 Calibration and Validation

The dataset D used in the MCMC simulation is generated by running experiments on two different oil types with viscosities 6.6 cP and 36.4 cP (see Table 4 in the Appendix). The measurements and the posterior samples from the MCMC with 99% credible intervals are plotted in Figure 8. Except for two points, for the case of 36.4 cP oil, all the pressure drops predicted by the model are within the 99% credible interval. That is,

at the calibration step, the model can describe most of the variations in the measurements. At this stage, without further measurements, it is difficult to explain the reason(s) for the two borderline outliers observed in the dataset for 36.4 cP oil.

The validation is conducted on a new dataset, which was not used in the estimation of the model parameters. This second dataset is generated by running the experiment on an oil with viscosity 12.6 cP. For this, we need to find the posterior predictive distribution.

Indeed, let $D_N = (\Delta p_{oN}, Q_{oN})$ denote the unobserved new data. Then the posterior predictive distribution is defined as $p(D_N \,|D, M, I)$. In order to be able to use the model M, one needs to know the model parameters.

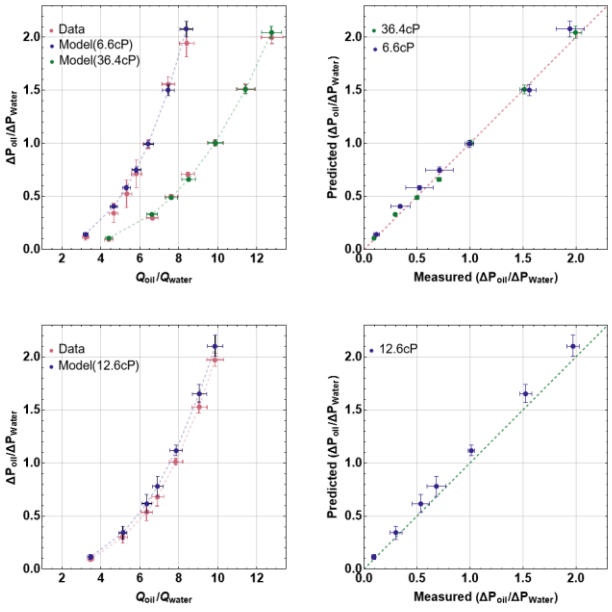

Figure 8. Calibration (top row) and validation (bottom row). The dashed lines are drawn for visualization purpose.

By application of the marginalization, we get

$$p(D_N \,|D, M, I) = \int_\Lambda p(D_N \,, \theta, \omega | D, M, I) d\theta d\omega \quad (9)$$

Note that by the product rule, the integrant can be expressed as

$$p(D_N \,, \theta, \omega | D, M, I) = p(D_N \,|\theta, \omega, D, M, I) \times p(\theta, \omega | D, M, I) \quad (10)$$

The observant reader recognizes that the second term on the right-hand side is the joint posterior distribution defined by Eq. (8). The first term on the right-hand side is called the *sampling distribution* and its functional form is same as the likelihood. The difference is that unlike likelihood, which is a function of the model parameters, the sampling distribution is a function of D_N and is normalized to unity over the domain of D_N. By applying the following algorithm, one can generate samples from the posterior predictive distribution,

1. Generate (θ_i, ω_i) from $p(\theta, \omega | D, M, I)$
2. Generate D_{Ni} from $p(D_N \,|\theta_i, \omega_i, D, M, I)$
3. $i = i + 1$, go to step 1.

The above algorithm is iterated a given number of times. The histogram of the generated samples D_{Ni} can then be considered as an estimate for the posterior predictive distribution defined by Eq. (9). Note that we are already in disposition of the samples (θ_i, ω_i). They are the samples generated from the joint posterior distribution during the calibration step. Thus, we only need to conduct the step 2 in the above algorithm. From the product rule, and the nature of measurements noise, follows that the sampling distribution can be expressed as product of two normal distributions

$$p(D_N \,|\theta, \omega, D, M, I) = p(\Delta p_{oN} \,|\mathrm{M}(\theta, \omega), Q_{oN}, D, I) \times p\left(Q_{oN} \,|q_{oN}, \sigma_q, I\right) \quad (11)$$

in which

$$p(\Delta p_{oN} \,|\mathrm{M}(\theta, \omega), Q_{oN}, D, I) = \mathcal{N}(\Delta p_{oN} | \mathrm{M}(\theta, \omega), Q_{oN}, D) \quad (12)$$

and

$$p\left(Q_{oN} \,|q_{oN}, \sigma_q, I\right) = \mathcal{N}\left(Q_{oN} | q_{oN}, \sigma_q\right). \quad (13)$$

In the above expressions q_{oN} is the given flow rate for which one seeks to calculate the corresponding pressure drop. The algorithm for generating samples from the sampling distribution can be formulated as follows

2.1. Generate Q_{oNi} from $\mathcal{N}\left(q_{oN}, \sigma_q\right)$
2.2. Generate Δp_{oNi} from $\mathcal{N}(\Delta p_{oN} | \mathrm{M}(\theta, \omega), Q_{oNi}, D)$

The result of the cross-validation with 99% credible error-bars is given in Figure 8. For low flow rates or equivalently low-pressure drops, the model prediction is within the 99% credible interval of the measurements. However, it appears that for high flow rates, the model has some tendency to over-predict the differential pressure over the valve.

8 Conclusions

In this paper, we demonstrated how the model and the measurement uncertainties can be quantified within the framework of the Bayesian statistics. In order to avoid complications due to dimensional inconsistency of the original model, we proposed a dimensionless version of the model. The result of our analysis revealed discrepancies, which could not be explained by the measurement noise or the uncertainty in the estimated parameters. The model inadequacy can be divided into global and local categories. The most serious problem observed was at the global level. Indeed, the predictions of the dimensionless model given by Eq. (5) had to be scaled down to 2.2%-3.2% of their values in order to be at the same level as the measurements. This has not been observed before or reported in literature. We believe that

the main reason for this is that this type of scaling would in general be absorbed into the a_{AICD} factor and hence would slip away unnoticed. Further studies are needed to determine the source(s) of this inconsistency. If one accepts the correction factor α and hence the modified dimensionless model given by Eq. (5), the deviation at the local level is less significant. The model validation has revealed that there is a tendency for the modified model to over-predict the pressure drop. A closer study of the results has revealed that a slight increase in oil viscosity during its passage through the valve can explain most of the overestimated pressure drop tendencies by the model. Further studies under more stringent conditions will be conducted in order to uncover the causes of these observations.

References

H. Aakre, B. Moldestad, B. Werswick, and V. Mathiesen. Autonomous Inflow Control Valve for Heavy and Extra-Heavy Oil. *In Proceedings- SPE Heavy and Extra Heavy Oil Conference. - Latin America, Medellín, Colombia*, 2014. doi: 10.2118/169233-MS.

H. Aakre, V. Mathiesen, and B. Moldestad. Performance of CO2 flooding in a heterogeneous oil reservoir using autonomous inflow control. *Journal of petroleum science & engineering,*167:654-663, 2018.

M. Halvorsen, M. Madsen, Mo. M. Vikøren, I. Mohd Ismail, and A. Green. Enhanced Oil Recovery on Troll Field by implementing Autonomous Inflow Control Device. *In Proceedings- SPE Bergen One Day Seminar. Bergen, Norway, 2016*. doi: 10.2118/169233-MS

J. Kruschke. *Doing Bayesian Data Analysis, A Tutorial with R,JAGS and Stan.* Elsevier Inc, Bloomington, USA, 2011.

K. Langaas,O. Urazovskaya, N. Gueze, E. Jeurissen. Attic Oil Recovery in the Alvheim Field. *In Proceedings-SPE Norway Subsurface Conference,Virtual. -Bergen, Norway,2020*. doi: 10.2118/169233-MS

V. Mathiesen, B. Werswick, H. Aakre, and G. Elseth. The Autonomous RCP Valve – New Technology for Inflow Control in Horizontal wells. *In Proceedings-SPE Offshore Europe Oil and Gas Conference and Exhibition, Aberdeen, 2011.* doi: 10.2118/169233-MS

V. Mathiesen , B. Werswick, and H. Aakre. The Next Generation Inflow Control the Next Step to Increase Oil Recovery on the Norwegian Continental Shelf. *In Proceedings - SPE Bergen one day seminar,2 April. - Bergen, Norway, 2014*. doi: 10.2118/169233-MS

I. Mohd Ismail, N.A .Che Sidik, F. Syarani wahi, G. Lin Tan, T. Focht, and F. Hillis. Increased Oil Production in Super Thin Oil Rim Using the Application of Autonomous Inflow Control Devices. *In Proceedings - SPE Annual Technical Conference and Exhibition, Dallas, Texas,2018*. doi: 10.2118/191590-MS

A. Moradi and B. Moldestad. A Proposed Method for Simulation of Rate-Controlled Production Valves for Reduced Water Cut. *SPE Prod & Oper*. 36(03): 669–684, 2021. doi: 10.2118/205377-PA

Stan development team Stan Reference Manual [Online]. -. - 2.27.2019. URL: https://mc-stan.org/docs/2_27/reference-manual/index.html

S. Taghavi, H. Aakre, S. Swaffield, and B.R. Brough. Verification of Autonomous Inflow Control Valve Flow Performance Within Heavy Oil-SAGD Thermal Flow Loop. *In Proceedings - SPE Annual Technical Conference and Exhibition. - Calgary, Alberta, Canada, 2019*. doi: 10.2118/196216-MS

B.A. Voll, I. Mohd Ismail, and I. Oguche. Sustaining Production by Limiting Water Cut And Gas Break Through With Autonomous Inflow Control Technology. *In Proceedings - SPE Russian Oil and Gas Exploration and Production Technical Conference and Exhibition. - Moscow,Russia,2014*. doi: 10.2118/171149-MS

Appendix

Table 1. Experimental results with model oil of different viscosities.

Differential Pressure [bar]	*Mass Flow [kg/h]*	*Density [kg/m3]*	*Temperature [°C]*	*Volume Flow [m3/h]*
Test#1; Oil 6.6 cP				
19.44	929.65	922.53	19.59	1.01
15.58	824.79	921.59	19.50	0.89
9.93	710.16	920.60	19.18	0.77
7.12	642.89	920.01	18.94	0.70
5.23	587.78	919.54	18.85	0.64
3.42	514.06	919.13	19.62	0.56
1.17	353.74	918.34	18.06	0.39
Test#2; Oil 12.6 cP				
19.73	1109.32	937.98	20.02	1.18
15.49	1021.85	937.51	19.34	1.09
10.12	882.52	936.54	19.25	0.94
6.82	774.99	935.77	18.93	0.83
5.36	712.71	935.48	19.11	0.76
3.02	575.30	934.97	18.61	0.62
0.92	388.95	934.03	19.57	0.42
Test#3; Oil 36.4 cP				
19.97	1460.89	953.18	21.95	1.53
15.13	1305.44	952.57	20.46	1.37
10.05	1126.45	951.34	20.31	1.18
7.08	966.33	951.62	20.28	1.02
4.99	868.67	952.29	20.54	0.91
2.96	760.25	953.07	20.88	0.80
0.93	503.04	950.56	20.05	0.53

Table 2. Accuracy of the test devices

Device	*Measured Property (ies)*	*Accuracy*
Coriolis	Mass flow, Temperature, Density	0.1 %
Pressure transmitter	Differential pressure	0.04 %
Viscometer	Viscosity	0.2 %

Table 3. Data and parameters description**.**

Name	*Description*
x, y, α	Model parameters
Δp_w	True differential pressure of water
Q_w	True volume flow rate of water
σ_μ	Standard deviation of oil viscosity
Q_o	True oil flow rate
μ_o	True oil viscosity
Δp_{od}	Measured differential pressure of oil
Q_{od}	Measured volume flow rate of oil
μ_{od}	Measured oil viscosity
ρ_o, ρ_w	Oil and water density
μ_w	Water viscosity $= 1$
σ_p	Standard deviations of the Δp measurements
σ_q	Standard deviations of the flow measurements
$\boldsymbol{\Delta p_o}$	True differential pressure of oil

Table 4. Calibration data set.

ρ_o *[kg/m3]*	Δp_{od} *[bar]*	σ_p *[bar]*	Q_{od} *[L/h]*	q_o *[L/h]*	σ_q *[L/h]*	μ_{od} *[cP]*	μ_{o1} *[cP]*
920	19.44	0.47	1007.72	1006.41	4.69	6.6	6.4
920	15.58	0.21	894.97	894.73	4.07	6.6	6.4
920	9.93	0.13	771.40	771.83	1.53	6.6	6.4
920	7.12	0.50	698.79	697.72	2.32	6.6	6.4
920	5.23	0.50	639.21	636.61	5.09	6.6	6.4
920	3.42	0.35	559.29	558.47	5.46	6.6	6.4
920	1.17	0.11	385.19	385.44	2.78	6.6	6.4
950	19.97	0.10	1532.66	1530.58	2.81	36.4	36.2
950	15.13	0.08	1370.44	1370.49	1.28	36.4	36.2
950	10.05	0.08	1184.07	1183.58	0.93	36.4	36.2
950	7.08	0.04	1015.46	1015.78	1.09	36.4	36.2
950	4.99	0.05	912.19	912.41	1.38	36.4	36.2
950	2.96	0.03	797.69	799.07	2.22	36.4	36.2
950	0.93	0.05	529.20	529.44	6.00	36.4	36.2

Paper 3

Performance Analysis of Autonomous Inflow Control Valve in a SAGD Late-Life Process with Non-Condensable Gases

SPE-208915-MS

This paper was prepared for presentation at the SPE Canadian Energy Technology Conference, Calgary, Alberta, Canada, 16-17 March 2022. Society of Petroleum Engineers

Paper presented by Soheila Taghavi

Authors: Soheila Taghavi, Haavard Aakre, and Britt M.E. Moldestad

SPE-208915-MS

Performance Analysis of Autonomous Inflow Control Valve in a SAGD Late Life Process with Non-Condensable Gases

Soheila Taghavi, University of South-Eastern Norway/InflowControl AS; Haavard Aakre, InflowControl AS; Britt M. E. Moldestad, University of South-Eastern Norway

 DOI 10.2118/208915-MS

This paper was prepared for presentation at the SPE Canadian Energy Technology Conference, Calgary, Alberta, Canada, 16-17 March 2022.

Abstract

The performance of an autonomous inflow control valve (AICV), used to restrict the inflow of unwanted fluids like gas and/or steam was simulated using an industrial reservoir simulator. The simulation results were used to determine how AICVs can improve the oil recovery in steam assisted gravity drainage (SAGD) operations. Utilizing inflow or flow control devices (ICDs/FCDs) in SAGD wells is a method with promising results. FCDs delay steam breakthrough and increase the oil recovery. The recently developed technology, AICV, further improves the oil recovery from SAGD operations. This paper provides a summary of the test data acquired from the full-scale flow loop testing that replicates the downhole operating conditions. Single and multiphase flow performance of an orifice type ICD and AICV is presented and compared. The results confirm the ability of the AICV to restrict the production of gas and/or steam. A performance analysis based on the results from the experiments and well case simulations is presented. The paper also presents an innovative approach on analyzing the well conditions which brings an insight into SAGD production wells completed with AICVs.

Simulations are performed in different scenarios of a SAGD late life process with non-condensable gases (NCGs), and these results confirmed a significant reduction in the gas liquid ratio (GLR), and an increased oil production when using AICV compared to the open hole case. Simulation results demonstrated that utilizing AICV in the SAGD production wells will reduce the gas and steam production by 64%. The reduction of steam production from the breakthrough zones allows a lower bottom hole pressure. This gives a higher sandface drawdown in the zones with less mobile oil, and thus a higher production from these zones. Further, this forces the steam chamber to be more evenly distributed along the different zones, resulting in increased oil recovery.

Considering the environmental aspect, AICV can contribute to a considerable reduction in the steam use which will consequently reduce the energy and water usage for steam generation. As a result, utilizing AICV in SAGD operations will improve the economics of SAGD projects.

Introduction

Bitumen and heavy oil reservoirs in western Canada utilize recovery methods such as steam assisted gravity drainage (SAGD) to obtain enhanced oil recovery (EOR). The viscosity of bitumen is in the range of 10^6 cP which makes it immobile and unable to flow towards the production well by gravity. The viscosity must be reduced dramatically to make the oil mobile. Hence, the high viscosity bitumen is heated by high quality steam injected continuously from an injection well which is located above the production well.

Steam from the injector form a steam chamber spreading towards the cold bitumen. Steam is transferring heat to the cold bitumen where the latent heat is released due to steam condensation. The transferred energy heats up the bitumen, resulting in decreasing the viscosity to below 20 cP and consequently increasing the oil mobility. As illustrated in Figure 1, the heated low viscous oil flows towards the production well. However, even steam distribution along the injector and steam conformance improvement must be attained to ensure an efficient SAGD process (Konopczynski, 2018). This can be achieved by deployment of flow control devices (FCDs) in the injector and/or the producer well. Deployment of flow/inflow control devices in the producer well can contribute to even influx of bitumen/water emulsion along the well and delay the onset of steam and water breakthrough. In industry, downhole FCDs are often referred to as inflow control devices (ICDs) (Banerjee & Hascakir, 2018) hence, in this work ICDs and FCDs are used interchangeably.

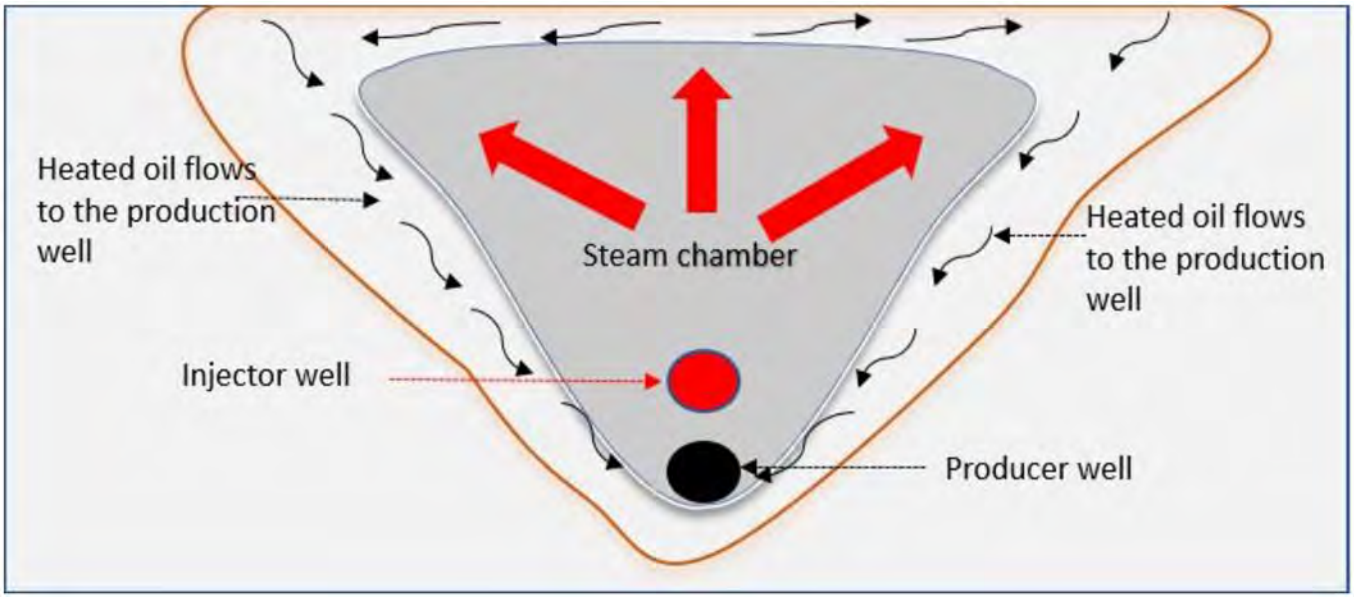

Figure 1—SAGD process.(Taghavi et al., 2019)

At the later stage of the SAGD process, non-condensable gases (NCGs) such as methane, nitrogen, carbon dioxide is co-injected with the steam to maintain the pressure and assist the bitumen to flow towards the producer well. The partial pressure of the steam is lowered, and consequently the temperature is being decreased from 230°C to about 160°C. This process is known as steam and gas push (SAGP) (Butler, 1999). As the non-condensable gases have lower density than steam, these gases tend to rise upwards towards the top edge of the steam chamber. The high concentrated gas on the top surface of the steam chamber acts as a barrier preventing thermal loss to the overburden. As a result, a significant amount of steam is saved. In addition, the gas at the top displaces oil downwards towards the producer well assisting the gravity drainage (Austin-Adigio & Gates, 2019; Butler, 1999). Although SAGP can cause some drawbacks (Canbolat et al., 2004; Sharma et al., 2012), several studies have demonstrated improved thermal efficiency of SAGD, increased oil production and reduced steam oil ratio (SOR) when SAGD is combined with NCG injection (Austin-Adigio & Gates, 2019; Bagci & Gumrah, 2004; Butler et al., 2001).

One of the disadvantages of SAGP is the reduced mobility of bitumen. Due to the presence of NCGs, the partial pressure of steam is lower, resulting in lower condensation temperature, and thereby lower mobility of bitumen (Austin-Adigio & Gates, 2019). It is important to maintain the required gas in the steam chamber to obtain an effective SAGP process, and therefore the production of gas should be limited. Limited gas production can be achieved by installing FCDs distributed on the tubing along the producer well.

Uneven liquid inflow from the reservoir to the well can result in steam and gas breakthrough in some parts of the well. This limits the heavy oil/bitumen production and consequently increases the SAGD operation cost. Therefore, reducing the steam and gas to oil ratio in the SAGD operation is essential to obtain an efficient bitumen recovery.

Passive FCDs have been successfully deployed in conventional reservoirs to reduce the production of unwanted fluids such as water and/or gas and increase the oil recovery. In comparison to conventional reservoirs, application of FCDs in SAGD wells is new. The application of FCDs in Surmont Field in Alberta in 2009, was accompanied by excellent steam-chamber development and overall performance (Stalder, 2013). Vachon et al. (2015) provide an overview of the initial necessary flow loop considerations for thermal FCD testing. Results from laboratory testing and preliminary field data of a FCD specifically designed for thermal operation showed successful performance (Lastiwka et al., 2019).

However, the way these passive FCDs delay the unwanted fluid breakthrough is not ideal. The fundamental problem of passive FCDs is that in confronting gas and/or steam, they appear to experience lower pressure drop than they do for oil. This will result in higher flow rate of gas and/or steam in the zones with breakthrough, which results in a potential problem of non-conforming profile over time. Autonomous FCDs restrict the production of unwanted fluids by increasing the pressure drop locally in the breakthrough section. This will contribute to an improved conformance profile along the well over time. (Banerjee & Hascakir, 2018)

Autonomous inflow control devices (AICDs) have not been widely used in SAGD wells so far, however, results from the laboratory tests and simulation analysis demonstrate promising performance in balancing the flow along the well, delaying steam breakthrough, and consequently providing uniform reservoir depletion (Konopczynski, 2018; Least et al., 2014).

The recently developed technology, autonomous inflow control valve (AICV), has the ability to restrict the production of unwanted fluids like water, gas and steam significantly. AICVs have been deployed worldwide for different applications from water control in the heavy oil reservoirs (Buwauqi et al., 2021) to gas control in the light oil reservoirs suffering from high gas oil ratio (Abd El-Fattah et al., 2021). AICV multiphase flow performance for a light oil reservoir with 1.02 cP oil viscosity and its significant impact on reservoir recovery are presented in previous author's work (Taghavi et al., 2021). In addition, both laboratory full scale testing and well production data demonstrate advantages of this technology in EOR wells. The advantages of AICVs over ICDs in CO_2-EOR were presented by (Aakre et al., 2018) in a trial well in the Midale carbonate field. In addition, results from full-scale high temperature laboratory flow loop that replicates the downhole operating conditions of a SAGD well demonstrated that a considerable reduction in steam consumption is possible by using AICV. This will contribute in less steam needed, reduced water usage, and consequently reduced greenhouse gas emissions for each barrel of oil produced, thus improving the economics of SAGD projects (Taghavi et al., 2019). In SAGD applications, the AICV can be designed to favor the production of the most viscous fluids, encouraging the cooler sections of the horizontal well to produce, and thereby enabling more uniform production along the well. This can also result in a reduction in SOR.

AICV Technology

The AICV functionality is based on utilizing the viscosity differences between reservoir fluids. The AICV will keep open for oil that has higher viscosity than water, steam, and gas.

As shown in Figure 2, AICV consists of two flow paths: the main flow path and the pilot flow path. The main flow flows over the piston as indicated by the green arrows, while the pilot flow path is shown by dashed red arrows. The pilot flow consists of two flow restrictors which act based on viscosity and density differences of the passing fluids. A small portion of the total flow is guided through the pilot flow. The pressure of the fluids through the flow restrictors, will drop depending on their viscosity and density. The governing equation of the first flow restrictor is Darcy-Weisbachs equation:

$$\Delta P = f \times \frac{L\rho v2}{2D} = \frac{64}{Re} \times \frac{L\rho v2}{2D} = \frac{32\mu vL}{D^2}, \quad (1)$$

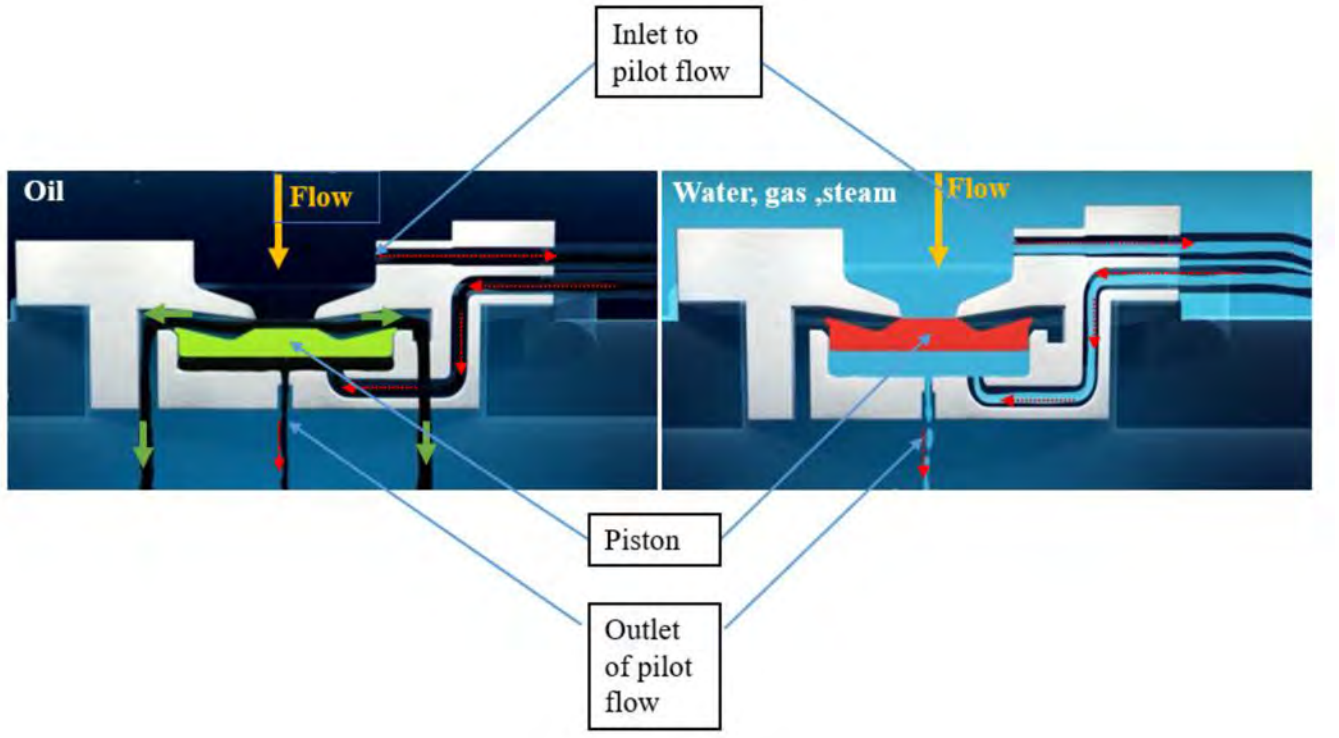

Figure 2—AICV is open for oil (left) and closed for water, gas, steam (right).

where ΔP is the pressure drop through the restrictor, *f* is the friction factor (64/Re), Re is Reynolds number, *ρ*, μ,*and v* are the fluid density, viscosity, and velocity respectively. *L* and *D* are the length and diameter of the flow restrictor. After passing through the first flow restrictor, fluid enters a chamber where the piston and the second flow restrictor is located. The pressure drop across the second flow restrictor as described by Bernoulli, is calculated using the equation:

$$\Delta P = \frac{C}{2}\rho v2, \quad (2)$$

in which, *C* is a geometrical constant.

The resulting pressure acting on the piston determines the piston movement, either upwards or downwards. If the pressure acting on the piston is high enough, then the resulting force will push the piston upwards closing the AICV for water, gas and/or steam. When the AICV is closed, the only flow to the production well is the flow through the pilot flow (the outlet of the pilot flow in the figure to the right). Lower pressure acting on the piston will keep the piston at its neutral position that maintains the oil production from both the main flow and the pilot flow (the small green arrows and the outlet of pilot flow in the figure to the left). The concept and principle of AICV is described in detail in earlier SPE paper (Aakre et al., 2014).

As illustrated in Figure 3, AICV can be mounted in isolated zones in the sand screens. The blue arrows in the figure show the flow path from the reservoir towards the sand screen, passing through the AICV,

entering the production tubing, and ultimately flowing to the surface together with the fluids from the other serial connected joints.

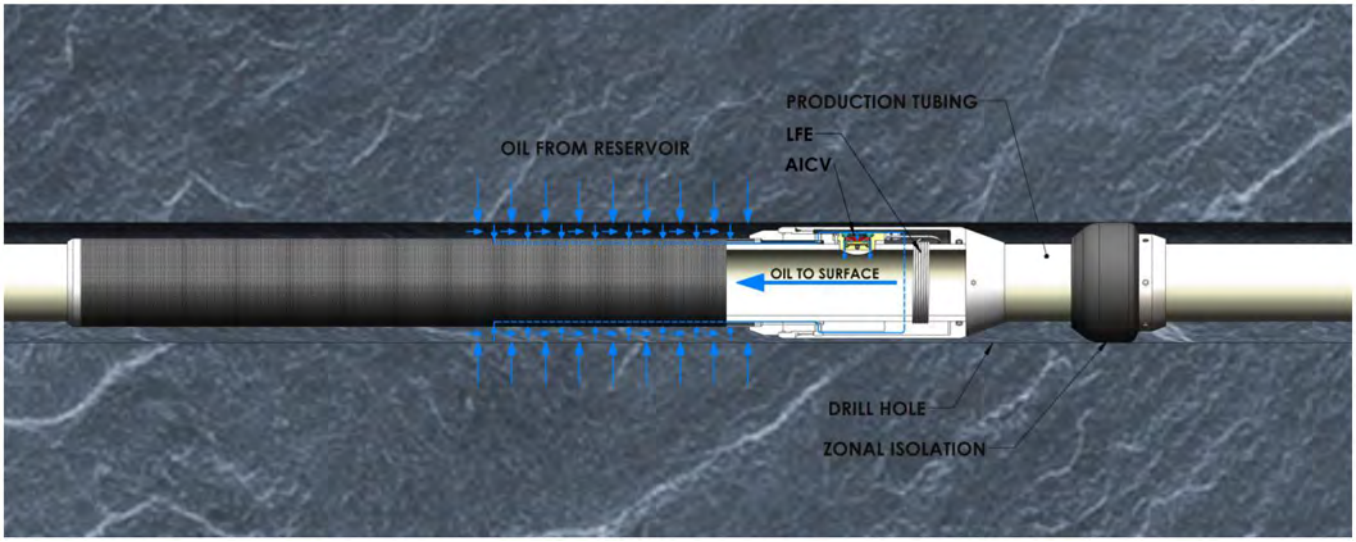

Figure 3—AICV mounted into the sand screen joints.

AICV Performance Under SAGD Conditions

Both single and multiphase flow tests were performed at the InflowControl multiphase test facility located in Porsgrunn, Norway. A simplified schematic of the test rig showing the equipment and key measurement locations is shown in Figure 4.

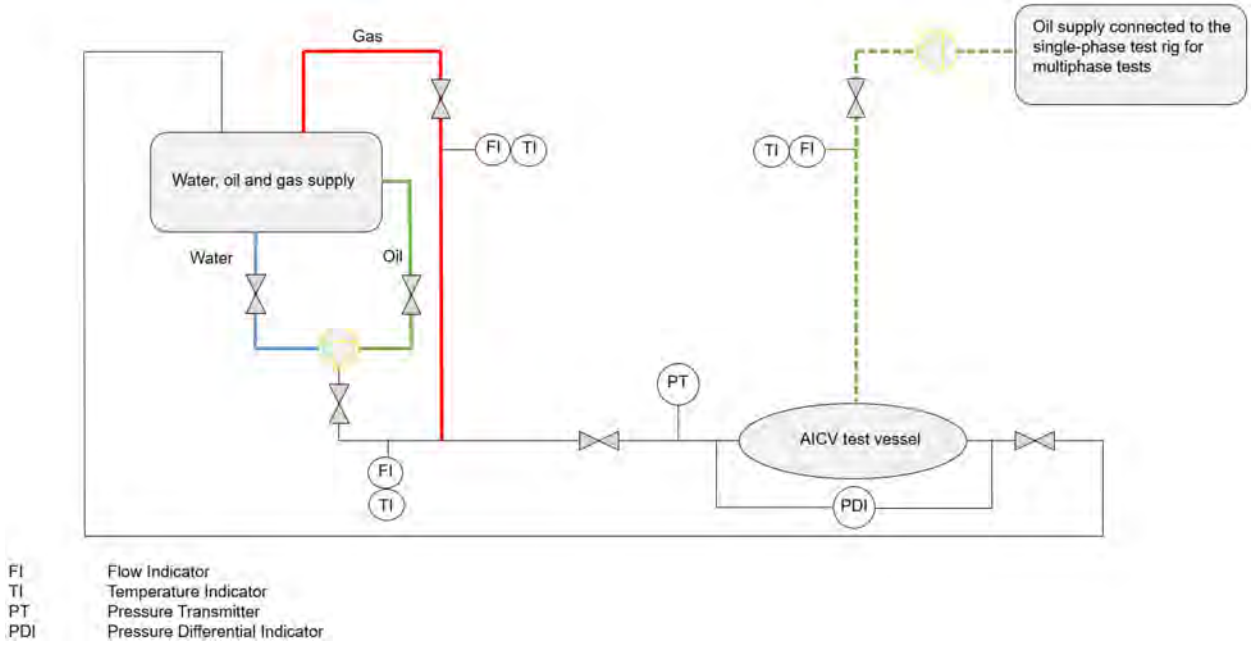

Figure 4—Schematic of the experimental flow loop.

The tests can be carried out using water, pressurized air, and oil as the test fluids. The test facility is designed for single- and multiphase oil, water, and gas tests. The desired test pressure for oil and water is obtained by regulating a multistage centrifugal pump. Compressed air at room temperature can be regulated to the desired pressure for each case, up to a maximum of 200 bar. A Coriolis flowmeter measures the flow rate, density, and temperature close to the inlet of the AICV test vessel. A pressure transmitter measures the inlet pressure, whereas a differential pressure transmitter measures the differential pressure over the test vessel. Multiphase flow tests can be performed by injecting the desired oil flow rate to the test vessel, which is already filled with gas. The desired oil flow rate is injected from a separate test rig, which is connected to the single-phase test rig. The green dashed line in Figure 4 shows the multiphase test flow path.

The test conditions applied in the experiments represent the conditions of a late life SAGD reservoir. The gas density was 11.5 kg/m^3 and the oil and water viscosity were measured to be 2.5 cP and 0.40 cP respectively. Tests with 44 cP oil were also performed in order to have a realistic oil viscosity range representing a late life SAGD reservoir. The gas density is equivalent to the hydrocarbon gas density at the reservoir condition. Also, the steam density is approximately the same as the hydrocarbon gas density at the SAGD late life condition. The mixture of NCGs and steam in a SAGD late life reservoir will behave as gas through the valve. Thus, in the simulations and the experiments, the gas represents the mixture of steam and hydrocarbon gas. The test matrix and system conditions are shown in Table 1.

Table 1—Test and system conditions.

Description	Fluid type	System conditions and/ fluid properties	Differential pressure across AICV [bar]
Single-phase test	Gas	≈11 bar, ρ ≈11.5 kg/m^3	1-8
Single-phase test	Water	≈ 70˚C / 0.40 cP	1-8
Single-phase test	Oil	44 cP and 2.5 cP	1-8
Multi-phase test	Oil and gas	≈11 bar	1-5

Single-phase flow tests

The single-phase performance data of the AICV and an orifice type ICD are presented in Figure 5. The ICD has equivalent size to the AICV. The tests were performed by establishing the desired differential pressure across the test unit where AICV is installed and measuring the stabilized flow rate.

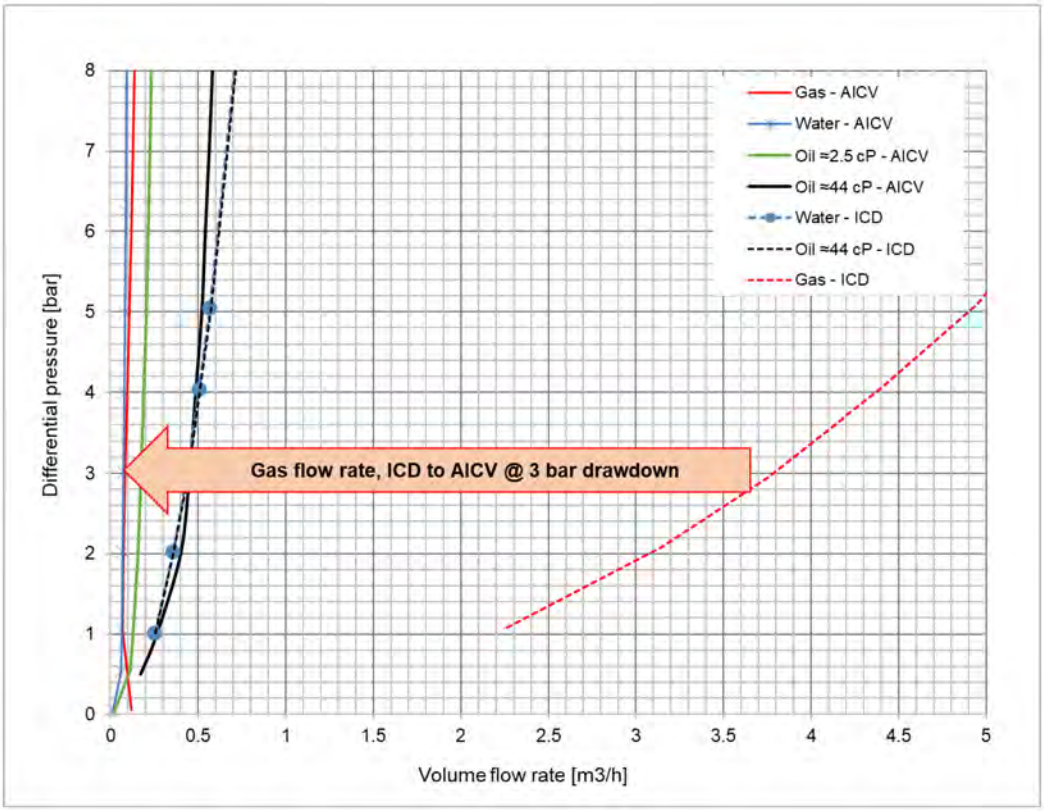

Figure 5—Comparison of single-phase flow performance of the ICD (dashed lines) and AICV (solid lines) for oil, water, and gas.

The pressure drops across the AICV and ICD as a function of the volumetric flow rates of the fluids are illustrated in Figure 5. The oil flow rate through the ICD is matched with AICV for 3 bar differential pressure. When the oil flow rates are equal, the gas flow rate through the ICD (red dashed line) and the AICV (red solid line) are compared. The gas flow rate at 3 bar for the ICD is about 3.8 m^3/h while it is about 0.1 m^3/h for the AICV indicating that the gas reduction by using AICV is significant. The ICD behavior is mainly density dependent and therefore the flow rate of oil and water is almost the same (the dashed black and blue lines respectively). The AICV is able to choke the water considerably (solid blue line). This is favorable when an aquifer is present in the reservoir and water breakthrough will likely occur. The results indicate that AICV compared to ICD is able to improve the oil recovery and production significantly by reducing the production of water, gas and/or steam fluids.

Multi-phase flow tests

Figure 6 shows two-phase oil/gas tests performed at 1, 2, 3 and 5 bar differential pressure across the AICV along with the single-phase performance of oil and gas for reference. The tests were performed by regulating the desired amount of oil flowing through the test unit filled with gas at targeted stable differential pressures.

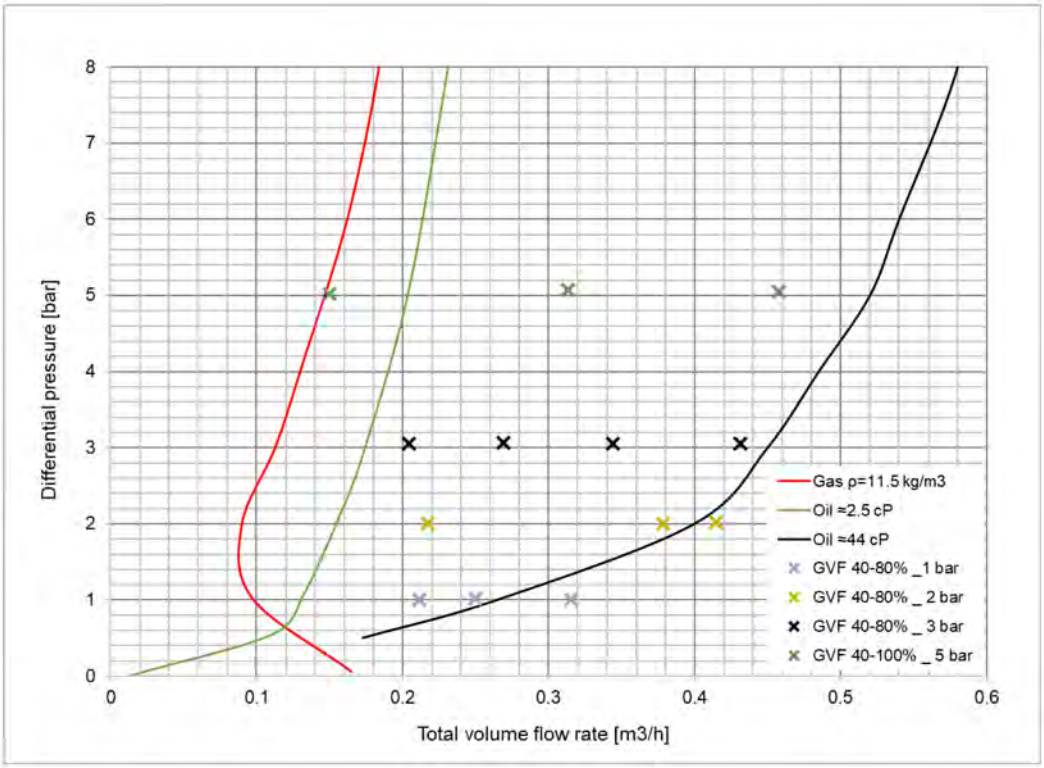

Figure 6—Two-phase performance of AICV at 1,2,3, and 5bar differential pressure together with single phase tests of AICV.

The pressure drop as a function of the total volume flow rate of the fluids is plotted. The total volume flow rate is the volume flow rate of gas together with the oil. The tests were performed in the gas volume fraction (GVF) range of 40-80 %. The AICV gradually opens when the oil/gas mixture flows through the valve. However, the AICV restricts the gas flow when the GVF is getting higher, until pure gas flows through the valve. The green point over the red curve (pure gas) at 5 bar is an illustration of 100 % GVF when the valve is closed, and the gas is only flowing through the pilot flow.

Modeling and simulation case study

The performance of the AICV in a SAGD reservoir is simulated using NETool. NETool is a one-dimensional steady state near well simulation tool which can be used for analysis of various types of inflow control devices. One of the most important benefits of using NETool for performance analysis of different inflow control technologies, is providing a user-friendly modeling for relative complex wells within a short simulation time.

AICV model

Equinor developed a mathematical model in 2011 which describes the performance of the rate controlled production (RCP) valve (Mathiesen et al., 2011) :

$$dP_{Tot} = \left(\frac{\rho_{mix}^2}{\rho_{cal}}\right) \cdot \left(\frac{\mu_{cal}}{\mu_{mix}}\right)^{y} \cdot a_{AICD} \cdot Q^{x}, \tag{3}$$

where ΔP_{Tot} is the differential pressure across the AICV, ρ_{cal} and μ_{cal} are the calibration fluid density and viscosity, and ρ_{mix} and μ_{mix} are the mixture fluid density and viscosity. The calibration fluid is water, and the mixed viscosity and density are calculated in NETool based on the fraction of the different fluids in the mixture. The parameter a_{AICD} is a valve characteristic given by the ICD strength, Q is the volumetric mixture flow rate, and x and y are constants.

By using the classical least square method, the model parameters are estimated and fitted to the experimental data and the results are shown in Figure 7. The dashed lines represent the modeled performance while the solid lines are data from the experiments. The model data is in relatively good agreement with the experimental data. There are some indications that the model do not explain all the variations in the data (Langaas et al., 2020). The author of this work has done uncertainty analysis of the model (Taghavi & Ghaderi, 2021). Results from the analysis revealed some inadequacy in the model which could not be explained by the measurement noise or the uncertainty in the estimated parameters. The author concluded that the original RCP model needs revision.

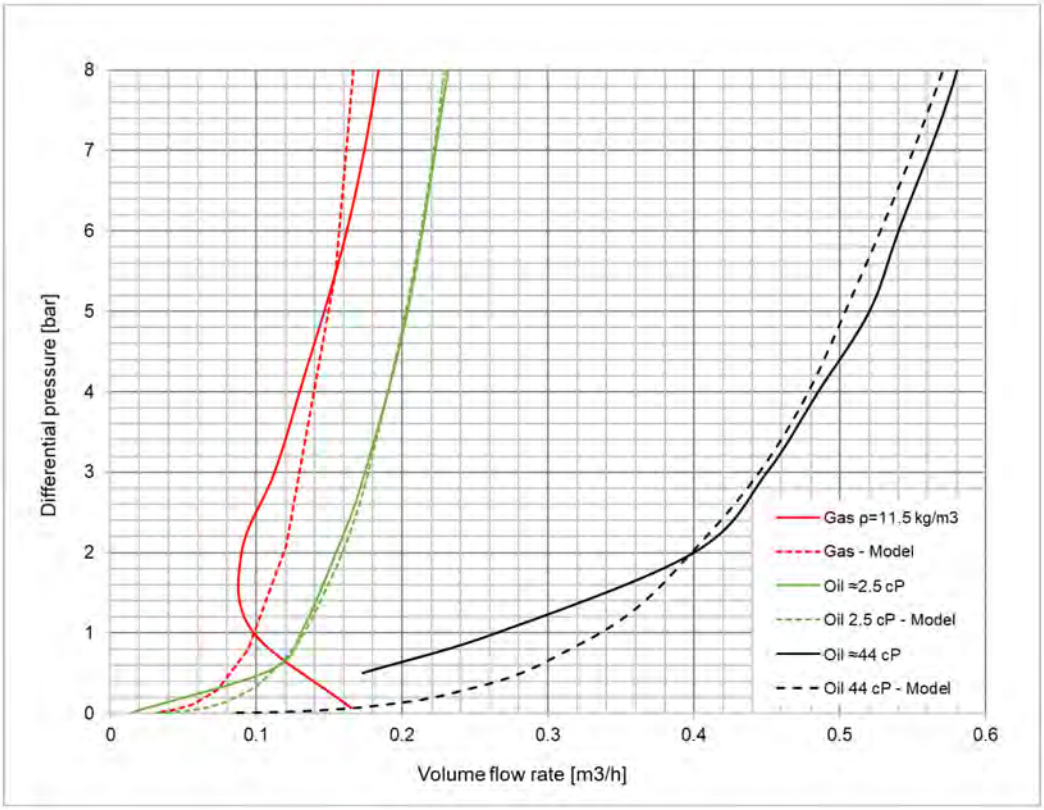

Figure 7—AICV model vs. experimental data.

Despite the discrepancies in the model, the existing model is used to model the AICV performance. Based on the assumed temperature profile along the well and the measured bitumen viscosity in the reservoir shown in Figure 8 and Figure 9 respectively, the AICV performance is modeled for the corresponding bitumen/water emulsion viscosities. The bitumen viscosity data as a function of temperature was selected from the literature (Jahanbani et al., 2012). It is common that bitumen/water emulsion is present in a SAGD reservoir, hence the AICV performance is modeled for the bitumen/water emulsion viscosity. In addition, if the other characteristics inherent in the emulsion are neglected, it is assumed that the AICV performance is only viscosity dependent for this range of viscosities. The model data shown in Figure 10 illustrates the differential pressure over the AICV as a function of the volumetric flow rate of emulsions with different viscosities.

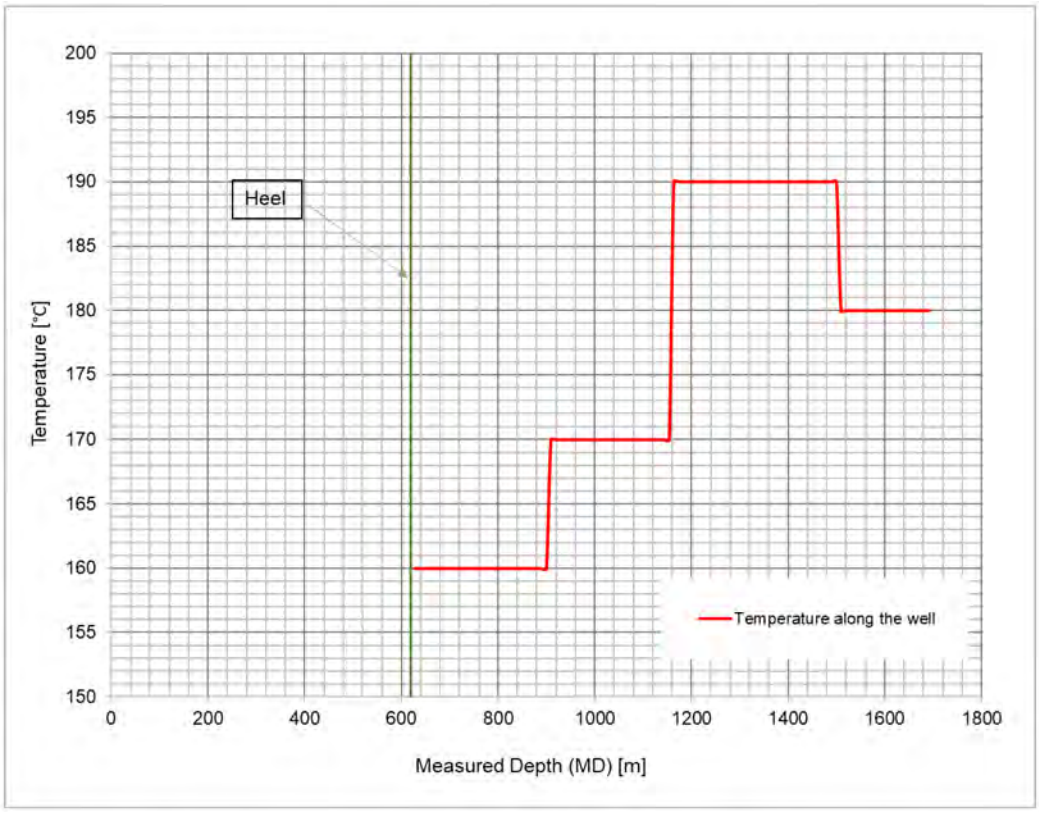

Figure 8—Temperature profile along the well.

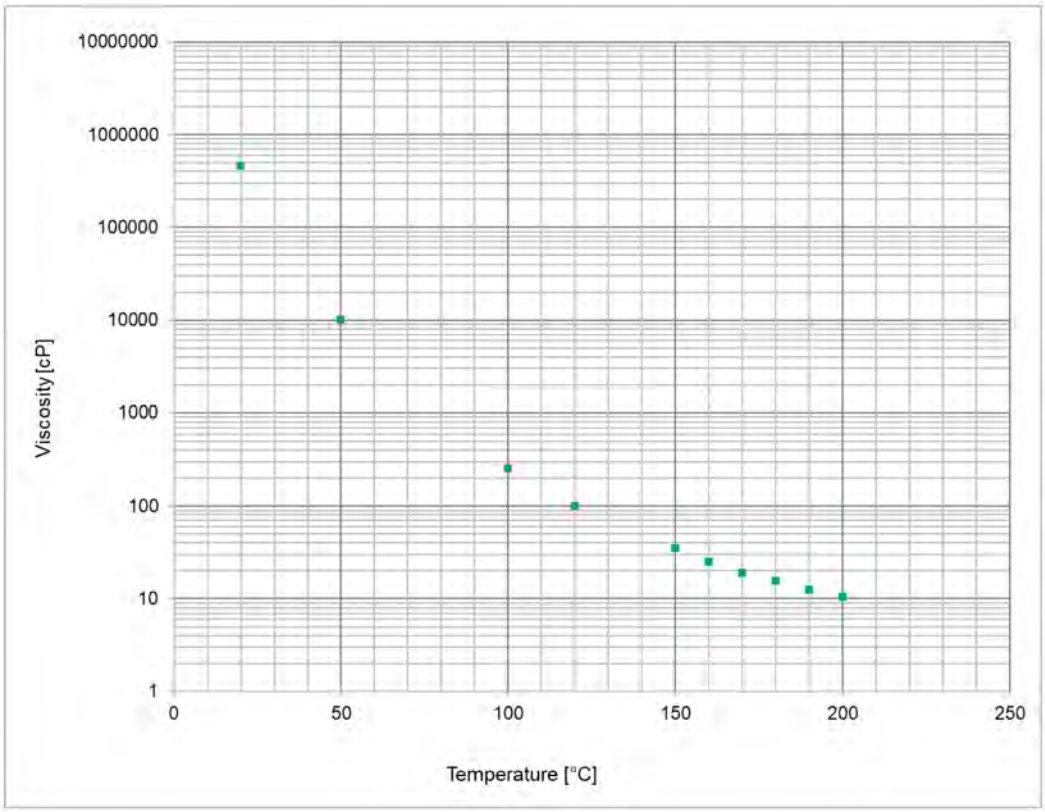

Figure 9—Viscosity as a function of temperature (Jahanbani et al., 2012).

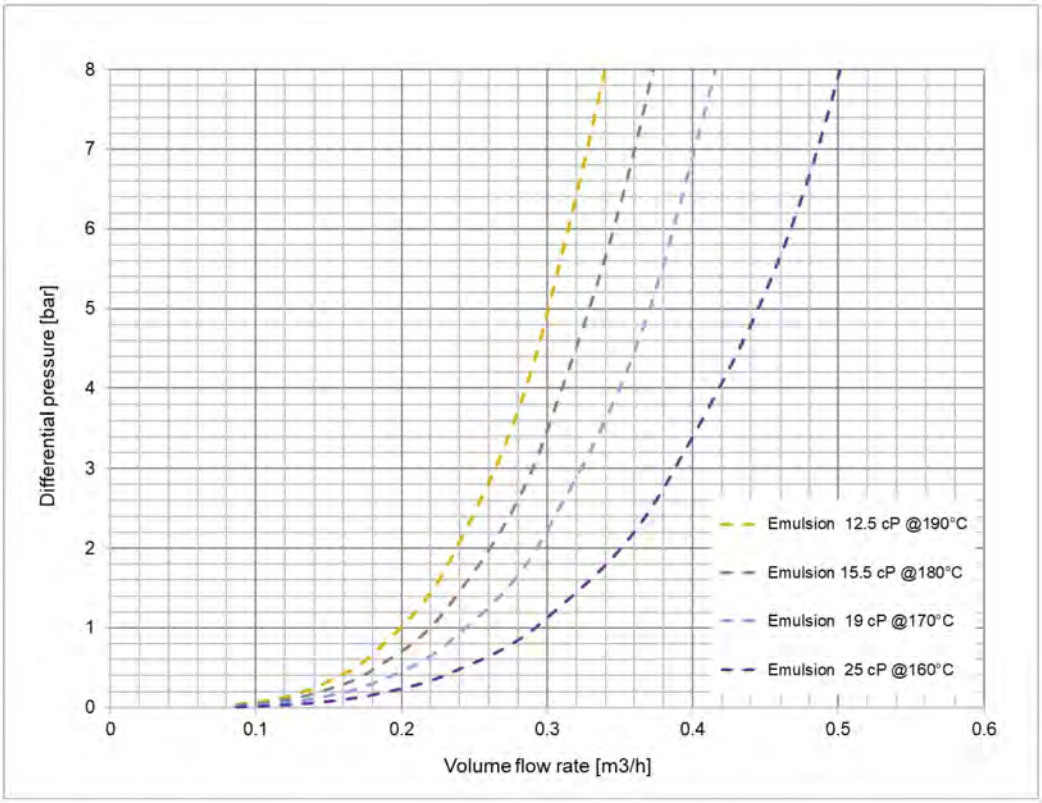

Figure 10—The modeled AICV performance.

The RCP model is available in NETool, and it is possible to adjust the functionality of the implemented AICVs by applying the model parameters and coefficients. The estimated model parameters, a_{AICD}, *x and y*, for different viscosities, as well as the density and viscosity for water as the calibration fluid, have been implemented in NETool.

Well case study

To analyze the AICV performance, a homogenous sandstone reservoir with a SAGD production well is assumed. NETool is used to carry out the performance analysis under SAGD late life condition. The implemented Black-oil model is used in the simulations carried out in this study and the Joshi model is chosen to model the inflow from the reservoir to the wellbore. The Joshi model assumes a constant pressure boundary and a centered well in the reservoir.

In this simulation case, the reservoir pressure is 27.5 bar, and it is assumed that the temperature along the well varies. The temperature profile along the well for the simulation case is illustrated in Figure 8. The temperature varies from 160°C to 190°C and the corresponding viscosity range is 25 cP to 12.5 cP. The open hole length is about 1045 m, the top measured depth is 620 m, and it is assumed that the production well is horizontal. Based on the temperature differences along the well, the production well is divided into four zones. The temperature and viscosity of the fluid in each zone are illustrated in Figure 11. The AICVs (black circles) are distributed in 21 compartments isolated by packers (red rectangles).

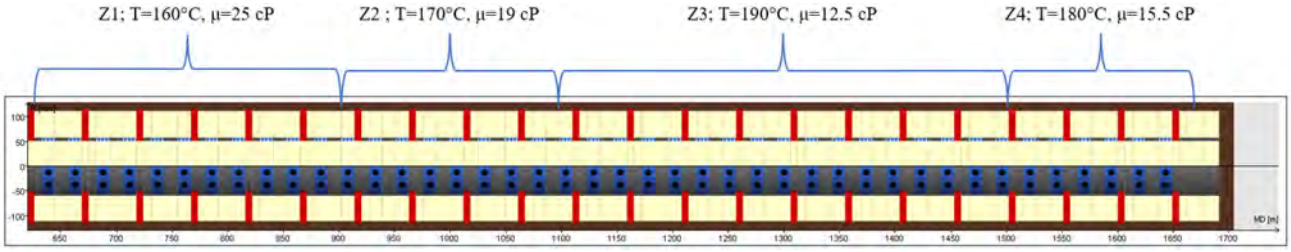

Figure 11—Fluid temperature and viscosity along the well.

The key information as well as the number of AICVs in each zone are listed in Table 2.

Table 2—The key information of the zones.

Production zones, Z	Zone length, L [m]	Number of AICVs	Temperature, T [°C]	Viscosity, μ [cP]
Z1	300	24	160	25
Z2	200	16	170	19
Z3	400	32	190	12.5
Z4	150	12	180	15.5

The base pipe is a precision punched screen (PPS) liner with OD 177.8 mm and the wellbore diameter is 222 mm. It is assumed that the reservoir pressure is less than the bubble point pressure and that the oil is saturated.

Different permeabilities and saturations are specified for the production zones. Production zone 3 has the highest gas saturation as it is the warmest zone, which implies the high probability of gas breakthrough from this zone. It is assumed that zone 3 has a gas saturation of 0.03, whereas zones 1, 2 and 4 are 100% saturated with oil. The horizontal permeability of the zones 1, 2, and 4 is set to 3000 mD, while the horizontal permeability of zone 3 is 6000 mD. The vertical permeability is 6/10 of the horizontal permeability. The data used as input to NETool is presented in Table 3.

Table 3—Input data to NETool

Parameter	Value	Unit
Top measured depth, *MD*	620	m
Well length, *L*	1045	m
Wellbore diameter, *ID*	222	mm
Base pipe outer diameter, *OD*	4.5	inch
Reservoir pressure, P_R	27.5	bar
Reservoir temperature, T_R	See Figure 8	–
Emulsion viscosity, μ	See Figure 9	–
Reservoir thickness	20	m
Reservoir width	500	m
Vertical /horizontal permeability, k_v/k_h	0.6	–
Gas density, ρ	11.5	Kg/m^3
Gas viscosity, μ	0.016	cP
Saturation in zone 1	S_g=0, S_o=1	–
Saturation in zone 2	S_g=0, S_o=1	–

Parameter	Value	Unit
Saturation in zone 3	S_g=0.03, S_o=0.97	–
Saturation in zone 4	S_g=0, S_o=1	–
Horizontal permeability in zone 1, K_h	3000	mD
Horizontal permeability in zone 2, K_h	3000	mD
Horizontal permeability in zone 3, K_h	6000	mD
Horizontal permeability in zone 4, K_h	3000	mD
Target oil production, Q	423	Sm^3/d

It is assumed that methane and steam are injected from the steam injection well and the objective is to analysis how AICV can prevent gas production and consequently improve oil production and recovery.

Results and Discussions

Simulations are performed with the three following scenarios and the results are compared:

1. Open hole: The target oil production is around 423 Sm^3/d with 0.75 bar drawdown.
2. 84×AICV (42×dual AICV) distributed equally along the well isolated by 22 packers: The target oil production is around 423 Sm^3/d with 3.5 bar drawdown.
3. 84×AICV (42×dual AICV) distributed equally along the well isolated by 22 packers: The target drawdown is 5 bar.

The drawdown represents the total drawdown which is the sum of the drawdown through the sandface and across the completion. As mentioned earlier, in the experiments and the simulation results, the oil represents bitumen/water emulsion, and the gas represents the mixture of steam and methane. The assumed horizontal permeability along the well at different production zones is illustrated in Figure 12.

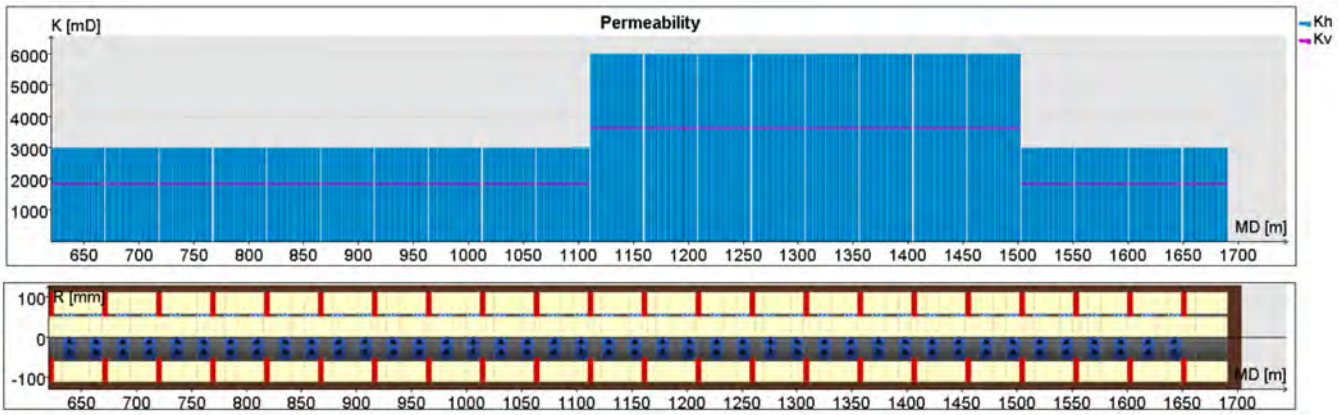

Figure 12—Permeability along the well.

Figure 13 shows comparison of the stock tank oil and the gas rates from the reservoir to the well together with the pressure profile along the well for the three simulation cases. The flow rates are given as $Sm^3/day/m$ of the well length. As can be seen from the figure, gas breakthrough occurs in zone 3, from MD 1100 m to 1500 m, as the gas saturation was highest in this zone. However, gas production is much higher in the case of open hole compared to the AICV cases. In the production zone 3, where the gas saturation is high, the AICV restricts the gas flow significantly. This allows reducing the bottom hole pressure and thus increasing the drawdown.

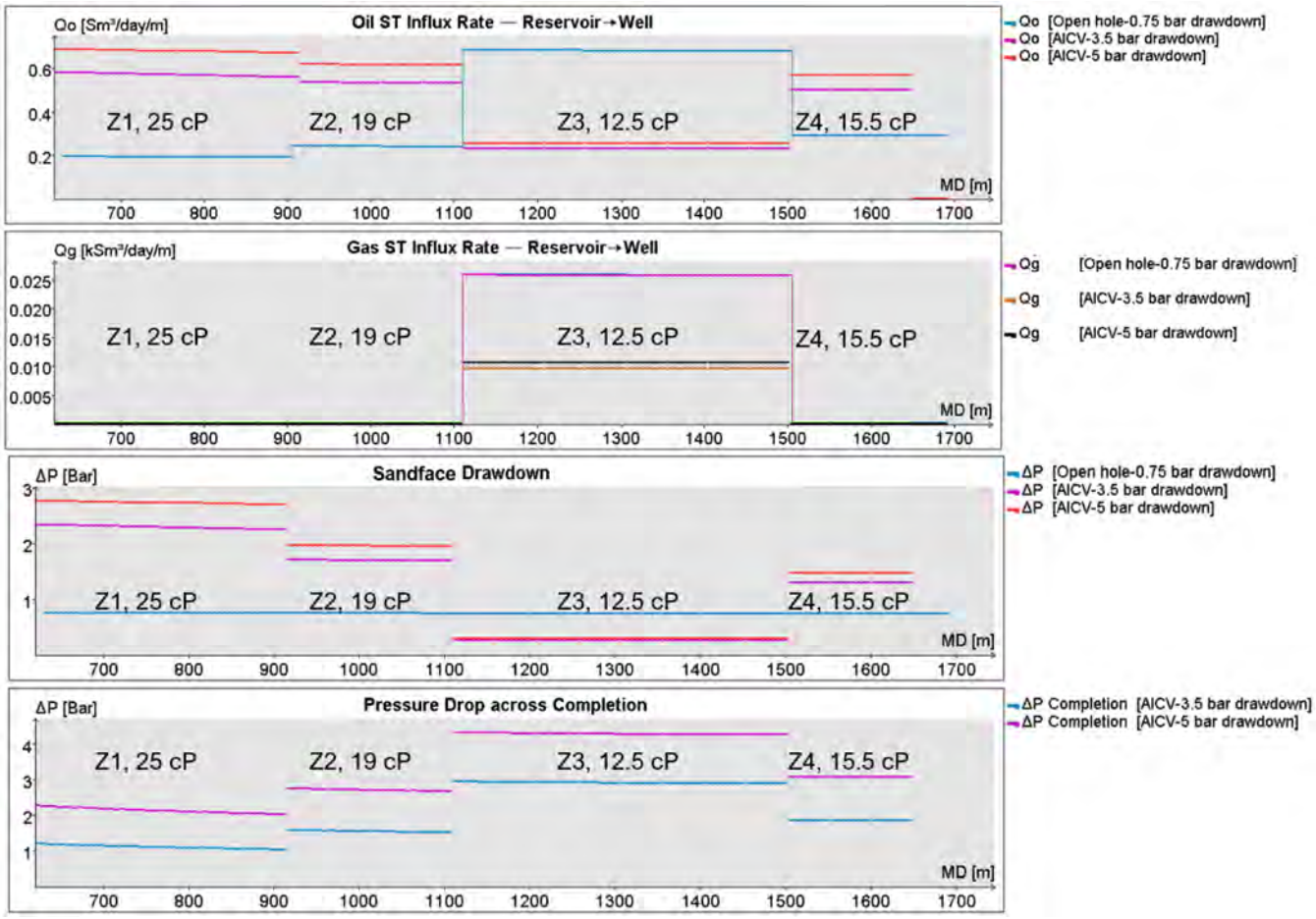

Figure 13—Oil and gas production and pressure profile along the well for three simulation cases.

By decreasing the bottom hole pressure to 22.5 bar, the AICV is still able to restrict the gas flow in the zone 3. Since the bottom hole pressure is being decreased, a higher drawdown in the sandface from zones, 1, 2, and 4 is obtained. Thus, a higher production from the zones with less mobile oil is achieved, and thereby forcing the steam chamber to be more evenly distributed along the different zones resulting in increased oil recovery. When the total drawdown is increased to 5 bar, the oil production from all zones is increased as well, compared to the open hole case and the AICV case with 3.5 bar total drawdown.

To check if the simulated oil production agrees with the modeled AICV performance, the production zone 1 in Figure 13 is considered. For the case of AICV with 3.5 bar total drawdown, the pressure drop across the AICV is around 1.2-1.1 bar along the zone length. The simulated oil production for this zone is approximately 0.58 Sm^3/day/m. As the zone length is 300 m, the oil production from this zone is equal to 7.25 m^3/h. According to Table 2, there are 24 AICVs installed in this zone which implies an oil production of 0.3 m^3/h per AICV. Figure 10 demonstrates that at 1.2-1.1 bar differential pressure across AICV, the flow rate of the 25 cP emulsion is around 0.3 m^3/h as well. This indicates that NETool is able to give a good prediction of the oil production.

It can be seen from the Figure 13 that as the bitumen/water emulsion viscosity increases, the sandface drawdown gets higher as well. This is according to Darcy's law in porous media which implies that the pressure drop across the porous media is directly dependent on the fluid viscosity:

$$\Delta P = \frac{Q \mu L}{k A} \tag{4}$$

ΔP is pressure drop across the rock sample, and Q and μ are the fluid flow rate and viscosity respectively. L is the rock sample length, A is the cross-sectional area of the rock sample, and *k* represents the permeability.

The production zone 1 has the highest fluid viscosity which is 25 cP. The pressure drop across the AICV in this production zone is lowest which indicates that the AICV is more open, producing the colder viscous bitumen/water emulsion. AICV is able to distinguish between the fluid viscosities and adjust the performance accordingly.

The results summery of the simulation cases are shown in Table 4. The initial reservoir pressure was the same for the three simulation cases. The target production rate for the cases with open hole and AICV with 3.5 bar drawdown was set to approximately 423 Sm^3/d. NETool predicts that the AICV case gives a gas reduction of 64% from 10.16 kSm^3/d to 3.67 kSm^3/d compared to the open hole case. If the bottomhole pressure is reduced from 24 bar to 22.5 bar, the production of the bitumen/water emulsion is increased by 15% from 423.72 Sm^3/d to 490.40 Sm^3/d. Also, 60% gas reduction compared to the open hole case is obtained.

Table 4—Comparison of the results for three simulation cases.

Case	Reservoir pressure [bar]	Bottomhole pressure (BHP) [bar]	Emulsion rate [Sm^3/d]	Gas rate [kSm^3/d]	Gas liquid ratio (GLR) [Sm^3/Sm^3]	Emulsion increase	Gas reduction
Open hole-0.75 bar drawdown	27.50	26.75	423.00	10.16	24.01	–	–
AICV-3.5 bar drawdown	27.50	24.00	423.72	3.67	8.66	0.16 %	64 %
AICV-5 bar drawdown	27.50	22.50	490.40	4.10	8.31	15 %	60 %

Conclusions

A homogenous sandstone reservoir with a SAGD production well was assumed as the case study to evaluate the performance of autonomous inflow control valve, AICV, when SAGD is combined with non-condensable gas injection. The single and multiphase flow performance data of a conventional ICD and AICV were presented, discussed, and compared. Results from the tests confirm the advantage of the AICV over the ICD in significantly restricting the production of gas and/or steam.

Simulations were performed with NETool, which is a steady state one dimensional near well simulation tool. The modeled AICV performance and the assumed SAGD reservoir conditions were used to run the simulations. Simulations were performed in different scenarios comparing an open hole well and an AICV completed well with two different drawdowns. The results indicate that AICV can decrease the production of gas and steam by 64 % compared to an open hole completion. In addition, the emulsion production can be increased by 15 % when AICV is used at higher drawdown.

Utilizing AICV in SAGD wells results in a considerable reduction in steam consumption which will consequently reduce the energy usage for steam generation. As less energy and steam are needed, the overall economics of SAGD projects will be improved.

References

Aakre, H., Halvorsen, B., Werswick, B., & Mathiesen, V. (2014). Autonomous Inflow Control Valve for Heavy and Extra-Heavy Oil. SPE Heavy and Extra Heavy Oil Conference: Latin America,

Aakre, H., Mathiesen, V., & Moldestad, B. (2018). Performance of CO2 flooding in a heterogeneous oil reservoir using autonomous inflow control. *Journal of Petroleum Science and Engineering*, **167**, 654–663. https://doi.org/https://doi.org/10.1016/j.petrol.2018.04.008

Abd El-Fattah, M., Fahmy, A. M., Wahaibi, H., Shibli, A., & Zuhaimi, K. (2021). Autonomous Inflow Control Valve Applications Creating Better Wells: A Review of Design Optimization and Associated Benefits. International Petroleum Technology Conference,

Austin-Adigio, M., & Gates, I. (2019). Non-condensable gas Co-Injection with steam for oil sands recovery. *Energy*, **179**, 736–746. https://doi.org/https://doi.org/10.1016/j.energy.2019.05.034

Bagci, A. S., & Gumrah, F. (2004). Effects of CO2 and CH4 Addition to Steam on Recovery of West Kozluca Heavy Oil. SPE International Thermal Operations and Heavy Oil Symposium and Western Regional Meeting,

Banerjee, S., & Hascakir, B. (2018). Design of flow control devices in steam-assisted gravity drainage (SAGD) completion. *Journal of Petroleum Exploration and Production Technology*, **8**(3), 785–797. https://doi.org/10.1007/s13202-017-0393-4

Butler, R. (1999). Steam and gas push (SAGP) [Article]. *Journal of Canadian Petroleum Technology*, **38**(3), 54–61. https://doi.org/10.2118/99-03-05

Butler, R. M., Jiang, Q., & Yee, C. T. (2001). Steam and Gas Push (SAGP)-4;Recent Theoretical Developments and Laboratory Results Using Layered Models. *Journal of Canadian Petroleum Technology*, **40**(01). https://doi.org/10.2118/01-01-06

Buwauqi, S., Jumah, A. A., Shabibi, A., Harrasi, A., Kalyani, T., Fahmy, A., & Ismail, I. M. (2021). Application of Autonomous Inflow Control Valve AICV in Increasing the Field Recovery in One of the Matured Fields in the Sultanate of Oman: Case Study. SPE Annual Caspian Technical Conference,

Canbolat, S., Akin, S., & Kovscek, A. R. (2004). Noncondensable gas steam-assisted gravity drainage. *Journal of Petroleum Science and Engineering*, **45**(1), 83–96. https://doi.org/https://doi.org/10.1016/j.petrol.2004.04.006

Jahanbani, A., Jelmert, T., Kleppe, J., Ashrafi, M., Souraki, Y., & Torsæter, O. (2012). *Investigation of the Applicability of Thermal Well Test Analysis in Steam Injection Wells for Athabasca Heavy Oil*. https://doi.org/10.2118/154182-MS

Konopczynski, M. (2018). Thermodynamic Analysis of a Modified Autonomous Flow Control Device for SAGD Sub-Cool Management. SPE Thermal Well Integrity and Design Symposium,

Langaas, K., Urazovskaya, O., Gueze, N., & Jeurissen, E. (2020). *Attic Oil Recovery in the Alvheim Field*. https://doi.org/10.2118/200719-MS

Lastiwka, M., Burke, L. H., Booy, D., Chineme, E. C., Gaviria, F., & Ortiz, J. D. (2019). Laboratory and Field Testing of a Steam-Limiting Flow Control Device Developed for Thermal Applications. SPE Annual Technical Conference and Exhibition,

Least, B., Greci, S., Huffer, R., Rajan, R. V., & Golbeck, H. (2014). Steam Flow Tests for Comparing Performance of Nozzle, Tube, and Fluidic Diode Autonomous ICDs in SAGD Wells. SPE Heavy Oil Conference-Canada,

Mathiesen, V., Aakre, H., Werswick, B., & Elseth, G. (2011). The Autonomous RCP Valve – New Technology for Inflow Control In Horizontal Wells. SPE Offshore Europe Oil and Gas Conference and Exhibition,

Sharma, J., Moore, R. G., & Mehta, S. A. (2012). Effect of Methane Co-Injection in SAGD--Analytical and Simulation Study. *SPE Journal*, **17**(03), 687–704. https://doi.org/10.2118/148917-pa

Stalder, J. L. (2013). Test of SAGD Flow-Distribution-Control Liner System in the Surmont Field, Alberta, Canada. *Journal of Canadian Petroleum Technology*, **52**, 95–100.

Taghavi, S., Aakre, H., Swaffield, S., & Brough, R. B. (2019). Verification of Autonomous Inflow Control Valve Flow Performance Within Heavy Oil-SAGD Thermal Flow Loop. SPE Annual Technical Conference and Exhibition,

Taghavi, S., & Ghaderi, A. (2021). On Uncertainty Analysis of the Rate Controlled Production (RCP) Model. First SIMS EUROSIM Conference on Modelling and Simulation, Finland.

Taghavi, S., Gisholt, E., Aakre, H., Håland, S., & Langaas, K. (2021). *Autonomous Inflow Control Valve Multiphase Flow Performance for Light Oil*. Offshore Technology Conference,

Vachon, G. P., Klaczek, W., Erickson, P. J., Langer, D. C., Booy, D., & Baugh, A. (2015). Use of Flow Control Devices (FCDs) to Enforce Conformance in Steam Assisted Gravity Drainage (SAGD) Completions. SPE Canada Heavy Oil Technical Conference,

Paper 4

Application of Autonomous Inflow Control Valve for Enhanced Bitumen Recovery by Steam Assisted Gravity Drainage

This paper is published in the Proceeding of 63rd International Conference of Scandinavian Simulation Society, SIMS 2022, Trondheim, Norway, September 20-21, 2022

Paper presented by Soheila Taghavi

Authors: Soheila Taghavi, Farzan Farsi Madan, Ramesh Timsina, and Britt M. E. Moldestad

Application of Autonomous Inflow Control Valve for Enhanced Bitumen Recovery by Steam Assisted Gravity Drainage

Soheila Taghavi[a,b], Farzan Farsi Madan[a] , Ramesh Timsina[a], Britt M. E. Moldestad[a]

[a] *Department of Process, Energy and Environmental Technology, University of South-Eastern Norway, Norway,*
[b]*InflowControl AS, Norway*
corresponding author: soheila.t.hosnaroudi@usn.no

Abstract

Steam assisted gravity drainage is a thermal method for enhanced bitumen recovery. In this method, steam is injected to bitumen and heavy oil to reduce the viscosity and make the oil mobile. However, early breakthrough of steam in some parts of the well results in loss of the required amount of steam in contact with the cold bitumen, and poor distribution of the steam chamber. This limits the oil production and increases the SAGD operation cost. Autonomous inflow control valve (AICV) is able to prevent the steam breakthrough and restrict the production of steam. The objective of this paper is to investigate the performances of AICV and passive inflow control device (ICD) in a SAGD production well. This is achieved by developing a dynamic wellbore-reservoir model in the OLGA-ROCX simulator. Reservoir and fluid properties have been specified in ROCX, and the wellbore model has been developed in OLGA. Coupling OLGA and ROCX enable the user to simulate the fluid production from the reservoir into the well. The simulation results demonstrate the significant benefit of AICV in steam to oil ratio (SOR) reduction compared to ICD. Indeed, the simulation results show that utilizing AICV in the SAGD production wells will reduce the steam production by 88% after 300 days of production. From environmental aspect, reduction in the steam to oil ratio by utilizing AICV will reduce the energy demand for steam generation. This will eventually improve the economics of SAGD projects. Also, reduction in the steam and energy demand will consequently contribute to lower the intensity of greenhouse gas (GHG) emissions.

1.Introduction

Steam assisted gravity drainage is a thermal recovery method based on gravity drainage for extraction of bitumen and heavy oil. More than 80% of the world's annual heavy oil production is by means of deploying this technology [1]. As the bitumen and heavy oil viscosity are as high as 10^6 cP, the mobility is very low. Thus, the viscosity must be reduced drastically to make the bitumen mobile and extractable. Therefore, the SAGD method is used, where the oil is heated to temperatures around 200°C and higher. At this temperature range, the oil viscosity is below 20 cP (see Figure 1) which implies that the oil is mobile and is able to flow towards the production well by gravity.

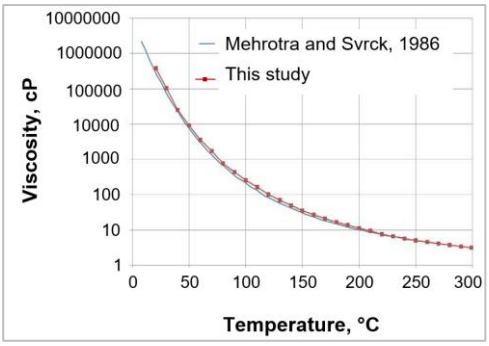

Figure 1:Viscosity of Athabasca bitumen sample versus temperature. [2]

The SAGD process is shown in Figure 2. Steam is injected continuously from the steam injection well which is located about 4-6m above the production well. As steam is injected, it forms a growing steam chamber with uniform temperature, called a depletion chamber. The continuous injected steam flows to the interface and condenses in contact with the cold bitumen. As a result, the latent steam energy is released leading to the higher oil temperature, lower oil viscosity, and consequently greater oil mobility. The low viscous mobile oil and condensate flow continuously from the edge of the steam chamber towards the production well.

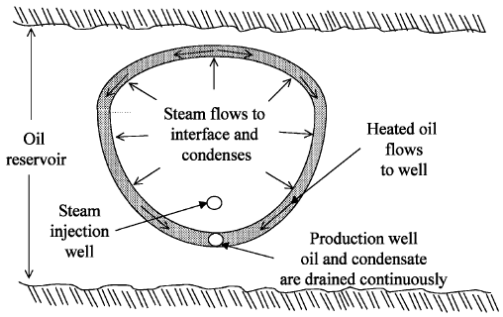

Figure 2:SAGD process. [3]

One of the key parameters of an efficient SAGD operation is attaining an even steam distribution

along the injection well. This can be achieved by deploying inflow control devices (ICDs) which balance the steam outflow to the reservoir. The role of ICD installation on the injection well is of great importance specially in the early phases of steam chamber growth, since it encourages more uniform steam development. [4]

One of the challenges in the SAGD wells is steam and water breakthrough in some parts of the well. This reduces the heavy oil/bitumen production and will consequently increase the SAGD operation cost. ICDs initially and autonomous inflow control devices (AICDs) latterly have been used to overcome this challenge. The newest generation of AICD is autonomous inflow control valve (AICV). AICV is able to delay the onset of steam and water breakthrough and ensure an even influx of oil along the well. In addition, in case of breakthrough of unwanted fluids like steam and/or water, AICV restricts the production of these fluids significantly. The ratio of steam injection to oil production (SOR) is of great importance in the SAGD process. From both environmentally and economically aspects, it is crucial to implement technologies which contribute to decrease the SOR.

The aim of this paper is to examine the impact of the ICD and AICV technology on reducing SOR and consequently improving the SAGD economics.

2. Inflow control technologies; ICD and AICV

Inflow control technologies such as ICDs and AICVs were introduced to the oil industry in order to overcome the early water and gas breakthrough challenges associated with heel-toe effect in horizontal wells. The heel-toe effect refers to the variations of the inflow rate of the fluid along the well, from toe to heel, due to the frictional pressure losses [5]. In addition, these technologies promote a balance drainage of long horizontal wells, and in general increase the oil production and recovery.

The following sub-sections present the functionality and performance curves of passive and autonomous inflow control device.

2.1. ICD

Figure 3 shows a pipe section with nozzle-type ICD completion. Fluid from the reservoir (red arrows) flows through the sand-screen, traverses along the annulus, and enters the production tubing through the ICD.

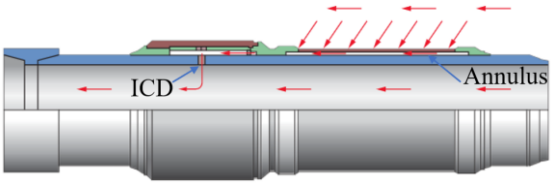

Figure 3: Nozzle-type ICD mounted on the pipe.[6]

The governing equation of the nozzle-type ICD is as follows [7]:

$$\Delta P = \frac{8\rho Q^2}{d^4\pi^2 n^2 {C_D}^2} \quad (1)$$

Where ΔP is the pressure drop through the nozzle, ρ is the fluid density, Q is the volumetric flow rate of the fluid through the nozzle, d is the diameter of the nozzle, n is the number of tested nozzles, and C_D is the discharge coefficient. C_D is mostly a function of the Reynolds number (Re) [7]. It can be interpreted from the equation (1) that the pressure drop through the nozzle is mainly dependent on the fluid density. The performance curve of a nozzle type ICD for water, oil and gas is shown in Figure 4. A nozzle type ICD with 4.75 mm diameter is used in the simulations. By performance curve, it means that the pressure drop through the device is plotted as a function of the volume flow rate of the fluid.

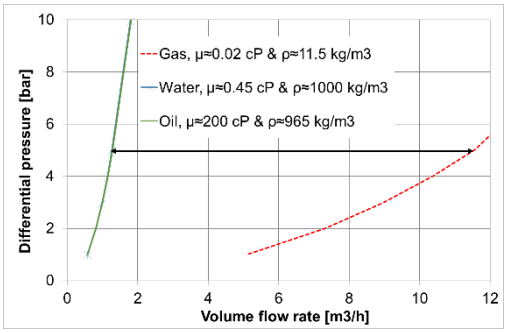

Figure 4: ICD performance curves.[8]

As it is illustrated in Figure 4, at constant pressure drop, the volume flow rate of oil and water differ slightly as the density differences are minor (1000 kg/m^3 for water vs 965 kg/m^3 for oil), while the volume flow rate of gas is much higher due to the much lower density (about 11.5 kg/m^3). This indicates that when gas breakthrough occurs, ICD will not restrict the gas production significantly.

2.1. AICV

Figure 5 shows a pipe section with sand screen and AICV completion.

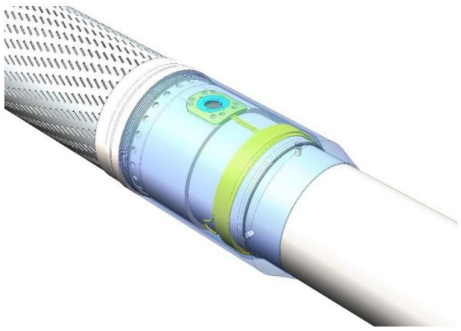

Figure 5:AICV mounted in a base-pipe with sand screen.[9]

The mathematical model describing the performance of the AICV can be described as:

$$\Delta P_{Tot} = \left(\frac{\rho_{mix}^2}{\rho_{cal}}\right) \cdot \left(\frac{\mu_{cal}}{\mu_{mix}}\right)^{y} \cdot a_{AICD} \cdot Q^{x} \qquad (2)$$

where ΔP_{Tot} is the differential pressure across the AICV, ρ_{cal} and μ_{cal} are the calibration fluid density and viscosity, and ρ_{mix} and μ_{mix} are the mixture fluid density and viscosity respectively. The parameter a_{AICD} is a valve characteristic given by the ICD strength, Q is the volumetric mixture flow rate, and x and y are constants. [10]

It can be interpreted from equation (2) that the pressure drop through the AICV is much more viscosity dependent than density dependent. The concept and principle of AICV is described in detail in earlier scientific works [11, 12].

The performance curve of AICV for water, oil and gas is shown in Figure 6.

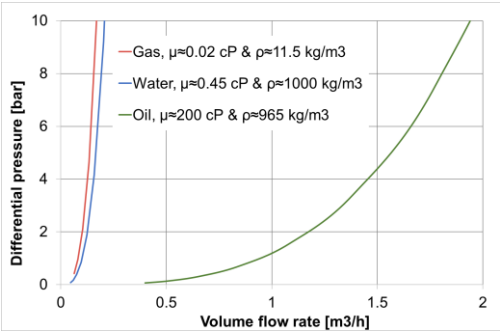

Figure 6:AICV performance curves.[8]

As it is illustrated in Figure 4 and Figure 6, at constant pressure drop the volume flow rates of oil with 200 cP viscosity through the ICD and the AICV are almost the same, while the gas flow rate is significantly higher through the ICD than the AICV. The location of performance curves of the gas and water for AICV have changed compared to the performance curves through ICD. The gas and water curve are now located far away to the left side of the oil curve. This indicates that when gas and water breakthrough occur, AICV will restrict the gas and water production significantly while maintaining a high oil production.

3. OLGA-ROCX set up

In this study, OLGA-ROCX is used to describe and compare the behavior of ICD and AICV in the SAGD reservoir, and to illustrate the impact of AICV completion on increased oil recovery. OLGA-ROCX is an integrated transient well/reservoir model. The reservoir model and the wellbore model are coupled in an implicit way [13]. Reservoir and fluid properties are specified in ROCX, and the wellbore model is developed in OLGA. Coupling OLGA and ROCX enable the user to simulate the fluid production from the reservoir into the well. NETool was used to simulate the AICV performance in a SAGD reservoir in previous author's work [8]. NETool is a static one-dimensional steady state simulation tool that shows the instantaneous inflow profile along the well, while OLGA/ROCX is a robust transient simulation tool to perform integrated well-reservoir simulations.

3.1. Reservoir model, ROCX

The black oil model which simulates the multiphase fluid transport in porous media is selected in ROCX. Input data to the model are grid dimensions, fluid, and reservoir properties. Reservoir properties such as permeabilities and porosities of the porous medium, and in addition thermal properties of the rock and fluids are among the input data. Initial conditions such as fluid saturations and temperature together with the boundary conditions at the well and at the outer near well boundary are needed. [14]

The boundary conditions of the reservoir grid elements are matched with inflow points of the components placed in the wellbore model. This will define the flow from the reservoir model. So, the pressure boundary for the reservoir model is provided by the wellbore model while the reservoir model provides the flow and the fluid temperatures into the pipeline[14]. The shape of the reservoir drainage area is considered to be rectangular, and the dimensions are given in Table 1.

Table 1:The dimensions of the drainage area.

Direction	Length (m)	Number of blocks	Block size (m)
X	1000	10	100
Y	117	15	20,20,5,5,3,3, 2,1,2,3,3,5,5, 20,20
Z	40	10	4

As the fluid properties varies significantly around the well and in the Y-Z plane, a finer mesh is considered in the grid setup to achieve more accurate results. The size of the blocks varies along the y direction while a uniform mesh along the z and x-direction is defined. Finer mesh along the x-direction will have insignificant impact on the overall flow rate [15]. The well length is 1000 m containing 10 segments with a length of 100 m each. One equivalent ICD/AICV is placed in each segment.

Since the purpose of this study is to evaluate the ICD/AICV performance in case of steam breakthrough, the well is located as near as possible to the bottom of the drainage area to delay the probable steam breakthrough. The schematic of the drainage area geometry and the well location is shown in Figure 7.

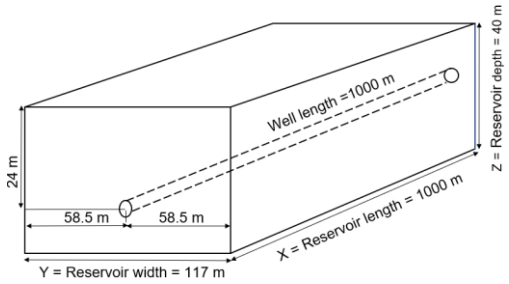

Figure 7:The schematic of the drainage area geometry.

The grid in three dimensions is shown in Figure 8.

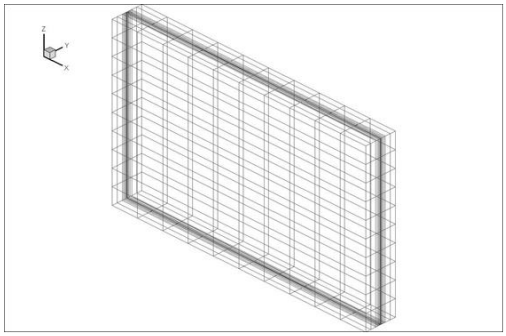

Figure 8:3-D view of grid.

As seen from the figure, the mesh in the y-direction and towards the well located in the middle of the drainage area is finer than in the z and x-direction.

3.1.1 Fluid and reservoir properties

The black oil model which estimates the pressure volume temperature (PVT) relations is selected in ROCX. The basic modeling assumption is that the gas may dissolve in the liquid oil phase, but no oil will dissolve in the gaseous phase. This implies that the composition of the gaseous phase is assumed the same at all pressure and temperatures [12],[16].In other words, the black oil model assumes that the oil components will always be in the liquid phase despite any changes in the conditions [15] .

The reservoir pressure at initial conditions is 27 bar and it is assumed to be constant. The fluid properties used for the simulation are listed in Table 2. The oil viscosity is measured at 180°C at atmospheric pressure [2].

Table 2: Fluid properties as input in ROCX.

Property	Value
Oil viscosity [cP]	15.50
Oil specific gravity [-]	0.90
Gas specific gravity [-]	0.64
Gas oil ratio (GOR) [Sm^3/Sm^3]	150

A gas cap is placed at the top of the reservoir in the boundary conditions section. Hence a gas feed in addition to oil feed are defined. The feed streams are presented in Table 3.

Table 3:Feed streams.

Feed stream	Fraction type	Fraction
Oil	GOR	150
Gas	OGR	0.99

The reservoir porosity is assumed to be constant 0.3 throughout the reservoir. Different permeabilities are specified for each block in order to simulate a heterogenous reservoir. It is assumed that the area close to the toe section of the well has a higher permeability in all directions. The permeability of the heterogenous reservoir in both x and y-direction, varies from 3000 mD in relatively low permeable zones to 6000 mD in relatively high permeable zones. The vertical permeability is specified in each block of the reservoir, and it varies from 300 to 600 mD for relatively low permeable and relatively high permeable zones respectively. The vertical permeability profile of the heterogenous reservoir is illustrated in Figure 9

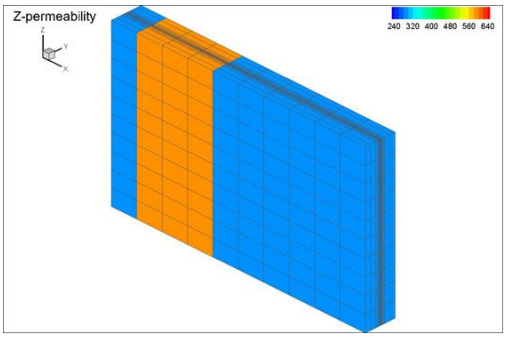

Figure 9:Vertical permeability profile.

Generally, it is challenging to obtain information about relative permeability for different fields. Data for relative permeabilities are set manually in table

form in Rocx. The "Stone II" model with exponent 2 is used to evaluate the oil phase relative permeability while the Corey correlation with exponent 1.5 is used to estimate the gas phase relative permeability. The relative permeability curves for oil and gas are presented in Figure 10.

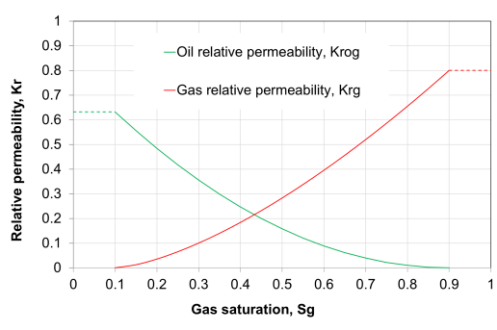

Figure 10: Relative permeability curves for the SAGD reservoir.

3.1.2 Initial and boundary conditions

Initially, it is assumed that the fraction of the black oil feed is equal to one. The initial oil and gas saturation of in the reservoir are set to 0.9 and 0.1. Pressure and temperature of the reservoir are 27 bar and 180°C, respectively.

3.2. Wellbore model, OLGA

In OLGA, separate continuity equations are applied for the gas, for the oil (or condensate) and water liquids and also for oil (or condensate) and water droplets. Three momentum equations are also used: one for each of the continuous liquid phases (oil/condensate and water) and one for the combination of gas with liquid droplets. One mixture energy equation is also applied. Totally, seven conservation equations and one equation of state to be solved: the seven conservation equations are three for mass, three for momentum, and one for energy, while the equation of state is for pressure.[17]

3.2.1 Mass Transport Equations:

$$\partial_t m_i + \partial_z (m_i U_i) = \sum_i \Psi_{ji} + G_i \qquad (3)$$

where m_i and U_i denote mass field (gas, oil in liquid layers, water in liquid layers, oil droplets in gas layer, and water droplets in gas layer) and velocity respectively. In addition, ∂_t denotes differentiation in time, ∂_z denotes spatial differentiation, Ψ_{ji} denotes the rate of mass transfer between the j-th and i-th mass field, that is, dispersions, droplet deposition and entrainment, and phase transitions, and G_i denotes any mass source/sink.

3.2.2 *Momentum Balance Equations*

$$\partial_t (m_i U_i) + \partial_z \left(m_i {U_i}^2\right) = m_i . g . \cos(\varphi) + \not{p}_i + G_i U_i + \sum_j \left(\Psi_{ji}^{+} U_i - \Psi_{ji}^{-} U_i\right) + \sum_j F_{ji}^{I} \left(U_j - U_i\right) - F_i^{w} U_i \qquad (4)$$

where ∂_t denotes differentiation in time, ∂_z denotes spatial differentiation. g is the acceleration of gravity, φ is the pipe angle relative to the gravitational vector, P_i is the pressure force, $G_i U_i$ is the momentum contribution corresponding to the mass source/sink G_i. Also, F^{I}_{ji} are friction forces between the i-th and j-th mass field, and F^{w} denotes the wall friction. Ψji denotes momentum contributions corresponding to the mass transfer between the j-th and i-th mass field. In the equation (4), Ψ^{+}_{ji} accounts for a net contribution from mass field i to j while Ψ^{-}_{ji} accounts for a net contribution from mass field j to i.

3.2.3 Energy balance equation

$$\partial_t (m_i E_i) + \partial_z (m_i U_i H_i) = \mathcal{S}_i + \mathcal{Q}_i + \sum_i T_{ij} E_j \qquad (5)$$

where E_i denotes the field energy, H_i denotes the field enthalpy, S denotes enthalpy source/sink, Q is the heat flux through the pipe wall, and T_{ij} models the energy transfer between fields.

3.3 OLGA set-up

In this work, a basic case is selected to generate the wellbore model in OLGA. The model consists of two pipes: pipeline and flowpath. The flowpath represents the production tubing, and the pipeline represents the annulus and the inflow from annulus to the well. On the pipeline, the flow components such as inflow controls and packers are placed. The characteristics and dimensions of the two pipes are listed in Table 4.

Table 4:The characteristics of pipeline and flowpath.

Pipe	Length (m)	Diameter (mm)	Roughness (mm)
Pipeline	1000	222	0.028
Flowpath	1000	114	0.050

Figure 11 shows the set-up in OLGA for one production zone which consists of two sections. This set-up was developed and proposed for the first time in 2012 [12] and results were presented in a scientific paper [11].

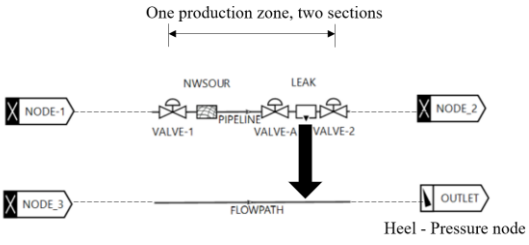

Figure 11:Set-up of a single production zone with inflow controller in OLGA.

The pipeline (PIPELINE) includes a near-well source (NWSOUR) which connects the ROCX file

as input data. The near-well source is the flow source from the reservoir to the annulus. In addition, the pipeline consists of one inflow controller (VALVE-A), two packers (VALVE-1 and 2 with zero opening), and leak (LEAK) which outflows the flow through the inflow control to the production well (FLOWPATH) and towards the heel (OUTLET). Each production zone is divided into two sections and is isolated by packers. The near-well source and the leak is placed in each section and the packers, and the inflow controllers are the section boundaries. Each pipe is divided into 10 production zones each 100 m long which implies that there are totally 20 sections.10 nozzle type ICDs with a diameter of 15 mm is distributed in the 10 production zones. The flow area of this ICD in one production zone (100 m) corresponds to the flow area of 10*4.75 mm ICDs. Usually, in the industry, the ICDs are installed in approximately 10-11 m long joints. So, the flow area of one equivalent ICD in a 100 m production zone is approximately the same as the flow area of 10 ICDs with 4.75 mm diameter which are installed in 10-11 meters long joints.

A comprehensive and step by step workflow for modelling of the rate controlled production (RCP) valves in the OLGA simulator was proposed in a scientific paper [18]. In this new method, a controller is used to chock the RCP valve based on the characteristics of the RCP valve and the reservoir fluid mixture. This method can also be used for AICVs. Set-up of a single production zone with AICV in OLGA is illustrated in Figure 12 .

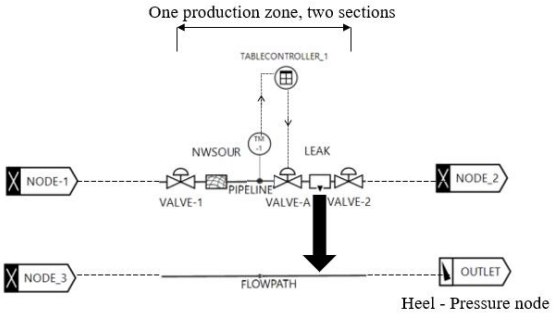

Figure 12:Set-up of a single production zone for AICV in OLGA.

Based on the single-phase (Figure 6) and multi-phase gas/oil performance of the AICV, a table controller (TABLECONTROLLER-1) is created. This table controller gets the measured gas volume fraction (GVF) data from the transmitter (TM-1) and provides corresponding control signals for chocking the AICV. The multiphase gas/oil behavior of the AICV for SAGD conditions was presented earlier in a scientific paper [8] . According to the experimental results provided in that paper, the AICV gradually opens when the oil/gas mixture flows through the valve. However, the AICV restricts the gas flow when the GVF is getting higher, until pure gas flows through the valve and the valve is almost closed.

The control signal table in the OLGA simulator for controlling the AICV, consists of independent and dependent variables. In this case, the percentage of the valve opening is a function of the GVF. Indeed, the valve opening is getting less and less by increasing the GVF.

4. Results and discussion

In this chapter, the obtained simulation results which are conducted for two cases are presented. The simulation cases are as follows:

1. Heterogeneous reservoir with ICDs
2. Heterogeneous reservoir with AICVs

The gas density and viscosity in the simulations performed by OLGA/ROCX, are set to 11.5 kg/m^3 and 0.02 cP respectively. In the simulations and the experiments, the gas represents steam.

In order to study the performance of ICD and AICV in a specific well production period, the accumulated oil and gas for AICV and ICD completions are compared. Figure 13 illustrates the accumulated oil and gas produced from the well after 300 days of production.

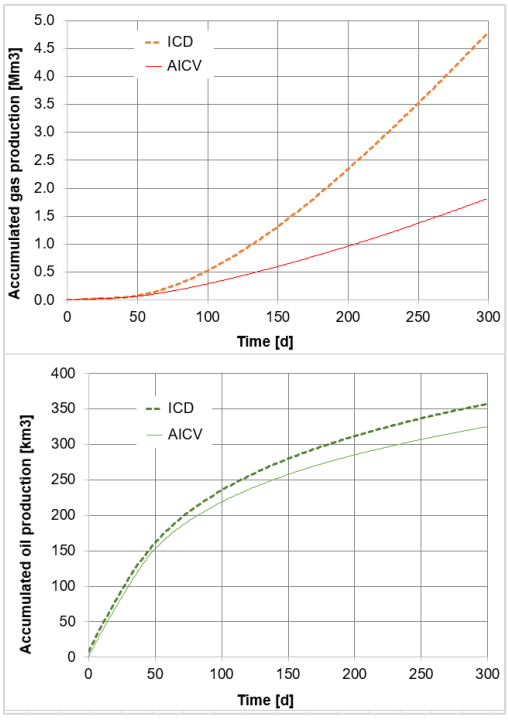

Figure 13:Accumulated oil and gas from the well completed with AICVs and ICDs.

As can be seen in this figure, after 300 days of production, the accumulated oil in the AICV and ICD cases differs marginally. However, due to the better performance of AICV in both single and multiphase flow regions, the amount of accumulated gas drops significantly from 4.8 Mm^3 to 1.9 Mm^3 after 300 days of production.

When the gas breakthrough occurs, AICV starts to chock the gas production gradually. Indeed, AICV chocks the gas production consistently by increasing GOR. This behavior, which is based on experimental data [8], was implemented in the Table Control module in OLGA.

Figure 14 Shows the comparison of oil and gas production rates for AICV and ICD completion for 300 days of production. The oil production rate for both cases reach its maximum at the start of the production. The oil production decreases slightly as the gas production increases simultaneously. Gas production grows suddenly and rapidly at 35th day of production, which implies that gas breakthrough has occurred. At the time of gas breakthrough, gas enters the well rapidly due to its high mobility. This restricts the production of oil significantly, and as a result, the oil production rate drops drastically. However, oil production is continued at an acceptable level until the end of the production time.

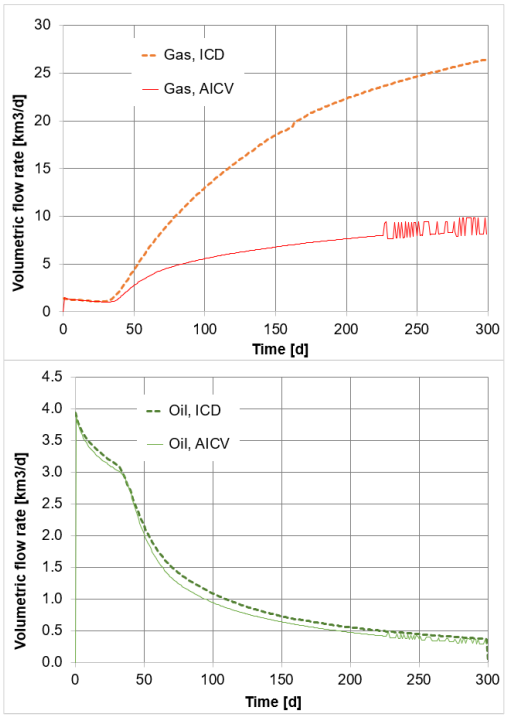

Figure 14:Voumetric flow rate of oil and gas for the well completed with AICVs and ICDs.

As can be seen from the figure, the volumetric oil flow rate of ICD is on average slightly higher than the volumetric oil flow rate of AICV during the whole period of production. However, the gas breakthrough occurs a few days later for the AICV case than for the ICD case. Also, the development of gas breakthrough is much faster for the ICD case compared to the AICV case. It can be concluded from the figure that the well completed with AICVs reduces the gas production by approximately 88% compared to using ICDs after 300 days of production.

Figure 15 shows the GOR at standard conditions as a function of accumulated oil production. This figure illustrates how the GOR varies with accumulated oil. Usually in the wells, the total allowable gas production is limited, since the total gas processing capacity is an active constraint [19]. This highlights the importance of developing new inflow control technologies which guarantee a higher maximum oil production while meeting the GOR constraint.

As it can be seen from the figure, the accumulated oil at a specific GOR, for example 600, for the AICV case is 15% more than the accumulated oil for the ICD case.

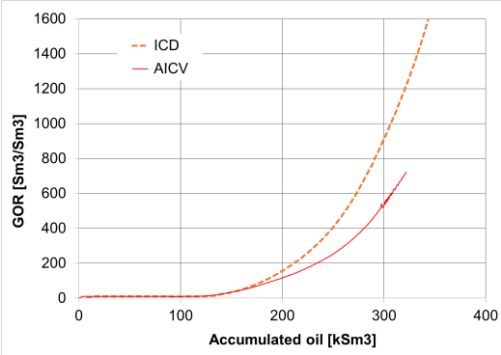

Figure 15: Accumulated oil production versus gas oil ratio for AICV and ICD.

4. Conclusions

The performances of AICV and ICD in a SAGD production well are investigated. This is achieved by developing a dynamic wellbore-reservoir model in the OLGA-ROCX simulator. Reservoir and fluid properties are specified in ROCX, and the wellbore model is developed in OLGA. Coupling OLGA and ROCX enable the user to simulate the fluid production from the reservoir into the well.

The simulation results demonstrate the significant benefit of AICV in SOR reduction compared to ICD. Indeed, simulation results show that utilizing AICV in the SAGD production wells will reduce the gas (steam) production by 88% after 300 days of production. Reduction in SOR, will improve the overall SAGD operation performance. This will also result in more cost-effective oil production.

From environmental aspect, reduction in the steam to oil ratio by utilizing AICV, will reduce the energy demand for steam generation. This will improve the economics of SAGD projects. Also, reduction in the steam and energy demand will consequently contribute to lower the intensity of greenhouse gas (GHG) emissions.

Acknowledgment

The author would like to thank the university of South-Eastern Norway for providing the necessary software arrangements for this work.

References

[1] Z. Xu, S. Li, B. Li, D. Chen, Z. Liu, and Z. Li, "A review of development methods and EOR technologies for carbonate reservoirs," *Petroleum Science*, pp. 1-24, 2020.

[2] A. Jahanbani, T. Jelmert, J. Kleppe, M. Ashrafi, Y. Souraki, and O. Torsæter, "Investigation of the Applicability of Thermal Well Test Analysis in Steam Injection Wells for Athabasca Heavy Oil," 06/04 2012, doi: 10.2118/154182-MS.

[3] R. Butler, "SAGD Comes of AGE!," *Journal of Canadian Petroleum Technology*, vol. 37, no. 07, 1998, doi: 10.2118/98-07-da.

[4] B. Least, S. Greci, R. Huffer, R. V. Rajan, and H. Golbeck, "Steam Flow Tests for Comparing Performance of Nozzle, Tube, and Fluidic Diode Autonomous ICDs in SAGD Wells," in *SPE Heavy Oil Conference-Canada*, 2014, vol. Day 3 Thu, June 12, 2014, D031S013R005, doi: 10.2118/170083-ms. [Online]. Available: https://doi.org/10.2118/170083-MS

[5] V. M. Birchenko, K. M. Muradov, and D. R. Davies, "Reduction of the horizontal well's heel–toe effect with inflow control devices," *Journal of Petroleum Science and Engineering*, vol. 75, no. 1, pp. 244-250, 2010/12/01/ 2010, doi: https://doi.org/10.1016/j.petrol.2010.11.013.

[6] T. Jokela *et al.*, "Inflow Control Devices — Raising Profiles," 2010.

[7] J. E. Lauritzen and I. B. Martiniussen, "Single and Multi-phase Flow Loop Testing Results for Industry Standard Inflow Control Devices," in *SPE Offshore Europe Oil and Gas Conference and Exhibition*, 2011, vol. All Days, SPE-146347-MS, doi: 10.2118/146347-ms. [Online]. Available: https://doi.org/10.2118/146347-MS

[8] S. Taghavi, H. Aakre, and B. M. E. Moldestad, "Performance Analysis of Autonomous Inflow Control Valve in a SAGD Late Life Process with Non-Condensable Gases," in *SPE Canadian Energy Technology Conference*, 2022, vol. Day 1 Wed, March 16, 2022, D011S011R002, doi: 10.2118/208915-ms. [Online]. Available: https://doi.org/10.2118/208915-MS

[9] H. Aakre, V. Mathiesen, and B. Moldestad, "Performance of CO2 flooding in a heterogeneous oil reservoir using autonomous inflow control," *Journal of Petroleum Science and Engineering*, vol. 167, pp. 654-663, 2018/08/01/ 2018, doi: https://doi.org/10.1016/j.petrol.2018.04.008.

[10] S. Taghavi and A. Ghaderi, "On Uncertainty Analysis of the Rate Controlled Production (RCP) Model," in *First SIMS EUROSIM Conference on Modelling and Simulation*, Finland, 2021: Linköping Electronic Conference Proceedings, 2021.

[11] H. Aakre, B. Halvorsen, B. Werswick, and V. Mathiesen, "Smart Well With Autonomous Inflow Control Valve Technology," in *SPE Middle East Oil and Gas Show and Conference*, 2013, vol. All Days, SPE-164348-MS, doi: 10.2118/164348-ms. [Online]. Available: https://doi.org/10.2118/164348-MS

[12] H. Aakre, n. o. m. f. Høgskolen i Sørøst-Norge Fakultet for teknologi, and S.-N. Høgskolen i, "The impact of autonomous inflow control valve on increased oil production and recovery," no. 32, University College of Southeast Norway, Faculty of Technology, Natural Sciences and Maritime Sciences, Kongsberg, 2017.

[13] G. Chupin, B. Hu, T. Haugset, J. Sagen, and M. Claudel, "Integrated Wellbore/Reservoir Model Predicts Flow Transients in Liquid-Loaded Gas Wells," in *SPE Annual Technical Conference and Exhibition*, 2007, vol. All Days, SPE-110461-MS, doi: 10.2118/110461-ms. [Online]. Available: https://doi.org/10.2118/110461-MS

[14] J. Sagen, T. Sira, A. Ek, S. Selberg, M. Chaib, and H. Eidsmoen, "A Coupled Dynamic Reservoir and Pipeline Model – Development and Initial Experience," in *13th International Conference on Multiphase Production Technology*, 2007, vol. All Days, BHR-2007-G1.

[15] N. C. I. F. Ramesh Timsina, Britt M. E. Moldestad, "Modeling and simulation of light oil production using inflow control devices," in *58th Conference on Simulation and Modelling (SIMS 58) Reykjavik, Iceland*, 2017: Linköping Electronic Conference Proceedings doi: http://dx.doi.org/10.3384/ecp17138180.

[16] "Black-Oil Simulations." wikitext. https://dwsim.org/wiki/index.php?title=Black-Oil_Simulations (accessed.

[17] K. H. Bendlksen, D. Malnes, R. Moe, and S. Nuland, "The Dynamic Two-Fluid Model OLGA: Theory and Application," *SPE Production Engineering*, vol. 6, no. 02, pp. 171-180, 1991, doi: 10.2118/19451-pa.

[18] A. Moradi and B. M. E. Moldestad, "A Proposed Method for Simulation of Rate-Controlled Production Valves for Reduced Water Cut," *SPE Production & Operations*, vol. 36, no. 03, pp. 669-684, 2021, doi: 10.2118/205377-pa.

[19] A. Mjaavatten, R. Aasheim, S. Saelid, and O. Groenning, "A Model for Gas Coning and Rate-Dependent Gas/Oil Ratio in an Oil-Rim Resevoir," in *SPE Russian Oil and Gas Technical Conference and Exhibition*, 2006, vol. All Days, SPE-102390-MS, doi: 10.2118/102390-ms. [Online]. Available: https://doi.org/10.2118/102390-MS

Paper 5

The Impact of Autonomous Inflow Control Valve on Enhanced Bitumen Recovery in a SAGD Late Life Reservoir: Lab Experiment and Simulation

SPE-212783-MS

This paper was prepared for presentation at the SPE Canadian Energy Technology Conference and Exhibition held in Calgary, Alberta, Canada, 15-16 March 2023. Society of Petroleum Engineers

Paper presented by Soheila Taghavi

Authors: Soheila Taghavi, Haavard Aakre, and Britt M.E. Moldestad

SPE-212783-MS

The Impact of Autonomous Inflow Control Valve on Enhanced Bitumen Recovery in a SAGD Late Life Reservoir: Lab Experiment and Simulation

Soheila Taghavi, University of South-Eastern Norway/InflowControl As; Haavard Aakre, InflowControl As; Britt M.E. Moldestad, University of South-Eastern Norway

 DOI 10.2118/212783-MS

This paper was prepared for presentation at the SPE Canadian Energy Technology Conference and Exhibition held in Calgary, Alberta, Canada, 15-16 March 2023.

Abstract

Steam assisted gravity drainage (SAGD) is an effective thermal recovery method for enhanced bitumen recovery. However, the success of SAGD operation depends on several factors. Reduction in gas and steam production is a crucial factor to achieve a successful SAGD operation. Autonomous inflow control valve (AICV) restricts the inflow of steam and/or gas in the zones where breakthrough occurs and improves recovery from SAGD operations. This can be achieved by restricting the excessive steam and/or gas production in a well that is perfectly isolated by packers. This paper presents the performance analysis of AICVs, and passive inflow control devices (ICDs) based on the results from experiments and simulations.

Experiments which illustrate the performance of an orifice type ICD and AICV is presented and compared. The results confirm the significantly better ability of the AICV to restrict the production of gas and/or steam. Simulations are performed with OLGA/ROCX which provides a dynamic wellbore-reservoir model. Simulation results show that utilizing AICV in the SAGD production wells will reduce the gas and steam production by 74% after 365 days of production. The results confirmed the significant benefit of AICV in steam and/or gas reduction and consequently increased oil production. Reduction in steam production will improve the overall SAGD operation performance. This will also result in more cost-effective oil production.

In addition, the annular flow in a well completed by inflow controllers was studied by using OLGA and NETool. Almost all the reservoir simulators calculate the multiphase flow properties in annulus with no-slip. This study was an attempt to initiate discussions and provide an insight into a fundamental problem that almost all the reservoir simulators are dealing with.

Introduction

Steam assisted gravity drainage (SAGD) is an effective thermal recovery method for enhanced heavy oil and bitumen recovery. Due to the technical success of the SAGD process, it is used widely by all the major operators in Athabasca and Cold Lake reservoirs in Alberta, Canada (Gates and Leskiw, 2010).

The in-situ oil viscosity in a typical bitumen reservoir exceeds 1 million cP; this implies that bitumen is immobile (Høhrbye et al., 2016). To make bitumen mobile and extractable under gravity drainage, the

viscosity must be reduced drastically. After heating to over 200 °C, the oil viscosity drops to less than 10 cP which makes it mobile under gravity towards the production well (Mehrotra and Svrcek, 1982).

SAGD process consists of two parallel horizontal wells, as shown in Fig. 1. Steam is circulated in both the injection and production wellbore for up to 3 months to initiate a steam chamber (Banerjee and Hascakir, 2018). After establishing thermal and hydraulic communication between two wellbores, high quality steam is injected continuously from the injection well to the reservoir. The continuous injection of steam creates a chamber with uniform temperature. Steam chamber expands towards the interface and to the immobile bitumen. The latent heat is released due to steam condensation at or near the edges of the steam depletion chamber (Gates and Leskiw, 2010). The transferred energy heats up the bitumen, resulting in decreasing the viscosity to below 10 cP and consequently increasing the oil mobility. The low viscosity heated oil and steam condensate flow along the chamber edges and towards the production well under the action of gravity.

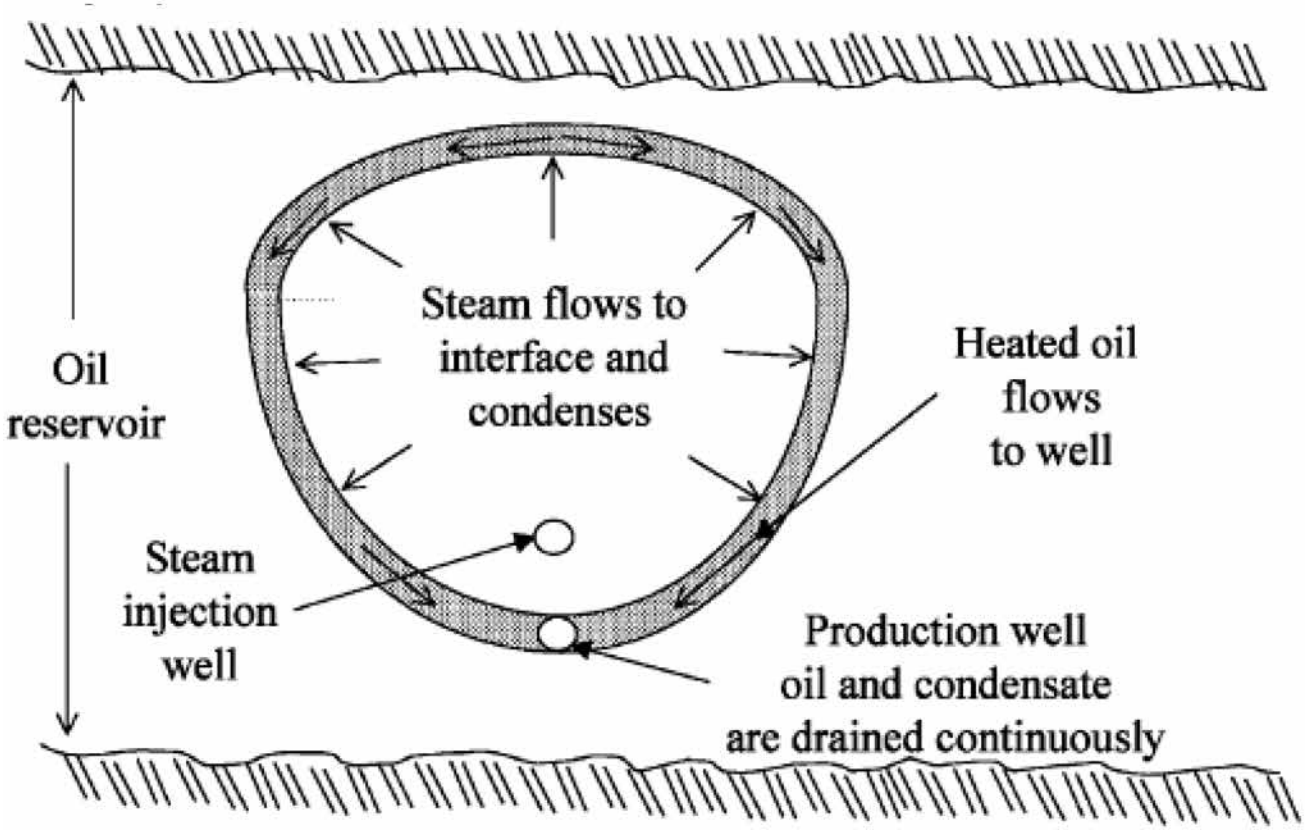

Figure 1—SAGD process (Butler, 1998).

At the later stage of the SAGD process, non-condensable gases (NCGs) such as methane, nitrogen, carbon dioxide are co-injected with the steam to maintain the pressure and assist the bitumen to flow towards the producer well. It is important to maintain the required gas in the steam chamber to obtain an effective SAGD late life process, and therefore the production of gas should be limited. (Soheila Taghavi et al., 2022)

There are several features of a SAGD system that reduce the thermal efficiency of the process. These features include but are not limited to heat losses to the overburden, uneven steam distribution, and bypassing of steam directly from injection to production well.

To obtain an efficient SAGD process, the residence time for steam in the reservoir must be long enough for the steam to condense and for the latent energy to be released and transferred to the cold bitumen. Also, if there is no barrier or resistance in the production well, the injected steam into the formation escapes from the chamber and flows directly to the production well without condensing and reaching any bitumen. This reduces the thermal efficiency of the SAGD process significantly.

Even distribution of steam along the length of the wells can be achieved by a variety of methods including but not limited to deploying concentric tubing strings, perforated tubing, and nozzle type passive inflow control devices (ICDs) along the length of the injector well (Konopczynski, 2018). Operation of the SAGD wells with as small a sub-cool value as possible is important. The temperature difference between the injected steam and produced fluids is called subcool. By operating in small subcool values, the distance between the injector and producer wellbore can be reduced (Konopczynski, 2018). This results into a less time required for steam to be saturated at the start-up phase of the process. Less steam injection in the start-up phase leads to a significant reduction in energy consumption before first hot bitumen production (Konopczynski, 2018). Also, a small subcool means the temperature of the fluid at the liquid pool is high and nearer to the steam temperature resulting in a lower viscosity of the bitumen. This makes bitumen mobile and easy to produce under gravity. As the produced fluids are nearer the steam temperature this means that steam is near the production wellbore or flows directly into it. Bypassing steam directly from injection to production well and steam breakthrough is a consequence of operating a SAGD well with small subcool. Advanced completion technologies like passive flow control devices (ICD or FCD) and autonomous inflow control valve (AICV) can ensure an even steam distribution and prevent or stop steam breakthrough and steam production. This will make it possible to operate a SAGD well with as small subcool value as possible.

Although the SAGD process is a viable thermal recovery method, generating the required amount of steam for the process is highly energy demanding. Based on field data, between 2 and 5 tons of steam are injected into the reservoir to produce each ton of bitumen (Gates and Leskiw, 2010). So, to justify the operation of the SAGD process, it is necessary to reduce the cost of generating steam by reducing the quantity of steam required for the process.

Inflow control technologies can overcome the aforementioned SAGD operation challenges. They can be effective in managing subcool, preventing gas and steam breakthrough, and subsequently reducing the amount of required steam for each ton of bitumen produced.

Passive ICDs are being used in SAGD injection wells to equalize steam delivery along the lateral length ensuring an even steam distribution (Ghesmat and Zhao, 2015). Deploying passives ICDs in production wells may create uniform inflow along the length of the wellbore by creating additional pressure drop and delay the steam breakthrough, but once the breakthrough occurs, they are not able to stop the steam production. Steam compared to oil will flow through ICDs at a higher rate with less pressure drop. This will create further pressure drop in the steam chamber and more steam flashing. This situation may only be alleviated by increasing the back pressure on the entire well (Konopczynski, 2018).

In contrast, AICV can stop the production of steam when breakthrough occurs. Results from full-scale laboratory flow loop that replicates the downhole operating conditions of a SAGD well demonstrated that a considerable reduction in steam production and steam to oil ratio (SOR) were achieved by using AICV (Taghavi et al., 2019). Simulation performed in previous author's work with industry standard reservoir simulators also indicates the significant benefit of AICV in produced steam and gas reduction compared to open hole and ICD completions (Soheila Taghavi et al., 2022), and (Soheila Taghavi et al., 2022).The success of ICDs and AICV completion rely on packers, seal bores, swell packers or even wellbore collapse around the liner to provide zonal isolation of the production wellbore (Konopczynski, 2018).An open annulus with no barrier implies a high flow capacity in which reservoir fluids travel along the completion with different velocities. Gas and steam will move much faster than oil along the annulus due to the higher mobility.

Installing annular swell packers have become common practice in the Troll reservoir in Norway since 2006 (Halvorsen et al., 2012). Compartmentalization and sectioning the annulus in the reservoir will result in different annulus pressure in sections between packers. In a heterogeneous reservoir like Troll, this will contribute to lower drawdown in sections with high rock permeability and higher drawdown in sections with lower rock permeability (Halvorsen et al., 2012). In addition, installing swell packers in stand-alone

screens with ICDs or AICVs may control annular movement of abrasive particles by minimizing annular velocity and consequently mitigate screen failure due to 'hot spotting' (Regulacion and Shahreyar, 2011).

The aim of this paper is to show the importance of using inflow control technologies in improving the economics of SAGD projects. Two different types of inflow control technology, a nozzle type ICD and AICV, are used to study their impact on improving the economics of SAGD projects. The multiphase oil/gas flow test data of AICV at different gas volume fractions are presented and these data are implemented in OLGA to regulate the closure system of AICV. The performance of AICV and ICD in SAGD late life conditions are simulated and compared using OLGA/ROCX. Also, the annular flow in a well is studied by using OLGA and NETool. This study is an attempt to provide an insight into a fundamental problem that almost all the reservoir simulators are dealing with.

Passive and autonomous inflow control device: experiments

AICV and a nozzle type ICD are used in the experiments and simulations to examine the impact of these technologies on reducing gas and steam production and consequently improving the SAGD economics. The pressure drop through the nozzle is mainly dependent on the fluid density while, the pressure drop through the AICV is much more viscosity dependent than density dependent. The AICV keeps open for high viscous fluids like oil and closes for fluids like gas, steam, and water (Aakre et al., 2018). The concept and principle of AICV is described in detail in earlier scientific works (Aakre et al., 2013), and (Aakre, 2017). Fig. 2 shows an AICV valve and an AICV installed in a base pipe with sand screen.

Figure 2—AICV; mounted in a base pipe with sand screen.

The ICD strength is the pressure drop over the valve when the oil flow rate is equal to 1 m^3/h. By using the same strength for AICV and orifice ICD, the performance curve for oil is the same. As it is illustrated in Fig. 3, at constant pressure drop the volume flow rates of oil with 200 cP viscosity through the ICD and the AICV are almost the same, while the gas flow rate is significantly higher through the ICD than the AICV. In the experiments, the gas pressure is approximately 11 bar and tests are performed for differential pressures up to 7 bar. Experimental results for ICD illustrate that at constant pressure drop, the volume flow rate of oil and water differ slightly as the density differences are minor (1000 kg/m^3 for water vs 965 kg/m^3 for oil), while the volume flow rate of gas is much higher due to the much lower density (about 11.5 kg/m^3). This indicates that when a gas breakthrough occurs, ICD will not restrict the gas production.

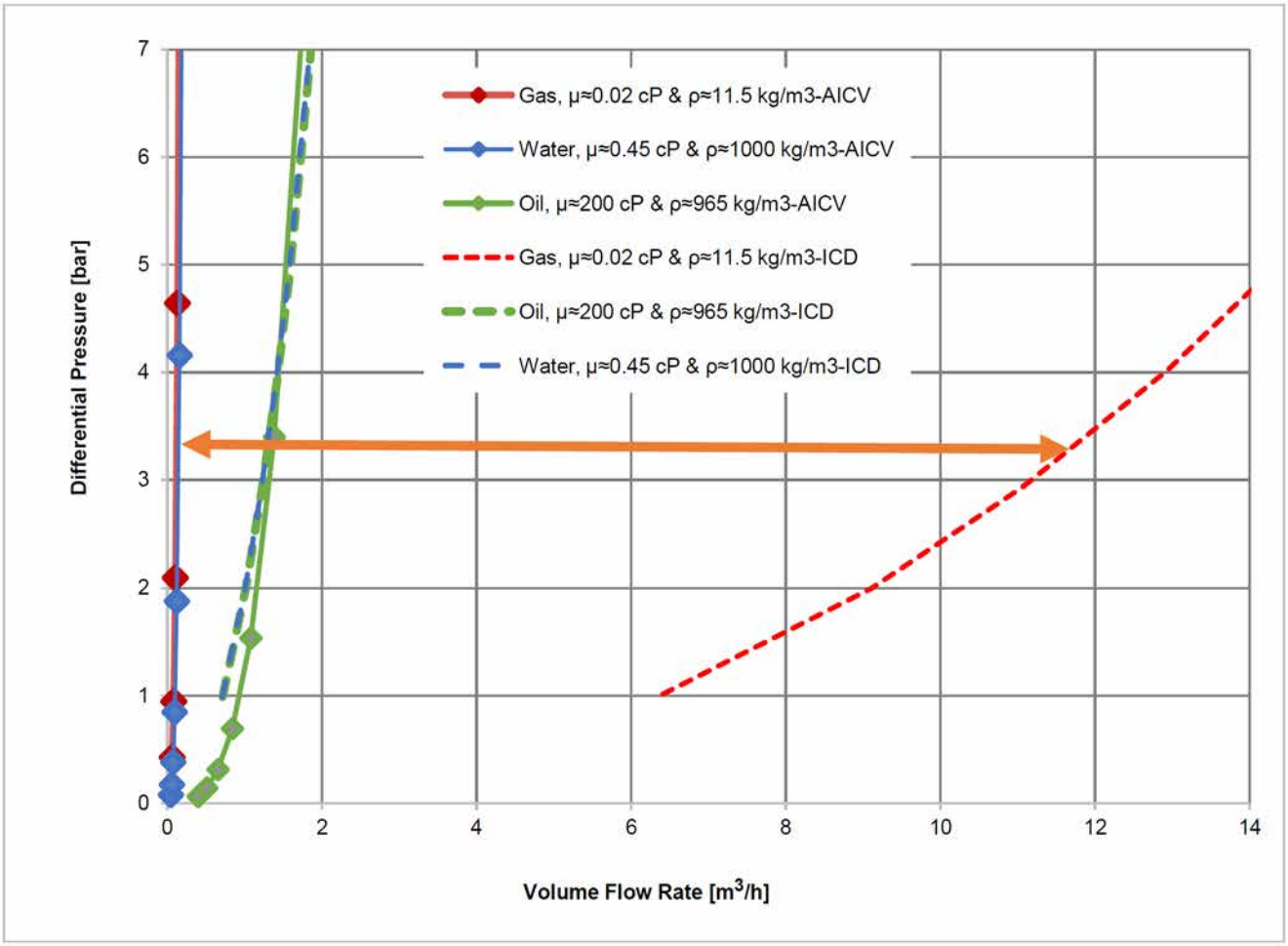

Figure 3—Comparison of single-phase flow performance of the ICD (dashed lines) and AICV (solid lines) for oil, water, and gas.

Two-phase oil/gas tests performed at 1, 2, 3 and 5 bar differential pressure in the gas volume fraction (GVF) range of 40-80 % are presented in previous authors' work (Soheila Taghavi et al., 2022) and is shown in Fig. 4.

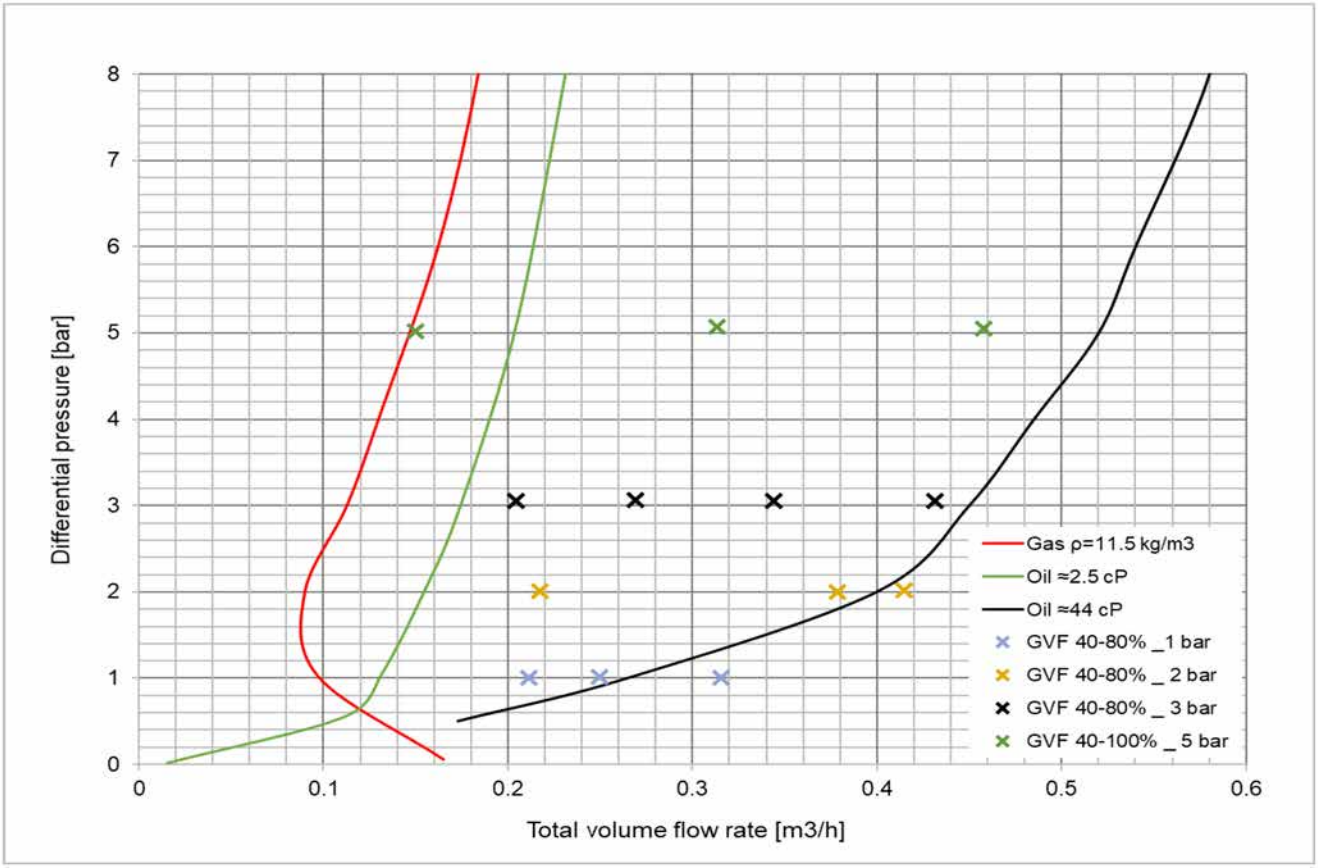

Figure 4—Two-phase performance of AICV at 1,2,3, and 5bar differential pressure together with single phase tests of AICV.

The GVF pattern of these data points are being used to generate the control signal table for table controllers in the OLGA set-up which regulates the opening and closing of the valve. The AICV restricts the gas flow when the GVF is getting higher, until pure gas flows through the valve. The green point over the red curve (pure gas) at 5 bar drawdown is an illustration of 100 % GVF when the valve is closed, and a minor amount of gas is flowing through the valve. (Soheila Taghavi et al., 2022)

Near well simulation with OLGA-ROCX

In this study, OLGA-ROCX is used to describe and compare the behavior of ICD and AICV in the SAGD late life reservoir, and to illustrate the impact of AICV completion on gas and steam reduction. OLGA/ROCX is a robust transient simulation tool to perform integrated well-reservoir simulations. The reservoir and the wellbore model are coupled in an implicit way (Chupin et al., 2007).

The near-well reservoir and fluid properties are specified in ROCX, and the wellbore model is developed in OLGA. Coupling OLGA and ROCX enables the user to simulate the fluid production from the reservoir into the well. The fluid properties are defined by the black oil option in ROCX. Reservoir properties including porosity, permeability, residual saturations, temperature, and pressure are specified in ROCX. The reservoir and well conditions are summarized in Table 1.

Table 1—Reservoir and well condition.

Oil viscosity [cP]	15.5
Oil and gas specific gravity [-]	0.9 and 0.64
Porosity [-]	0.3
Temperature °C	180

Pressure [bar]	27
Horizontal permeability and vertical permeability [mD]	3000 and 500
Wellbore diameter ID, and tubing outer diameter OD [in]	8.74 and 4.5
Reservoir length, width, height [m]	1000,117,40
Height of the oil column [m]	36
Drawdown (Preservoir - Pwell) [bar]	7

The well is 1000 m long and is divided into 10 zones of 100 m each. As the fluid properties vary significantly around the well and in the Y-Z plane, a finer mesh is considered in the grid setup to achieve more accurate results. The grid resolution in the Y-Z, and X-Z plane and the well location is shown in Fig. 5.

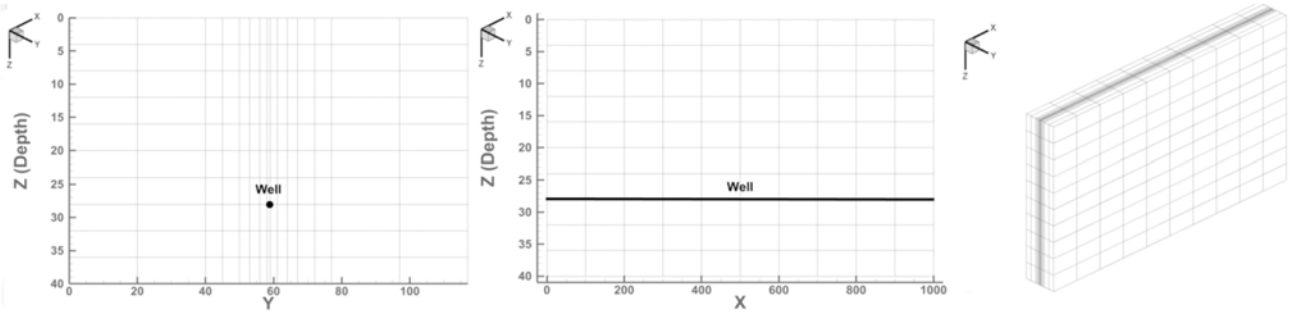

Figure 5—Grid resolution in Y-Z, and X-Z plane and the well location.

A homogenous reservoir is assumed. In addition, it is assumed that the well has been in production for several years and at the late life stage a strong gas breakthrough (high gas saturation) has occurred in the toe section of the production well. Fig. 6 shows the initial oil saturation profile of the reservoir.

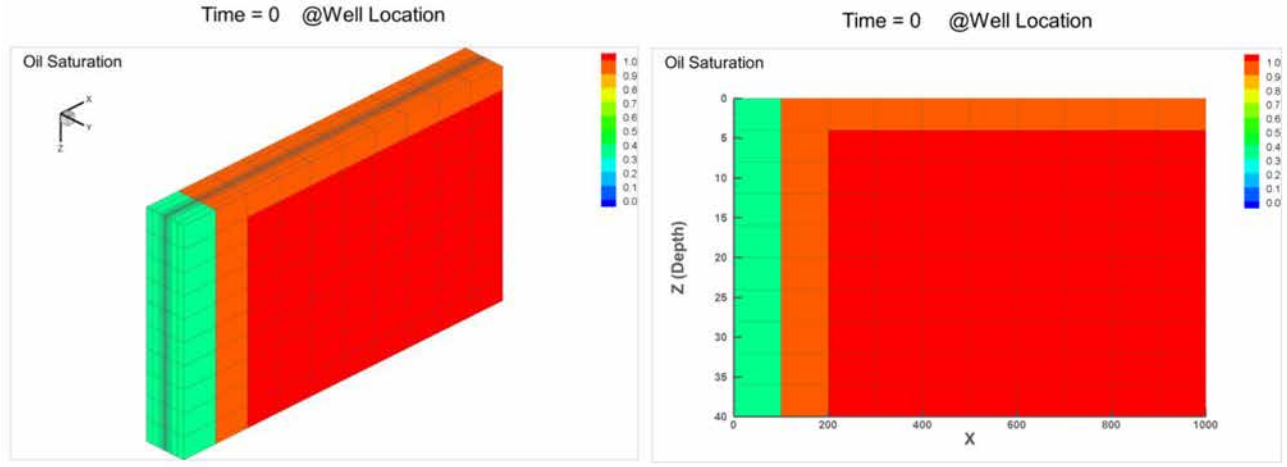

Figure 6—3D plot of initial oil satuartion (left) and 2D plot in x-z direction (right).

The well set-up in OLGA for ICD and AICV completion which is tubing deployed is shown in Fig. 7 and Fig. 8 respectively. A zoom view of one pipe section including packer, near-well source, inflow controller and leak is presented in Fig. 9. This set-up was developed and proposed for the first time in 2012 (Aakre, 2017), and results were presented in a scientific paper (Aakre et al., 2013).

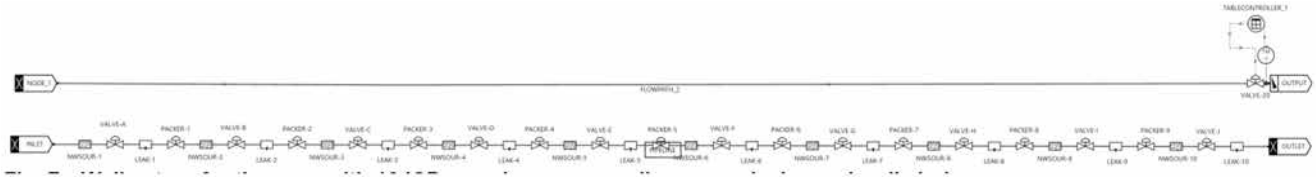

Figure 7—Well set-up for the case with 10 ICDs, packers, near-well sources, leaks, and well choke.

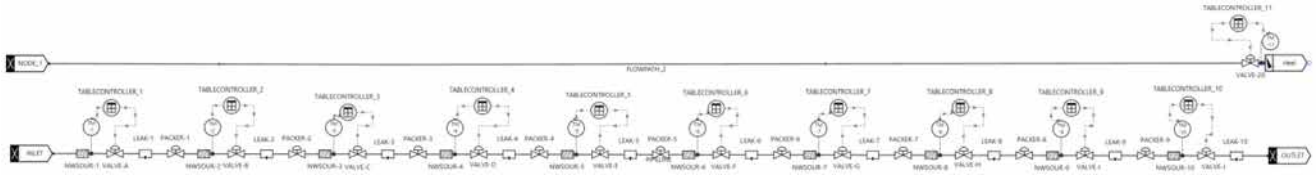

Figure 8—Well set-up for the case with 10 AICVs, table controllers, packers, near-well sources, leaks, and well choke.

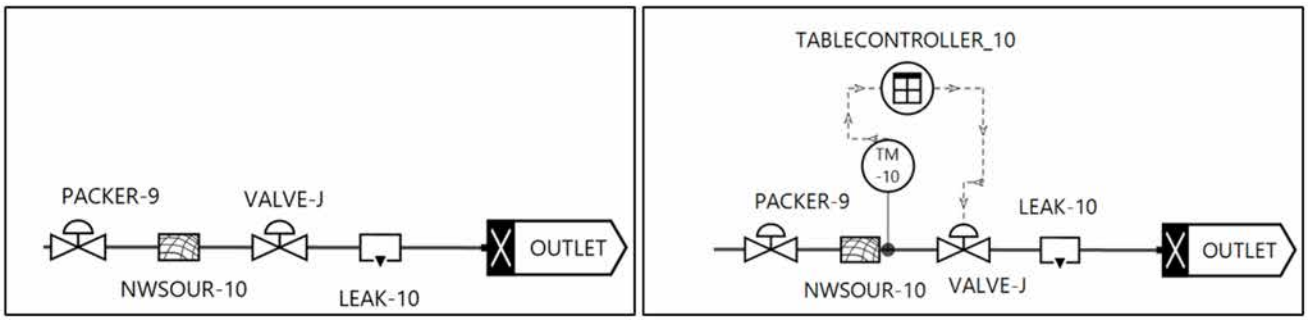

Figure 9—set-up of one pipe section for ICD (left) and AICV (right) case in OLGA.

This set-up consists of near-well sources which get input data from the ROCX file, inflow controllers, packers, and leaks from which fluids flow to the production well (FLOWPATH). The well consists of 10 segments, each 100 m long. One equivalent orifice valve is considered for every segment of the well, meaning one equivalent orifice valve for every 8 AICVs and ICDs in a standard completion where the joint length is 12.4 m.

A comprehensive and step by step workflow for modelling of the rate-controlled production (RCP) valves in the OLGA simulator was proposed in a scientific paper (Moradi and Moldestad, 2021). In this new method, a controller is used to chock the RCP valve based on the characteristics of the RCP valve and the reservoir fluid mixture. This method is used in this work to regulate the closure system of AICVs. This table controller gets the measured GVF data from the transmitter (TM) and provides corresponding control signals for chocking the AICV. Control signal table is generated based on the GVF data gained from experiments illustrated in Fig. 4 and data shown in Fig. 10. According to the experimental data, the AICV restricts the gas flow when the GVF is getting higher meaning the percentage of valve opening is getting less and less by increasing the GVF percentage.

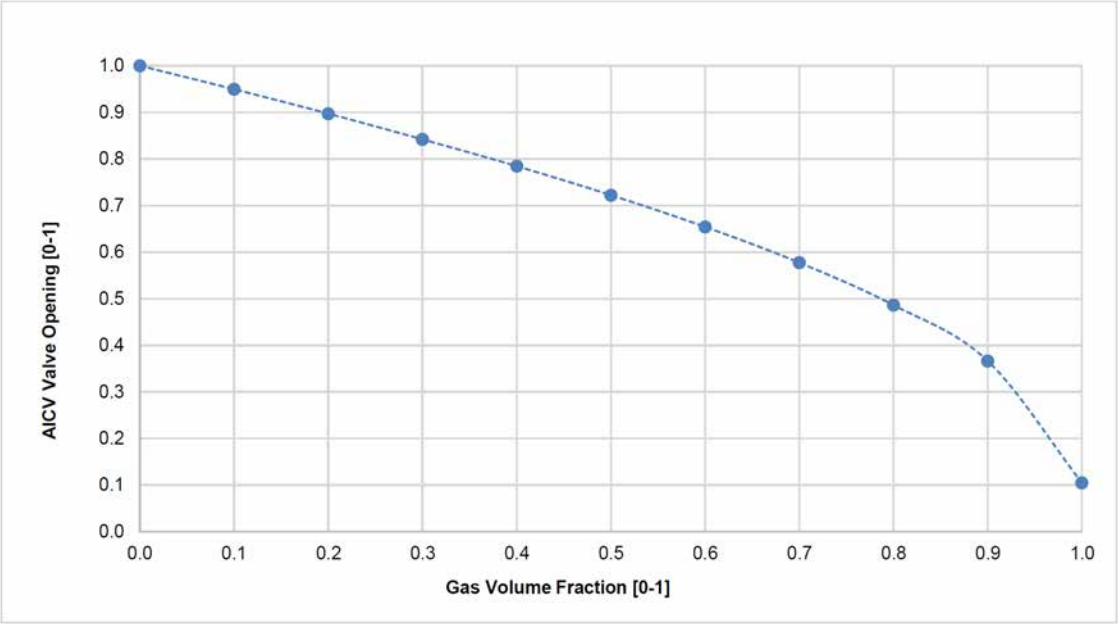

Figure 10—Valve opening versus GVF for AICV valve.

Results and discussion, AICV and ICD

As shown in Fig. 10, the minimum opening of the AICVs was specified as 10% of fully open AICV. Fig. 11 shows the output signal of AICV controllers with time. The first AICV which is installed in the toe section of the well starts choking to the minimum opening of the AICV, since the gas saturation was highest in the toe section of the well and GVF is equal to one. The gas reaches the second AICV near the toe (GVF is equal to 0.58) and starts choking to 70% of fully open AICV. On day 58, gas reaches the heel section of the well due to heel-toe effect. The AICV at the heel section of the well starts choking and consequently the remaining AICVs starts to choke the gas flow. At the end of the production time, all the AICVs except the AICV at the toe section of the well, chokes to 40% of fully open AICV meaning GVF is approximately 0.9, see Fig. 10.

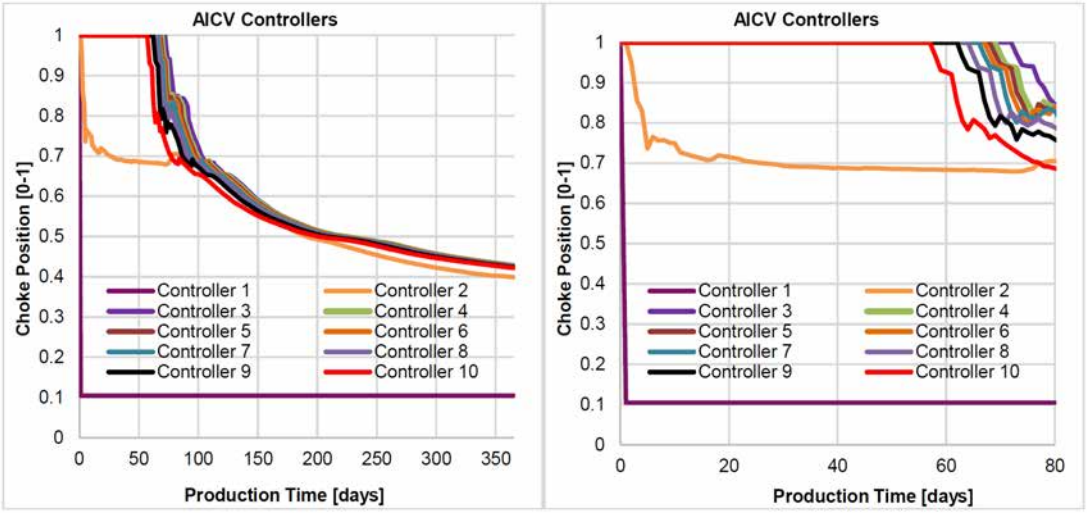

Figure 11—Choke position of AICVs with time: 365 days (left), the first 80 days (right).

Fig. 12 shows the gas oil ratio (GOR) development for both ICD and AICV case and how a well completed with AICVs and ICDs is choked consequently. Fig. 13 shows a 2D plot of the reservoir in the x-z direction

including all the production zones and the well location. The plot shows the oil saturation right after the breakthrough (day 58) and after 365 days of production.

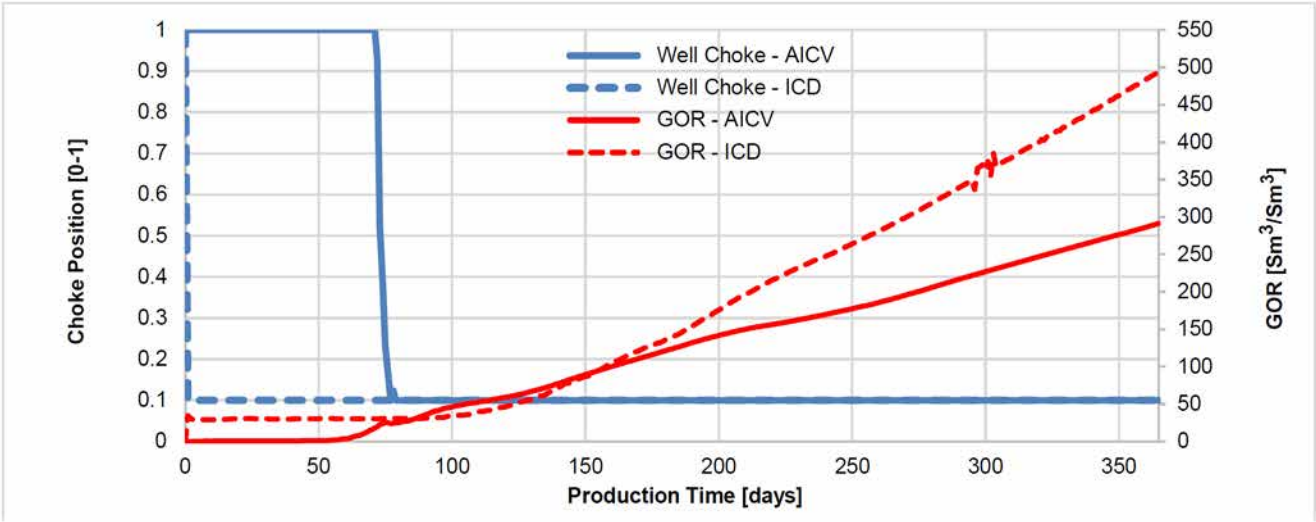

Figure 12—GOR development and well choke position.

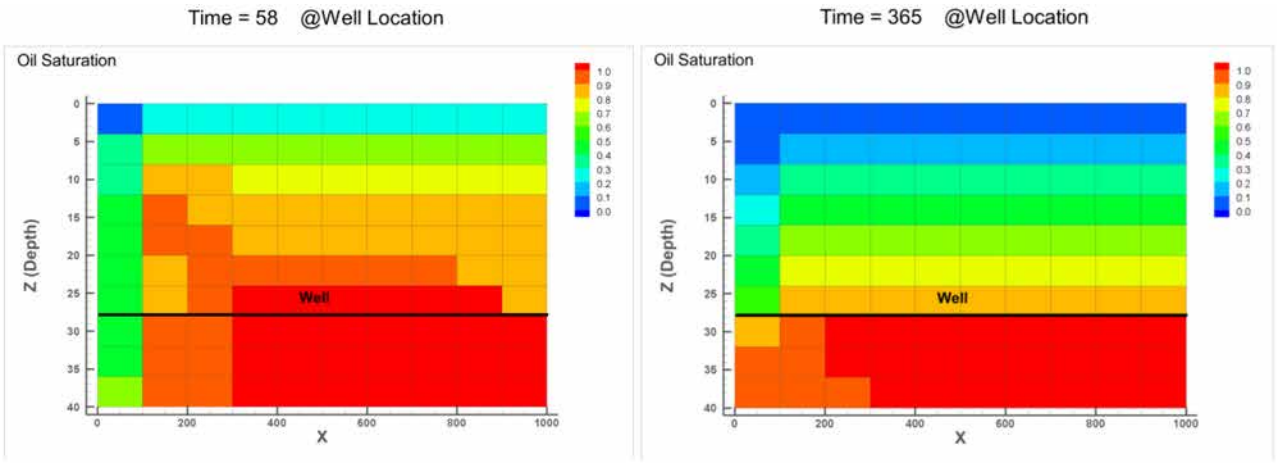

Figure 13—Oil saturation in the reservoir in the x-z direction after 58 days (left) and after 365 days (right).

In this simulation the well choke is regulated with table controller. This table controller gets the measured GOR data from the transmitter and provides corresponding control signals for chocking the well. The minimum possible opening of the choke is set to 10 % opening when GOR [Sm^3/Sm^3] reaches to 20. This shows that ICD chokes instantly to its minimum value as the gas enters the well and GOR is equal to 20 Sm^3/Sm^3. There is no controller for ICDs so the ICDs do not restrict gas production. However, those AICVs that are installed in the toe and adjacent zone, restrict the gas production, keeping the GOR low and the well choke in fully open position. On day 58, gas reaches the heel section of the well due to the heel-toe effect, and GOR increases. This is shown in Fig. 13 to the left, where the oil saturation in the heel is less than the oil saturation in the adjacent zones. When the GOR passes 20 due to the gas breakthrough in the heel, the controller starts to reduce the choke opening and chokes the well. The choke position reaches its minimum after almost 80 days of production. After this the valve position is constant at its minimum opening and the GOR gradually increases.

Fig. 14 shows the cumulative oil and gas production versus time. In the ICD case, the gas is produced from the beginning of the production time, while for AICV case is from day 58; when the breakthrough

occurs at heel. For the ICD case, the well choking begins from the first day, see Fig. 12. This choking leads to reduction of the drawdown in the gas production zone, and consequently reduction of the oil production. This continues until the breakthrough occurs in the heel (day 58) and the GOR increases until day 80. In this period, the cumulative oil production for AICV case is 48 % higher than for the ICD case. At day 80, when the GOR passes 20, the controller starts to reduce the choke opening and chokes the well for the AICV case. At the end of the production period, the accumulated oil for the AICV case is about 3% more than for the ICD case. Also, it can be concluded from Fig. 14 that the amount of accumulated gas is reduced significantly from 1.68 Mm3 for the ICD case to 0.97 Mm3 for the AICV case (74% reduction) after 365 days of production. Although excessive amount of gas is produced from the ICD well, the oil reduction compared to the AICV well is only 3%. This is most probably due to the relative permeability curves that are being used for the simulations. To our knowledge and experience (Halvorsen et al., 2012), dynamic reservoir simulators tend to underpredict the oil production after gas breaks through the well.

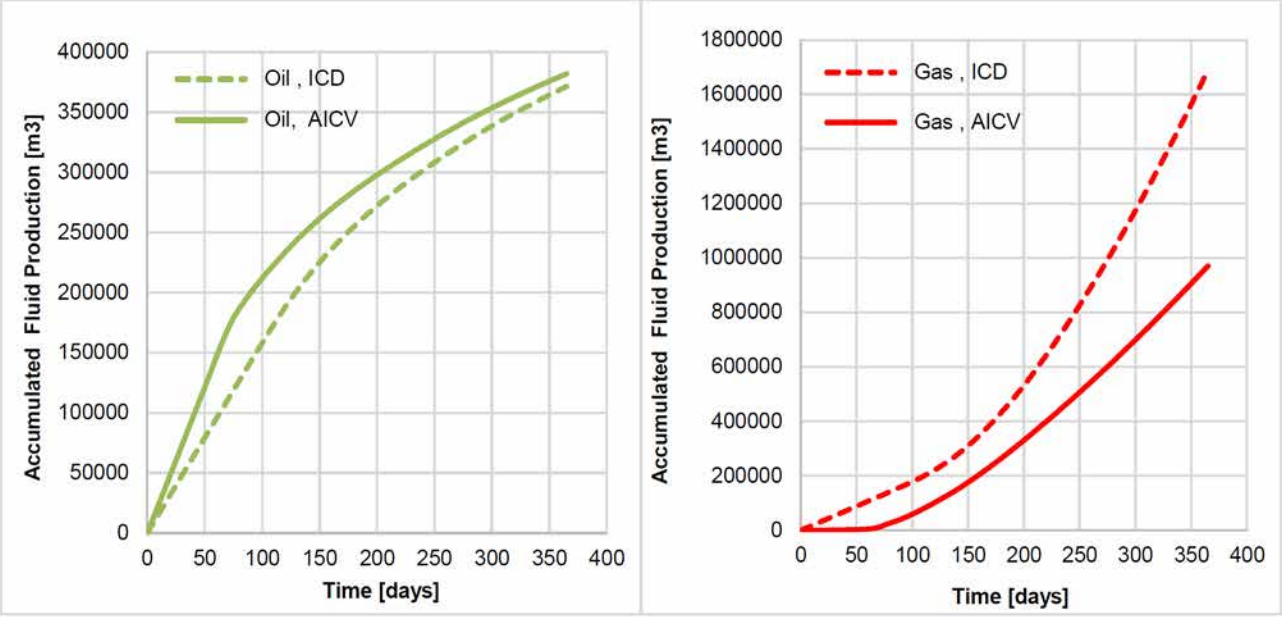

Figure 14—Cumulative oil (left) and gas (right) production with time.

Annulus flow simulation with OLGA and NETool

Almost all the reservoir simulators calculate the multiphase flow properties in annulus with no-slip. The no-slip correlation assumes homogeneous flow with no slippage between the phases. The difference in velocity between the gas and liquid is defined as slip ratio and is as follows:

$$S = \frac{A_o}{A_g}\frac{U_{sg}}{U_{so}} = \frac{1-\varepsilon_g}{\varepsilon_g}\frac{U_{sg}}{U_{so}} \quad (1)$$

Where U_{sg} and U_{so} are the superficial velocity of gas and oil, A_g and A_o are area of a pipe segment occupied by the gas and oil, and εg and εo are the actual or the in-situ area fraction or hold-up of gas and oil respectively. (Elseth, 2001)

Two cases are simulated in OLGA and NETool simulator. It is possible to perform the simulations in OLGA with and without slip while the calculations in NETool is without slip. NETool uses the modified Darcy's law for flow in annulus filled with formation or gravel:

$$v = k\left(\frac{k_{ro}}{\mu_o} + \frac{k_{rg}}{\mu_g}\right)\frac{\partial p}{\partial x} \quad (2)$$

Where, v is the total volumetric flux, $\partial p/\partial x$ is the pressure gradient, μg and μo are gas and oil viscosity, K is gravel permeability, k_{rg} and k_{ro} are gas and oil relative permeabilities and are calculated as:

$$k_{ro} = \alpha^c \tag{3}$$

$$k_{rg} = (1-\alpha)^c \tag{4}$$

C is Corey index and the value of 2 is commonly used, and α is the oil fraction.

This model considers both gas and oil flow along the annulus through the gravel and the effect of relative permeability on this flow via the Corey Index. This is a homogeneous model which assumes that all phases travel with same speed in the form of a mixture. Thus, NETool allows only a single true velocity at each node, the slip effect captured by many of the regime closure models is not fully utilized in the output results.

Two cases are studied in the OLGA/ROCX simulator to study the annuls flow, one with calculation of slip between the phases, and one without slip calculation. It is assumed that gas and oil enter the annulus from the toe section of the well. One ROCX near-well source for gas and one for oil are placed in the toe section of the well and leaks with fixed openings are distributed along the annulus. The fluid from the near-well sources flows through the leaks into the annulus. The well set-up for this case is shown in Fig. 15. Localized reduction in the annular area resulting from hole collapse is not considered in this study.

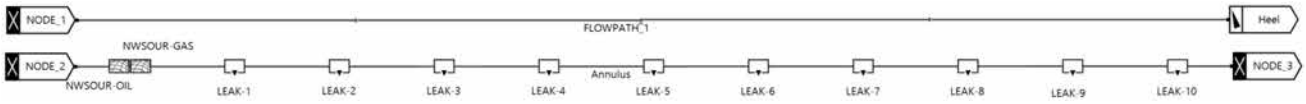

Figure 15—Simulation set-up consists of near-well sources and leaks in annulus.

In addition, one case is studied using NETool. In this case, the annulus of the production well is filled with high permeability gravel (which resembles almost an open annulus) and the well is completed with 10 (blue rectangles) with the same diameter as OLGA case, see Fig. 16. It is assumed that the gas saturation near the toe section is significantly high, whereas the other sections are 100% saturated with oil.

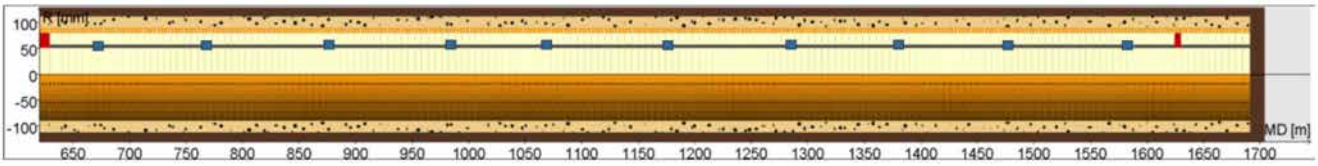

Figure 16—sketch of the production well and annulus which is filled with high permeable gravel.

Results and discussions, Annulus Flow

The simulations are performed for the cases in NETool, and OLGA and the results are presented in this section.

OLGA simulations

Fig. 17 shows the actual velocity of gas and oil along the annulus by considering slip and without slip between phases. Fig. 18 shows the flow regime along the annulus where the different regimes are categorized by different IDs in which 1= stratified, 2= annular, 3=slug, 4=bubble. For the case without slip, the actual velocity of oil and gas in the annulus is equal and the flow regime is mainly bubble, as there is no slip between the phases. However, in the case with slip, the actual velocity of gas is higher than oil and the flow regime is stratified. The actual velocity of gas is highest in the toe section of the well; meaning that the area of the pipe that is occupied by gas is lowest in the toe section. This is the opposite of what is illustrated by the results from NETool explained in the next section.

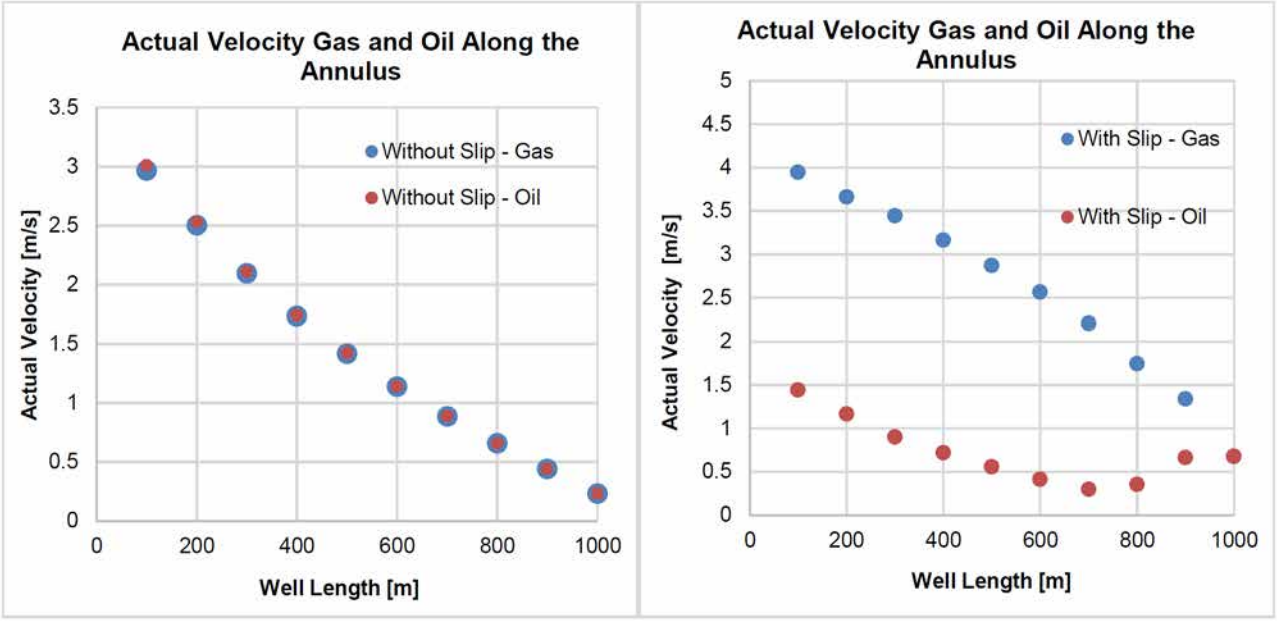

Figure 17—Actual velocity of gas and oil along the annulus with and without slip.

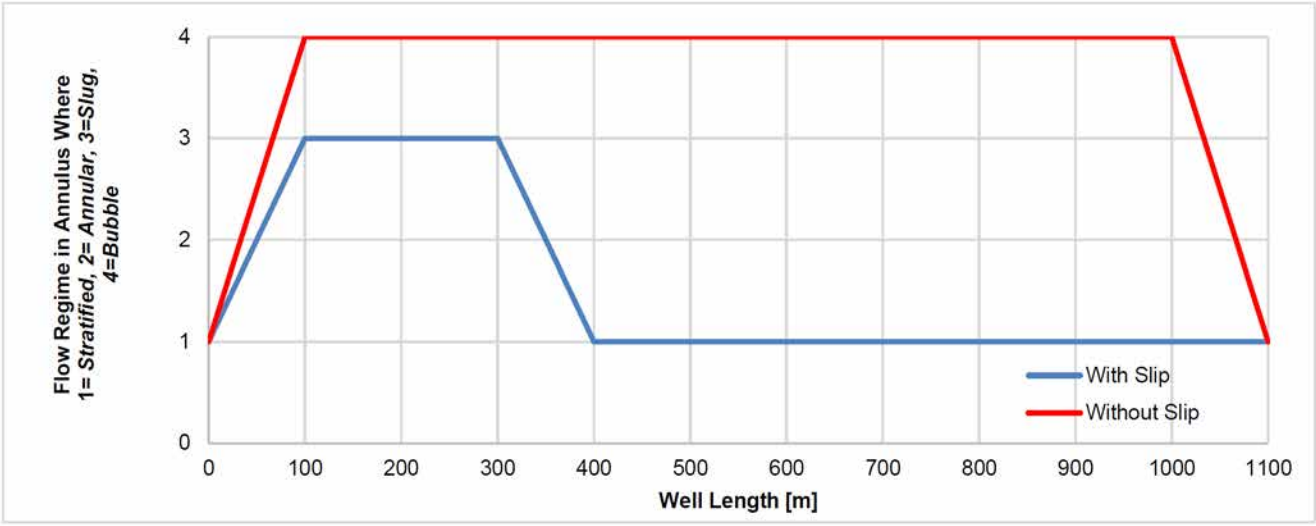

Figure 18—Flow regime along the annulus with and without slip.

The flow regime for the case with slip is defined as slug in the toe section where the gas enters the well, while it becomes stratified in the other sections along the well towards the heel. The flow regime for the case without slip is defined as bubble along the whole length of the well, indicating that an oil continuous flow contains gas bubbles and there is no slip between the phases.

NETool simulations

The phase volumetric flow fraction from reservoir to the well and across the inflow control are presented in Fig. 19. The gas saturation is set to 1(red bars) at one section of the well close to the toe, giving a GVF of 1. The GVF is almost constant along the annulus towards the heel. NETool uses a homogeneous model which assumes that all phases travel with same speed in the form of a mixture (no slip). However, in case of gas breakthrough in a real case, the gas travels much faster than oil along the annulus with low pressure gradients because of much lower gas viscosity compared to the oil viscosity.

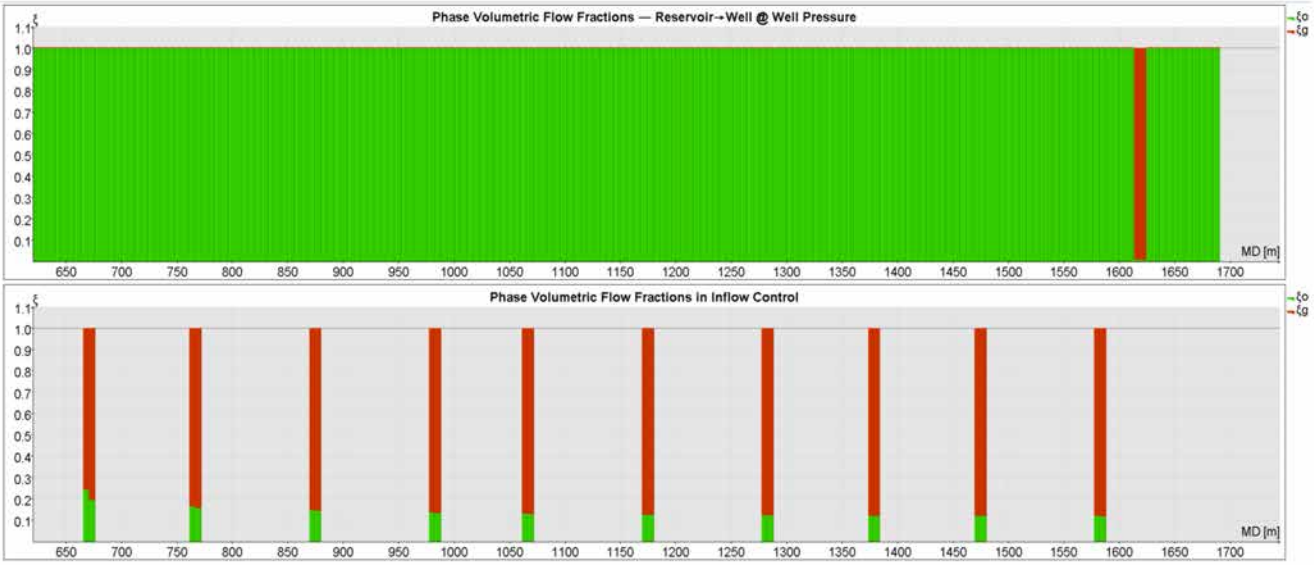

Figure 19—Phase volumetric flow fractions from reservoir to well and across inflow control as a function of position.

Fig. 20 shows the comparison of the GVF behavior along the annulus in OLGA (with and without slip) and NETool (without slip). The GVF performance along the annulus is almost the same for the NETool case and OLGA case with no slip assumption. The GVF performance along the annulus simulated using NETool and OLGA illustrates how different reservoir simulators behave for similar cases. This can be due to the fact that NETool and most of the reservoir simulators (except for OLGA) calculate the multiphase flow properties in annulus with no-slip assumption.

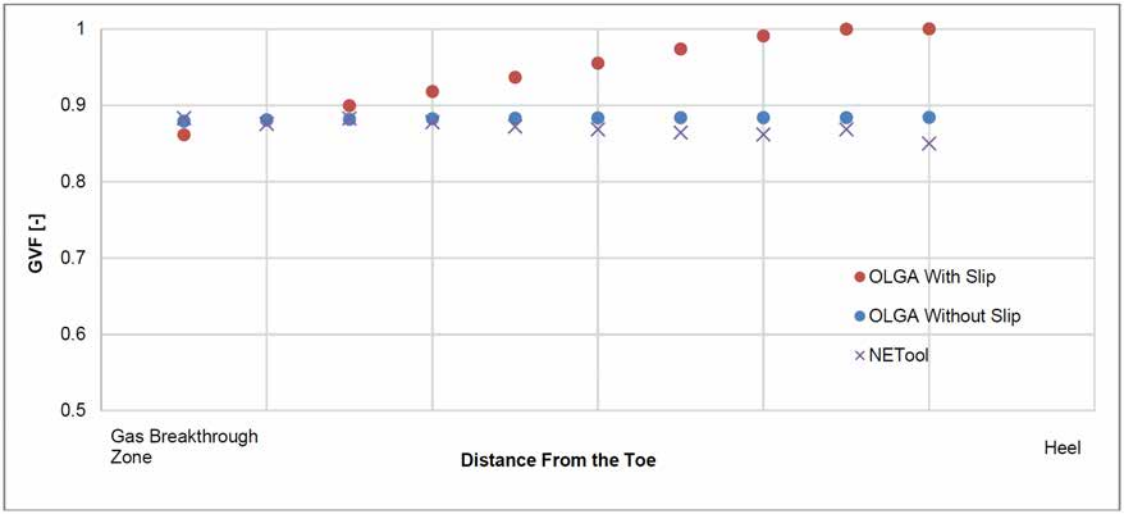

Figure 20—Comparison of GVF behavior along the annulus in OLGA and NETool.

Conclusion

AICV restricts the inflow of steam and/or gas in the zones where breakthrough occurs. A SAGD production well completed with ICDs and AICVs was modeled in OLGA. The reservoir properties and specifications were defined in ROCX. ROCX is a near-wellbore reservoir simulator and can be coupled to OLGA which is a dynamic multiphase flow simulator. Coupling OLGA and ROCX enables the user to perform integrated reservoir-well simulations. The simulations in OLGA/ROCX show that the recovery with AICV is increased with approximately 3% compared to passive ICD.

Indeed, simulation results show that utilizing AICV in SAGD production wells will reduce the gas and steam production by 74% after 365 days of production. The results confirm the significant benefit of AICV in steam and/or gas reduction and consequently increased oil production. Reduction in steam production will improve the overall SAGD operation performance. This will also result in more cost-effective oil production.

In addition, the annular flow in a well completed by inflow control devices was studied by using OLGA and NETool. Almost all the reservoir simulators calculate the multiphase flow properties in annulus with no-slip. In this paper, the effect of using slip and no-slip between the phases was investigated for one case. The study was an attempt to initiate discussions and provide an insight into a fundamental problem that almost all the reservoir simulators are dealing with.

References

Aakre, H. (2017). *The impact of autonomous inflow control valve on increased oil production and recovery* University College of Southeast Norway, Faculty of Technology, Natural Sciences and Maritime Sciences]. Kongsberg.

Aakre, H., Halvorsen, B., Werswick, B., and Mathiesen, V. (2013). Smart Well With Autonomous Inflow Control Valve Technology. SPE Middle East Oil and Gas Show and Conference, https://doi.org/10.2118/164348-MS

Aakre, H., Mathiesen, V., and Moldestad, B. (2018). Performance of CO2 flooding in a heterogeneous oil reservoir using autonomous inflow control. *Journal of Petroleum Science and Engineering*, **167**, 654–663. https://doi.org/10.1016/j.petrol.2018.04.008

Banerjee, S., and Hascakir, B. (2018). Design of flow control devices in steam-assisted gravity drainage (SAGD) completion. *Journal of Petroleum Exploration and Production Technology*, **8**(3), 785–797. https://doi.org/10.1007/s13202-017-0393-4

Butler, R. (1998). SAGD Comes of AGE! *Journal of Canadian Petroleum Technology*, **37**(07). https://doi.org/10.2118/98-07-da

Chupin, G., Hu, B., Haugset, T., Sagen, J., and Claudel, M. (2007). Integrated Wellbore/Reservoir Model Predicts Flow Transients in Liquid-Loaded Gas Wells. SPE Annual Technical Conference and Exhibition, https://doi.org/10.2118/110461-MS

Elseth, G. (2001). *An Experimental Study of Oil/Water Flow in Horizontal Pipes* (Publication Number 125012) [*Doctoral thesis*, Telemark University College]. POrsgrunn, Norway. http://hdl.handle.net/11250/231212

Gates, I. D., and Leskiw, C. (2010). Impact of steam trap control on performance of steam-assisted gravity drainage. *Journal of Petroleum Science and Engineering*, **75**(1), 215–222. https://doi.org/10.1016/j.petrol.2010.11.014

Ghesmat, K., and Zhao, L. (2015). SAGD Well-Pair Completion Optimization Using Scab Liner and Steam Splitters. *Journal of Canadian Petroleum Technology*, **54**(06), 387–393. https://doi.org/10.2118/170076-pa

Halvorsen, M., Elseth, G., and Nævdal, O. M. (2012). Increased oil production at Troll by autonomous inflow control with RCP valves. SPE Annual Technical Conference and Exhibition, https://doi.org/10.2118/159634-MS

Høhrbye, E.-M. J., Mathiesen, V., and Moldestad, B. M. E. (2016). Heavy Oil Production With Energy Effective Steam-assisted Gravity Drainage.

Konopczynski, M. (2018). Thermodynamic Analysis of a Modified Autonomous Flow Control Device for SAGD Sub-Cool Management. *SPE Thermal Well Integrity and Design Symposium*, https://doi.org/10.2118/193365-MS

Mehrotra, A. K., & Svrcek, W. Y. (1982). Correlations For Properties of Bitumen Saturated With CO2, CH4 And N2, And Experiments With Combustion Gas Mixtures. *Journal of Canadian Petroleum Technology*, **21**(06). https://doi.org/10.2118/82-06-05

Moradi, A., and Moldestad, B. M. E. (2021). A Proposed Method for Simulation of Rate-Controlled Production Valves for Reduced Water Cut. *SPE Production and Operations*, **36**(03), 669–684. https://doi.org/10.2118/205377-pa

Regulacion, R., and Shahreyar, N. (2011). Inflow Control Devices Minimize Annular Velocity in Gas Wells with Stand-Alone Screen Completions. SPE European Formation Damage Conference,https://doi.org/10.2118/142700-MS

Taghavi, S., Aakre, H., and Moldestad, B. M. E. (2022). Performance Analysis of Autonomous Inflow Control Valve in a SAGD Late Life Process with Non-Condensable Gases. SPE Canadian Energy Technology Conference, https://doi.org/10.2118/208915-MS

Taghavi, S., Aakre, H., Swaffield, S., and Brough, R. B. (2019). Verification of Autonomous Inflow Control Valve Flow Performance Within Heavy Oil-SAGD Thermal Flow Loop. SPE Annual Technical Conference and Exhibition, https://doi.org/10.2118/196216-MS

Taghavi, S., Farsi Madan, F., Timsina, R., and Moldestad, B. M. E. (2022). Application of Autonomous Inflow Control Valve for Enhanced Bitumen Recovery by Steam Assisted Gravity Drainage. The 63rd International Conference of Scandinavian Simulation Society, SIMS 2022, Trondheim, Norway.https://doi.org/10.3384/ecp192009

Paper 6

The Impact of Autonomous Inflow Control Valve on Enhanced Oil Recovery in SAGD Application

This paper is published in the Proceeding of 64th International Conference of Scandinavian Simulation Society, SIMS 2023, Västerås, Sweden, September 26-27, 2023

Paper presented by Soheila Taghavi

Authors: Farhan Hasin Alam, Seyed Amin Tahami, Nora C.I. Furuvik, Britt M.E. Moldestad, and Soheila Taghavi

The Impact of Autonomous Inflow Control Valve on Enhanced Oil Recovery in SAGD Application

Farhan Hasin Alam [a], Seyed Amin Tahami [a], Nora C.I. Furuvik [a], Britt M.E. Moldestad [a], Soheila Taghavi [a & b, *]

[a] *Department of Process, Energy and Environmental Technology, University of South-Eastern Norway, Norway*
[b] *InflowControl AS, Norway*

*corresponding author: soheila.taghavi.hosnaroudi@gmail.com
soheila.t.hosnaroudi@usn.no

Abstract
The demand for non-conventional oil has increased globally. Non-conventional oil is categorized as extra heavy oil and bitumen. In reservoirs with extra heavy oil and bitumen, thermal methods are used to reduce the oil viscosity. Steam assisted gravity drainage (SAGD) is a thermal recovery method to enhance the bitumen recovery. In this method, steam is injected to bitumen and heavy oil to reduce the viscosity and make the oil mobile and extractable. To obtain an efficient SAGD process, the residence time for steam in the reservoir must be long enough for the steam to condense and release the latent energy to be transferred to the cold bitumen. Early breakthrough of steam in some parts of the well will eventually limit the oil production and must be avoided. Autonomous inflow control valve (AICV) can prevent the steam breakthrough and restrict the excessive production of steam. The objective of this paper is to investigate the performance of AICV and its impacts on increased oil production in a SAGD production well. This is achieved by focusing on the implementation, and performance evaluation of inflow control devices (ICDs) and AICVs compared with standard well perforations. CMG STARS, a multi-phase, multi-component thermal reservoir simulator, is used to perform numerical simulation studies. The simulation results demonstrate the significant benefit of AICV in steam reduction compared to ICD and well perforations. The simulation results demonstrate that utilizing AICV in a SAGD reservoir will lead to higher oil production, less steam production, and a more uniform temperature distribution, and steam chamber conformance. Reduction in steam production, will improve the overall SAGD operation performance. This will also result in more cost-effective oil production, as less steam is needed to be generated for production of each barrel of oil.

1. Introduction

The demand for non-conventional oil has increased globally. Non-conventional oil is categorized as extra heavy oil and bitumen. The mobility of bitumen is quite poor since the viscosity can be as high as 10^6 cP (Ghahfarokhi et al., 2012). In reservoirs with extra heavy oil and bitumen, thermal methods such as steam assisted gravity drainage (SAGD) are used to reduce the oil viscosity and make the bitumen mobile and extractable. More than 80 percent of the world's annual output of heavy oil is accomplished through the utilization of this technique (Xu et al., 2020).

The SAGD well configuration typically consists of a pair of horizontally aligned wells that are between 500 and 1000 meters in length (Shen, 2013). The top wellbore is utilized for steam injection which is located about 4-6m above the production well, and the lower wellbore is utilized for oil production. When horizontal wellbores are used in SAGD, reservoir contact, and the overall well productivity are both significantly improved (Shen, 2013). Steam is injected into the reservoir from the injection well. This creates steam chambers at the interfaces as shown in Figure 1. These steam chambers expand both vertically and laterally (Shen, 2013). Latent heat from the steam is transferred to the bitumen at the interface, making it less viscous and more mobile. Due to the action of gravitational forces, the steam condensate, and the mobile bitumen flow downwards into the producer well. SAGD has been shown to be a successful and cost-effective way to get bitumen out of heavy oil reservoirs.

Several technologies have been created to optimize the performance of the SAGD process. Advanced well completion devices such as inflow control devices (ICDs) and autonomous inflow control valves (AICVs) can be used for improving bitumen recovery in SAGD operations. ICDs are intended to control fluid flow within a wellbore and assuring uniform distribution of steam. AICVs, on the other hand, are adjustable valves that regulate the openings automatically based on the fluid viscosities. The AICVs are thereby preserving

balanced production rates and are controlling the inflow profiles.

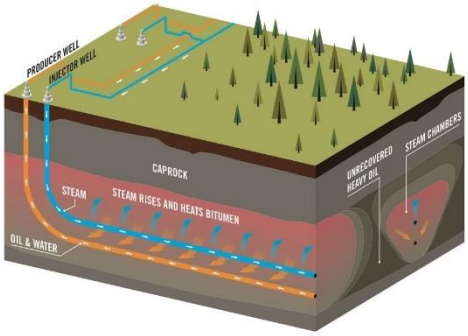

Figure 1: Principles of SAGD operation (staff, 2016)

The use of ICDs and AICVs in SAGD operations has the potential to solve several issues associated with steam injection and bitumen recovery. These issues include steam chamber conformance, early steam breakthrough, irregular fluid distribution, water and gas coning, and excessive production of undesirable fluids. By strategically employing ICDs and AICVs, operators can optimize thermal performance, maximize bitumen recovery, and reduce operating expenses.

The objective of this paper is to investigate the performance of AICVs, and its impacts on increased oil production in a SAGD production well. This is achieved by focusing on the implementation, and performance evaluation of ICDs and AICVs compared with standard well perforations. The novelty of this work is to simulation of the AICV and ICD behavior in a dynamic reservoir simulator under SAGD conditions. The functionality of the AICV and ICD is simulated through tabulated data based on the experiments presented in previous author's work (Taghavi et al., 2022). CMG STARS, a multi-phase, multi-component thermal reservoir simulator, is used to perform numerical simulation studies.

2. Advanced Wells with Inflow Control Technologies; ICD and AICV

Inflow control technologies such as ICDs and AICVs were introduced to the oil industry to overcome the early water and gas breakthrough challenges associated with the heel-toe effect in horizontal wells. Drilling long horizontal wells can increase reservoir contact, resulting in improved oil recovery. The pressure difference between the toe and heel sections of the well becomes large in long horizontal wells due to the pressure drop induced by friction between the inner pipe surface and fluid flowing through the pipe. This pressure difference in the well generates a higher pressure drawdown between the wellbore and the reservoir at the heel than at the toe, resulting in a greater inflow of reservoir fluid in the heel rather than in other areas of the well as shown in Figure 2. This phenomenon is known as the heel-toe effect. Because of heel-toe effect, early breakthrough of water and/or gas occurs at the heel section of the well, decreasing oil recovery efficiency.

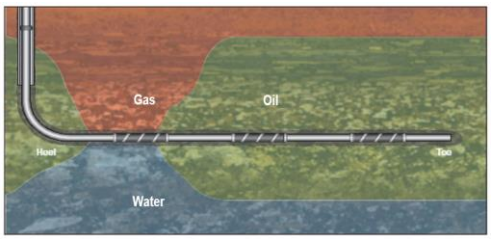

Figure 2: Gas and water breakthrough at the heel section of the well (Ellis et al., 2009).

2.1. ICDs in advanced wells

ICD is used to restrict the flow of fluid entering the base pipe from the annulus. It is a passive inflow control device, meaning it has no active components that can be regulated or altered to regulate the flow through it.

The governing equation of the nozzle-type ICD, as shown in Figure 3, is as follows (Lauritzen & Martiniussen, 2011):

$$\Delta P = \frac{8\rho Q^2}{d^4\pi^2 n^2 {C_D}^2} \qquad (1)$$

Where ΔP is the pressure drop through the nozzle, ρ is the fluid density, Q is the volumetric flow rate of the fluid through the nozzle, d is the diameter of the nozzle, n is the number of tested nozzles, and C_D is the discharge coefficient. C_D is mostly a function of the Reynolds number (Re) (Lauritzen & Martiniussen, 2011).

The pressure drop through the nozzle is mainly dependent on the fluid density.

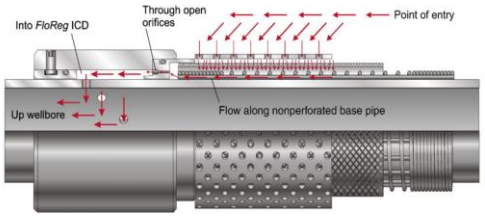

Figure 3 : Nozzle-type ICD (Birchenko et al., 2010).

2.2. AICVs in advanced wells

AICV is a novel inflow control system that combines the most advantageous characteristics of inflow controllers. AICVs are autonomous, meaning that they operate without the need of external control systems and constant human involvement. For oil production, AICV offers minimal flow restriction and the capability to close for water and gas/steam while simultaneously producing oil from other zones along the well. The valves in zones where gas/steam

and water break through into the well, will close locally. Figure 4 shows AICV in closed and open position. Figure 4a shows that valve is open and producing oil as gas/steam is approaching the valve. Figure 4b illustrates that the gas/steam has reached the valve inlet, and valve is closed for gas/steam.

(a)

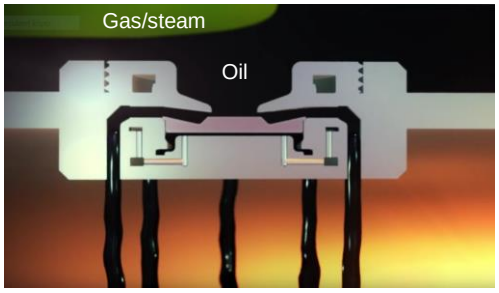

(b)

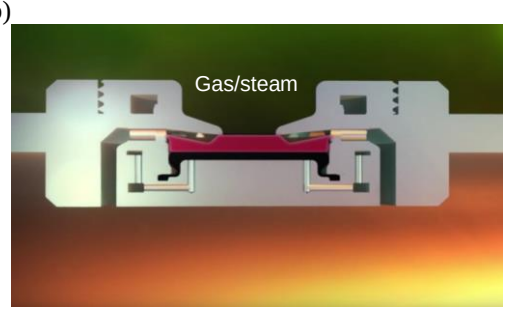

Figure 4: AICV in open (a) and closed (b) position (Aakre et al., 2018).

The mathematical model describing the performance of the AICV can be described as:

$$\Delta P_{Tot} = \left(\frac{\rho_{mix}^2}{\rho_{cal}}\right) \cdot \left(\frac{\mu_{cal}}{\mu_{mix}}\right)^{y} \cdot a_{AICD} \cdot Q^{x} \qquad (2)$$

where ΔP_{Tot} is the differential pressure across the AICV, ρ_{cal} and μ_{cal} are the calibration fluid density and viscosity, and ρ_{mix} and μ_{mix} are the mixture fluid density and viscosity respectively. The parameter a_{AICD} is a valve characteristic given by the ICD strength, Q is the volumetric mixture flow rate, and x and y are constants (Taghavi & Ghaderi, 2021). It can be interpreted from equation (2) that the pressure drop through the AICV is much more viscosity dependent than density dependent. The concept and principle of AICV is described in detail in earlier scientific works (Aakre, 2017; Aakre et al., 2013).

3. Reservoir and Wellbore Model in CMG

CMG 2022.10 general release by Computer Modeling Group Ltd. is used for accomplishing the objectives of this paper. The software has thirteen modules, each for a specific purpose. Reservoir grid modeling, well modeling, creation of fluid models, rock fluid properties and importing previously created well, reservoir and component properties are done using the Builder module of the CMG software. CMG STARS is responsible for conducting thermal and steam additive simulations. Thermal oil recovery methods such as SAGD, can be simulated with the help of STARS.

3.1. Reservoir construction in CMG Builder

A cuboid shaped reservoir has been considered where gravitational force is acting along the k-direction (vertical). The reservoir grid building constraints have been shown in Table 1.

Table 1:The dimensions of the drainage area.

Direction	No. of Blocks	Block size distributions (No. of blocks*block length) [m]
I (x)	30	30*50
J (y)	15	2*20, 10, 8, 5, 4, 3, 1, 3, 4, 5, 8, 10, 2*20
K (z)	20	11*3.5, 1, 2*3, 1, 3*3, 2*5

The areas marked in blue in Figure 5 represent the location of the injector and producer wells. All the cells within the blue area are very small in dimensions.

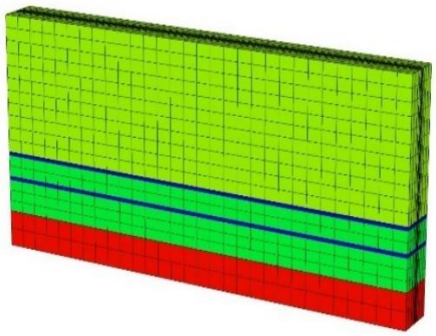

Figure 5: Reservoir 3D view

The details regarding the reservoir characteristics and parameters for initialization are presented in Table 2.

Table 2: Reservoir Characteristics initialization details.

Property	Value
Porosity	30 %
Rock wettability	Water wet
Reservoir top depth	400 m
Initial pressure at top of the reservoir	1500 kPa
Initial temperature	12°C
Initial water saturation	0.10
Reference depth	430 m
Water-oil contact depth	455.5 m
Oil mole fraction (dead oil)	0.80
Oil mole fraction (solution gas)	0.20

3.1.1. Reservoir rock and fluid properties

The reservoir rock and fluid thermal properties are given in Table 3.

Table 3: Reservoir rock and fluid thermal properties.

Property	Value
Formation compressibility	2.90×10^{-6} 1/kPa
Rock volumetric heat capacity	2.35×10^{6} J/(m^3·C)
Rock thermal conductivity	6.60×10^{5} J/(m·day.C)
Oil thermal conductivity	1.25×10^{4} J/(m.day.C)
Water thermal conductivity	5.35×10^{4} J/(m.day.C)
Gas thermal conductivity	3.20×10^{3} J/(m.day.C)
Over/Under-burden volumetric heat capacity	2.35×10^{6} J/ (m^3.C)
Over/Under-burden thermal conductivity	1.496×10^{5} J/(m.day.C)

The viscosity changes of bitumen as a function of temperature is taken from the experimental work of (Ghahfarokhi et al., 2012) and is shown in Figure 6. The oil viscosity at standard pressure decreases radically with the increase in temperature.

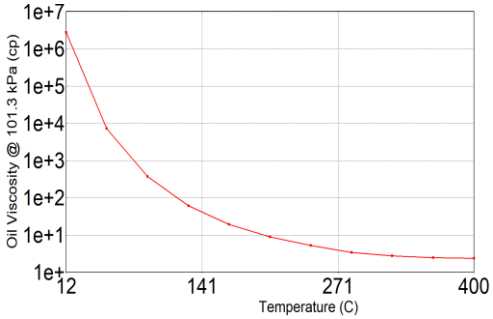

Figure 6:Viscosity of Athabasca bitumen sample versus temperature.

Generally, it is challenging to obtain information about relative permeability for different fields. Data for relative permeabilities are set manually in table form in CMG Builder. Two-phase relative permeabilities for liquid-gas and water-oil are shown in Figure 7 and Figure 8 respectively. The datasets have been calculated based on the Stone II model.

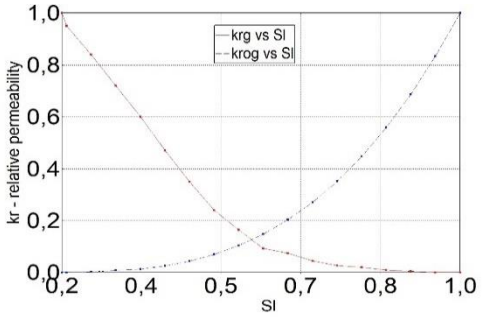

Figure 7: Liquid - gas relative permeability curves.

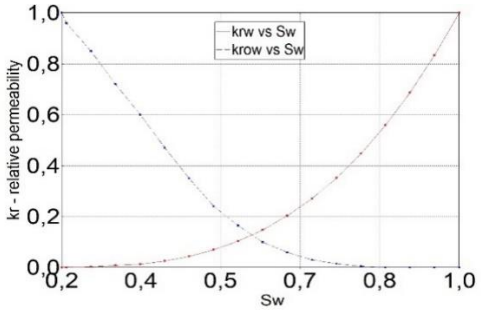

Figure 8: Water-oil relative permeability curves.

Sl is the liquid saturation, Kr is the endpoint relative permeability, krg is the relative permeability to gas at Sl, krog is the relative permeability to oil in the presence of gas at liquid saturation Sl = 1-Sg. In addition, Sw is the water saturation, krw is the relative permeability to water at Sw and krow is the Relative permeability to oil at Sw.

3.2. Well modelling in Builder

The simulation time has been set to 10 years for the SAGD operation and these 10 years have been divided into two phases. The first phase, also known as the circulation period, starts from 1st of January 2023 and continue for six months until 1st of July 2023. The SAGD period starts from 1st of July 2023 and continue until 1st of January 2033. Each well is 1201 meters long horizontally. Eight wells have been defined for accomplishing the whole SAGD process. Their names and period and mode of operation are shown in Figure 9. The FlexWell (FW) model is developed by CMG and is used to model the fluid flow in the wellbore and between the wellbore and the reservoir. FW is an advanced discretized mechanistic wellbore model which models the complex well completions (Mohd Ismail et al., 2021). The injector FWs are placed 6 meters above the producer FWs maintaining the optimum vertical distance. Figure 10 and Figure 11present the wells trajectories during the circulation phase and the SAGD phase respectively.

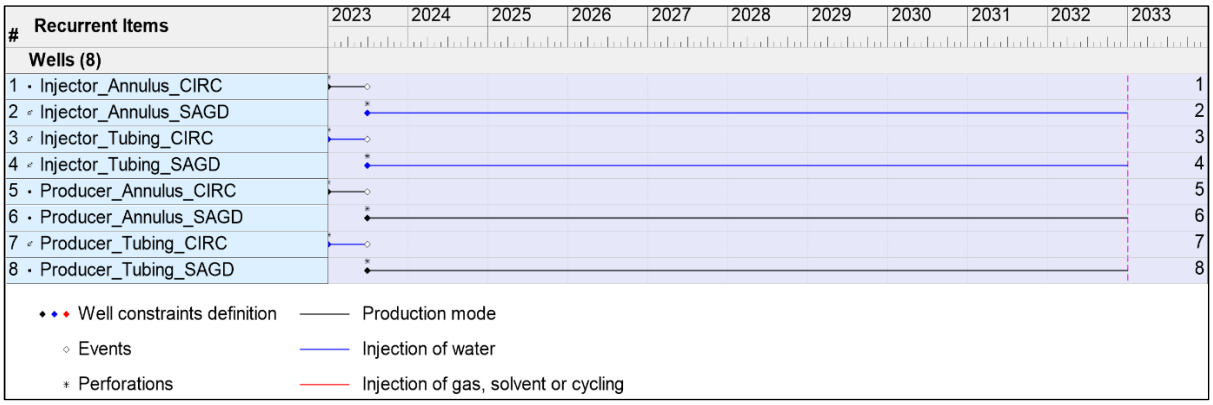

Figure 9: Timeline view of well operation data.

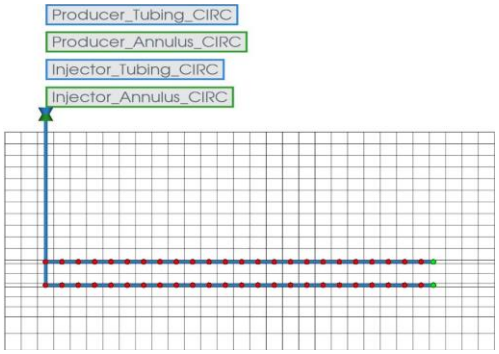

Figure 10: Well trajectories during circulation phase.

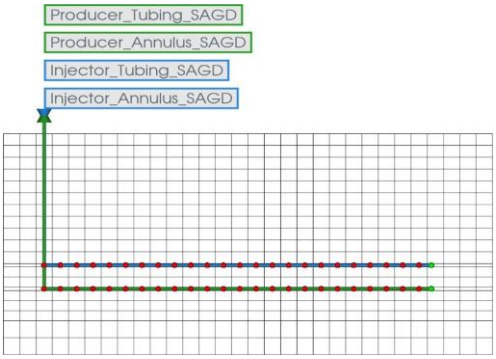

Figure 11:Well trajectories during SAGD phase.

The wells have been modeled this way in order to maintain similarity with the real-world conditions as the wells working during the circulation stage are completely turned off as the SAGD stage starts, rendering them nonexistent by CMG. Essentially, the wells present during the circulation stage are neither active nor present during the SAGD stage.

The well constraints for circulation and SAGD phases are listed in Table 4 and Table 5.

Table 4 : Circulation period well constraints.

FWs	Name	Function	Constraints
Injector FW_ CIRC	Injector_ Annulus _CIRC	Producer	MIN BHP 3500 kPa
			MAX STL 150 m^3/day
	Injector_ Tubing _CIRC	Injector	MAX BHP 4000 kPa
			MAX STW 100 m^3/day
			Injection temperature 250°C
			Steam quality 0.9
Producer FW_ CIRC	Producer_ Annulus _CIRC	Producer	MIN BHP 3500 kPa
			MAX STL 150 m^3/day
	Producer_ Tubing_ CIRC	Injector	MAX BHP 4000 kPa
			MAX STW 100 m^3/day
			Injection temperature 250°C
			Steam quality 0.9

Table 5: SAGD period well constraints.

FWs	Name	Function	Constraints
Injector FW_ SAGD	Injector_ Annulus_ SAGD	Injector	MAX BHP 4000 kPa
			MAX STW 500 m^3/day
			Injection temperature 250°C
			Steam quality 0.9
	Injector_ Tubing_ SAGD	Injector	MAX BHP 4500 kPa
			MAX STW 500 m^3/day
			Injection temperature 250°C
			Steam quality 0.9
Producer FW_ SAGD	Producer_ Annulus_ SAGD	Producer	MIN BHP 2000 kPa
			MAX STL 1500 m^3/day
	Producer_ Tubing_ SAGD	Producer	MIN BHP 2000 kPa
			MAX STL 1500 m^3/day

BHP is bottom hole pressure, STW is the surface water rate, and STL is the surface liquid rate.
The dimensions of the annulus and tubing are listed in Table 6.

Table 6: Diameters of annulus and tubing.

Parameter	Size
Tubing wall inner diameter	0.104 m
Tubing wall outer diameter	0.114 m
Annulus wall inner diameter	0.166 m
Annulus wall outer diameter	0.177 m

4. Results and Discussions

The main well of interest for this study is the Producer_Annulus_SAGD, the annulus of Producer FW_SAGD. Depending on the case definitions, Producer_Annulus_SAGD annulus will either have only perforations or be equipped with ICDs or AICVs for comparing oil recovery. The rest of the wells will operate with well perforations.

4.1 Simulation cases

Six cases have been established for simulation purposes. The simulation cases are well perforations (without any inflow controllers), well completed with 4 ICDs in each 50 meters of the horizontal length, and well completed with 4 AICVs in each 50 meters of the horizontal length in both homogenous and heterogeneous reservoir. The horizontal permeability of the homogeneous reservoir is 1800 mD in all blocks. The permeability distribution of the heterogeneous reservoir is illustrated in Figure 12.

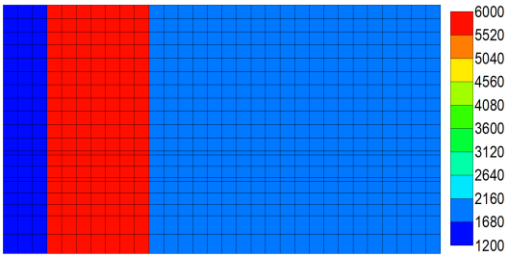

Figure 12: Permeability distribution of heterogeneous reservoir (I-K plane view).

4.2 Simulation results in the homogenous reservoir

During the circulation period, steam is injected from both wells. This is to establish thermal communication between the injector and producer and warm up the reservoir. Figure 13 shows the temperature distribution at the end of the circulation period which is between 70-100 ºC.

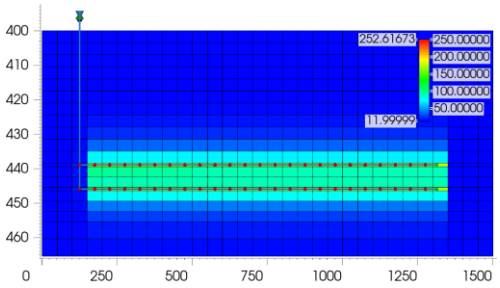

Figure 13: Temperature distribution at the end of the circulation period (I-K plane view).

In order to study the performance of ICD and AICV, the accumulated oil, gas (steam), and water for the AICV and ICD completion cases are compared to the case without any inflow controllers (perforations), see Figure 14. Under homogeneous conditions, the perforation case (red line) falls behind the case with ICDs (dashed green line) and the case with AICVs (solid green line), having the lowest cumulative oil production for the highest cumulative gas and water production. Based on cumulative oil and gas production, the AICV case outperforms the ICD case having higher oil production and lower gas production as shown in Figure 14.

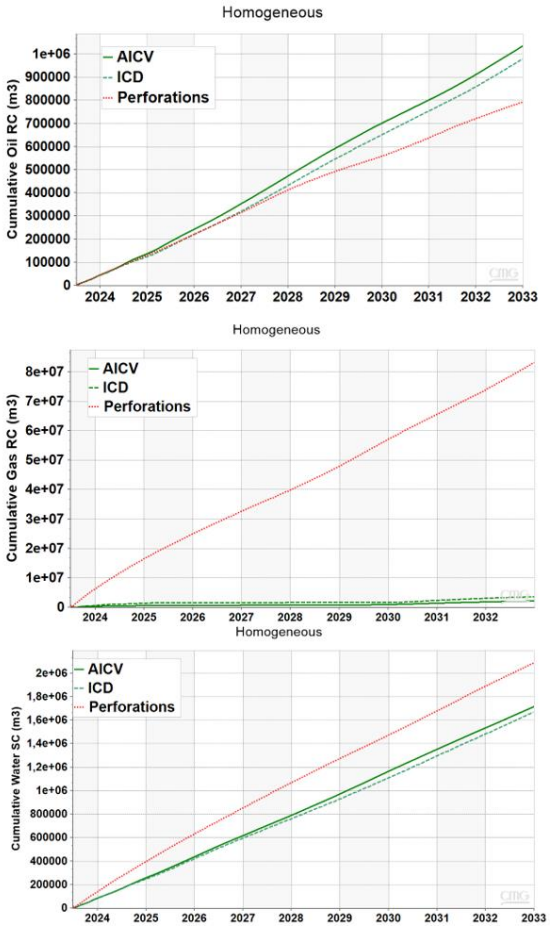

Figure 14 : Cumulative oil, gas, and water production for perforations, ICDs and AICVs in a homogenous reservoir.

Understanding the formation of steam chambers and temperature distribution across the reservoir is an important aspect of the SAGD process. Steam chamber patterns and temperature distributions can also be used to indicate in which case there is more steam production. From Figure 15, it can be interpreted that due to the high steam production for well perforations, the steam chamber has not reached the maximum temperature after 5 years, see Figure 15a. Looking closely along J-K plane shown in Figure 15c, illustrates that the AICV case has a slightly better steam distribution than the ICD case shown in Figure 15b. This means that AICVs are better in handling steam breakthroughs than ICDs and well perforations.

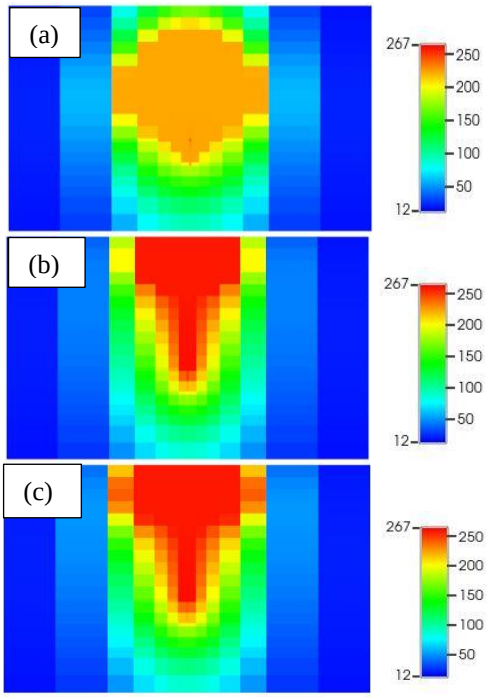

Figure 15 : Steam chamber conformance along J-K plane for (a) perforations, (b) ICDs, and (c) AICVs.

4.3 Simulation results in the heterogeneous reservoir

Figure 16 illustrates that the AICV case outperforms the ICD and perforations cases in terms of having the highest cumulative oil production and the least cumulative gas and water production. The perforation case (red line) falls behind the case with ICDs (dashed green line) and the case with AICVs (solid green line), having the lowest cumulative oil production for the highest cumulative gas and water production.

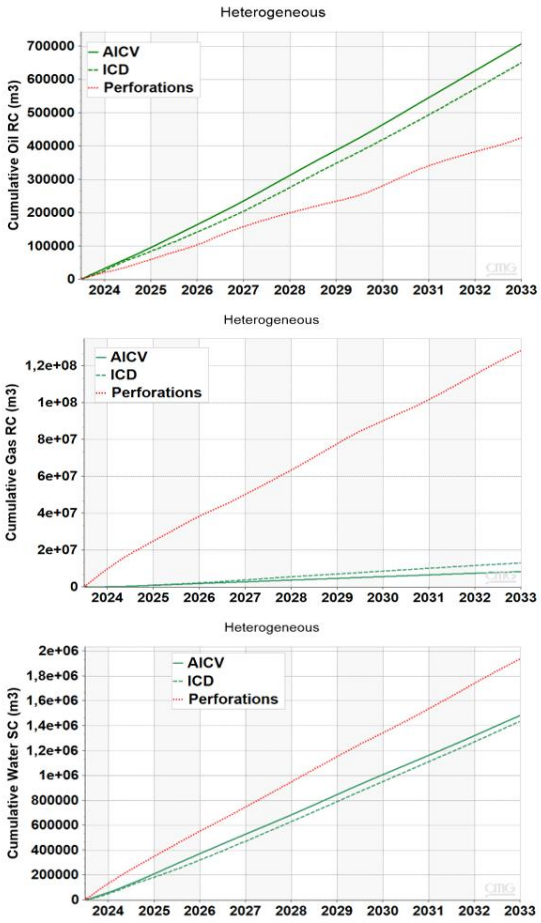

Figure 16: Cumulative oil, gas, and water production for perforations, ICDs and AICVs in a heterogeneous reservoir.

This directly indicates that AICVs are better in recovery of heavy oil and in resisting gas (steam), and water production compared to ICDs and well perforations when subjected to heterogeneous reservoir conditions, similar to that under homogenous conditions.

As illustrated by Figure 17a, the perforation case does not have a uniform steam chamber conformance and temperature distribution after 5 years. Both ICDs and AICVs show uniform steam chamber conformance which has reached maximum temperature after 5 years as shown in Figure 17b and Figure 17c respectively.

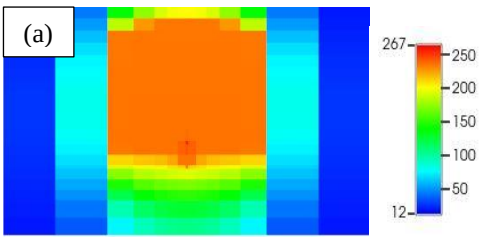

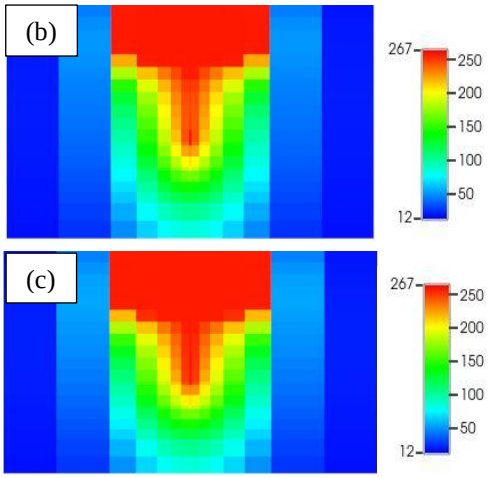

Figure 17 : Steam chamber conformance along J-K plane for (a) perforations, (b) ICDs, and (c) AICVs.

Analysis of Figure 15 and Figure 17 demonstrates that ICDs and AICVs are much better in maintaining proper temperature distribution across the reservoir and in formation of uniform steam chamber compared to well perforations. When looked from the J-K plane, it is seen that steam chamber conformations with well perforations in both homogeneous and heterogeneous cases do not reach the maximum steam injection temperature. On the contrary, ICDs and AICVs evidently show better steam chamber conformance by reaching maximum injection temperatures.

5. Conclusions

The impact of AICV on enhanced oil recovery in a SAGD production well is investigated. This is achieved by developing a wellbore-reservoir model in the CMG STARS simulator.

Both homogenous and heterogeneous reservoirs are studied by considering ICD and AICV completion and well perforations only.

The simulation results demonstrate that utilizing AICV in a SAGD reservoir will lead to higher oil production, less steam production, and a more uniform temperature distribution, and steam chamber conformance.
Reduction in steam production, will improve the overall SAGD operation performance. This will also result in more cost-effective oil production, as less steam is needed to be generated for production of each barrel of oil. Less steam generation means less energy demand, that consequently contribute to lower the intensity of greenhouse gas emissions.

References

Aakre, H. (2017). *The impact of autonomous inflow control valve on increased oil production and recovery* University College of Southeast Norway, Faculty of Technology, Natural Sciences and Maritime Sciences]. Kongsberg.

Aakre, H., Halvorsen, B., Werswick, B., & Mathiesen, V. (2013). Smart Well With Autonomous Inflow Control Valve Technology. SPE Middle East Oil and Gas Show and Conference, https://doi.org/10.2118/164348-MS

Aakre, H., Mathiesen, V., & Moldestad, B. (2018). Performance of CO2 flooding in a heterogeneous oil reservoir using autonomous inflow control. *Journal of Petroleum Science and Engineering*, *167*, 654-663. https://doi.org/https://doi.org/10.1016/j.petrol.2018.04.008

Birchenko, V. M., Muradov, K. M., & Davies, D. R. (2010). Reduction of the horizontal well's heel–toe effect with inflow control devices. *Journal of Petroleum Science and Engineering*, *75*(1), 244-250. https://doi.org/https://doi.org/10.1016/j.petrol.2010.11.013

Ellis, T., Erkal, A., Goh, G., Jokela, T., Kvernstuen, S., Leung, E., Moen, T., Porturas, F., Skillingstad, T., Vorkinn, P. B., & Raffn, A. G. (2009). Inflow control devices - Raising profiles. *21*, 30-37. https://doi.org/https://studylib.net/doc/18336329/inflow-control-devices%E2%80%94raising-profiles

Ghahfarokhi, A. J., Jelmert, T. A., Kleppe, J., Ashrafi, M., Souraki, Y., & Torsaeter, O. (2012). Investigation of the Applicability of Thermal Well Test Analysis in Steam Injection Wells for Athabasca Heavy Oil. SPE Europec/EAGE Annual Conference, https://doi.org/10.2118/154182-MS

Lauritzen, J. E., & Martiniussen, I. B. (2011). Single and Multi-phase Flow Loop Testing Results for Industry Standard Inflow Control Devices. SPE Offshore Europe Oil and Gas Conference and Exhibition, https://doi.org/10.2118/146347-MS

Mohd Ismail, I., Mathiesen, V., Abraham, A., Ranjbar, E., Zarei, F., & Walter, J. (2021). An Innovative Modelling Approach in Characterization of Autonomous Inflow Control Valve Performance to Maximizing Oil Recovery in Heavy Oil-SAGD Application. SPE Thermal Well Integrity and Design Symposium, https://doi.org/10.2118/203859-MS

Shen, C. (2013). Chapter 17 - SAGD for Heavy Oil Recovery. In J. J. Sheng (Ed.), *Enhanced Oil Recovery Field Case Studies* (pp. 413-445). Gulf Professional Publishing. https://doi.org/https://doi.org/10.1016/B978-0-12-386545-8.00017-8

staff, J. (2016, 2016). *Temporarily shutting in oilsands SAGD wells might not be as harmful as you think*. Retrieved February from https://www.jwnenergy.com/article/2016/5/26/temporarily-shutting-oilsands-sagd-wells-might-not/

Taghavi , S., & Ghaderi, A. (2021). On Uncertainty Analysis of the Rate Controlled Production (RCP) Model. First SIMS EUROSIM Conference on Modelling and Simulation, Finland. https://doi.org/10.3384/ecp21185271

Taghavi, S., Aakre, H., & Moldestad, B. M. E. (2022). Performance Analysis of Autonomous Inflow Control Valve in a SAGD Late Life Process with Non-Condensable Gases. SPE Canadian Energy Technology Conference, https://doi.org/10.2118/208915-MS

Xu, Z.-X., Li, S.-Y., Li, B.-F., Chen, D.-Q., Liu, Z.-Y., & Li, Z.-M. (2020). A review of development methods and EOR technologies for carbonate reservoirs. *Petroleum Science*, *17*(4), 990-1013. https://doi.org/10.1007/s12182-020-00467-5

Paper 7

Performance Analysis of Autonomous Inflow Control Valve in a Heterogenous Reservoir Using CO_2 Enhanced Oil Recovery

SPE-215153-MS

This paper was prepared for presentation at the 2023 SPE Annual Technical Conference and Exhibition held in San Antonio, Texas, USA, 16-18 October 2023. Society of Petroleum Engineers

Paper presented by Soheila Taghavi

Authors: Soheila Taghavi, Seyed Amin Tahami, Haavard Aakre, Nora C.I. Furuvik, and Britt M.E. Moldestad

SPE-215153-MS

Performance Analysis of Autonomous Inflow Control Valve in a Heterogenous Reservoir Using CO_2 Enhanced Oil Recovery

Soheila Taghavi, Department of Process, Energy and Environmental Technology, University of South-Eastern Norway, Porsgrunn, Norway / InflowControl AS, Porsgrunn, Norway; Seyed Amin Tahami, Department of Process, Energy and Environmental Technology, University of South-Eastern Norway, Porsgrunn, Norway; Haavard Aakre, InflowControl AS, Porsgrunn, Norway; Nora C.I. Furuvik and Britt M.E. Moldestad, Department of Process, Energy and Environmental Technology, University of South-Eastern Norway, Porsgrunn, Norway

 DOI 10.2118/215153-MS

This paper was prepared for presentation at the 2023 SPE Annual Technical Conference and Exhibition held in San Antonio, Texas, USA, 16 - 18 October 2023.

Abstract

CO_2 flooding is a proven method to mobilize the immobile oil in the reservoirs for enhanced oil recovery (EOR). Using CO_2 for EOR has been commercially used for several decades in onshore and offshore oil fields in North America, Canada, and Brazil. The injection of CO_2 will both improve oil recovery and contribute significantly to reduction of greenhouse gas emissions. Breakthrough and direct reproduction of CO_2, and production of corrosive carbonated water are among the challenges with CO_2 EOR projects. Breakthrough of CO_2 leads to poor distribution of CO_2 in the reservoir and low CO_2 storage. Carbonated water production results in corrosion of process equipment on the platform. Autonomous inflow control valve (AICV) is capable of autonomously restricting the reproduction of CO_2 from the zones with CO_2 breakthrough, and at the same time produce oil from the other zones with high oil saturation. In addition, AICV can reduce the production of carbonated water.

The objective of this paper is to investigate the impact of AICV on oil production in a heterogeneous reservoir where CO_2 is injected for EOR. The AICV performance is simulated with a dynamic reservoir simulator in a CO_2 EOR oil reservoir. AICV restricts the inflow of unwanted fluids such as pure water, gas, carbonated water, and pure CO_2. To achieve the objective, experiments and simulations are conducted. Experiments are carried out with realistic reservoir fluids to generate single phase flow performance curves for AICV and for an orifice type inflow control device (ICD). Simulations are performed using CMG STARS, which is a multi-phase, multi-component reservoir simulator. The performance of AICV is evaluated and compared with perforated casing completion. The experimental results confirm the significant benefit of AICV regarding water and CO_2 reduction compared to ICD. Under the same conditions and at a given differential pressure, AICV compared to ICD, reduces the water and CO_2 volume flow rate by approximately 58% and 82%, respectively. Experimental AICV performance curves are used to generate the flow control device (FCD) tables in CMG STARS.

The FCD tables are used to simulate the AICV behavior. The simulation results indicate that AICV reduces the water cut significantly. The cumulative water production is reduced by approximately 25% by using AICVs compared to the perforated casing completion. Indeed, reduction in carbonated water production will minimize the recirculation of CO_2. Also, reduction in production of carbonated water will mitigate the problem related to the corrosion of the producing wells and process equipment on the platform. In addition, simulation results show that the AICV completion delivers the highest cumulative oil production after five years of production. From the environmental aspects, utilizing AICV in CO_2 EOR projects will contribute significantly to reduction of greenhouse gas emissions. A better distribution of CO_2 in the reservoir contributes to a larger storage capacity and thereby more CO_2 storage.

Introduction

Power production and other use of fossil energy is the largest source of greenhouse gas emissions leading to global warming (Halland et al., 2012). Carbon capture utilization and storage (CCUS) offers a potential solution to mitigate the effects of anthropogenic CO_2 (Safi et al., 2016). Applying CCUS approach to reduce the direct CO_2 emissions from stationary sources into the atmosphere, is known as a lucrative financially approach (Safi et al., 2016). In this approach, the captured CO_2 can be injected into the oil fields for enhanced oil recovery (EOR). CO_2 for EOR has been commercially used for several decades in onshore and offshore oil fields in North America, Canada, and Brazil. The Norwegian petroleum directorate (NPD) has conducted several screening studies to evaluate the possibility and potential of using the captured CO_2 for EOR at the Norwegian continental shelf (NCS) (Halland et al., 2014; Halland et al., 2019). According to NPD, the average oil recovery rate for the Norwegian offshore oil fields is approximately 47% urging the industry to find new methods for improved oil recovery (IOR) (Petroleum, 2022). Fig. 1 shows that in the 25 largest oil fields on the NCS, about half of the oil on average is remaining in the reservoir after shutting down the wells. About 50% of this oil is categorized as immobile oil (Halland et al., 2019). To the authors knowledge, neither CO_2 EOR nor any other EOR methods to extract the immobile oil have been implemented on a full field scale at NCS.

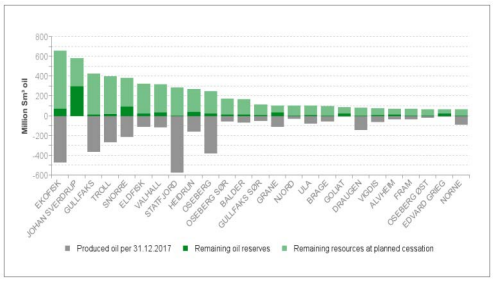

Figure. 1—Distribution of oil reserves and resources for the largest oil fields in Norway (Halland et al., 2019).

CO_2 is often injected in carbonate reservoirs which usually have low permeable sands (Aakre et al., 2018). However, carbonate reservoirs, may contain high permeable zones and fractures that are prone to breakthrough and direct reproduction of CO_2 to the well. To improve the sweep efficiency of CO_2 flooding, applying the alternating injection of CO_2 and water is a common practice (WAG) (Halland et al., 2012). Water alternating CO_2 injection often experience significant problems and challenges with short circuiting of CO_2 and water between the injectors and producers (Aakre et al., 2018).This is illustrated in Fig. 2.

Consequently, the CO_2 is reproduced without contributing to enhanced oil recovery. Also, in miscible CO_2 EOR process, if the reservoir pressure drops below the minimum miscible pressure (MMP) of CO_2 in oil, CO_2 will break through the production well (Zhang et al., 2015). Direct reproduction of CO_2 to the well

also results in poor distribution of CO_2 in the reservoir. Therefore, the challenge is to stop or restrict the reproduction of CO_2 (Aakre et al., 2018). Avoiding reproduction of CO_2 is especially important if high-cost anthropogenic CO_2 is used for EOR and storage operations (Gozalpour et al., 2005). In addition, insufficient supplies of available CO_2 that needs to be injected for EOR purpose is a major challenge of CCUS.

Another CO_2 EOR challenge is that the mixture of CO_2 and water is extremely corrosive. The reaction between CO_2 and formation water, forming a weak acidic solution, is as follows (Oomole & Osoba, 1983):

$$H_2O + CO_2 + CaCO_3 \leftrightarrow Ca(HCO_3)_2 \quad (1)$$

In case of breakthrough, this corrosive mixture can cause problems in the producing wells and in the process equipment on the platform (Halland et al., 2012). This is a key factor economically for offshore developments.

Autonomous inflow control valve (AICV) is capable of autonomously restricting the reproduction of CO_2 from the zones with CO_2 breakthrough, and at the same time produce oil from the other zones (Aakre et al., 2018). Choking back CO_2 gas or super critical CO_2 by AICV may give a better distribution of CO_2 in a larger area of the reservoir. This leads to a broader contact between CO_2 and the residual oil in the reservoir, resulting in increased EOR. Choking back CO_2 by AICV also may result in increased drawdown in the zones with high oil saturation, and thereby increased oil production and recovery. In addition, AICV can reduce the production of carbonated water. This will mitigate the problem related to the corrosion of the producing wells and process equipment on the platform.

The main objective of this work is to investigate the impact of AICV on oil production in a heterogeneous reservoir where CO_2 is injected for enhanced oil recovery. AICV restricts the inflow of unwanted fluids such as pure water, gas, carbonated water, and pure CO_2. The main objective is achieved by performing experiments and simulations of the AICV performance using an industrial reservoir simulator, CMG.

CO_2 EOR Mechanism and Potential

CO_2 flooding is a proven method to mobilize the immobile oil. Injection of super-critical dense CO_2 after a waterflood phase is a widespread practice. CO_2 may be injected continuously, altered with water in a WAG process, or simultaneous with water (Ettehadtavakkol et al., 2014). Fig. 3 shows a cross section of a reservoir with CO_2 WAG in which oil and CO_2 displacement is illustrated. CO_2 is injected into the oil fields and can be dissolved in water. The injection process may help to maintain the reservoir pressure above the MMP of the oil, securing a more desirable miscible flood. After injection, CO_2 encounters the trapped oil in the pores, and under miscible condition the CO_2 is mixed with oil. The volume of oil that exists in the reservoir pore spaces swells and moves towards the production well. Four primary factors that affect the oil swelling in the presence of CO_2 are API oil gravity, temperature, CO_2 concentration and pressure (Ahmadi et al., 2018). Interaction between oil and CO_2 can be immiscible and miscible or multi-contact miscible process (Gozalpour et al., 2005). CO_2 extracts the intermediate components of the oil through repeated contacts. In this process, the oil evaporates into lean gas. CO_2 and oil achieve multi-contact miscibility when CO_2 is sufficiently enriched with the intermediate components during vaporization (Council, 2021). According to (Taber et al., 1997), the favorable reservoir condition in which the injected CO_2 is miscible in the residual oil is when the oil gravity is API >22° and depth is >1200m.The best effect is achieved when CO_2 is miscible in oil in the reservoir (Halland et al., 2012).

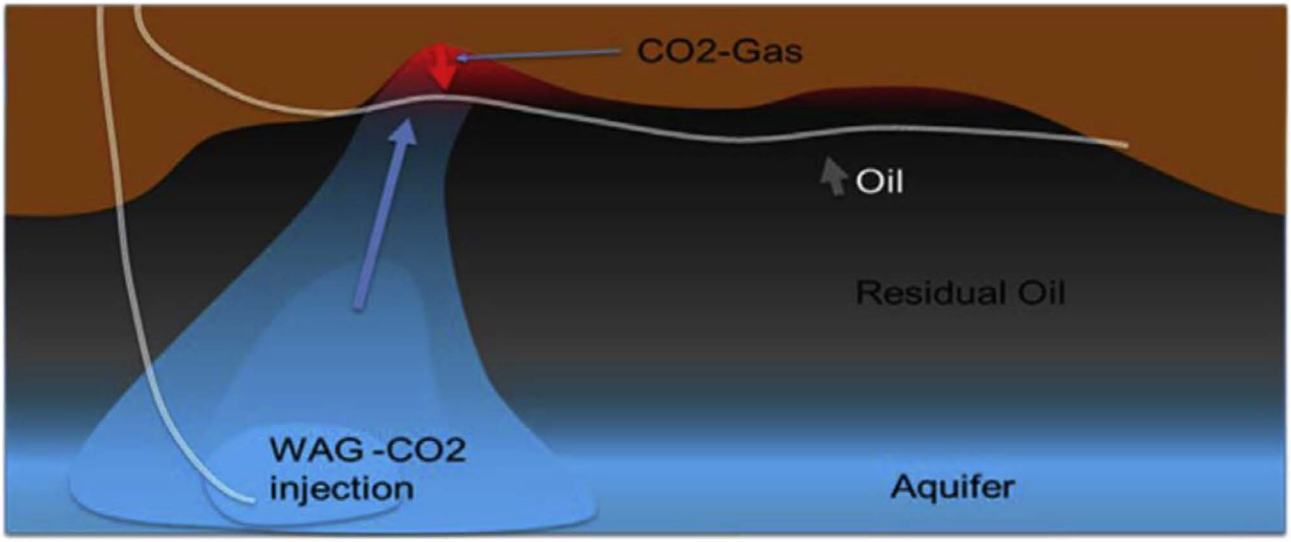

Figure. 2—Short circuiting of CO_2 and water between injector and producer in WAG CO_2 injection process (Aakre et al., 2018).

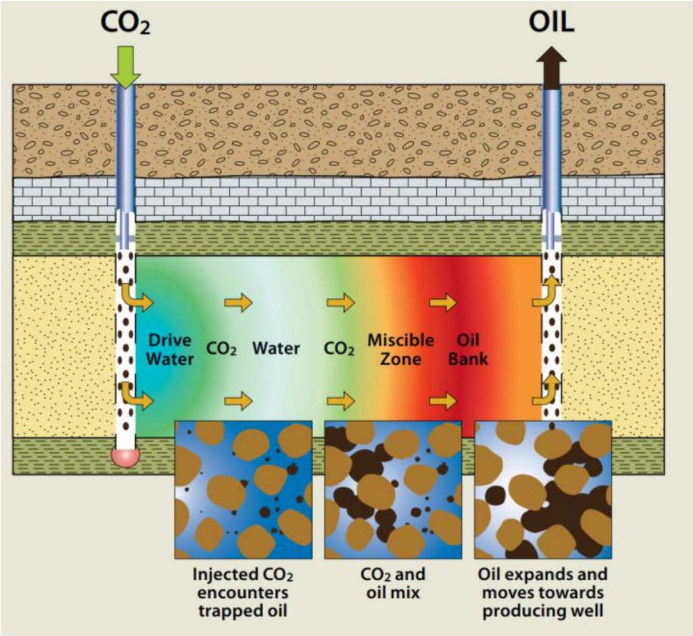

Figure. 3—Cross section of a reservoir with CO_2 WAG (Halland et al., 2012).

Residual oil zones (ROZs) are of great interest employing CO_2 EOR due to the mostly immobile nature of the oil in ROZs (West, 2014). When CO_2 is injected in miscible condition, oil in ROZs becomes mobile and this makes it possible to produce oil from both natural residual oil zones and residual oil zones from oil production (Halland et al., 2019).

At supercritical condition, CO_2 forms a phase with a density close to a liquid density, typically around 0.6-0.8 g/cm^3, and a viscosity close to a gas viscosity (Mansour et al., 2019). Dense phase CO_2, compared to the gas phase CO_2, can extract hydrocarbon components from oil easier. Dissolved CO_2 causes the oil to swell and improves the oil mobility. This may result in an additional oil recovery of 5 to 20% of the original oil in place (OOIP) (Stevens et al., 200; Halland et al., 2019). Swelling is defined as the increase in the volume of the saturated liquid phase compared to the initial reference volume (Mansour et al., 2019). Oil swelling is increased as more CO_2 dissolves into the liquid phase. The swollen oil droplets force fluids to move out of the pores, hence causing drainage effect and consequently decreases the residual oil saturation

(Aakre et al., 2018). In addition, CO_2 is soluble in water, can evaporate and extract the oil and it reduces the surface tension between oil and water (Halland et al., 2019).

Asphaltene precipitation can happen during CO_2 flooding. Precipitation and deposition of asphaltene during CO_2 flooding may reduce the porosity and permeability resulting in reduced recovery. On the other hand, the precipitation of asphaltene, reduces oil density and viscosity, making the oil more mobile. So in oil reservoirs containing asphaltene, there is a competition between positive and negative effects of asphaltene precipitation and deposition (Tahami et al., 2014).

Another effect of CO_2 on oil is observed in the relative permeability characteristics. According to (Potter, 1987; Zekri et al., 2013), CO_2 flooding will affect the reservoir wettability making the rock slightly more water-wet. When the rock becomes more water- wet, a favorable oil displacement efficiency is achieved. The endpoint relative permeabilities, kr, which are irreducible water saturation and residual oil saturation, and also the shape of the curves are changed. By this, it can be interpreted that CO_2 flooding reduces the mobility ratio, M, between water and oil. The mobility, Z, is defined as the ratio between the end point relative permeability, k_r, and dynamic viscosity, μ:

$$\lambda = \frac{k_r}{\mu} \tag{2}$$

Mobility ratio is defined as the ratio of the displacing fluid mobility, e.g., Zw, to that of the displaced fluid, e.g., Z0, and is expressed as (Ahmed, 2010) :

$$M = \frac{\lambda_w}{\lambda_o} = \frac{k_{rw}}{k_{ro}} \cdot \frac{\mu_o}{\mu_w} \tag{3}$$

The subscripts o and w refer to the oil and water phase, respectively. Making the rock more water-wet, reduces the residual oil saturation and increases the irreducible water saturation as shown in Fig. 4.This implies that the relative permeability of oil is increased. In addition, the oil viscosity is decreased, and the sum up effect results in reduction in the mobility ratio, which will increase the oil recovery efficiency (Aakre et al., 2018).

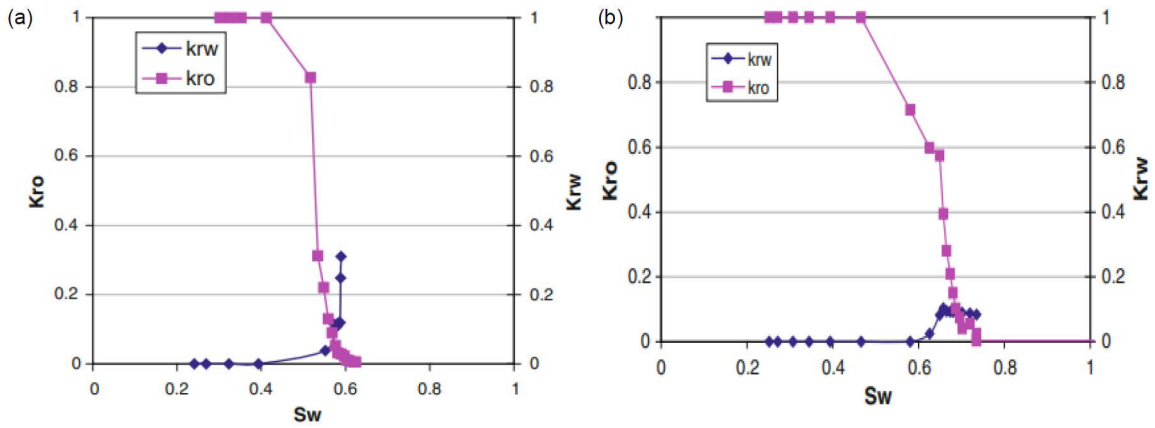

Figure. 4—Oil-water relative permeability prior to (a) and after (b) CO_2 flood (Zekri et al., 2013).

The expected EOR potential varies between vertical and horizontal miscible flooding processes. In a vertical miscible flooding, the expected EOR potential is in the range of 15-40% OOIP compared to upward water flood, while in a horizontal miscible flooding process, the expected EOR factor is 5-15% OOIP. The low EOR potential in horizontal miscible flooding may be associated with gravity override, viscous fingering and poor control of injection profiles (Gozalpour et al., 2005). A study carried out by the NPD indicates an EOR potential of 3-7% from fields of interests (Halland et al., 2012). Industry experience from onshore North America and the simulation results from the Brage field in the North Sea indicate an EOR

potential of 4-12% OOIP and 9-12% OOIP, respectively (Gozalpour et al., 2005). Also, a research carried out by the department of energy in the USA suggests that, CO_2 EOR could improve the recovery factor by as much as 3-5% from unconventional shale reservoirs (Council, 2021).

AICV Technology and Design for CO_2 EOR

The functionality of AICV is based on viscosity and density differences between reservoir fluids. AICV is a valve with a movable piston. The piston acts either upwards or downwards. If high viscous fluids like oil pass through the valve, the movable piston acts downwards keeping the valve open to produce the oil. If low viscous fluids like pure CO_2 and/or carbonated water pass through the valve, the movable piston acts upwards keeping the valve closed for those fluids. Fig. 5 shows AICV in closed and open position. Fig. 5a shows that the valve is open and is producing oil as gas is approaching the valve. Fig. 5b illustrates that the gas has reached the valve inlet, the movable piston has moved upward, and the valve is closed for gas. For ultra-light oil, AICV takes advantage of the density difference between water and oil. The functionality and principle of AICV are described in detail in earlier studies (Aakre, 2017; Aakre et al., 2014).

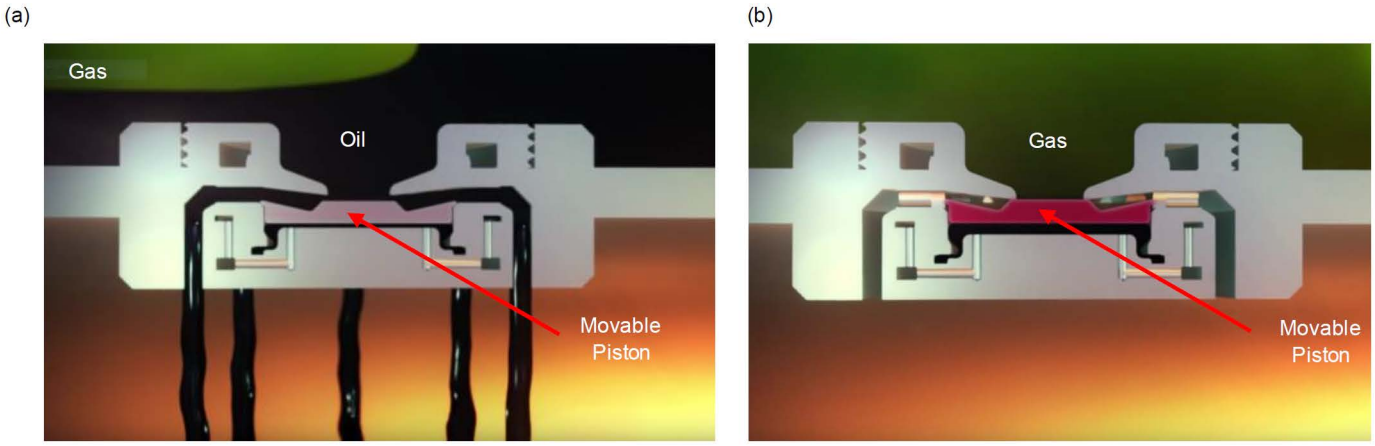

Figure. 5—AICV in open (a) and closed (b) position.

The AICV performance curves for reservoir fluids based on experimental data are presented in Fig. 6. The figure illustrates the differential pressure, Δp, over the AICV as a function of volume flow rates for oil with various viscosities, water, and supercritical CO_2. The original viscosity of the oil is 3 cp. The injected CO_2 has an effect on the oil viscosity. By increasing the CO_2 concentration up to a certain level, the viscosity of oil is reduced. The AICV performance curves clearly illustrate the viscosity dependency of the valve for different fluids. As the fluid viscosity is reduced, AICV restricts the volume flow rate of the fluid at given Δp. Even though the oil viscosity is getting as low as 0.7 cp, AICV produces almost 40% more oil than water. In this case, AICV can distinguish between ultra-light oil and water even when the viscosities are almost similar. The reason could be that AICV is responding to viscosity changes through changes in the Reynolds numbers and density differences (Killie et al., 2021). Additionally, the results confirm that AICV restricts the production of CO_2 and water under miscible injection of CO_2.

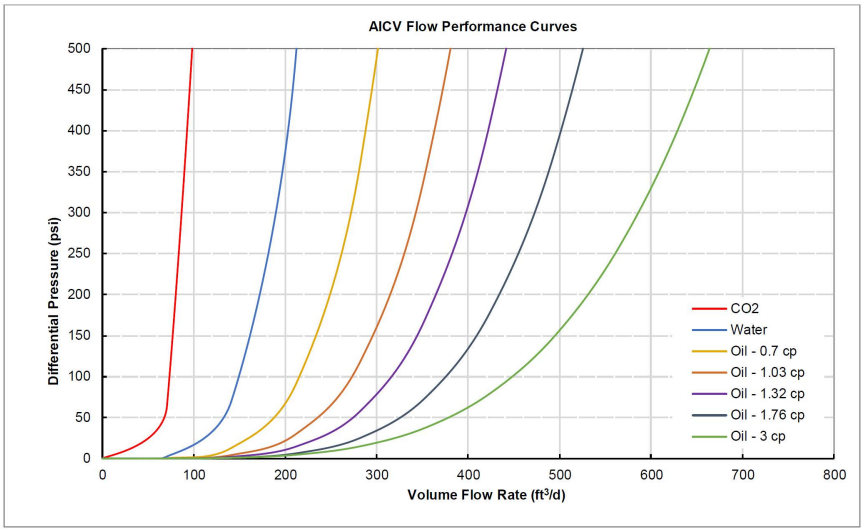

Figure. 6—Flow performance curves of the AICV for oil, water, and CO_2.

Fig. 7 compares the performance curves of AICV and an orifice type ICD for CO_2 and water. The orifice type ICD has the same strength as the AICV meaning that the pressure drop across the ICD is the same as the pressure drop across the AICV when the oil flow rate is equal to 1 m^3/h. Under the same conditions and at a given Ap, AICV compared to ICD, reduces water and CO_2 volume flow rate by approximately 58% and 82% respectively. The results indicate that the gas and water reduction by using AICV is significant. According to the experimental results, the volume flow rate of unwanted fluids like gas and water is always less than oil flow rate at a given Ap, as AICV is mainly viscosity dependent.

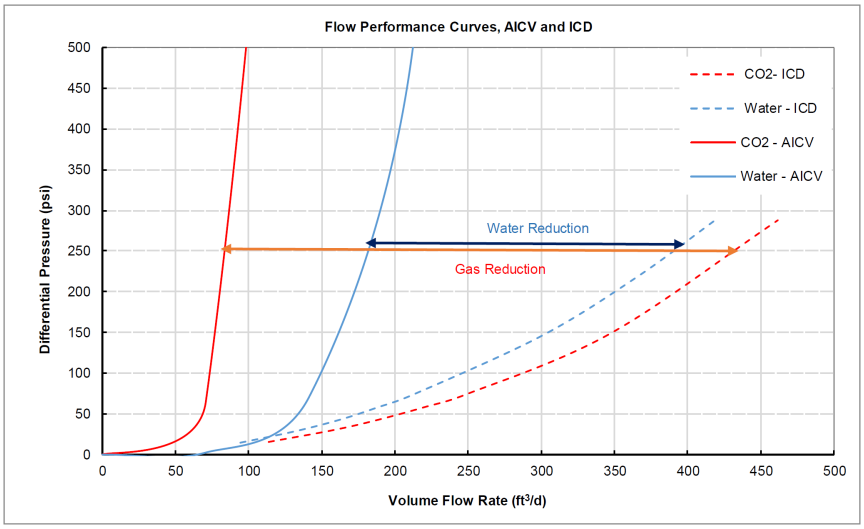

Figure. 7—Comparison of flow performance curves of the ICD and AICV.

Development of the Reservoir and Well Model in the CMG Simulator

CMG 2022.10 general release by Computer Modeling Group Ltd. is used for accomplishing the objectives of this paper. WinProp is a software in CMG suite package that applies an equation of state methodology to generate PVT data by analyzing oil and gas samples within a laboratory environment. WinProp is used for fluid characterization, matching the experimental data, and construct phase diagram. For our sample, the calculated MMP by WinProp at the reservoir temperature condition (186 °F) is 3217 psi. The phase

behavior of the reservoir fluid constructed by WinProp is shown by the pressure-temperature (P-T) diagram in Fig. 8. Also, the oil viscosity as a function of temperature and pressure is shown in Fig. 9.

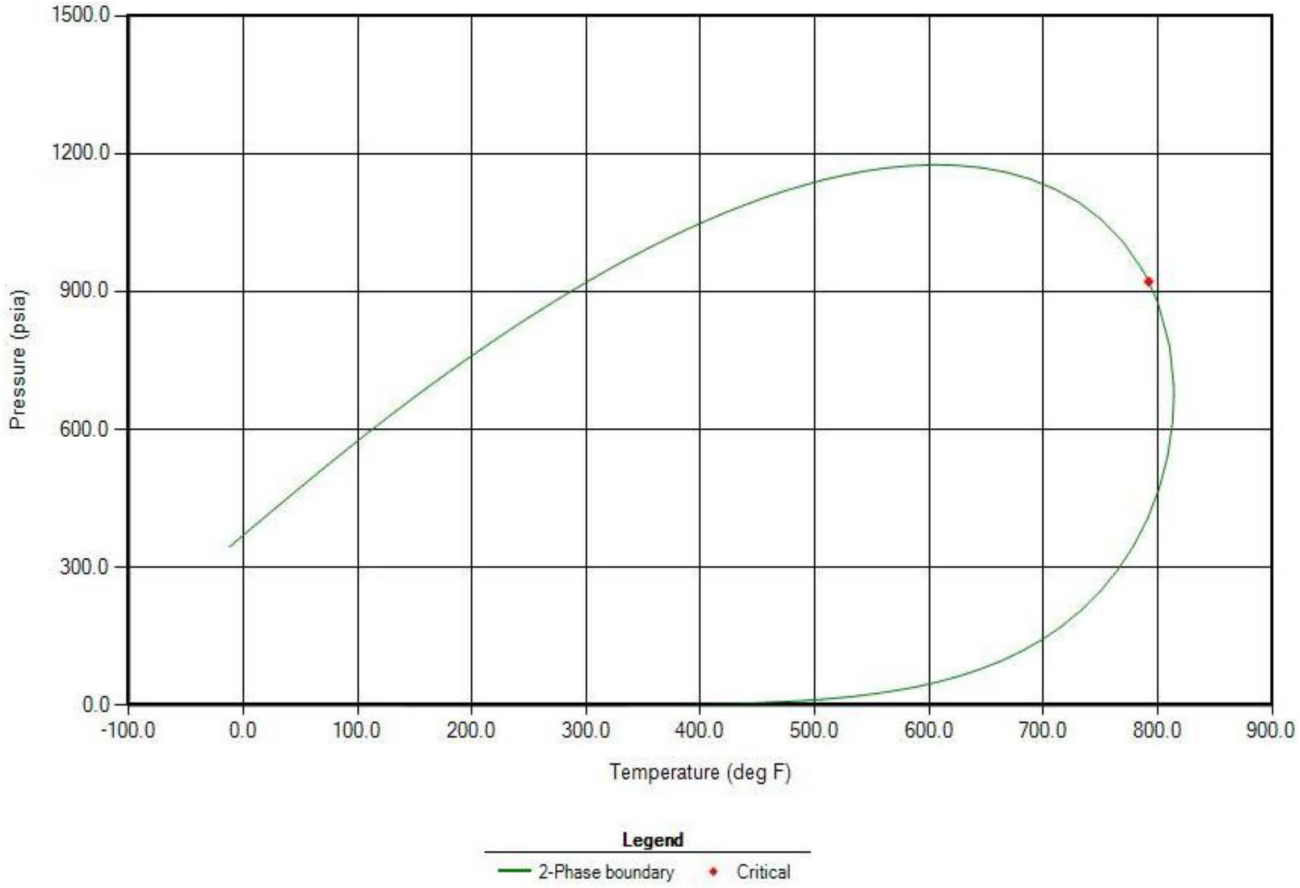

Figure. 8—P-T diagram of the reservoir fluid.

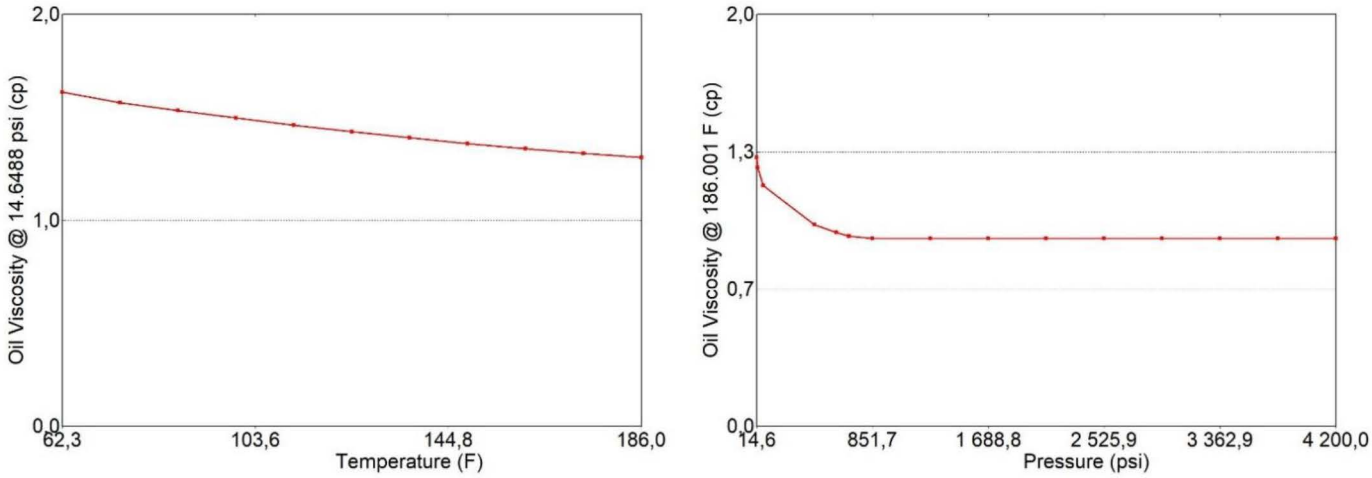

Figure. 9—Oil viscosity as a function of temperature (left) and pressure (right).

The two-phase relative permeability curves utilized in this study are shown in Fig. 10. The datasets have been calculated based on the Stone II model. Subscripts o, w, g, and l refer to the oil, water, gas, and liquid phase, respectively.

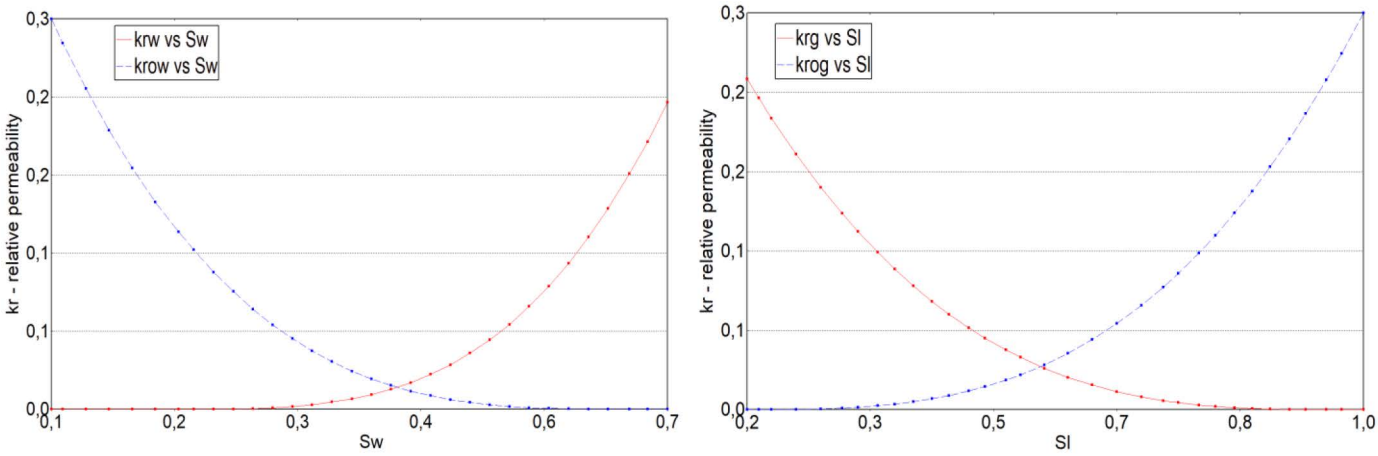

Figure. 10—Water-oil (left) and gas-liquid (right) relative permeabilities.

Fig. 11 shows the distribution of porosity and horizontal permeability in the heterogeneous reservoir. The porosity ranges from 0.23 to 0.32 and the horizontal permeability varies from 0 to 2588 mD. The top of the reservoir is at a defined depth of 5835 ft, while the bottom is at a depth of 6016 ft. Dimensions of the reservoir model are 3116 ft in both I and J directions, and 181 ft in K-direction with 25*25*15 grid blocks in I, J, and K directions. The reservoir temperature is considered constant and equal to 186 °F. To assure that the reservoir pressure is always higher than MMP, the initial reservoir pressure at the top and bottom of the reservoir are 4184 and 4248 psi, respectively. Also, CO_2 is injected by a constraint of a maximum bottomhole pressure of 5000 psi.

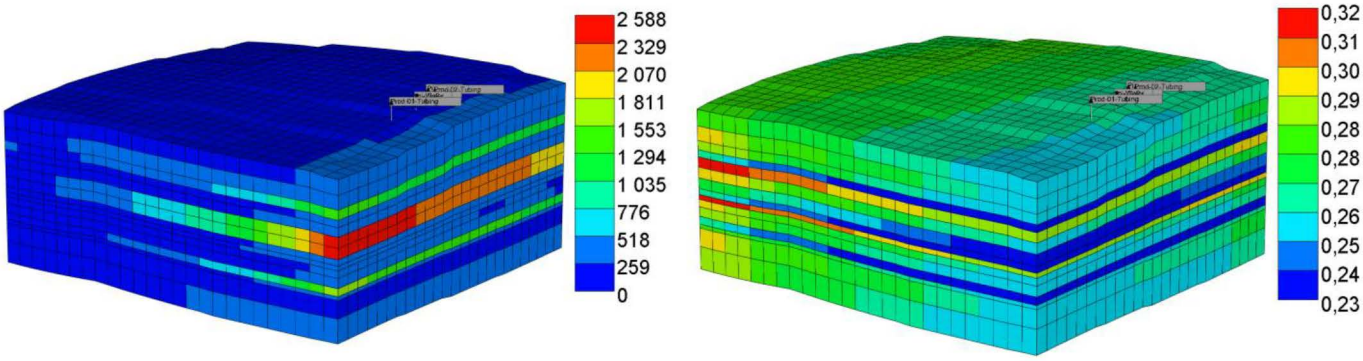

Figure. 11—Distribution of permeability (left) and porosity (right).

Two horizontal wells as producers and one horizontal well as injector are considered to develop the well model. The length of the wells is approximately 2200 ft, and they are placed in the J-direction. The injector well is placed between the two producer wells, see Fig. 12.

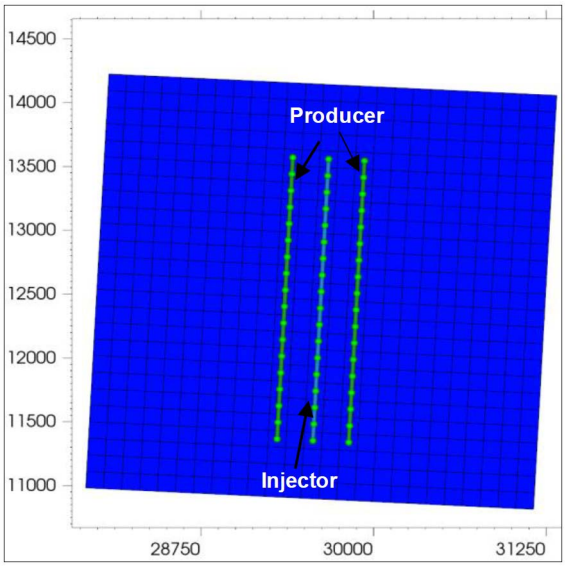

Figure. 12—The producer and injector wells.

The simulations are conducted for five years; from January 2023 to February 2028. The CO_2 WAG injection starts with water injection in three months followed by CO_2 injection in three months. This cycle is repeated in almost five years. Fig. 13 and Table 1 represent the timeline during the CO_2 WAG period, and the injector and producer wells constraints, respectively. BHP is the bottom hole pressure, STW is the surface water rate, STG is the surface gas rate, and STL is the surface liquid rate.

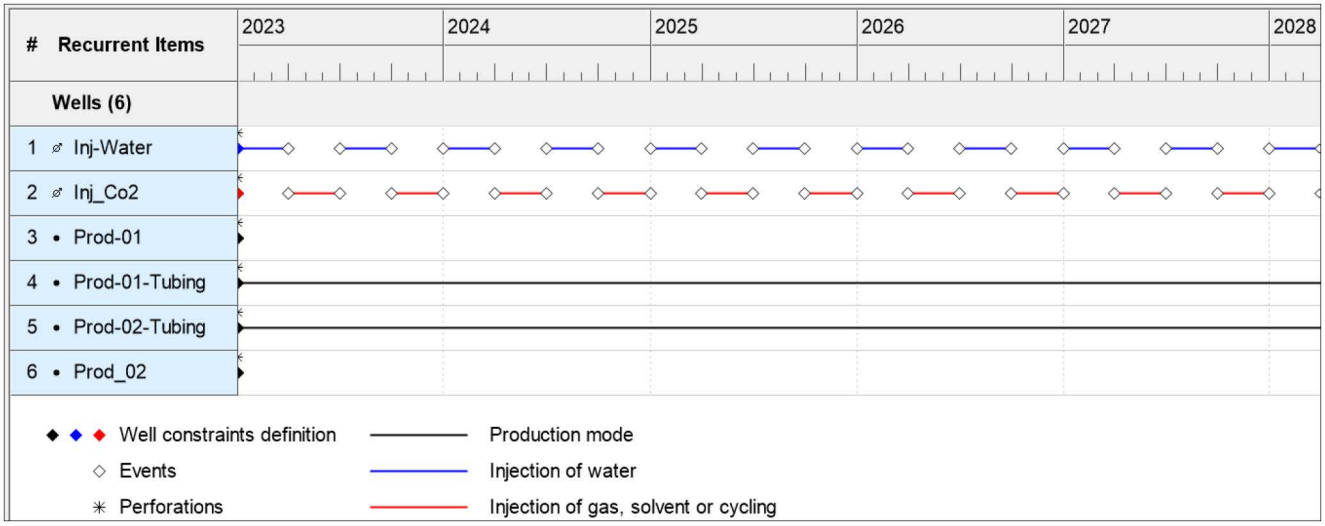

Figure. 13—Timeline view of the CO_2 WAG.

Table 1—The injector and producer wells constraints.

Wells	Function	Constraints
Injector	Water Injection	MAX BHP 5000 psi MAX STW 5000 bbl/day
	CO_2Injection	MAX BHP 5000 psi MAX STG 3000000 ft^3/day
Producer	Prod-01-Tubing	MIN BHP 500 psi MAX STL 2000 bbl/day
	Prod-02- Tubing	MIN BHP 500 psi MAX STL 2000 bbl/day

Simulation Results and Discussion

The CO_2 EOR process is modelled using CMG STARS. The AICVs are used for the producer well and the injector well is perforated casing completion. Three different cases are presented here: one case without any completion on the producer wells, one case with AICV completion on the producer wells, and one case with AICV in one producer well and without AICV in another producer well. There are in total 18 production zones in each case. The production zones are isolated by packers. The completion scenarios are presented in Table 2.

Table 2—Completion scenarios.

Case No.	Completion Scenario	Number of Production Zones
1	Two perforated casing wells	18
2	Two wells with AICV	18
3	One well with AICV and one well with perforated casing	18

AICV is designed to close for carbonated water and pure CO_2 gas or supercritical CO_2. Flow control device (FCD) tables are developed to simulate the single phase and two-phase behavior of AICV. The FCD table in CMG allows to characterize a FCD through tabulated data. This table is generated based on experimental data shown in Fig. 6. The dependent variables to generate the FCD tables are the gas mass fraction, water cut and volume flow rate. The independent variable is the pressure drop which is calculated accordingly.

Fig. 14 shows the cumulative oil and water production for case No.3. The producer wells are at the same height in the reservoir and under the same conditions. The cumulative oil production for the producer well completed with AICVs is approximately 5 % more than the producer well with perforated casing. Also, the water production with AICV completion is approximately 5 % less than the perforated case. Fig. 15 shows the water cut vs. time for the simulated cases. The water cut reaches to over 50% for the perforated case (case No.1) at the last year of the simulation time. The water cut is lowest for the AICV case (case No.2) compared to other cases. Also, the water breakthrough occurs later for the AICVs (case No.2) compared to the perforated case (No.1). This indicates that AICV both delays water breakthrough and restricts the water production. Fig. 16 illustrates the produced gas-oil ratio at standard condition vs. time for the AICV and the perforated case. As can be seen from this figure, the GOR for the two scenarios at the start of production is the same as the initial solution gas oil ratio (Rs), but as time passes, they separate from each other. At the beginning and till the end of 2027, the GOR in the perforated case is higher than in the AICV case. This is because the oil produced from the high permeable zones has more solution gas, as the injected gas moves easier in these zones, and more gas dissolves in oil. At the same time water also moves easier in these high permeable zones and causes the water cut to increase. So, in the AICV case as the water cut is increasing due to the contribution from the high permeable zones in the production, AICV operates and chocks back the production from these zones. Thus, in this period, the GOR is less for the AICV case compared to the perforated case. However, the contribution from the low permeable zones in the oil production in the AICV case increases as time passes. After the end of 2027, the contribution from the low permeable zones — that have been exposed to injected CO_2 for a longer period— dominates more in the production for the AICV case. As these layers have more dissolved gas, the GOR in the AICV case becomes higher than in the perforated case from the third quarter of 2027.

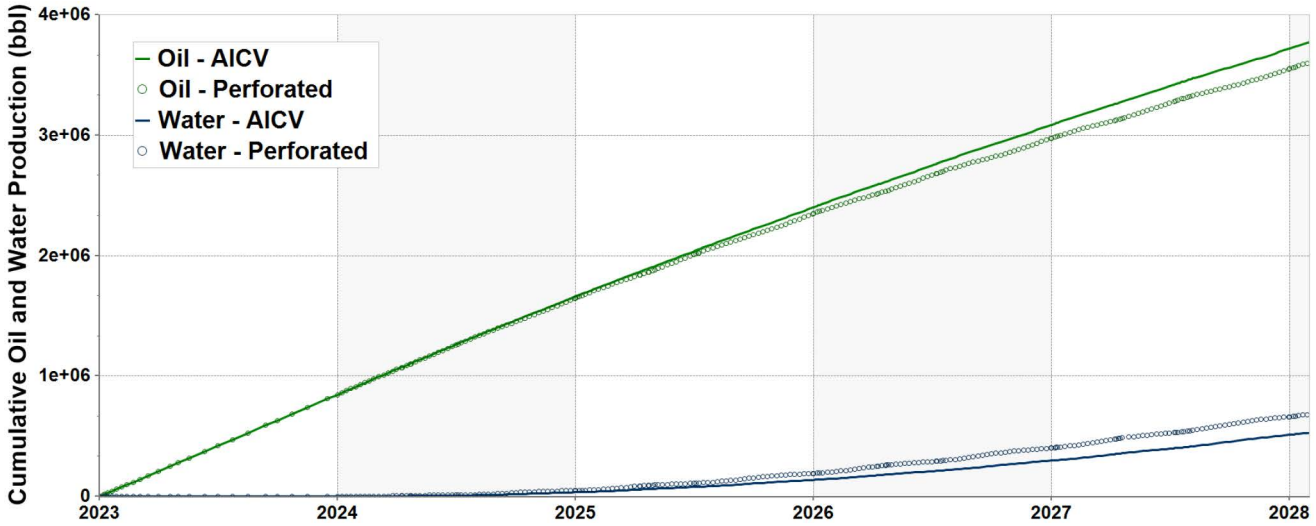

Figure. 14—Cumulative oil and water production for simulation case No.3.

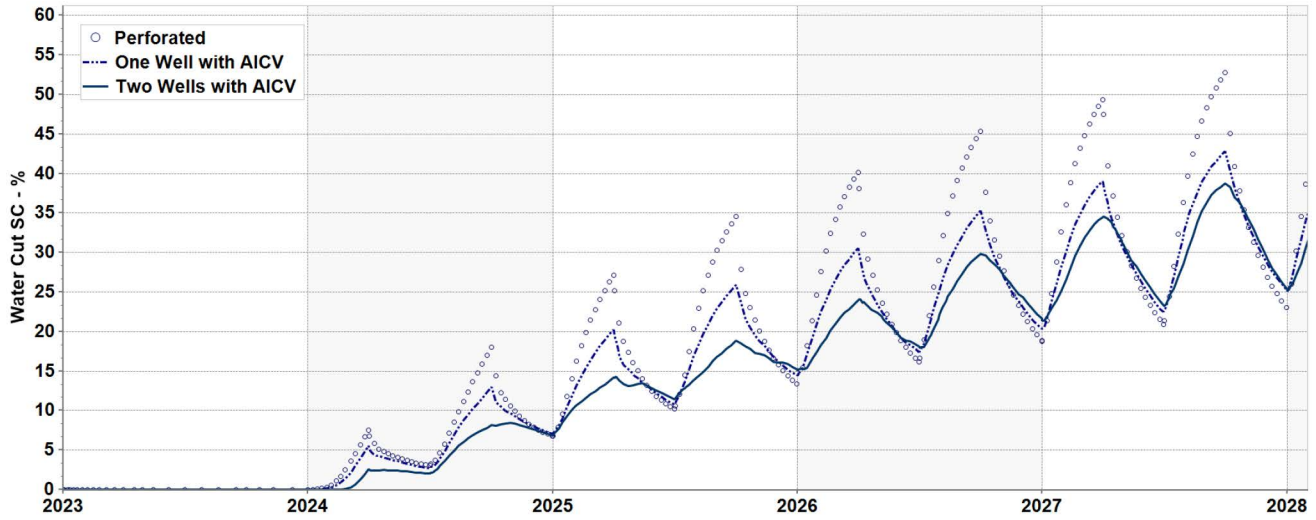

Figure. 15—Water cut vs. time for different completion scenarios.

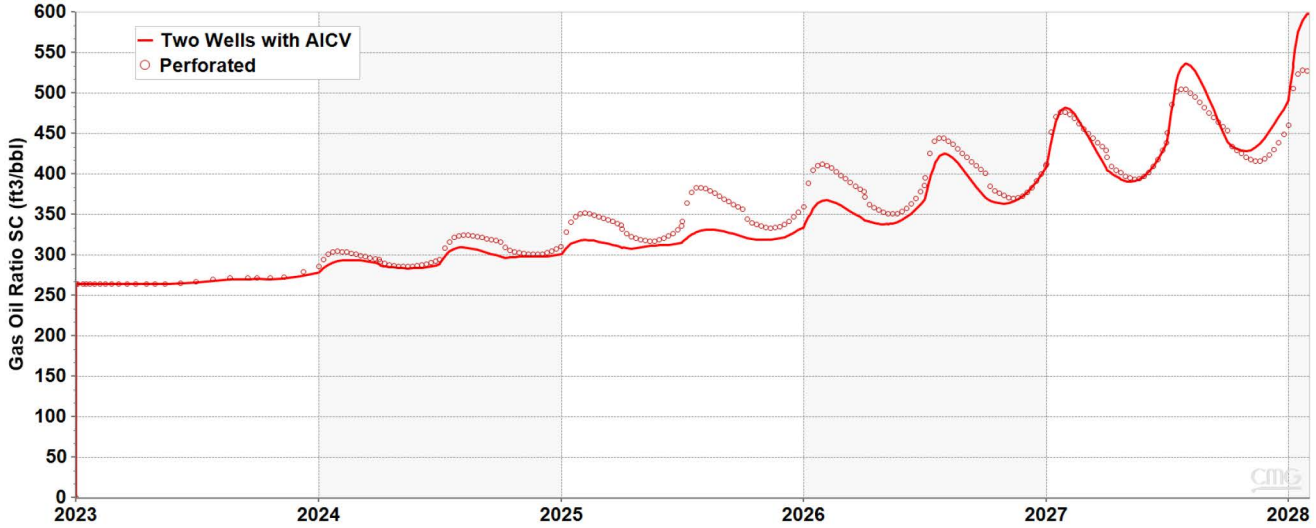

Figure. 16—Gas-oil ratio at standards condition vs. time for different completion scenarios.

Fig. 17 and Fig. 18 show the field cumulative oil and water production for different completion scenarios. The results indicate that the wells completed with AICVs have the highest oil production with lowest water production. The cumulative water production is reduced by approximately 25% by using AICVs compared to the perforated casing completion. It is assumed that the CO_2 is dissolved in water and oil, indicating that reduction in water production will minimize the recirculation of CO_2. The results confirm the significant benefit of AICV regarding water reduction and consequently increased oil production. The increased oil production and reduced water and gas production obtained by using AICV are demonstrated in several field installations worldwide and results are presented in several studies (Alakberi et al., 2023; Buwauqi et al., 2021; Kearns et al., 2022). Also the significantly better performance of AICV compared to ICD was demonstrated by experimental tests in this work and in previous work performed by the author (Taghavi et al., 2021). However, the dynamic reservoir simulators tend to underestimate the oil production and recovery compared to reality and actual well tests (Halvorsen et al., 2016).

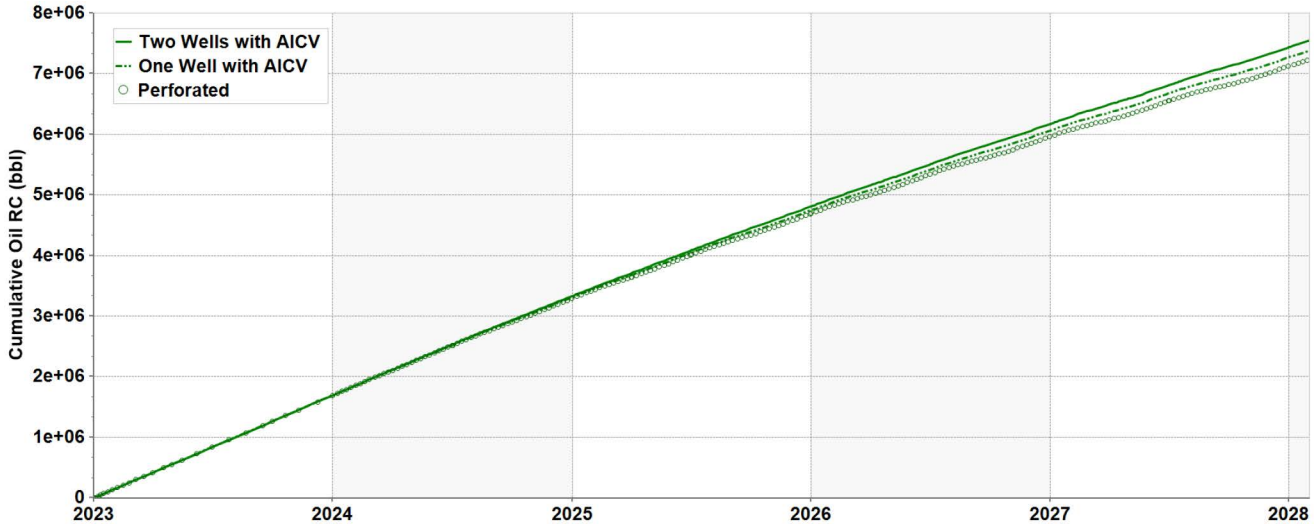

Figure. 17—Field cumulative oil production of different completion scenarios.

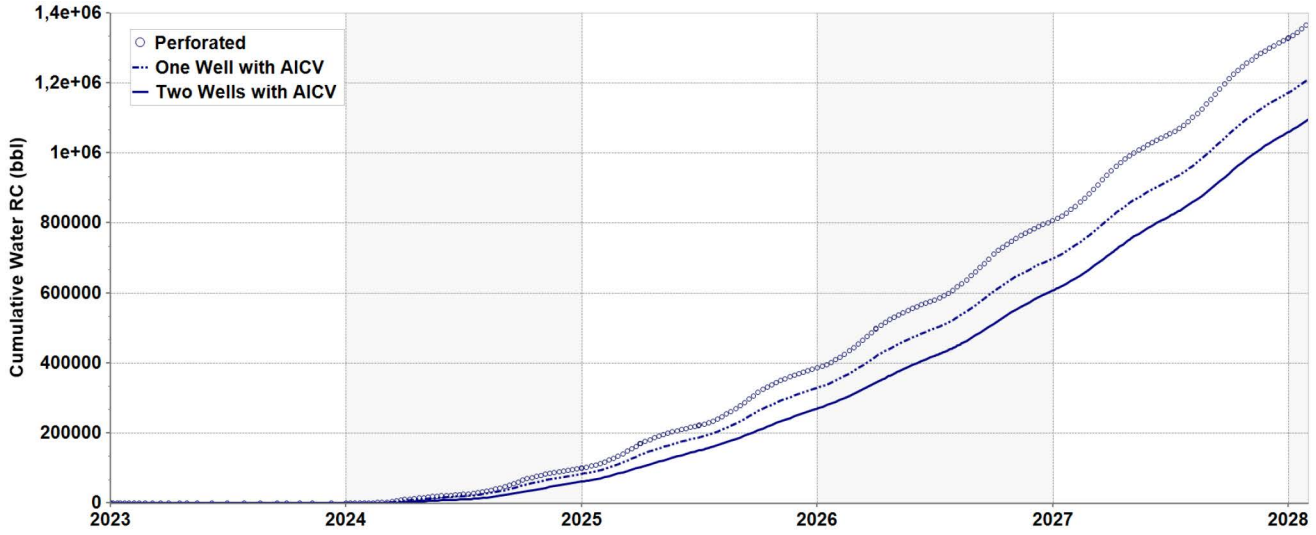

Figure. 18—Field cumulative water production of different completion scenarios.

Conclusions

The AICV performance and its impact on oil production in a heterogeneous reservoir where CO_2 is injected for enhanced oil recovery are investigated. This is achieved by performing experiments and simulation of the AICV performance using an industrial reservoir simulator, CMG STARS. The AICV performance by using CMG simulator in a CO_2 EOR oil reservoir is simulated for the first time.

Experiments are carried out with realistic reservoir fluids to generate single phase flow performance curves for AICV and an orifice type ICD. The experimental results confirm the significant benefit of AICV compared to ICD regarding water and CO_2 reduction. Under the same conditions and at a given differential pressure, AICV compared to ICD, reduces the water and CO_2 volume flow rate by approximately 58% and 82% respectively. ICD cannot choke locally for water and CO_2, and this leads to high production of these unwanted fluids compared to AICV. Simulations are performed using CMG STARS, which is a multi-phase, multicomponent reservoir simulator. Three simulation cases are studied in a heterogenous reservoir with CO_2 WAG injection. The experimental performance curves for the AICV are used to generate the FCD tables in CMG STARS to simulate the AICV behavior. The simulation results indicate that AICV reduces the water cut significantly. The cumulative water production is reduced by approximately 25% by using AICVs compared to the perforated casing completion. Indeed, reduction in water production will minimize the recirculation of CO_2. Also, reduction in production of carbonated water will mitigate the problem related to the corrosion of the producing wells and process equipment on the platform. In addition, the AICV completion scenario delivers the highest cumulative oil production after five years of production.

From the environmental aspects, utilizing AICV in CO_2 EOR projects will contribute significantly to reduction of greenhouse gas emissions. A better distribution of CO_2 in the reservoir contributes to a larger storage capacity of CO_2 in the reservoir, and thereby more CO_2 storage.

References

Aakre, H., Mathiesen, V., & Moldestad, B. (2018). Performance of CO_2 flooding in a heterogeneous oil reservoir using autonomous inflow control. *Journal of Petroleum Science and Engineering*, **167**, 654–663 https://doi.Org/10.1016/j.petrol.2018.04.008.

Aakre, H. (2017). The impact of autonomous inflow control valve on increased oil production and recovery University College of Southeast Norway, Faculty of Technology, Natural Sciences and Maritime Sciences]. *Kongsberg*.

Aakre, H., Halvorsen, B., Werswick, B., & Mathiesen, V. (2014). Autonomous Inflow Control Valve for Heavy and Extra-Heavy Oil. SPE Heavy and Extra Heavy Oil Conference: Latin America, https://doi.org/10.2118/171141-MS

Ahmadi, M. A., Zendehboudi, S., & James, L. A. (2018). Hybrid connectionist model determines CO_2-oil swelling factor. *Petroleum Science*, **15**(3), 591–604. https://doi.org/10.1007/s12182-018-0230-5

Ahmed, T. (2010). Chapter 14 - Principles of Waterflooding. In T. Ahmed (Ed.), *Reservoir Engineering Handbook* (Fourth Edition) (pp. 909–1095). Gulf Professional Publishing. https://doi.org/10.1016/B978-1-85617-803-7.50022-5

Alakberi, R. S., Igein, O. F., & Aljasmi, S. A. (2023). Successful Smart Completion Deployment of Autonomous Inflow Control Valve with 13 Open Hole Segmentation Lower Completion Using a Light Workover Rig. *SPE/IADC Middle East Drilling Technology Conference and Exhibition*, https://doi.org/10.2118/214582-MS

Buwauqi, S., Jumah, A. A., Shabibi, A., Harrasi, A., Kalyani, T., Fahmy, A., & Ismail, I. M. (2021). Application of Autonomous Inflow Control Valve AICV in Increasing the Field Recovery in One of the Matured Fields in the Sultanate of Oman: Case Study. SPE Annual Caspian Technical Conference, https://doi.org/10.2118/207069-MS

Council, N. P. (2021). MEETING THE DUAL CHALLENGE; A Roadmap to At-Scale Deployment of CARBON CAPTURE, USE, AND STORAGE. https://www.energy.gov/sites/default/files/2022-10/CCUS-Chap_8-030521.pdf

Ettehadtavakkol, A., Lake, L. W., & Bryant, S. L. (2014). CO_2-EOR and storage design optimization. *International Journal of Greenhouse Gas Control*, **25**, 79–92. https://doi.org/10.1016/j.ijggc.2014.04.006

Gozalpour, F., Ren, S. R., & Tohidi, B. (2005). CO_2 EOR and Storage in Oil Reservoir. *Oil & Gas Science and Technology - Rev. IFP*, **60**(3), 537–546. https://doi.org/10.2516/ogst:2005036

Halland, E. K., Johansen, W. T., & Riis, F. (2012). CO_2 Storage ATLAS Norwegian Sea. *Directorate N. P.*. https://www.npd.no/en/facts/publications/CO2-atlases/CO2-storage-atlas-of-the-norwegian-sea/

Halland, E. K., Johansen, W. T., & Riis, F. (2014). CO_2 Storage Atlas Norwegian Continental Shelf Directorate N. P.. https://www.npd.no/en/facts/publications/CO2-atlases/CO2-atlas-for-the-norwegian-continental-shelf/

Halland, E. K., Pham, V., Riis, F., & Hansen, A.-H. (2019, 21-26 October 2018). CO_2 for EOR Combined with Storage in the Norwegian North Sea 14th Greenhouse Gas Control Technologies Conference (GHGT-14), *Melbourne*. http://dx.doi.org/10.2139/ssrn.3365602

Halvorsen, M., Madsen, M., Vikøren Mo, M., Isma Mohd, I., & Green, A. (2016). Enhanced Oil Recovery On Troll Field By Implementing Autonomous Inflow Control Device. *SPE Bergen One Day Seminar*, https://doi.org/10.2118/180037-MS

Kearns, K., Rios, F., Montero, J., Uzcategui, A. A., Fipke, S., Molina, J. L., & Mohd Ismail, I. (2022). Autonomous Inflow Control Valves Restore Oil Production by Controlling Gas and Water Breakthrough in Acordionero Field, Colombia: A Case Study. SPE Annual Technical Conference and Exhibition, https://doi.org/10.2118/210163-MS

Killie, R., Paterson, G. J., & Lager, T. (2021). Delivering Automated Reservoir Management with Birth of the First Ever Universal Inflow Control System UICS. SPE Annual Technical Conference and Exhibition, https://doi.org/10.2118/205868-MS

Mansour, E. M., Al-Sabagh, A. M., Desouky, S. M., Zawawy, F. M., & Ramzi, M. (2019). A laboratory investigati on of carbon dioxide-enhanced oil recovery by focusing on CO_2-oil physical properties. *Egyptian Journal of Petroleum*, **28**(1), 21–26. https://doi.org/10.1016/j.ejpe.2018.10.004

Oomole, O., & Osoba, J. S. (1983). Carbon Dioxide - Dolomite Rock Interaction During CO_2 Flooding Process. Annual Technical Meeting, Banff, May 1983, https://doi.org/10.2118/83-34-17

Potter, G. F. (1987). The Effects of CO_2 Flooding on Wettability of West Texas Dolomitic Formations. SPE Annual Technical Conference and Exhibition, https://doi.org/10.2118/16716-MS

Petroleum, N. (2022). Effective resource management in mature areas https://www.norskpetroleum.no/en/developments-and-operations/resource-management-in-mature-areas/

Safi, R., Agarwal, R. K., & Banerjee, S. (2016). Numerical simulation and optimization of CO_2 utilization for enhanced oil recovery from depleted reservoirs. *Chemical Engineering Science*, **144**, 30–38. https://doi.org/10.1016/j.ces.2016.01.021

Stevens, S. H., Kuuskraa, V. A., Gale, J., & Beecy, D. (2001). CO_2 Injection and Sequestration in Depleted Oil and Gas Fields and Deep Coal Seams: Worldwide Potential and Costs. *Environmental Geosciences*, **8**(3), 200–209. https://doi.org/10.1046/j.1526-0984.2001.008003200.x

Taber, J. J., Martin, F. D., & Seright, R. S. (1997). EOR Screening Criteria Revisited— Part 1: Introduction to Screening Criteria and Enhanced Recovery Field Projects. *SPE Reservoir Engineering*, **12**(03), 189–198. https://doi.org/10.2118/35385-pa

Tahami, S. A., Dabir, B., Asghari, K., & Shahvaranfard, A. (2014). Modeling of Asphaltene Deposition During Miscible CO_2 Flooding. *Petroleum Science and Technology*, **32**(18), 2183–2194. https://doi.org/10.1080/10916466.2010.504937

Taghavi, S., Gisholt, E., Aakre, H., Haland, S., & Langaas, K. (2021). Autonomous Inflow Control Valve Multiphase Flow Performance for Light Oil. Offshore Technology Conference, Autonomous Inflow Control Valve Multiphase Flow Performance for Light Oil | OTC Offshore Technology Conference | OnePetro

West, L. M. (2014). A Regional Assessment of Residual Oil Zones in the Permian Basin and Their Potential for Carbon Dioxide Capture Usage and Storage. *Energy Procedia*, **63**, 7884–7890. https://doi.org/10.1016/j.egypro.2014.11.824

Zekri, A. R. Y., Shedid, S. A., & Almehaideb, R. A. (2013). Experimental investigations of variations in petrophysical rock properties due to carbon dioxide flooding in oil heterogeneous low permeability carbonate reservoirs. *Journal of Petroleu m Exploration and Production Technology*, **3**(4), 265277. https://doi.org/10.1007/s13202-013-0063-0

Zhang, L., Ren, B., Huang, H., Li, Y., Ren, S., Chen, G., & Zhang, H. (2015). CO_2 EOR and storage in Jilin oilfield China: Monitoring program and preliminary results. *Journal of Petroleum Science and Engineering*, **125**, 1–12. https://doi.org/10.1016/j.petrol.2014.11.005

Paper 8

The Impact of Autonomous Inflow Control Valve on Improved Oil Recovery in a Thin-Oil-Rim Reservoir

This paper is published in SPE Journal, April 2024, Volume 29, Issue 04

Authors: Soheila Taghavi, Haavard Aakre, Seyed Amin Tahami, and Britt M.E. Moldestad

The Impact of Autonomous Inflow Control Valve on Improved Oil Recovery in a Thin-Oil-Rim Reservoir

Soheila Taghavi[1,2*], Haavard Aakre[2], Seyed Amin Tahami[1], and Britt M. E. Moldestad[1]

[1]University of South-Eastern Norway
[2]InflowControl AS

Summary

Oil production from thin-oil-rim fields can be challenging as such fields are prone to gas coning. Excessive gas production from these fields results in poor production and recovery. Hence, these resources require advanced recovery methods to improve the oil recovery. One of the recovery methods that is widely used today is advanced inflow control technology such as autonomous inflow control valve (AICV). AICV restricts the inflow of gas in the zones where breakthrough occurs and may consequently improve the recovery from thin-oil-rim fields. This paper presents a performance analysis of AICVs, passive inflow control devices (ICDs), and sand screens based on the results from experiments and simulations. Single- and multiphase-flow experiments are performed with light oil, gas, and water at typical Troll field reservoir conditions (RCs). The obtained data from the experiments are the differential pressure across the device vs. the volume flow rate for the different phases. The results from the experiments confirm the significantly better ability of the AICV to restrict the production of gas, especially at higher gas volume fractions (GVFs). Near-well oil production from a thin-oil-rim field considering sand screens, AICV, and ICD completion is modeled. In this study, the simulation model is developed using the CMG simulator/STARS module. Completion of the well with AICVs reduces the cumulative gas production by 22.5% and 26.7% compared with ICDs and sand screens, respectively. The results also show that AICVs increase the cumulative oil production by 48.7% compared with using ICDs and sand screens. The simulation results confirm that the well completed with AICVs produces at a beneficial gas/oil ratio (GOR) for a longer time compared with the cases with ICDs and sand screens. The novelty of this work is the multiphase experiments of a new AICV and the implementation of the data in the simulator. A workflow for the simulation of AICV/ICD is proposed. The simulated results, which are based on the proposed workflow, agree with the experimental AICV performance results. As it is demonstrated in this work, deploying AICV in the most challenging light oil reservoirs with high GOR can be beneficial with respect to increased production and recovery.

Introduction

In a typical thin-oil-rim field, a thin oil layer lies between a gas cap and an underlying aquifer. Oil may be produced from such fields by drilling long horizontal wells or long multilateral horizontal wells. Oil production from such fields will, over time, cause gas coning in some locations along the well. Generally, thin-oil-rim reservoirs are prone to gas coning (Hasan et al. 2010). Excessive gas production from a gas cap will result in upward movement and smearing of the tiny oil column (Langaas et al. 2020). Therefore, oil production from a thin-oil-rim field can be challenging. The Troll field in the northern part of the North Sea is characterized as a thin-oil-rim reservoir.

The major challenge in oil production is to increase the recovery factor. The Norwegian Continental Shelf is one of the leading regions in oil recovery, but still about half of the oil on average is remaining in the reservoir after shutting down the wells. These resources require the implementation of other methods beyond the methods in the plan for development and operation to improve the oil recovery.

Well placement, well type, well path, and completion methods are among the important factors that must be evaluated to achieve enhanced well performance and improved recovery (Chan et al. 2014; Carpenter 2015). Several measures regarding the production of the thin remaining oil columns at the Troll oil field have been in focus in recent years. These measures include, but are not limited to, developing and implementing new technologies for cost-effective drilling, more accurate well placement, and technology for constraining water and gas production from the oil wells (The Norwegian Petroleum Directorate 2021). Constraining the water and gas production and consequently increasing the oil production can be achieved by deploying passive and autonomous inflow control devices (ICDs and AICDs). Both data from experiments in laboratories and the application of AICDs in reservoirs with high GOR have demonstrated that utilizing AICDs is a robust method in restriction of gas production and improving oil recovery (Konopczynski et al. 2022; Langaas et al. 2019; Tusimin et al. 2020). The production results from the well completed with rate-controlled production (RCP) valves at Troll show approximately 20% higher cumulative oil production compared with ICDs (Halvorsen et al. 2012). In addition, the GOR in wells completed with ICDs is three times the GOR in wells completed with RCPs (Halvorsen et al. 2012). Also, analysis of the output from oil wells at Troll demonstrates a clear improvement in the production rate after AICD installation (The Norwegian Petroleum Directorate 2019). The AICD completion in a superthin-oil-rim reservoir in the East and West Belumut fields in Malaysia demonstrates 50% more oil production compared with the offset ICD wells (Mohd Ismail et al. 2018).

There is an incentive to keep the production of oil at a high liquid rate before gas from the gas cap breaks through into the well. Also, it is important to keep a high oil production rate after the gas breakthrough occurs. This can be achieved by using AICVs. AICD is an autonomous inflow control device covering a wide range of devices, while AICV is one type of AICD. The effective flow area of the AICV is changing because of its dynamic and autonomous behavior, while a passive ICD has a constant flow area. AICV delays the onset of breakthrough and restricts the gas production locally when the gas breaks through into the well as it is shown in **Fig. 1** (Aakre et al. 2014)**.** The figure shows a horizontal well completed with AICVs in a heterogeneous reservoir. The pressure drops at different reservoir locations are plotted. Gas and water breakthrough occurs in high-permeability zones in heterogeneous reservoirs. In high-permeability zones, the

*Corresponding author; email: soheila.taghavi@inflowcontrol.no

Original SPE manuscript received for review 30 May 2023. Revised manuscript received for review 13 November 2023. Paper (SPE 218393) peer approved 26 November 2023.

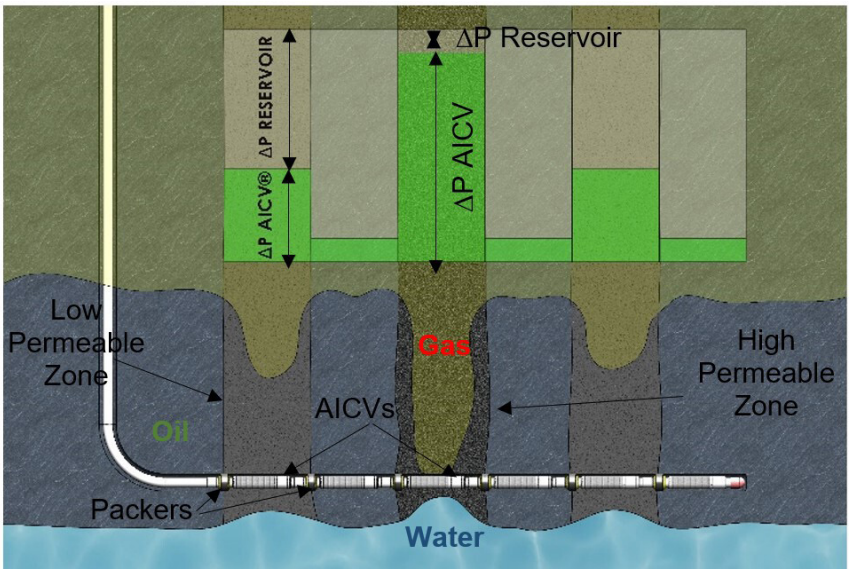

Fig. 1—High pressure drop across AICV in high-permeability zones with gas and water breakthrough (Aakre et al. 2014).

low resistance in the reservoir gives a high flow rate of fluids resulting in a higher pressure drop through the AICV, indicating that the AICV is choking. However, in low-permeability zones, the pressure drop in the reservoir is higher and as the total pressure drop from the reservoir to the well is constant, the pressure drop over the AICV is lower. The reduction of gas production from the breakthrough zones allows to keep a low bottomhole pressure. This keeps a higher sandface drawdown in the zones with oil and thus keeps the oil production from these zones. This results in maximizing the oil production and recovery. The increased oil production and reduced water and gas production obtained by using AICV are demonstrated in several field installations worldwide, and the results are presented in several studies (Alakberi et al. 2023; Buwauqi et al. 2021; Kearns et al. 2022).

According to Halvorsen et al. (2012), the RCP valves have increased the cumulative oil production by 20%. The single- and multiphase behaviors of the new AICV presented in this work are evaluated to find if the AICV can additionally increase the cumulative oil production. This new AICV has a better performance in multiphase flow compared with previous versions of AICVs.

The objective of this paper is to evaluate the performance of the new AICV in a thin-oil-rim reservoir and its impact on reservoir recovery. This is achieved by performing experiments and simulations. The experimental study includes one-phase and multiphase flow tests for orifice ICD and AICV using water, gas, and oil as the reservoir fluids at realistic RCs. Simulations are performed using a commercial simulator. The impact of improved AICV performance on the reservoir recovery is evaluated, and the results are validated against the experimental data.

AICV Technology and Design for Light Oil

The technology developed by InflowControl AS (the AICV; see **Fig. 2a**) restricts the production of unwanted fluids such as water, gas, and steam significantly. By balancing the reservoir drawdown, AICV delays the onset of water and/or gas breakthrough, and in case of breakthrough, it will restrict the production of these unwanted fluids significantly. **Fig. 2b** shows an AICV mounted in a base pipe with sand screen. Annular swellable packers must be in place to provide robust zonal and annulus isolation. Perfect sectioning of the annulus will guarantee the functionality of AICV in long horizontal wells.

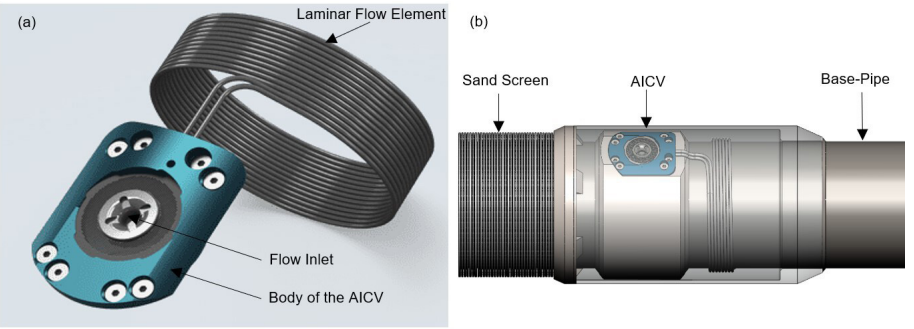

Fig. 2—AICV design for light oil (a) and AICV mounted in a base pipe with sand screen (b).

The AICV distinguishes between the reservoir fluids and reacts accordingly. The functionality is based on the viscosity and density of the reservoir fluids. The valve keeps open for viscous fluids like light oil and closes for lower viscous fluids such as water and gas. Light oil is defined as oil with a density of less than 875.7 kg/m^3 (API gravity greater than 30.1 °API) (Canadian Legal Information Institute 1996). In this paper, the viscosity of the oil is 2.1 cp and the density is 870 kg/m^3 at RCs, which is considered light oil.

The functionality of the AICV is controlled by a pilot flow parallel to the main flow, as it is illustrated in **Fig. 3.** The main body, inlet, and piston are the elements of the main flow path. The pilot flow consists of a pipe segment and a thin-plate orifice that are connected in series. The pipe segment serves as a laminar flow element (LFE) and the pressure drop through it is proportional to the fluid viscosity and the velocity. Eq. 1 describes the pressure drop through the LFE:

$$\Delta P = f \times \frac{L\rho v^2}{2D} = \frac{64}{\mathrm{Re}} \times \frac{L\rho v^2}{2D} = \frac{32\mu v L}{D^2}, \quad (1)$$

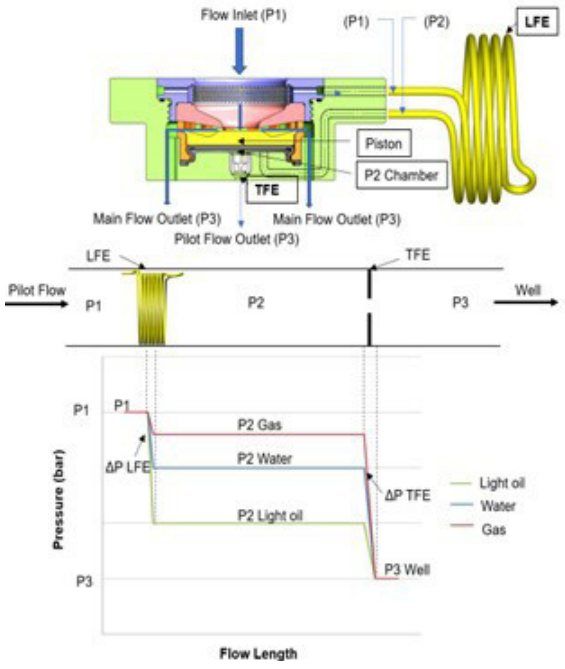

Fig. 3—Pressure drop of reservoir fluids through the AICV.

where ΔP is the pressure drop, f is the friction factor (64/Re), Re is Reynolds number, ρ is the fluid density, μ is the fluid viscosity, v is the fluid velocity, and L and D are the length and diameter of the LFE, respectively. A thin-plate orifice serves as a turbulent flow element (TFE) and the pressure drop through it is given by Eq. 2:

$$\Delta P = \frac{1}{2C_d^2}.\rho v^2, \quad (2)$$

in which C_d is the discharge coefficient that depends on the orifice design (Konopczynski et al. 2022). The discharge coefficient is a dimensionless number that is used to characterize the pressure loss behavior of an orifice or a nozzle and is defined as $C_d = A/A_{VC}$ (Moradi and Moldestad 2021). A is the cross-sectional area of the orifice hole and A_{VC} is the area in vena contracta. Vena contracta is the minimum jet area that appears just downstream of the orifice, where the fluid velocity is at its maximum.

As it is illustrated in **Fig. 3**, the reservoir fluid at reservoir pressure P1 enters the valve inlet, and a minor portion of the fluid is guided through the pilot flow elements, while the main flow passes through the small opening between the inlet seat and the piston. By passing through the LFE, the pressure of the fluid is reduced to P2 at a chamber called the P2 chamber. The fluid properties and the flow rate through the pilot flow determine the P2 pressure. The pilot flow is further led through the turbulent flow element in which the second pressure drop to the well pressure, P3, occurs. The P2 pressure in the P2 chamber controls the valve functionality. Different P2 pressures act on the piston based on the different fluids passing through the LFE. For higher viscosity fluids like oil, the pressure drop through the LFE is high, resulting in a lower P2 (see the lower plot in **Fig. 3**). Because the P2 pressure is low for oil, the generated force under the piston, which acts upward, is low as well. This will keep the piston in an open position, producing oil to the well through both the main flow and the pilot flow path. For lower viscosity fluids, such as gas and water, the pressure drop through the LFE is low, resulting in a higher P2 (see the lower plot in **Fig. 3**). Because the P2 pressure is high for gas and water, the generated force under the piston, which acts upward, is high as well. This will actuate the piston and the valve will close. The closed valve produces gas and water to the well only through the pilot flow path.

The LFE, the turbulent flow element, the inlet, and the piston design are adapted to the conditions, including the reservoir fluid properties and the requirements in the relevant field. The force balance around the piston is described in detail in earlier scientific works (Aakre et al. 2013, 2014).

Single- and Multiphase Flow Loops and Test Conditions

Fig. 4 shows the photo and the piping and instrumentation diagram of the flow loop test rig. The test facility is designed for single- and multiphase oil, water, and gas tests. Performance curves from single-phase tests with oil, gas, and water are obtained from the test rig. Performance curves describe the differential pressure of the AICV and ICD as a function of volumetric flow rate of the fluid. Also, the closure function of the AICV is obtained from the multiphase tests with oil and gas and/or oil and water.

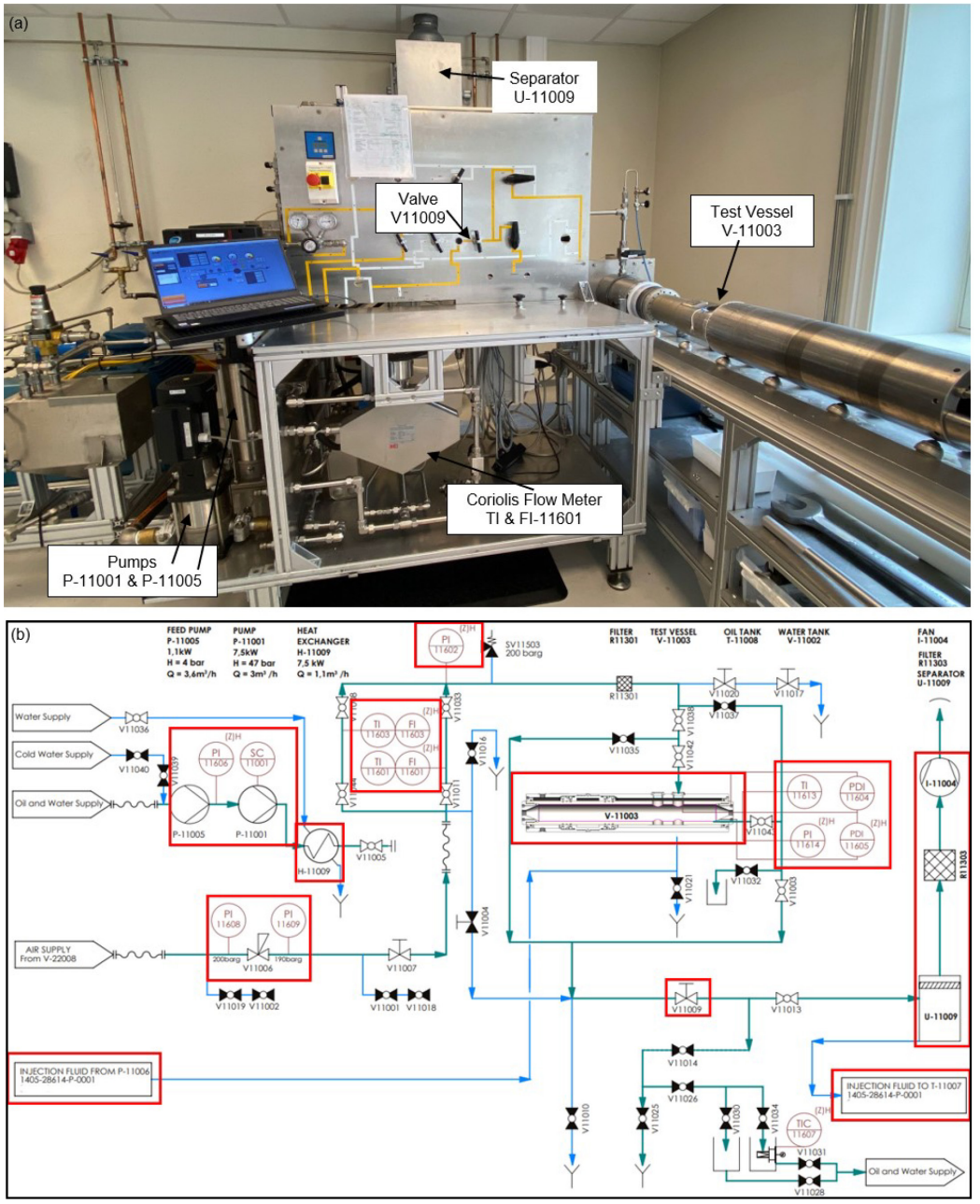

Fig. 4—Photo (a) and piping and instrumentation diagram (b) of the flow loop test rig showing the key elements and measuring instruments marked with red rectangles.

Two pumps, P-11005 and P-11001 in series, are used to increase the liquid pressure up to 50 bar from the oil and water supply. Compressed air at room temperature is regulated by V-11006 to the desired pressure for each case, up to a maximum of 200 bar. An AICV or ICD is installed in the test vessel, V-11003. Flow rates, density, and temperature are measured by the Coriolis flowmeters, TI & FI-11601 and TI & FI-11603, which are located close to the test vessel inlet. Pressure transmitter PI-11602 measures the inlet pressure, whereas the differential pressure transmitters, PDI-11604 and PDI-11605, measure the total differential pressure over the test vessel. Also, TI-11613 and PI-11614 measure the temperature and pressure of the outlet fluid, respectively. Valve V11009 is used to control and regulate the fluid flow rate. The fluids are circulated back to the oil and water supply and air exits to the atmosphere after passing through the separator, U-11009, and filter, R11303. The heat exchanger, H-11009, is used to regulate the temperature of the circulated fluid to the desired temperature. To study the multiphase behavior of the AICV or ICD, the test vessel is already filled with gas, and the desired amount of oil is injected by Pump P-11006 from a separate test unit that is connected to the single-phase test rig. After passing through the inflow device, oil and gas are separated in the separator where oil is circulated back to the oil supply tank, T-11007, in the injection rig and gas exits to the atmosphere after passing through the filter. All the key elements and measuring instruments of the test rig are marked with red rectangles in **Fig. 4b**.

The controlled and measured key variables for the test program were flow rates, differential pressure across the AICV or ICD, system conditions (pressure and temperature), and fluid properties, such as viscosity and density. The test matrix and system condition applied in the experiments are given in **Table 1.** These conditions represent the Troll field conditions. The tests are performed at different temperatures and pressures to obtain the viscosity and density of the fluids in the reservoir. The differential pressure across the AICV or ICD is

varied gradually between 1 bar and 20 bar. The flow rate and differential pressure are continuously measured as the differential pressure is gradually varied from 1 bar to 20 bar. The air density is equivalent to the hydrocarbon gas density at theRCs.

Description	Fluid Type	Density (kg/m^3)	Viscosity (cp)	Pressure (bar)	Temperature (˚C)	Differential Pressure (bar)
Single-phase test	Pressurized air	92	0.02	78	21	1–20
	Water	980	0.41	50	68	1–20
	Oil	870	2.1	50	21	1–20
Multiphase test	Oil and gas	–	–	78	21	10, 15, 20

Table 1—Test conditions.

Development of the Reservoir and Well Model in a Commercial Simulator

In this study, CMG STARS is used to model the performance of ICD and AICV in a light oil reservoir. The developed model investigates the performance of ICD and AICV and their effect on increased oil recovery. CMG STARS is a reservoir simulator capable of handling multiple phases and components. Besides, when modeling a well with CMG STARS, two options are available, which are the source/sink model and the advanced FlexWell (FW) model. The source/sink model is suitable for specific scenarios, such as short horizontal wells, uniform wellbore-reservoir communication, low flow rates, or large pipe diameters. FW is an advanced wellbore model that considers complex well completions, utilizing governing equations for mass, energy, momentum balance, and pipe flow with spatial discretization (Mohd Ismail et al. 2021). FW modeling incorporates a two-way interaction between the wellbore and reservoir simulator, capturing dynamic interactions. This modeling process involves solving the wellbore and reservoir models alternately at each timestep, with the reservoir slightly trailing behind by one iteration. As a result, to enhance the precision of the well modeling calculations, CMG STARS is used for reservoir modeling, and the FW option is chosen for modeling the wells equipped with ICDs and AICVs.

Reservoir Model. The reservoir properties at the Troll oil field are used to develop a thin-oil-rim reservoir model in the simulator. The Troll oil field is located in the North Sea, 80 km from the west coast of Norway. The oil production from the Troll West oil and gas province started in 1995. The thin oil layer was originally between 22 m and 26 m at the Troll West oil province, located at a depth of 1360 m (Mjaavatten et al. 2006). The thin oil layer lies between a large gas cap and a strong aquifer. The oil column is now reduced to only 1–5 m in thickness (The Norwegian Petroleum Directorate 2021). However, a significant volume of residual oil is encountered directly below the oil column (The Norwegian Petroleum Directorate 2021). The newly drilled long horizontal multilateral wells at the Troll oil field have a reservoir length of more than 3500 m. These wells are positioned close to the oil-water contact to avoid early gas breakthrough. The Troll reservoir mostly consists of high-permeability homogeneous sandstones with permeability ranging from 1 darcy to more than 20 darcies. In addition, the porosity ranges from 30% to 35% (Halvorsen et al. 2012).

Reservoir Fluid and Rock Properties. The temperature of the reservoir near the well is 68°C and the pressure at initial conditions is 12 500 kPa, and it is assumed to be constant. The most important properties of the fluid used for the simulation are presented in **Table 2.** The light oil viscosity as a function of pressure at reservoir temperature is shown in **Fig. 5.**

Parameter	Value at 68°C	Unit
Viscosity	2.1	cp
Density	870	kg/m^3
GOR	42	std m^3/std m^3
Bubblepoint pressure	12 500	kPa

Table 2—Oil properties.

The reservoir near the well has a total oil column of 7 m, starting from a depth of 2092 m. The effective porosity of sandstone near the well is 30%. Generally, it is challenging to obtain information about relative permeability for different fields. Veskimägi (2013) presented relative permeability data provided by the Equinor Troll department in his work. The study uses the standard type of unnormalized LET family of correlations (Lomeland and Orec 2018). The calculated LET relative permeabilities were a good match for the historic well production. The relative permeability curves for oil, water, and gas at the Troll reservoir are presented in **Fig. 6.**

The permeability of the heterogeneous reservoir in both *x*- and *y*-directions varies from 42 md in the low-permeability zones to 7,282 md in the relatively high-permeability zones. The vertical permeability is specified in each block of the reservoir, and it varies from 20 md to 5,058 md for the low-permeability and the relatively high-permeability zones, respectively. These values are the average permeabilities in each production zone (Veskimägi 2013). This is to illustrate a heterogeneous reservoir. The horizontal and vertical permeability profiles of the heterogeneous reservoir are illustrated in **Fig. 7.** The capillary forces are not included in this study. The objective of this work is to evaluate the AICV performance and compare it with ICD and screens under the same conditions. It is expected that the inclusion of capillary forces will not affect the outcome of this work.

Dimensions of the Reservoir Drainage Area and Grids. In this work, for simplicity, a rectangular drainage area is considered for developing the oil production model. The length of the drainage area is 4500 m, the length of the horizontal well is 3500 m, and the width of the drainage area is 201 m. The thin oil column is placed between a gas cap starting at the depth of 2026 m and an underlying aquifer. It is assumed that the well is located at a depth of 2096 m in the thin oil column and 4 m below the gas cap. The size of the blocks varies along the *y*- and *z*-directions, while a uniform mesh along the *x*-direction is defined. Based on the mesh-sensitivity analysis performed by Timsina et al. (2017), finer mesh along the *x*-direction will have an insignificant impact on the overall flow rate. The optimal required number of grids in (*x*, *y*, *z*) coordinates and their size for discretizing the reservoir near the well have been determined and are presented in **Table 3.**

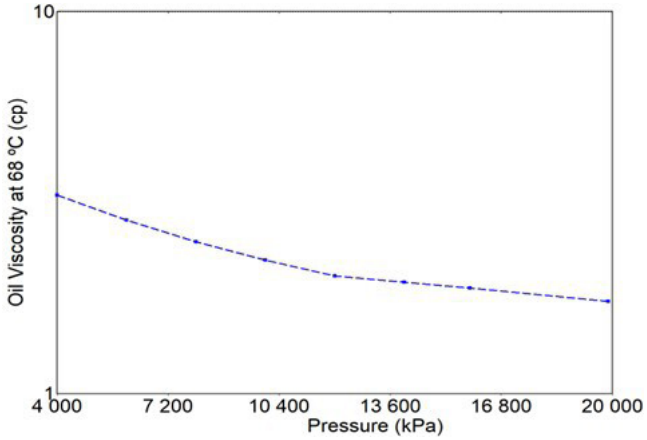

Fig. 5—Oil viscosity as a function of pressure.

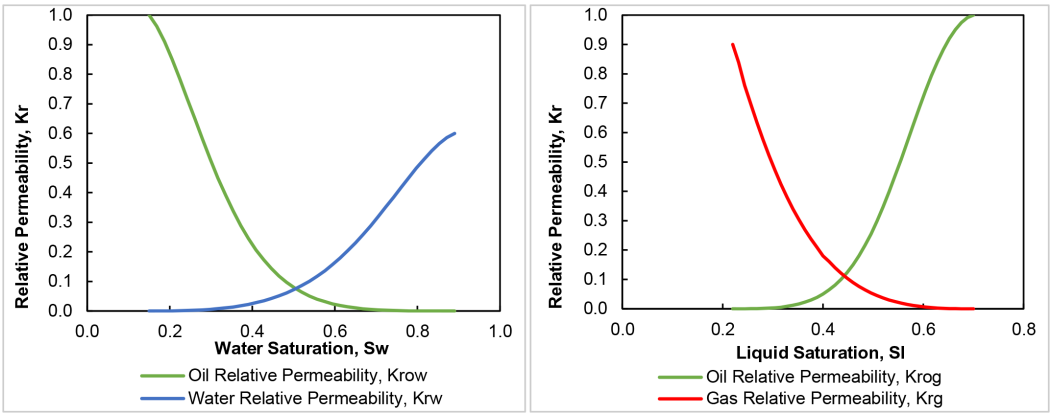

Fig. 6—LET relative permeability curves for the Troll reservoir (Veskimägi 2013).

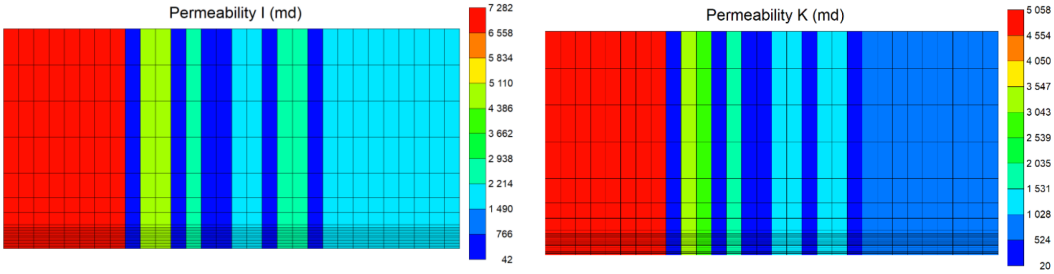

Fig. 7—Permeability profile of (left) horizontal permeability and (right) vertical permeability.

Direction	Length (m)	Number of Blocks	Block Size (m)
x	4500	30	150 (constant)
y	201	15	30, 24, 20, 12, 8, 4, 2, 1, 2, 4, 8,12, 20, 24, 30
z	73	22	12, 12, 12, 12, 8, 5, 4, 1, 0.5, 0.5, 0.5, 0.5, 0.5, 0.5, 0.5, 0.5, 0.5, 0.5, 0.5, 0.5, 0.5, 0.5, 0.5, 0.5

Table 3—Drainage area grid dimension.

Fig. 8 shows the grid resolution in IK-2D and JK-2D cross-sectional views and the position of the well. The scales are *Z*/*X*: 31:1 and *Z*/*Y*: 1.4:1.

Reservoir Initialization. The model is initialized without engaging the calculation of gravity equilibrium. The temperature of the reservoir is set at 68°C, while the initial pressure is considered constant (equal to 12 500 kPa) during the initialization. In Layers 1–8 in the *z*-direction, all the blocks are fully saturated with gas, whereas Layers 9–22 are initially set with 85% oil saturation and 15% water saturation.

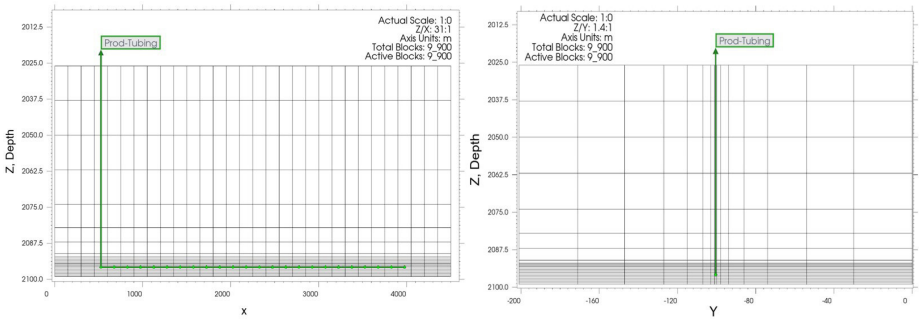

Fig. 8—Grid resolution in (left) IK-2D and (right) JK-2D cross-sectional views and the well position.

Wellbore Model. The model is run for 5 years to investigate the oil production. The minimum and maximum timesteps are set to 0.00001 days and 0.25 days, respectively. The well model consists of two pipes that represent the wellbore and the production tubing. The wellbore is a pipe with a length and inner diameter of 3500 m and 0.2159 m (8.5 in.), and the production tubing is a pipe with a length and inner diameter of 3500 m and 0.1397 m (5.5 in.).

To mechanistically model the simulation period, FWs were defined in the simulator. The FWs are annulus and tubing, both of the producer type. Three different completion scenarios are modeled and compared. Sand screens only, well completed with ICDs, and well completed with AICVs are simulated. By considering the target oil production rate and using the single-phase experimental data for oil shown in **Fig. 9,** the required number of AICVs and ICDs is determined. The oil flow rate through each AICV and ICD at around 10–15 bar drawdown is measured to be approximately 0.4 m^3/h. It is assumed that 2500 m^3/d oil is produced from 24 zones along the entire horizontal section. In each zone, 12 AICVs or 12 ICDs are used. To avoid the annular flow of the reservoir fluids, each production zone is isolated by packers installed in the annulus.

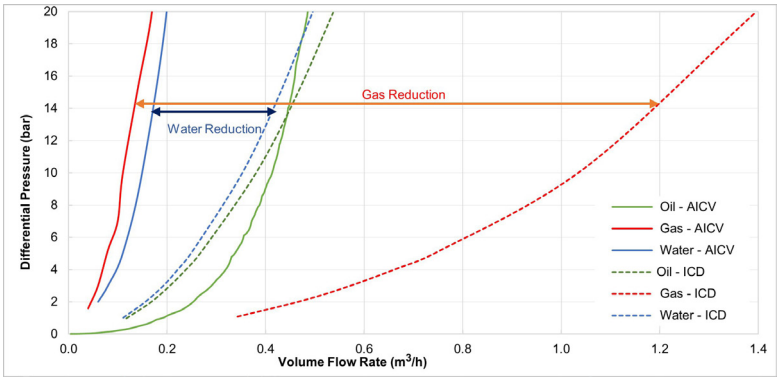

Fig. 9—Experimental performance curves for oil (2.1 cp), gas (0.02 cp), and water (0.41 cp) for ICD and AICV.

The production constraints are maximum surface liquid rate of 2500 m^3/d, minimum bottomhole pressure of 11 000 kPa, and GOR to stay below 600 std m^3/std m^3, with a cutback rate of 0.85 for the 5 years of production. The specifications of FWs and constraints for the production tubing are given in **Table 4.**

		Constraints			
Well	Well Size, Wall ID	Parameter	Limit/Mode	value	Action
Producer FW, annulus	0.2159 m (8.5 in.)	—	—	—	—
Producer FW, tubing	0.1397 m (5.5 in.)	Surface liquid rate	MAX	2500 m^3/d	Continue (CONT)
		Bottomhole pressure	MIN	11 000 kPa	Continue (CONT)
		GOR	STG	Upper limit	Continue (CONT)
				Cutback rate	

Table 4—Well configurations and constraints.

AICVs and ICDs are placed in the production tubing every 12.5 m, and their effects on oil production and gas reduction are investigated. In the simulations, AICV/ICD tables are developed and used to implement their behavior using the characteristics of the AICV/ICD and the reservoir fluid mixtures. The flow control device (FCD) table allows for characterization of an FCD through tabulated data. In this work, the AICV and ICD tables are based on experimental data shown in **Figs. 10 and 11.** The dependent variables to generate the FCD tables are the gas mass fraction and volume flow rate. A workflow for developing the AICV/ICD tables in the simulator is proposed in Appendix A.

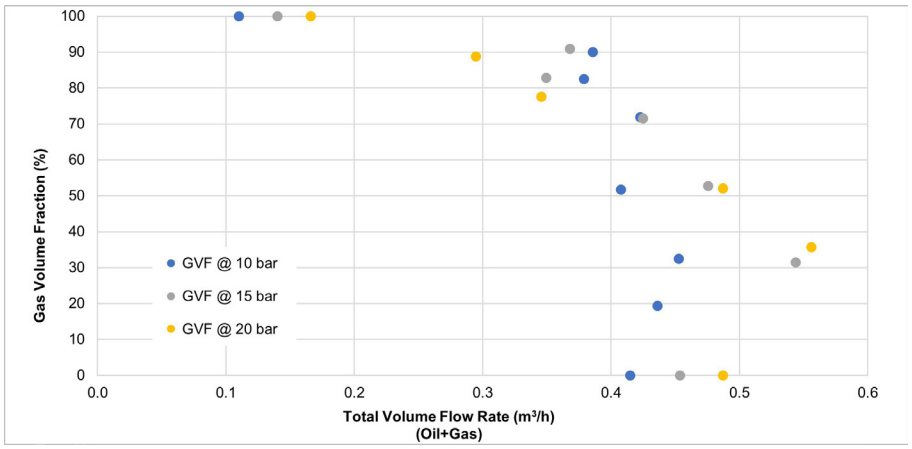

Fig. 10—Experimental GVF as a function of two-phase oil/gas volume flow of oil (2.1 cp) and gas at 10-bar, 15-bar, and 20-bar differential pressures across the AICV.

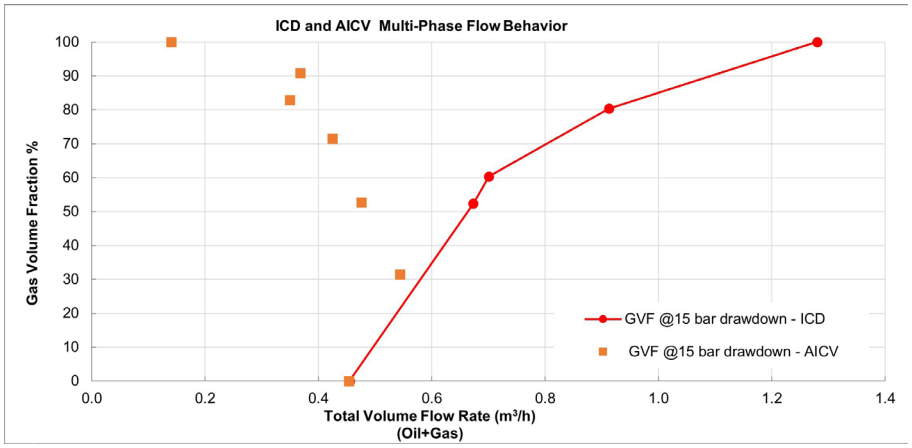

Fig. 11—Experimental multiphase flow behavior for ICD and AICV.

Simulation Cases. In this paper, the impact of AICV on improved oil recovery in a thin-oil-rim reservoir is evaluated. To achieve this purpose, in addition to the main study case with AICV completion, the simulations are conducted for similar cases with ICD completion and one case that represents sand screens only. AICV and ICD used in the experimental tests have the same strength. The strength of AICV or ICD is defined as the pressure drop over the valve when the oil flow rate is equal to 1 m^3/h. The completion scenarios are summarized in **Table 5.**

Completion Scenario	Number in Each 150-m Zone	Total Number	Diameter
Sand screens	12	288	8-mm ICD (as an approximation for sand screens only)
ICD	12	288	2.1 mm
AICV	12	288	Same strength as ICDs

Table 5—Completion scenarios.

The simulations for all the different cases have been performed for 5 years of production using the same well constraints as listed in **Table 4**.

Results and Discussion

The experiments and simulation results are presented and discussed in the following subsections.

Experimental Single-Phase Flow Test. AICV and an orifice-type ICD with 2.1-mm diameter and discharge coefficient of 0.65 for all the phases are used for the single-phase experiments under the Troll field conditions. The single-phase experimental results have been obtained for oil, water, and pressurized air. The results shown in **Fig. 9** represent the performance curves of the AICV and ICD. The performance curves illustrate pressure drop across the devices as a function of volumetric flow rate for single-phase fluids. At a 15-bar pressure drop, the oil/water ratio for AICV is 2.60, while it is 1.08 for ICD. Also, the oil/gas ratio at the same pressure drop for AICV

is 3.20, while it is 0.36 for ICD. The corresponding values of the oil/water ratio and oil/gas ratio for the RCP valve are 1.33 and 0.55, respectively, at a 15-bar pressure drop at Troll conditions (Halvorsen et al. 2016). The approximate fluid ratio values for the ICD, the RCP valve, and the AICV are summarized in **Table 6.**

Device	Oil/Water Ratio	Oil/Gas Ratio
ICD	1.08	0.36
RCP valve	1.33	0.55
AICV	2.60	3.20

Table 6—Approximate fluid ratio values for ICD, RCP valve, and AICV.

The oil flow rates through the ICD and AICV are equal at a 15-bar pressure drop, and the differences in the flow characteristics are studied. At a 15-bar pressure drop, the gas and water flow rates through the passive ICD are approximately 7.35 and 2.4 times more compared with AICV. The results indicate that the gas and water reduction by using AICV is significant. The ICD behavior is mainly density dependent, and therefore the flow rate of oil and water differs slightly, while the AICV chokes the water considerably. This is favorable when an aquifer is present in the reservoir and water breakthrough is likely to occur.

Experimental Two-Phase Flow Test. The multiphase behavior of inflow control technologies is of significant importance in controlling the breakthrough and restriction of unwanted fluids such as gas and water. **Fig. 10** shows the two-phase oil/gas tests performed at 10-bar, 15-bar, and 20-bar differential pressures across the AICV. The GVF vs. the two-phase oil/gas volume flow rate is presented in **Fig. 10**. The results demonstrate how AICV restricts the gas flow rate as the GVF increases. If oil flashes in the reservoir toward the inflow zones, gas is released from the oil. When the local GVF is up to 30%, the AICV opens, allowing all the oil together with gas to flow through the valve. The AICV closes gradually from 30% GVF until 100% pure gas flows through the valve. At this point, the AICV is closed for gas and the only remaining flow is through the pilot flow.

Fig. 11 shows the comparison of the oil/gas experimental results for ICD and AICV at 15-bar differential pressure. The oil flow rate at 15-bar differential pressure through both ICD and AICV is 0.45 m^3/h. As the amount of gas (GVF) increases, AICV chokes the gas flow, while ICD does not restrict the gas production. When the GVF reaches 100%, the volume flow rate through the ICD is 1.27 m^3/h, which is three times more than the volume flow rate for pure oil through the ICD. The AICV restricts the gas flow significantly, specifically at higher GVF, which is what makes this technology unique compared with other inflow control technologies.

Simulated Fluid-Flow Distribution, Pressure and Oil Production Along the Well. Fig. 12 illustrates the *y-z* view of the oil-saturation contours for the least permeable zone (42 md) by considering AICV completion. As shown in the contours, gas is coning toward the production well and oil is being produced as the oil saturation is less around the well location and the adjacent cells. Therefore, it can be interpreted that, by use of AICV, the low-permeability zones also contribute to the oil production.

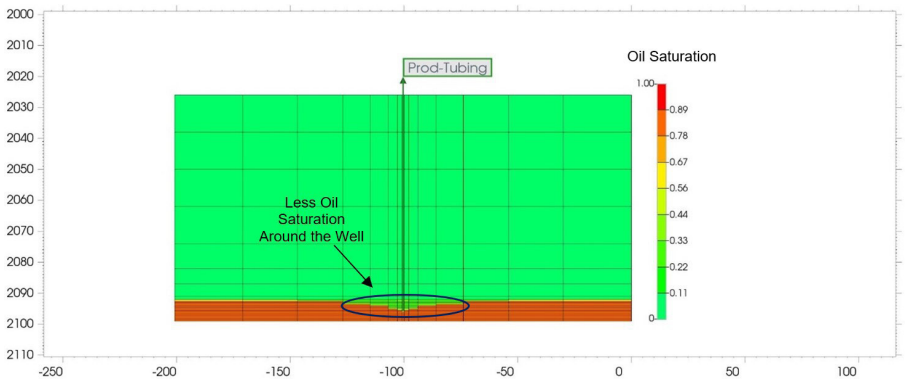

Fig. 12—Simulated oil-saturation distribution for the AICV completion in the least permeable zone.

Fig. 13 shows the tubing pressure and gas and oil flow rates along the horizontal length of the well for the cases with AICVs and sand screens at day 350 when excessive gas production occurs in the AICV case. This is to compare the best and the worst scenarios. The circles represent the flow influx from each zone, which is isolated by packers. In the high-permeability zones in the heel, which suffer from excessive gas production, the highest pressure drop occurs through the AICV, while the pressure drop with sand screens is negligible (see **Fig. 13a**). AICV chokes the gas flow rate entering the well, resulting in a higher pressure drop across the AICV in the heel while continuing to produce oil from the heel and other zones along the well (see **Figs. 13b and 13c**).

Fig. 14 illustrates the pressure in the tubing for the completion scenarios during the production period. As can be seen from the figure, AICV has the highest pressure drop ($P_{reservoir} - P_{tubing}$) over the whole production period. The higher pressure drop indicates that AICV chokes the gas flow entering the well for a longer period. This will delay the excessive gas production that will eventually take over the oil production.

Accuracy of the FCD Tables for Implementing the Behavior of the AICVs. To check if the simulated oil production agrees with the experiments, **Fig. 15** is considered. The plot to the left shows the simulated oil flow rate along the well and the tubing pressure. In production zone 1, for the case of AICVs, the pressure drop across the AICV ($P_{reservoir} - P_{tubing}$) is around 1500 kPa (15 bar) along the zone length shown by a blue ellipse. The simulated oil production for this zone is approximately 135 m^3/d. According to **Table 5**, there are 12

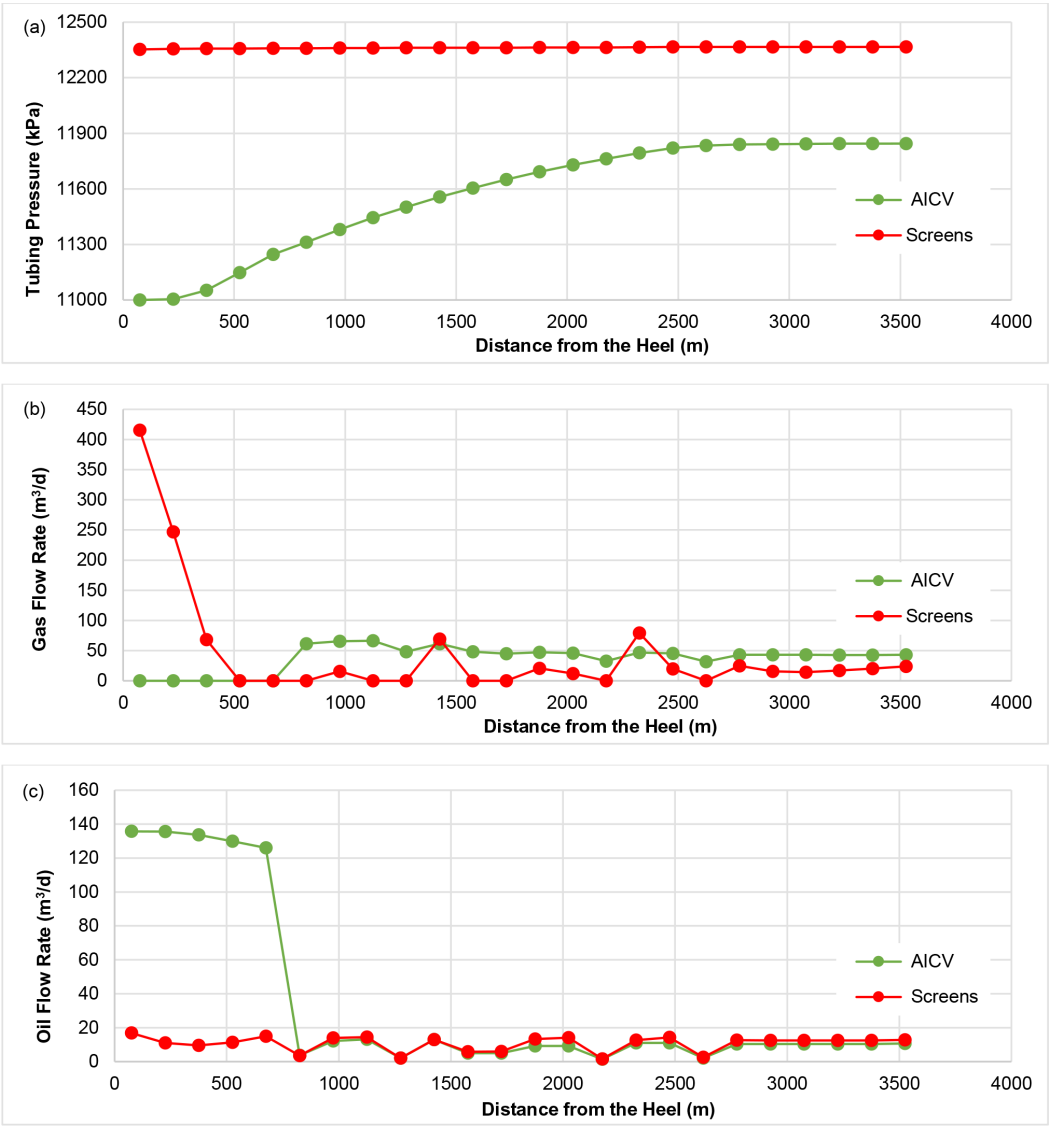

Fig. 13—Simulated tubing pressure (a), gas flow rate at RC (b), and oil flow rate at RC (c) along the well for the cases with AICV and sand screens.

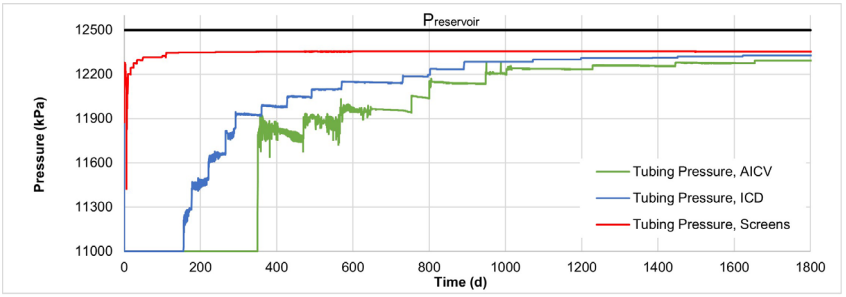

Fig. 14—Simulated pressure changes of the completion scenarios with time.

AICVs installed in this zone which implies an oil production of 11.25 m^3/d (0.46 m^3/h) per AICV. **Fig. 9** demonstrates that at around 15-bar differential pressure across the AICV, the oil flow rate is around 0.45 m^3/h. The plot to the right shows the comparison of simulated and experimental data for single-phase oil in production zone 1. The comparison indicates that the implementation of the workflow for generating the FCD table in the simulator has been successful.

Simulated GOR Development. One important parameter that must be considered for comparing the functionality of the AICVs with other types of completions is the GOR development. **Fig. 16a** illustrates the GOR development of the production well for a period

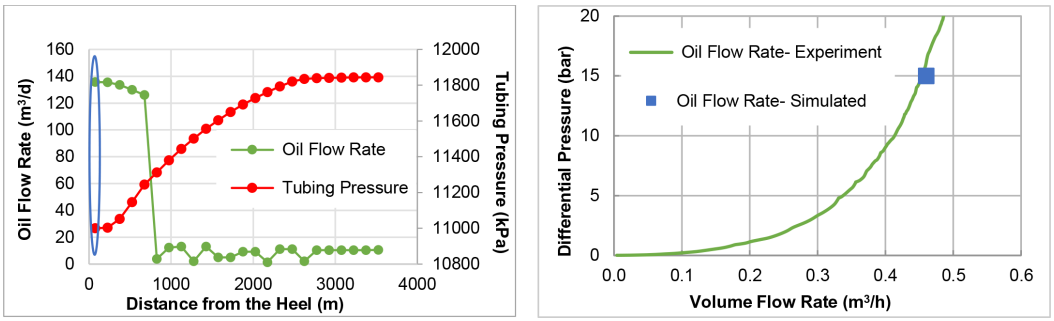

Fig. 15—Simulated oil flow rate and pressure drop across AICVs along the well (left) and oil flow rate from experiments and simulation (right).

of 1,825 days. **Fig. 16a** includes the GOR development by considering completions with both AICVs, ICDs, and sand screens. For challenging thin-oil-rim reservoirs, it is beneficial to have long-term oil production, as this limits the production from the gas cap. When the production from the gas cap is restricted, the upward movement and smearing of the oil column are limited (Langaas et al. 2020). As it can be seen from **Fig. 16a**, the early GOR level is highest with sand screens, delayed somewhat with ICDs, and even more with AICVs. The well is producing at a beneficial GOR for a longer time for the AICV case compared with the cases with ICDs and sand screens. Keeping the GOR at a relatively low level allows the production well to stay longer at a high liquid rate without needing to choke back because of high GOR.

Fig. 16b shows the GOR at standard conditions as a function of cumulative oil production at RC. This figure illustrates how the GOR varies with cumulative oil production. Usually in the wells, the total allowable gas production is limited, because the total gas processing capacity is an active constraint (Mjaavatten et al. 2006). This highlights the importance of developing new inflow control technologies that guarantee a higher maximum oil production while meeting the GOR constraint. As can be seen from **Fig. 16b**, the accumulated oil at a specific GOR (e.g., 400) for the AICV case is approximately four times more than the accumulated oil for the ICD case.

Simulated Cumulative Oil and Gas Production. Another important parameter that must be considered for comparing the functionality of the AICVs with other types of completions is the accumulated oil and gas. **Fig. 17** illustrates the cumulative oil and gas produced at RC by considering sand screens, ICD, and AICV completions along the well and by time. As it is shown in **Fig. 17a**, the cumulative oil production along the entire horizontal length of the well, at a given time, is higher for the AICV case compared with the case with screens. This implies that both the high- and low-permeability zones along the entire length of the wellbore contribute to the oil production by using AICVs. **Fig. 17b** shows that there is an insignificant difference between accumulated oil in the ICD and sand screen cases, whereas the accumulated gas drops by using ICDs compared with sand screens. However, the difference between accumulated oil in the AICV case compared with the two other cases is significant. Also, because of the choking effect of the AICVs on low-viscosity fluids like gas, the amount of accumulated gas drops significantly when the well is completed with AICVs. The values of accumulated oil and gas for the three simulated cases are presented in **Table 7.** According to **Table 7**, the cumulative oil production is 48.7% more when using AICVs

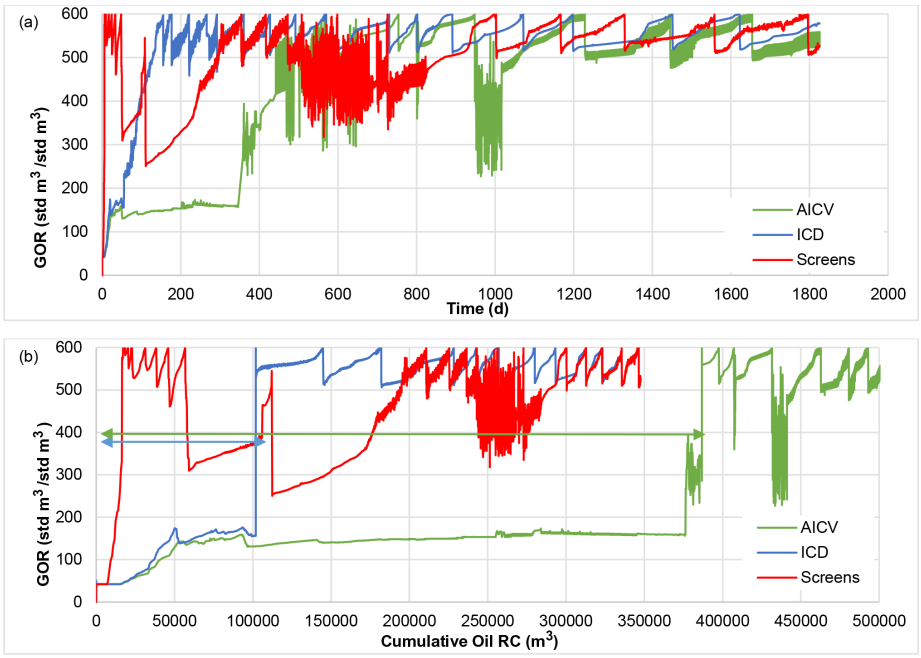

Fig. 16—Simulated GOR development for sand screens, AICVs, and ICDs simulation cases (a) and accumulated oil production vs. GOR for sand screens, ICDs, and AICVs (b).

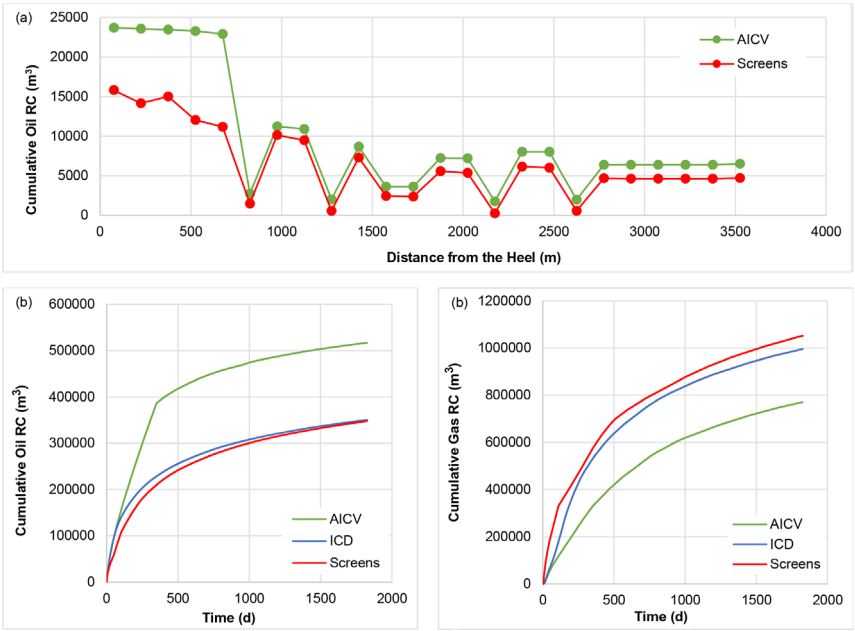

Fig. 17—Simulated accumulated oil along the well at a given time (a) and accumulated oil and gas from the well by time (b).

Completion Scenario	Accumulated Oil (m^3)	Accumulated Gas (m^3)	Relative Oil Increase from Sand Screens Case (%)	Relative Gas Reduction from Sand Screens Case (%)
Sand Screens	347 568	1 052 216	0	0
ICD	347 754	996 252	Negligible	–5.31
AICV	517 146	771 246	+48.7	–26.7

Table 7—Values of accumulated oil and gas after 1,825 days of oil production.

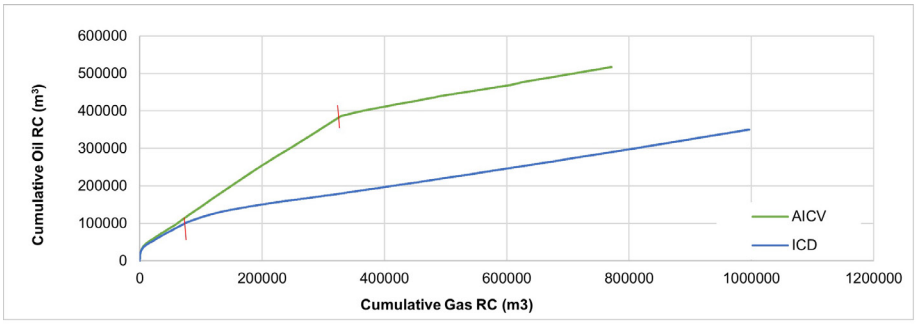

Fig. 18—Comparison of cumulative oil production as a function of cumulative gas production for well completions by ICDs and AICVs.

compared with using ICDs and sand screens. Owing to the better performance of AICV in both single- and multiphase flow regions, the amount of accumulated gas after 1,825 days of production is reduced by 22.5% and 26.7% relative to the ICD and sand screen cases, respectively. When the gas enters the well, AICV starts to choke the gas production gradually. Indeed, AICV chokes the gas production consistently as the gas mass fraction increases. This behavior, which is based on the experimental data, was implemented in the FCD control tables.

The flow influx along the horizontal well can be evened out by using AICVs. **Fig. 18** illustrates that the excessive gas production occurs much later for the case with AICVs than the case with ICDs. The small vertical red lines in **Fig. 18** indicate the change in the slope and the start of the decline in the oil production due to excessive gas production. It can be observed from the figure that the well completed by AICVs has produced about twice as much oil than the well completed by ICDs at a given cumulative gas production.

Conclusions

In this study, the performance of AICV in a thin-oil-rim reservoir and its impact on reservoir recovery are evaluated. This was achieved by performing experiments and simulations. Oil production from a thin-oil-rim field can be challenging because of early gas breakthrough and high GOR. The AICVs can restrict the inflow of gas in the zones where breakthrough occurs.

The experimental work consists of one-phase and multiphase flow tests for orifice ICD and AICV using water, gas, and oil as the reservoir fluids at realistic reservoir condition. Simulations are performed using a commercial simulator. The results from experiments show that AICV restricts the gas flow significantly compared with an orifice-type ICD, specifically at higher GVF. This behavior makes this technology unique when compared with other inflow control technologies.

In the simulations, AICV/ICD tables (FCD tables) are developed based on data from the experiments. The FCD tables are used to implement the behavior of the AICV/ICD using their characteristics and the reservoir fluid properties. Hence, a workflow for developing the AICV/ICD tables in the simulator is proposed.

According to the simulation results, by completion of the well with AICVs compared with using ICDs and sand screens only, the cumulative oil production is increased by 48.7% during the first 5 years of production. Besides, AICVs reduce the cumulative gas production by 22.5% and 26.7% relative to the ICD and sand screen cases, respectively. The simulated oil production agrees with the AICV performance results from the experiments. This shows that the implementation of the workflow for generating the FCD tables in the simulator has been successful. By evaluation of the simulation results, it can be concluded that the well is producing at a beneficial GOR for a longer time for the AICV case compared with the cases with ICDs and sand screens. Keeping the GOR at a relatively low level allows the production well to stay longer at a high liquid rate without needing to choke back because of high GOR. This can be achieved by using advanced inflow control technologies such as AICVs. As it is demonstrated in this work, deploying AICVs in the most challenging light oil reservoirs with high GOR can be beneficial with respect to increased production and recovery.

Nomenclature

a_{AICD} = RCP valve/AICV strength parameter
A_{vc} = area in vena contracta
C = geometrical constant
C_d = discharge coefficient
D = diameter, m
f = friction factor, 64/Re
K_r = relative permeability
K_{rg} = relative permeability of gas phase
K_{rog} = oil relative permeability at irreducible water saturation for an oil-gas system
K_{row} = oil relative permeability for a water-oil system
K_{rw} = relative permeability of water phase
L = length, m
Q = volumetric flow rate, m^3/d
Re = Reynolds number
x = user-input parameter
y = user-input parameter
ΔP = differential pressure, bar
μ = fluid viscosity, cp
μ_{cal} = calibration viscosity, cp
μ_{mix} = mixed-fluid viscosity, cp
ρ = fluid density, kg/m^3
ρ_{cal} = calibration density, kg/m^3
ρ_{mix} = mixed-fluid density, kg/m^3

References

Aakre, H., Halvorsen, B., Werswick, B. et al. 2013. Smart Well With Autonomous Inflow Control Valve Technology. Paper presented at the SPE Middle East Oil and Gas Show and Conference, Manama, Bahrain, 10–13 March. https://doi.org/10.2118/164348-MS.

Aakre, H., Halvorsen, B., Werswick, B. et al. 2014. Autonomous Inflow Control Valve for Heavy and Extra-Heavy Oil. Paper presented at the SPE Heavy and Extra Heavy Oil Conference, Medellín, Colombia, 24–26 September. https://doi.org/10.2118/171141-MS.

Alakberi, R. S., Igein, O. F., and Aljasmi, S. A. 2023. Successful Smart Completion Deployment of Autonomous Inflow Control Valve with 13 Open Hole Segmentation Lower Completion Using a Light Workover Rig. Paper presented at the SPE/IADC Middle East Drilling Technology Conference and Exhibition, Abu Dhabi, UAE, 23–25 May. https://doi.org/10.2118/214582-MS.

Buwauqi, S., Jumah, A. A., Shabibi, A. et al. 2021. Application of Autonomous Inflow Control Valve AICV in Increasing the Field Recovery in One of the Matured Fields in the Sultanate of Oman: Case Study. Paper presented at the SPE Annual Caspian Technical Conference, Virtual, 5–7 October. https://doi.org/10.2118/207069-MS.

Canadian Legal Information Institute. 1996. *National Energy Board Act Part VI (Oil and Gas) Regulations, SOR/96-244*. https://canlii.ca/t/52hmb.

Carpenter, C. 2015. Smart Horizontal Wells for Development of Thin-Oil-Rim Reservoirs. *J Pet Technol* **67** (11): 87–89. https://doi.org/10.2118/1115-0087-JPT.

Chan, K. S., Masoudi, R., Karkooti, H. et al. 2014. Smart Horizontal Well Drilling and Completion for Effective Development of Thin Oil-Rim Reservoirs in Malaysia. Paper presented at the International Petroleum Technology Conference, Kuala Lumpur, Malaysia. https://doi.org/10.2523/IPTC-17753-MS.

Halvorsen, M., Elseth, G., and Nævdal, O. M. 2012. Increased Oil Production at Troll by Autonomous Inflow Control with RCP Valves. Paper presented at the SPE Annual Technical Conference and Exhibition, San Antonio, Texas, USA, 8–10 October. https://doi.org/10.2118/159634-MS.

Halvorsen, M., Madsen, M., Vikøren Mo, M. et al. 2016. Enhanced Oil Recovery On Troll Field By Implementing Autonomous Inflow Control Device. Paper presented at the SPE Bergen One Day Seminar, Grieghallen, Bergen, Norway, 20 April. https://doi.org/10.2118/180037-MS.

Hasan, A., Sagatun, S., and Foss, B. 2010. Well Rate Control Design for Gas Coning Problems. Paper presented at the 49th IEEE Conference on Decision and Control (CDC), Atlanta, Georgia, USA, 15–17 December. https://doi.org/10.1109/CDC.2010.5717861.

Kearns, K., Rios, F., Montero, J. et al. 2022. Autonomous Inflow Control Valves Restore Oil Production by Controlling Gas and Water Breakthrough in Acordionero Field, Colombia: A Case Study. Paper presented at the SPE Annual Technical Conference and Exhibition, Houston, Texas, USA, 3–5 October. https://doi.org/10.2118/210163-MS.

Konopczynski, M., Moradi, M., Krishnan, T. et al. 2022. Case Study: Oil Production Optimized With Autonomous Inflow Control Devices Offshore Malaysia. *J Pet Technol* **74** (09): 44–51. https://doi.org/10.2118/0922-0044-JPT.

Langaas, K., Jeurissen, E. J., and Abay, H. K. 2019. Combining Passive and Autonomous Inflow-Control Devices in a Trilateral Horizontal Well in the Alvheim Field. *SPE Prod & Oper* **34** (03): 446–460. https://doi.org/10.2118/187288-PA.

Langaas, K., Urazovskaya, O., Gueze, N. et al. 2020. Attic Oil Recovery in the Alvheim Field. Paper presented at the SPE Norway Subsurface Conference, Virtual, 2–3 November. https://doi.org/10.2118/200719-MS.

Lomeland, F. and Orec, A. 2018. Overview of the LET Family of Versatile Correlations for Flow Functions. Paper presented at the International Symposium of the Society of Core Analysts, Trondheim, Norway, 27–30 August. SCA2018-056.

Mathiesen, V., Aakre, H., Werswick, B. et al. 2011. The Autonomous RCP Valve - New Technology for Inflow Control in Horizontal Wells. Paper presented at the SPE Offshore Europe Oil and Gas Conference and Exhibition, Aberdeen, UK, 6–8 September. https://doi.org/10.2118/145737-MS.

Mjaavatten, A., Aasheim, R., Saelid, S. et al. 2006. A Model for Gas Coning and Rate-Dependent Gas/Oil Ratio in an Oil-Rim Reservoir. Paper presented at the SPE Russian Oil and Gas Technical Conference and Exhibition, Moscow, Russia, 3–6 October. https://doi.org/10.2118/102390-MS.

Mohd Ismail, I., Che Sidik, N. A., Syarani Wahi, F. et al. 2018. Increased Oil Production in Super Thin Oil Rim Using the Application of Autonomous Inflow Control Devices. Paper presented at the SPE Annual Technical Conference and Exhibition. https://doi.org/10.2118/191590-MS.

Mohd Ismail, I., Mathiesen, V., Abraham, A. et al. 2021. An Innovative Modelling Approach in Characterization of Autonomous Inflow Control Valve Performance to Maximizing Oil Recovery in Heavy Oil-SAGD Application. *SPE Thermal Well Integrity and Design Symposium*. https://doi.org/10.2118/203859-MS.

Moradi, A. and Moldestad, B. M. E. 2021. A Proposed Method for Simulation of Rate-Controlled Production Valves for Reduced Water Cut. *SPE Prod & Oper* **36** (03): 669–684. https://doi.org/10.2118/205377-PA.

Taghavi, S. and Ghaderi, A. 2021. On Uncertainty Analysis of the Rate Controlled Production (RCP) Model. Paper presented at the First SIMS EUROSIM Conference on Modelling and Simulation, SIMS EUROSIM 2021, Oulu, Finland, 21–23 September. https://doi.org/10.3384/ecp21185271.

The Norwegian Petroleum Directorate. 2019. *Zone Control for Improved Recovery and Lower Costs*. https://www.npd.no/en/facts/publications/reports/resource-report/resource-report-2019/fields/Zone-control-for-improved-recovery-and-lower-costs/.

The Norwegian Petroleum Directorate. 2021. *NPD FactPages*. https://factpages.npd.no/en/field/PageView/Producing/46437.

Timsina, R., Furuvik, N. C. I., and Moldestad, B. M. E. 2017. Modeling and Simulation of Light Oil Production Using Inflow Control Devices. Paper presented at the 58th Conference on Simulation and Modelling (SIMS 58), Reykjavik, Iceland, 25–27 September. https://doi.org/10.3384/ecp17138180.

Tusimin, F., Riyanto, L., Ahmad Tajuddin, N. et al. 2020. Enhanced Oil Production with Autonomous Inflow Control Devices in a Thin Oil Rim Reservoir Malaysia. Paper presented at the Offshore Technology Conference Asia, Kuala Lumpur, Malaysia, 2–6 November. https://doi.org/10.4043/30363-MS.

Veskimägi, V. 2013. *Gas Coning Control with a Smart Horizontal Well in a Thin Oil Rim*. PhD dissertation, Delft University of Technology, Delft, Netherlands. https://repository.tudelft.nl/islandora/object/uuid:e05799fa-2d9d-459d-afa9-fb52efb423ef?collection=education.

Appendix A—Modeling of AICV/ICD in the CMG STARS Simulator

Modeling of the AICV/ICD by using FCD tables in the CMG STARS simulators can be established as the following workflow:

1. Obtain the necessary data related to the total production rates, number of compartments, reservoir type (sandstone or carbonate), oil viscosity and density, and the desired behavior as gas shutoff and water shutoff/choking.
2. Find the available experimental data related to the case study that describe the performance of AICV for single phases of oil, gas or steam, and water. If possible, find the multiphase data of AICV too.
3. Calculate the equivalent orifice diameter by considering the same oil rate at the same pressure drop for the AICV and ICD using the following equation (Langaas et al. 2019):

$$\Delta p = \frac{1}{2}\rho \cdot \left(\frac{Q}{A \cdot C_d}\right)^2, \tag{A-1}$$

   where ΔP is the pressure drop, ρ is the fluid density, A is the flow area of the orifice, C_d is the discharging coefficient, and Q is the volumetric flow rate of fluid. By calculating A, the diameter of the orifice can be obtained. When the experimental data for an equivalent ICD is not available, Step 3 is applied.
4. Calculate the corresponding gas and water rate through ICD using Eq. A-1.
5. Generate the standard FCD table for ICDs and AICVs with optional dependencies. The optional dependency in this work is the gas mass fraction (*GFR keyword in the simulator). Total mass flow rates (*RATES_MASS keyword in the simulator) are measured for different pressure drops. One value for each combination of pressure drops and optional dependency appears immediately after the keyword *RATES_MASS. The data used in the simulation of the AICV case are presented in **Table A-1**. As it is shown in the tables for six different GFRs and four different pressure drops, the mass flow rates are measured. The first-rate Q (1) on each row must be zero and the flow rate values must be increasing monotonically. In the case of not having measurements for one data point, *EXTP may be used to either interpolate or extrapolate from adjacent values on the same table row.
6. If experimental data are not available, drive a mathematical model for the AICV using the RCP model (Mathiesen et al. 2011):

$$\Delta P_{\text{tot}} = \left(\frac{\rho_{\text{mix}}^2}{\rho_{\text{cal}}}\right) \cdot \left(\frac{\mu_{\text{cal}}}{\mu_{\text{mix}}}\right)^y \cdot a_{\text{AICD}} \cdot Q^x, \tag{A-2}$$

   where ΔP_{tot} is the pressure drop through the AICV, ρ_{cal} and ρ_{mix} are the densities of the calibration fluid and mixture fluid, μ_{cal} and μ_{mix} are the viscosities of the calibration and mixture fluid, a_{AICD} is the valve strength, and Q is the volumetric flow rate of the fluid. There are several methods to estimate the x and y, which are the parameters of the RCP valve model. These methods include but not limited to curve fitting to the experimental data, linear regression (Moradi and Moldestad 2021), and Bayesian approach (Taghavi and Ghaderi 2021).

								Definitions
*DELP		0	1000	1500	2000			**Pressure drops (kPa)
*GFR		0	0.05	0.22	0.42	0.9	1	**Gas mass fractions
*RATES_ MASS		**Q (1)	**Q (2)	**Q (3)	**Q (4)			**Rates (kg/d) across 12 valves
	1	0	96 350	111 629	135 130			
	2	0	83 520	86 000	89 000			
	3	0	39 426	42 164	*EXTP			
	4	0	14 000	14 500	15 788			
	5	0	4500	5500	6000			
	6	0	3168	3456	3744			

Table A-1—FCD table for the AICV case used in the simulations.

7. Generate the performance curves for both single- and multiphase of oil/gas and/or oil/water that represent the behavior of the AICV up to the desired differential pressure.
8. Generate the standard FCD table for ICDs and AICVs with optional dependencies as Step 5.

Improved Multiphase Flow Performance Using AICV and its Potential Impact on Reservoir Recovery
Soheila Taghavi Hosnaroudi

Doctoral dissertations at the University of South-Eastern Norway no. 198

ISBN 978-82-7206-866-9 (print)
ISBN 978-82-7206-867-6 (online)

usn.no